

# **Organophosphorus Compounds as Fluorescent Probes for Cell Imaging**



**Antonio Alberto Sánchez Cid**

Submitted in fulfilment of the requirements for the  
degree of Doctor of Philosophy

School of Chemistry

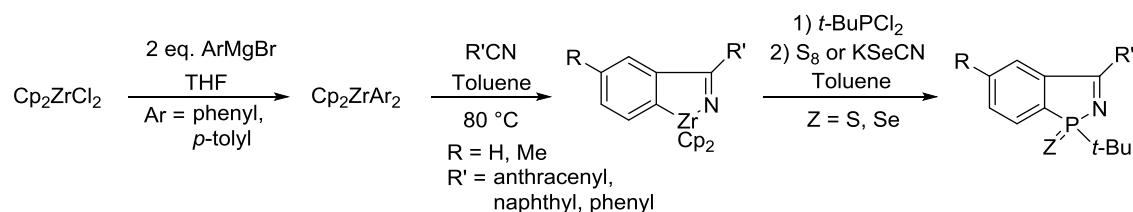
Newcastle University

December 2017

## Abstract

Small molecules containing fluorescent moieties can be used as a means of studying cell structure and function, as a result of the high sensitivity of fluorescence microscopy. This technique allows one to obtain specific information about the cell and has recently attracted considerable interest by many research groups. This work presents three projects in which the main aim was to develop multi-modal imaging agents. They will possess a fluorescent group and also another moiety which provides predictable biological properties. Our interest is centred on two types of fluorophore: Polycyclic Aromatic Hydrocarbons (PAHs) and 4,4-difluoro-4-bora-3a,4a-diaza-s-indacene (BODIPY).

The first project describes the synthesis of the phosphorus analogues of the biologically-active indazole core which remain rare in the literature. The synthesis presented here shows the versatility of our approach and allows for substitution on the phenyl ring of the newly formed phosphindole core simply by changing the nitrile used. Position 3 of the phosphindoles was also varied to bear different aromatic groups; the chosen aromatic systems were phenyl, naphthyl and anthracenyl. These were chosen in order to prepare a fluorescent and biologically-active core.

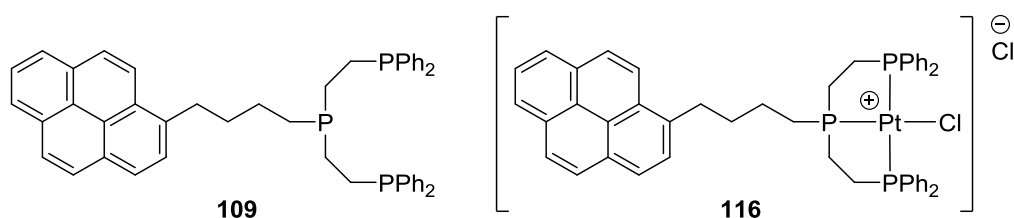


### Synthesis of novel phosphindoles containing a PAH

In practice, the phosphindoles showed near zero quantum yields. Photoinduced Electron Transfer and Dexter Energy Transfer seem to be the plausible responsible phenomena behind this lack of fluorescence. Temperature was found to be a key variable in the synthesis of phosphindoles since a temperature below 110 °C in the last step led to the formation of two chlorothiophosphonates. One of these unexpected chlorothiophosphonates showed strong activity against *Bacillus subtilis* and *Streptococcus pyogenes*.

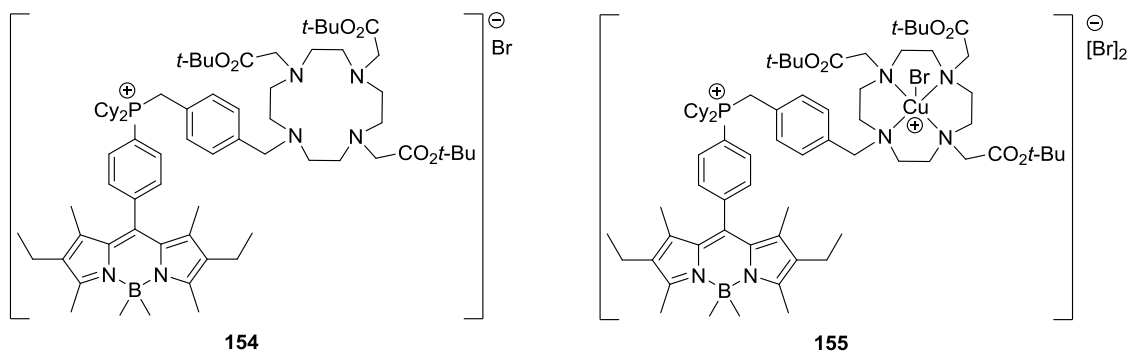
The second project describes the synthesis of the pyrene-based ligand **109**, which is significant as it was based on an air-stable alkyl primary phosphine. This remarkable stability is provided by the electronic properties that both the pyrene and the butyl linker

confer on the corresponding primary phosphine. The tridentate ligand **109** was obtained following a double hydrophosphination reaction of the primary phosphine, and **109** was subsequently used to create complexes with the transition metals from groups 9 and 10. These demonstrated demonstrated weak fluorescence despite the presence of a metallic core. The presence of the DNA intercalating pyrene unit and the presence of the square-planar Pt centre in complex **116** required an assessment of the cytotoxicity of the complex. In assays, **116** was shown to exert similar cytotoxicity towards bone osteosarcoma (U2OS) and transformed mammary cancer (HMLER) cell lines as the anticancer drug Cisplatin. The advantage of complex **116** is that it contains an intercalating function, a potential cytotoxic platinum centre and moderate/mild loss of fluorescence for cell imaging by optical microscopy.



**Ligand 109 and its Pt(II) complex 116**

The final project discussed in this thesis is the synthesis of a phosphonium salt containing BODIPY as fluorophore, bound to a macrocycle which is able to undergo complexation reactions with d-block metals. This is another example of a molecule capable of multi-modal functionality, since phosphonium salts have been shown to target mitochondria. Positively charged compounds freely diffuse across the negatively charged mitochondrial membrane and the BODIPY moiety allows for imaging of the compound's fate by optical microscopy. Finally, the tetraamine macrocycle of the molecule allowed ligand **154** to be reacted with  $[\text{Cu}(\text{OAc})_2]$  which gave the fluorescent Cu(II) complex **155**. This complex is interesting because it proves that coordination to Cu is possible. The next step in this research would be to prepare the  $^{64}\text{Cu}$  analogue, which would be a candidate for Positron Emission Tomography (PET) imaging. In this manner,  $^{64}\text{Cu}$ -**154** would be a fluorescent organelle-specific PET imaging agent.



**Ligand 154 and the BODIPY-phosphonium Cu(II) complex 155**

## **Acknowledgments**

Firstly, I would like to thank CONACyT, a Mexican governmental body which funded my research during the whole time I have been in the UK.

I would like to acknowledge foremost my supervisor Dr Lee J. Higham for his constant support, guidance, and encouragement throughout the course of this work. I would also like to thank my colleagues at Newcastle University and especially to the LJH research group for their friendship and support during this research.

I would like to thank Prof. W. Clegg, Dr P. Waddell and Dr M. Probert for X-ray crystallography, Prof. W. McFarlane and Dr C. Wills for assistance with NMR spectroscopy, and the EPSRC Mass Spectrometry Service, Swansea.

Finally I would like to thank my friends and family for their constant and unconditional support throughout my PhD.

## Abbreviations

### General:

$\alpha$	Alpha particle
CT	Computed Tomography
DLC	Delocalised Lipophilic Cation
DFT	Density Functional Theory
$E_\gamma$	Gamma Energy
$\gamma$	Gamma-ray
$t_{1/2}$	Half-life
HOMO	Highest Occupied Molecular Orbital
HPLC	High-Performance Liquid Chromatography
LUMO	Lowest Unoccupied Molecular Orbital
$m$	Metastable
MP	Melting Point
MIC	Minimum Inhibitory Concentration
MDR	Multidrug Resistant
MRI	Nuclear Magnetic Resonance Imaging
PeT	Photoinduced Electron Transfer
PAH	Polycyclic Aromatic Hydrocarbon
$\beta^+$	Positron
PET	Positron Emission Tomography
RC	Radical cation
rt	Room Temperature
SOMO	Singly Occupied Molecular Orbital
TLC	Thin Layer Chromatography
$\Delta\psi_m$	Transmembrane Potential

### Chemicals:

Ac	Acetate
Ac <sub>2</sub> O	Acetic anhydride
MeCN	Acetonitrile
ATP	Adenosine Triphosphate
Bn	Benzyl
Triphos	Bis(2-diphenylphosphinoethyl)phenylphosphine
Ct	Calf thymus
DCM	Dichloromethane
DDQ	2,3-Dichloro-5,6-dicyano-1,4-benzoquinone
BODIPY	4,4-Difluoro-4-bora-3a,4a-diaza-s-indacene
DIPEA	<i>N,N</i> -Diisopropylethylamine
CDCl <sub>3</sub>	Deuterated chloroform
CD <sub>2</sub> Cl <sub>2</sub>	Deuterated dichloromethane
cod	1,5-Cyclooctadiene
Cp	Cyclopentadienyl
Cy	Cyclohexyl
DAPI	4',6-Diamidino-2-phenylindole
DCM	Dichloromethane
DDQ	2,3-Dicyano-5,6-dichloroparabenzoquinone

DMSO	Dimethyl Sulfoxide
DNA	Deoxyribonucleic Acid
DPH	1,6-Diphenyl-1,3,5-hexatriene
EtOH	Ethanol
Fc	Fe( $\eta^5$ -C <sub>5</sub> H <sub>4</sub> ) <sub>2</sub>
NAD	Nicotinamide Adenine Dinucleotide
MeOH	Methanol
MeI	Methyl Iodide
KOH	Potassium Hydroxide
( <i>R</i> )-MOPH <sub>2</sub>	2-Phosphino-2'-methoxy-1,1'-binaphthyl
Nbd	Norbornadiene
nb	Norbornene
PBr <sub>3</sub>	Phosphorus Tribromide
<i>p</i> Tol	<i>para</i> -Tolyl
Ph	Phenyl
Pr	Propyl
py	Pyridine
TFA	Trifluoroacetic Acid
THF	Tetrahydrofuran
TMSCl	Trimethylsilyl Chloride

**Units:**

Å	Angstroms
cm	Centimetres
°	Degrees
°C	Degrees Celsius
Ci	Curies
eq	Equivalents
eV	Electron Volts
g	Grams
Hz	Hertz
H	Hours
IU	International Unit
Kcal/mol	Kilocalorie per mole
L	Litre
MeV	Megaelectron Volts
mg	Milligrams
mV	Millivolt
MHz	Megahertz
mmol	Millimolar
min	Minutes
M	Molar
nm	Nanometres
ns	Nanoseconds
ppm	Parts per million
s	Seconds

**NMR:**

br	Broad
$\delta$	Chemical Shift
d	Doublet
I	Nuclear Spin
J	Coupling Constant
m	Multiplet
NMR	Nuclear Magnetic Resonance
NOE	Nuclear Overhauser Effect
q	Quartet
s	Singlet
t	Triplet

**Infrared:**

br	Broad
FT-IR	Fourier Transform Infrared Spectroscopy
m	Medium
NIR	Near-Infrared Region
s	Strong
w	Weak

**Mass spectrometry:**

AP	Atmospheric Pressure
CI	Chemical Ionisation
EI	Electron Ionisation
ESI	Electrospray
FAB	Fast Atom Bombardment
HRMS	High Resolution Mass Spectrometry

**Photophysical Parameters:**

$\lambda_{\text{abs}}$	Absorption Maxima
$\lambda_{\text{em}}$	Emission Maxima
$S_1$	First Excited State
$T_1$	First Triplet State
$S_0$	Ground State
$\tau$	Lifetime
$\epsilon$	Molar Absorption Coefficient
$\Phi_F$	Quantum Yield
$S_2$	Second Excited State
$\Delta v_{\text{st}}$	Stokes Shift
UV	Ultra-Violet



# Table of Contents

## 1 Contents

1	Introduction .....	13
1.1	Overview .....	13
1.2	Targets .....	13
1.3	Primary phosphines .....	14
1.3.1	Predicting the air-stability of primary phosphines .....	16
1.4	Origins of luminescence .....	20
1.4.1	Fluorescence quenching .....	22
1.5	Fluorophores .....	25
1.5.1	Polycyclic Aromatic Hydrocarbons (PAH) .....	25
1.5.2	BODIPY .....	34
1.5.3	DNA probes .....	38
1.6	Radiotracers .....	40
1.6.1	Positron Emission Tomography (PET) .....	40
1.6.2	Isotopes of copper: $^{64}\text{Cu}$ and $^{62}\text{Cu}$ .....	42
2	Novel 1,2-azaphosphindoles .....	44
2.1	Introduction .....	44
2.1.1	1 <i>H</i> -indazole .....	44
2.1.2	Synthetic routes towards indazoles .....	46
2.2	Synthetic target .....	48
2.3	Synthesis of 1,2-azaphosphindoles .....	49
2.4	Structural and electronic properties of 1,2-azaphosphindoles .....	54
2.4.1	Phosphorus-selenium coupling constants in NMR .....	54
2.4.2	X-ray crystallographic analysis and molecular structures .....	56
2.4.3	Chlorothiophosphonates <b>80-81</b> .....	59

2.4.4	An investigation to the torsional angles between the phosphindole backbone and the PAH ancillary group.....	61
2.5	Photophysical data.....	63
2.5.1	UV-Vis absorption spectroscopy .....	63
2.5.2	Quantum yield.....	66
2.6	Biological activity of the novel synthesised phosphindazoles .....	73
2.6.1	Determination of Minimum Inhibitory Concentration (MIC) .....	74
2.7	Summary .....	77
2.8	Experimental .....	79
2.8.1	General Procedure.....	79
2.8.2	Diphenyl zirconocene <b>67</b> .....	79
2.8.3	3-Anthracen-9-yl-(phenyl-azazirconacyclopentene) <b>69</b> .....	80
2.8.4	3-Anthracen-9-yl-((1- <i>tert</i> -butyl)-1-sulfide-1 <i>H</i> -1,2-azaphosphindole) <b>73</b> .....	80
2.8.5	3-Naphthalen-1-yl-(phenyl-azazirconacyclopentene) <b>70</b> .....	81
2.8.6	3-Naphthalen-1-yl-((1- <i>tert</i> -butyl)-1-sulfide-1 <i>H</i> -1,2-azaphosphindole) <b>74</b> 81	
2.8.7	3-Phenyl-(phenyl-azazirconacyclopentene) <b>71</b> .....	82
2.8.8	3-Phenyl-((1- <i>tert</i> -butyl)-1-sulfide-1 <i>H</i> -1,2-azaphosphindole) <b>75</b> .....	83
2.8.9	Bis( <i>p</i> -tolyl) zirconocene <b>68</b> .....	83
2.8.10	3-Anthracen-9-yl-( <i>p</i> -tolyl-azazirconacyclopentene) <b>72a/b</b> .....	84
2.8.11	3-Anthracen-9-yl-((1- <i>tert</i> -butyl)-(4-methyl)-1-sulfide-1 <i>H</i> -1,2-azaphosphindole) / 3-Anthracen-9-yl-((1- <i>tert</i> -butyl)-(5-methyl)-1-sulfide-1 <i>H</i> -1,2-azaphosphindole) <b>76a/b</b> .....	85
2.8.12	3-Anthracen-9-yl-((1- <i>tert</i> -butyl)-1-selenide-1 <i>H</i> -1,2-azaphosphindole) <b>77</b> 86	
2.8.13	3-Naphth-1-yl-((1- <i>tert</i> -butyl)-1-selenide-1 <i>H</i> -1,2-azaphosphindole) <b>78</b> ...	86
2.8.14	3-Phenyl-((1- <i>tert</i> -butyl)-1-selenide-1 <i>H</i> -1,2-azaphosphindole) <b>79</b> .....	87

2.8.15	<i>N</i> -(Anthracen-9-yl(phenyl)methylene)- <i>P</i> -( <i>tert</i> -butyl)phosphonamidothioic chloride <b>80</b> .....	88
2.8.16	<i>N</i> -(Anthracen-9-yl( <i>p</i> -tolyl)methylene)- <i>P</i> -( <i>tert</i> -butyl)phosphonamidothioic chloride / <i>N</i> -(anthracen-9-yl( <i>m</i> -tolyl)methylene)- <i>P</i> -( <i>tert</i> -butyl)phosphonamidothioic chloride <b>81a/b</b> .....	89
3	Synthesis of a pyrene-based tridentate phosphine and its coordination chemistry in complexes of biological interest .....	90
3.1	Primary phosphines on aromatic backbones .....	90
3.2	Quantum chemical calculations.....	91
3.3	Synthesis of air-stable phosphines pyrene-based <b>93-95</b> .....	93
3.3.1	NMR experiments to determine the air stability of PyrCH <sub>2</sub> PH <sub>2</sub> <b>94</b> and Pyr(CH <sub>2</sub> ) <sub>4</sub> PH <sub>2</sub> <b>95</b> .....	102
3.4	Synthesis of the pyrene-based ligand <b>109</b> .....	104
3.4.1	Group 10 coordination chemistry of tridentate phosphine <b>109</b> .....	106
3.4.2	Group 9 coordination chemistry of tridentate phosphine <b>109</b> .....	116
3.5	Photophysical data.....	120
3.6	Cell studies with [PtCl( <b>109</b> )]Cl <b>116</b> .....	125
3.7	Summary .....	130
3.8	Experimental .....	131
3.8.1	General Procedure .....	131
3.8.2	Diethyl 1-pyrenylmethylene phosphonate <b>100</b> .....	132
3.8.3	1-Pyrenylmethylene phosphine <b>94</b> .....	132
3.8.4	1-(4-Bromobutyl)-pyrene <b>102</b> .....	133
3.8.5	Diethyl (4-(pyren-1-yl)butyl)phosphonate <b>103</b> .....	134
3.8.6	4-(Pyren-1-yl)butylphosphine <b>95</b> .....	134
3.8.7	4-(Pyren-1-yl)butyl- <i>P</i> - <i>bis</i> -(2-ethyl)phenylphosphino)phosphine <b>109</b> ..	135
3.8.8	[PtCl( <b>109</b> )]Cl <b>116</b> .....	136
3.8.9	[PdCl( <b>109</b> )]Cl <b>120</b> .....	136

3.8.10	[NiCl <sub>2</sub> ( <b>109</b> )] <b>121</b> .....	137
3.8.11	[RhCl( <b>109</b> )] <b>125</b> .....	137
3.8.12	[IrCl( <b>109</b> )] <b>129</b> .....	138
3.8.13	Absorption and Emission Spectroscopy .....	138
3.8.14	Quantum Yield Method.....	138
3.8.15	UV/Vis titration.....	139
3.8.16	Ethidium bromide displacement assay .....	139
3.8.17	ct-DNA precipitation assay .....	140
3.8.18	Cell lines and cell culture conditions .....	140
3.8.19	Cytotoxicity MTT assay.....	140
4	Synthesis of a fluorescent chelator ligand derived from 8-((4-dicyclohexylphosphino)phenyl)-4,4-diphenyl-1,3,5,7-tetramethyl-2,6-diethyl-4-bora-3a,4a-diaza-s-indacene .....	142
4.1	Mitochondria .....	142
4.1.1	Mitochondria as a drug target .....	143
4.2	Phosponium cations capable of binding Cu(II).....	145
4.3	BODIPY-derived ligand target.....	148
4.4	Synthesis of BODIPY-Cu(II) complex derived from a phosponium cation	151
4.5	Photophysical Data.....	161
4.6	Summary .....	165
4.7	Experimental .....	166
4.7.1	General procedure .....	166
4.7.2	8-(4-Bromophenyl)-4,4-difluoro-1,3,5,7-tetramethyl-2,6-diethyl-4-bora-3a,4a-diaza-s-indacene <b>149</b> .....	166
4.7.3	8-(4-Bromophenyl)-4,4-dimethyl-1,3,5,7-tetramethyl-2,6-diethyl-4-bora-3a,4a-diaza-s-indacene <b>150</b> .....	167
4.7.4	8-((4-Dicyclohexylphosphino)phenyl)-4,4-dimethyl-1,3,5,7-tetramethyl-2,6-diethyl-4-bora-3a,4a-diaza-s-indacene <b>151</b> .....	168

4.7.5	9-(4-(Bromomethyl)benzyl)-8-((4-dicyclohexyl)phenyl)-4,4-dimethyl-1,3,5,7-tetramethyl-2,6-diethyl-4-bora-3a,4a-diaza-s-indacene phosphonium bromide <b>152</b> .....	169
4.7.6	9-(4-((4,7,10-Tris(2-( <i>tert</i> -butoxy)-2-oxoethyl)-1,4,7,10-tetraazacyclododecan-1-yl)methyl)benzyl)-8-((4-dicyclohexyl)phenyl)-4,4-dimethyl-1,3,5,7-tetramethyl-2,6-diethyl-4-bora-3a,4a-diaza-s-indacene phosphonium bromide <b>154</b> .....	170
4.7.7	[CuBr( <b>154</b> )] [Br] <sub>2</sub> <b>155</b> .....	171
5	Future Work .....	172

# 1 Introduction

## 1.1 Overview

The use of fluorescent molecules in biological applications is a useful tool in contemporary research, and their ever increasing due to their flexibility, sensitivity and ability to provide data. Fluorescence methods are predominantly valuable due to the widespread use of confocal,<sup>1, 2</sup> two-photon<sup>3</sup> and epifluorescence light microscopy.<sup>4</sup> Furthermore, the development of new functional fluorescent compounds that can monitor intra- and extracellular events with high chemoselectivity is a promising avenue. The use of confocal<sup>5</sup> and multiphoton microscopy<sup>6</sup> provides optical sectioning (the process by which a suitable microscope can record clear images of cells in a thick sample). This type of probe uses fluorescent compounds that improve image quality. This thesis describes the results obtained during the development of three projects where the main objective was to prepare multi-modality organophosphorus fluorescent probes for use in the fields of bioscience. During the development of this work, the synthesis of novel primary phosphines was required in order to synthesise some of the essential phosphorus-containing compounds.

## 1.2 Targets

This thesis explores three main topics:

1) 1,2-Azaphosphindoles containing aromatic moieties and the biological characterization of **73**, **76** and **80**:

This type of compound is interesting as *N*-heterocycles are a common scaffold in medicine, while the analogous *P*-heterocycles have been much less studied. The Higham research group is interested in the use of primary phosphines as precursors – can be used to prepare organodichlorophosphines  $\text{RPCl}_2$  which in turn can be used to prepare the *P*–*N* heterocycles found in azaphosphindoles. Thus, the primary phosphine route offers a new avenue for the preparation of bioactive molecules.

2) Synthesis of a fluorescent pyrene-based tridentate phosphine with DNA intercalating properties:

The Higham research group has reported a BODIPY-based tridentate phosphine that was synthesised from the primary phosphine BODIPY- $\text{PH}_2$ . The tridentate BODIPY ligand proved to be a potential Single-Photon Emission Computed Tomography (SPECT) imaging agent. In this section, a fundamental question will be addressed – is

pyrene(CH<sub>2</sub>)<sub>4</sub>PH<sub>2</sub> air-stable? If so, this would be the first example of an *alkyl* primary phosphine which is air-stable, by virtue of remote  $\pi$ -conjugation. The synthesis of such a primary phosphine would also allow for the synthesis of a tridentate derivative capable of binding or intercalating with DNA. The pyrene-based ligand and its resulting complexes then had their biological and photophysical properties assessed, with promising results.

3) <sup>64</sup>Cu-BODIPY complex – synthesis of a mitochondria specific fluorescent PET imaging agent:

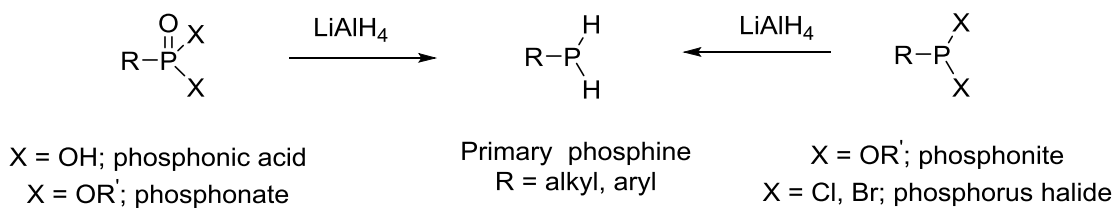
There have been previous reports of non-fluorescent phosphonium salt chelators of <sup>64</sup>Cu that are interesting in PET applications because they are selective for mitochondria. The nature of the mitochondrial membrane means that it possesses an electric potential,  $\Delta\psi_m$ ; it has been shown that this potential is higher in cancer cells than in healthy cells. This enhanced gradient in cancer cells offers an opportunity to target tumours. <sup>64</sup>Cu is an isotope used in radiotracing agents, therefore, phosphonium-<sup>64</sup>Cu compounds have been developed as radiotracer that can selectively accumulate in the mitochondria of cancerous cells. In this section, the development of a BODIPY-phosphonium-<sup>64</sup>Cu complex which could take advantage of the selective absorption of a phosphonium ion is described. This complex will allow for both PET and fluorescent cell imaging studies to be undertaken.

The features that make these molecules significant are discussed in the following sections.

### 1.3 Primary phosphines

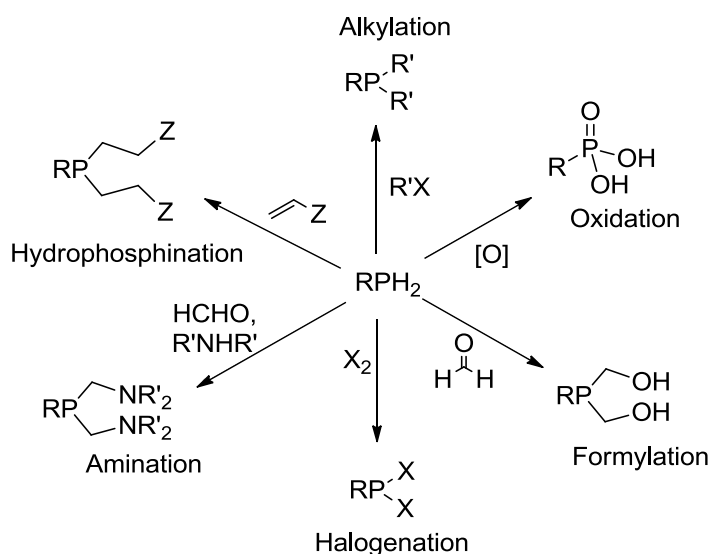
Primary phosphines are the keystone of the development of the proposed compounds.

Primary phosphines<sup>7-24</sup> have two hydrogens bonded to a phosphorus that is connected to an alkyl or aryl group. They are known for being unstable in air, as a number of examples decompose into an often random mixture of oxides and acids, due to the high enthalpy of formation of the P=O bond (bond dissociation energy of 128 to 139 kcal/mol). Some of these compounds can spontaneously ignite in the presence of air due to this high reactivity, making their handling a complicated procedure.<sup>25, 26</sup> Common protocols for the synthesis of primary phosphines include the reduction of dichloroalkyl/arylphosphines, phosphonic acid, phosphonate or their derivatives. The usual reducing reagent used is lithium aluminium hydride (Figure 1.1).<sup>8, 27</sup> The reduction of phosphonates often proceeds in a quantitative fashion using an equivalent of chlorotrimethylsilane as a co-reductant.



**Figure 1.1** Synthesis of primary phosphines starting from different phosphorus-containing compounds. The reducing agent is LiAlH<sub>4</sub> in this approach.

Despite their air-sensitivity, primary phosphines are flexible starting materials due to the possibility of functionalising the two phosphorus-hydrogen bonds. However, the low air stability of many such compounds has made them an under-utilised class of ligand. This kind of useful functional group can be employed in many different reactions including hydrophosphination additions to unsaturated hydrocarbon chains. They can also be substituted with acid halides and undergo alkylation and amination. These different reactions opened the door to new compounds, which have been shown to have applications in numerous fields, including medicinal chemistry,<sup>15,28,29</sup> polymer science,<sup>30</sup> carbohydrate modification,<sup>31</sup> macrocyclic research<sup>32</sup> and catalysis.<sup>33</sup>



**Figure 1.2** Functionalisation of primary phosphines showing a broad variety of reactions that primary phosphines can undergo.

Due to their reactive nature towards oxygen from the atmosphere, it is important to take into account the air stability of compounds containing this functional group.



### 1.3.1 Predicting the air-stability of primary phosphines

There are however a small number of air-stable primary phosphines which make synthetic preparations and purifications more time efficient and simpler technically, especially regarding a large scale synthesis. From the air-stable primary phosphines reported (Figure 1.3), there appears to be a range of structural types, including supermesitylphosphine **1**,<sup>9,10</sup> triptycylphosphine **2**,<sup>11</sup> (*R*)-MOPH<sub>2</sub> **3**,<sup>34</sup> diprimary **4**,<sup>14</sup> thioether **5**<sup>8</sup> and the ferrocene derivative **6**.<sup>12</sup> The first two compounds, **1-2**, are protected from oxidation due to steric encumbrance provided by the bulky substituents. However, the same argument cannot be used to rationalise the air-stability of the remaining compounds, **3-6**.

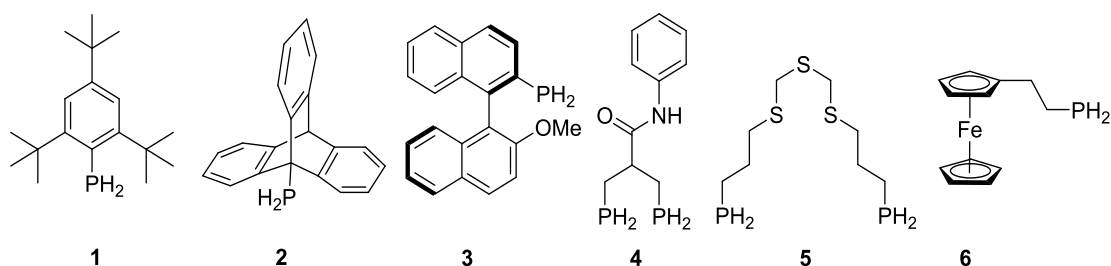


Figure 1.3 Air-stable primary phosphines.<sup>34</sup>

On the other hand, Figure 1.4 provides examples of primary phosphines that have proved to be unstable to air oxidation, which can lead them to spontaneously ignite if not handled under an inert atmosphere.

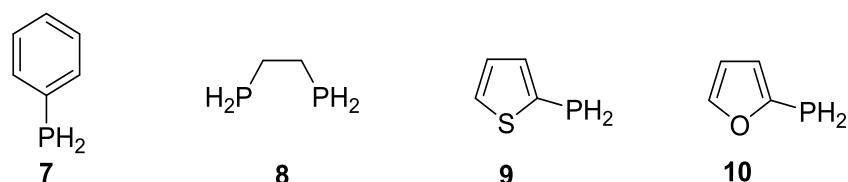


Figure 1.4 Air-sensitive primary phosphines.<sup>7</sup>

To understand the air-stability of the primary phosphines, where steric hindrance cannot be the protecting factor, the electronic nature of the molecule must be taken into account. The mechanism for the air-oxidation of phosphines has not yet been fully elucidated. However, it has been demonstrated that the generation of the corresponding radical cation of a given phosphine by photolysis<sup>35</sup> or radiolysis<sup>36</sup> led to its oxidation *via* the radical pathway shown below (Figure 1.5), which was confirmed spectroscopically.

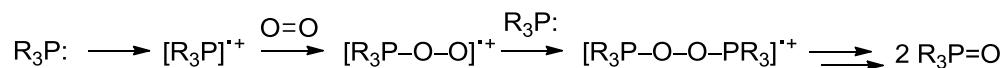


Figure 1.5 Postulated steps in the photolytic/radiolytic oxidation of phosphines.<sup>35, 36</sup>

Our research group therefore modelled the neutral phosphine and its radical cation in a series of Density Functional Theory (DFT) calculations using the B3LYP function with a 6-31G\* basis set, in an attempt to explain the observed stability/sensitivity of the different phosphines to aerobic oxidation. It was possible to observe a trend involving the highest occupied molecular orbital (HOMO), which corresponded to the experimental findings.

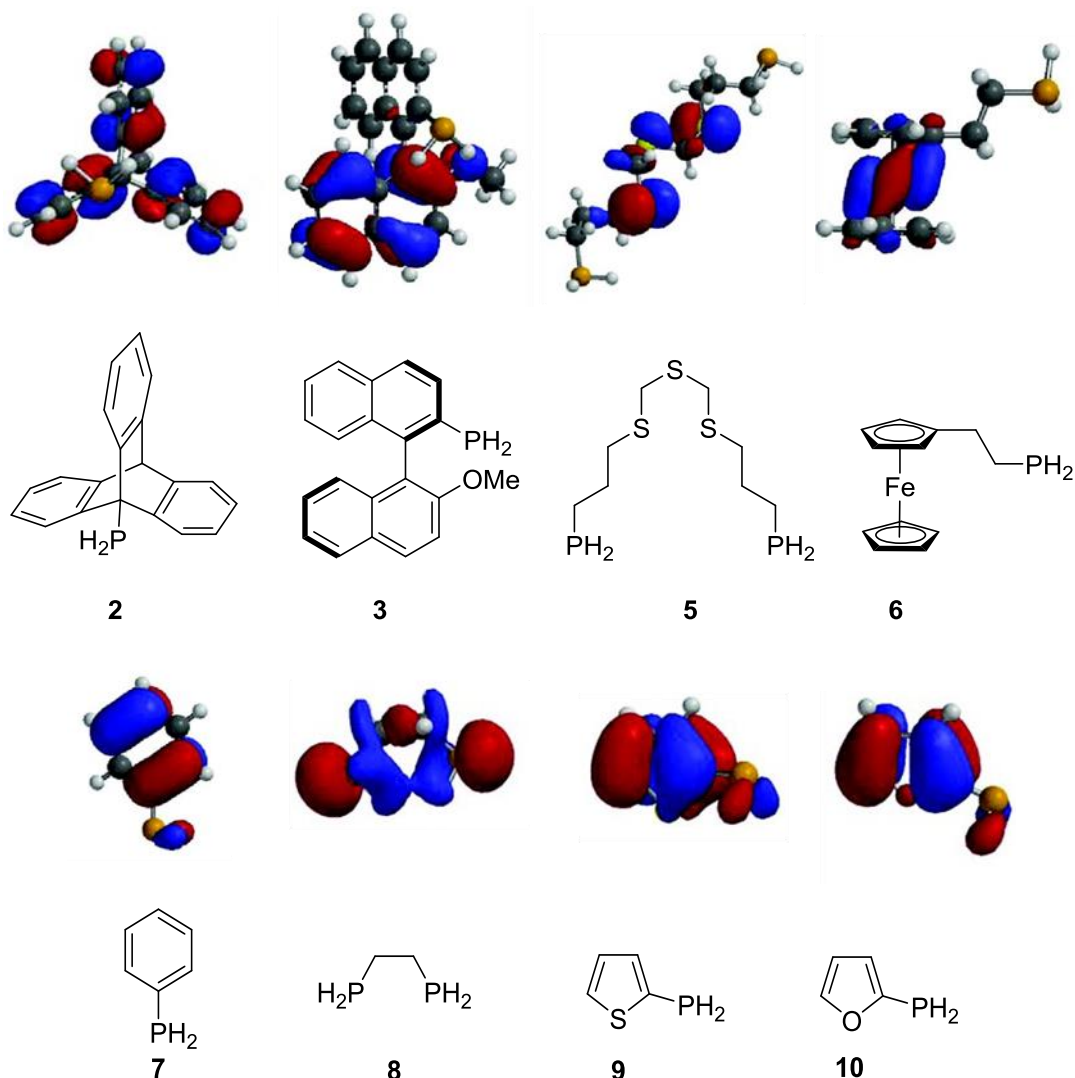


Figure 1.6 HOMO distributions of air-stable primary phosphines (top) and air-sensitive primary phosphines (bottom), obtained from B3LYP/6-31G\* DFT calculations.<sup>37</sup> Note that the phosphine does not participate in the HOMO of the air-stable compounds.

Air-stable primary phosphines with extended conjugation have a HOMO with no phosphorus character, whereas the primary phosphines shown to be sensitive to air oxidation demonstrate phosphorus character in the HOMO (Figure 1.6).<sup>37</sup> However, this trend *does not* predict the stability of triphenylphosphine since its HOMO is located on the phosphorus atom. Therefore, the location of the HOMO with respect to phosphorus is unlikely to be the causative factor of air-stability (unless the mechanism of oxidation of primary and tertiary phosphorus is due to different mechanisms). Increasing  $\pi$ -conjugation in the different compounds corresponded with increased stability towards oxidation, also producing higher energy HOMO orbitals (as expected). This indicates that a radical mechanism is likely to be involved. A radical cation generated from lower energy orbital would be more reactive than one generated from a compound with high  $\pi$ -conjugation. The radical cation Singly Occupied Molecular Orbital (SOMO) energies were therefore also calculated for each primary phosphine. The SOMO energies of the primary phosphines showed that those that are resistant towards air oxidation have a SOMO energy above an apparent threshold of  $-10$  eV, as depicted in Figure 1.7.<sup>37</sup> This infers that a radical cation produced from a more stable HOMO is reactive enough to combine with oxygen from the atmosphere and generate a peroxy radical, which ultimately results in irreversibly oxidation to the phosphine oxide.<sup>37</sup> This DFT model is a useful predictive tool which allows for new primary phosphines that may be air-stable to be modelled before synthesising them in the laboratory. Figure 1.7 contains examples of a wide variety of primary phosphines. The compounds above a SOMO energy of  $-10$  eV, represented by a red line in the figure below, are air-stable whereas those below this energy are unstable in the presence of air. Compounds **1** and **2** are stable due to the steric hindrance provoked by the structures in which the phosphine function is placed. However, compounds **4-6** do not contain bulky groups around their phosphorus atoms. In these cases, the air-stability is attributed to their electronic properties, since the three of them have SOMO values that are above the stability threshold of  $-10$  eV. Phosphines **7-10** do not contain any bulky groups around their phosphine functional groups and their SOMO energy is below the stability threshold. Therefore, it is no surprise that they are sensitive to air-oxidation.

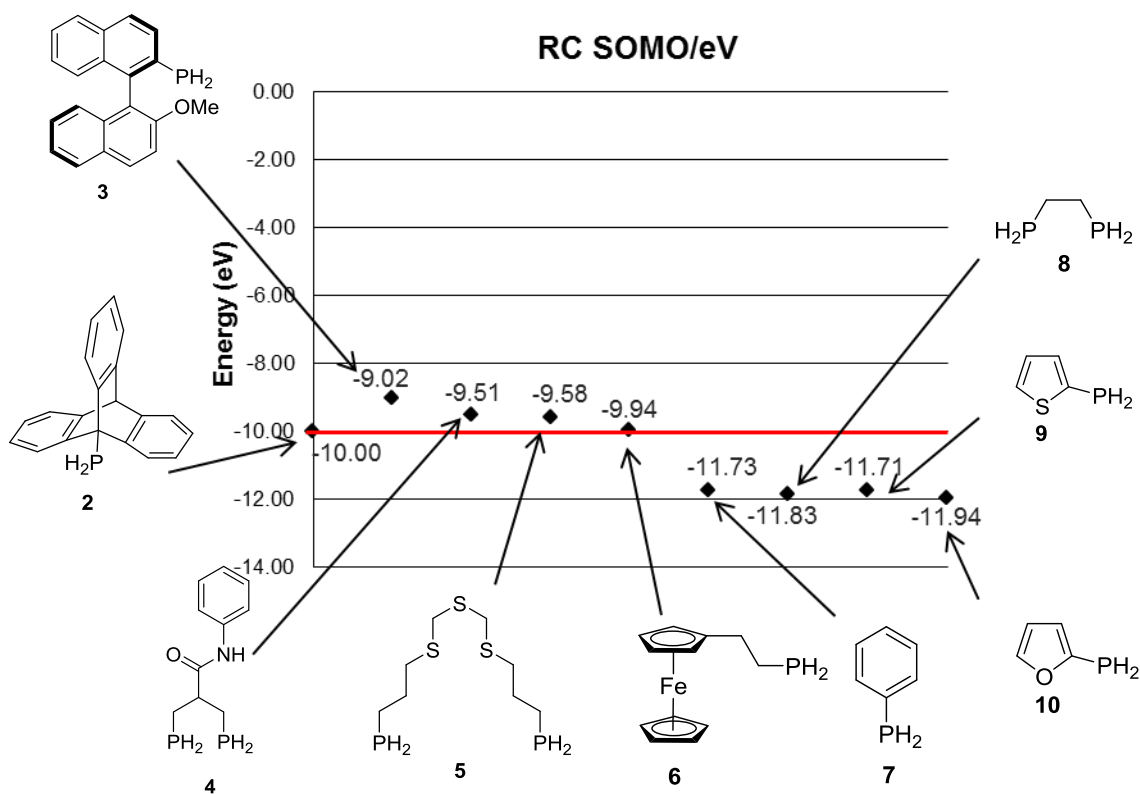
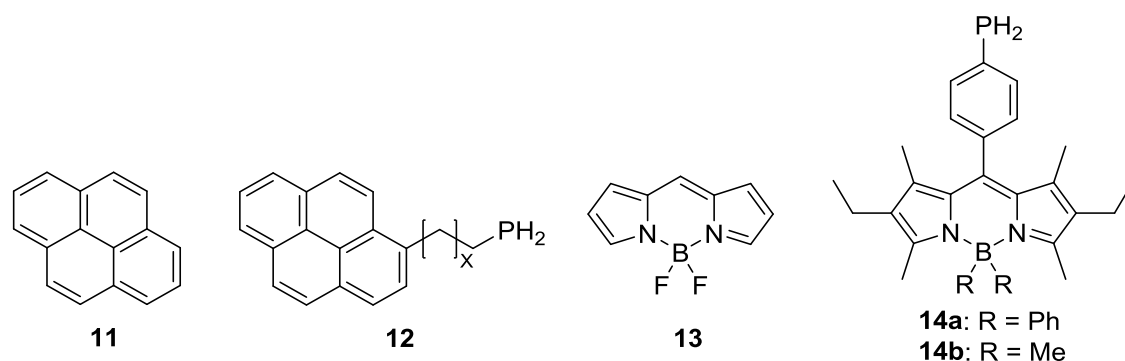


Figure 1.7 Plot of the radical cation SOMO energies for primary phosphines 2-10.<sup>37</sup>

A part of the research presented in this thesis is based on an air-stable primary phosphine that has as backbone pyrene **11**, which is separated from the phosphine by an alkyl chain. One important feature of the phosphines stabilised electronically is that they either contain heteroatoms, such as sulfur, oxygen or nitrogen, or have a direct aryl bond to phosphorus. This research group has previously synthesised stable fluorescent primary phosphines based on the known fluorophore 4,4-difluoro-4-bora-3a,4a-diaza-s-indacene **13** (BODIPY). The high conjugation of the BODIPY **13** core was key to the stability of the resulting phosphines **14a** and **14b** and this generated the first fluorescent air-stable primary phosphines.<sup>38</sup> The air-stability of these compounds is provided by the  $\pi$ -conjugation of the system. Nevertheless, this conjugation also confers a useful property, which has been subsequently exploited in medical imaging.<sup>39</sup>



**Figure 1.8** Fluorophores pyrene **11** and BODIPY **13**; phosphines **14a** and **14b** developed using **13** as fluorophore and the theoretical air-stable phosphine **12** using pyrene as core.

Both cores, pyrene **11** and BODIPY **13**, have a useful feature in common: fluorescence. Fluorescence has a special place in the life sciences, as many non-destructive techniques take advantage of this phenomenon in order to track or analyse biological molecules. This is possible because there are relatively few cellular components that are naturally fluorescent, which makes “non-labelled” cells invisible to fluorescence microscopy. By “labelling” a cell or a protein with a fluorescent compound which has a known emission wavelength, it is possible to follow it within the biological system. Fluorescent compounds which are used in this way are known as fluorescent probes.<sup>40</sup>

One of the main objectives of our research was to functionalise pyrene with a phosphino group to answer two related questions: does the conjugation provide the phosphine air-stability? Does the presence of the pyrene, a known DNA intercalator, allow for the development of new medicinal agents?

#### 1.4 Origins of luminescence

Pyrene is fluorescent which may be a feature we can exploit in medicinal imaging; therefore, a brief introduction to it will be discussed next.

Luminescence is the emission of light from an electronically excited species and it can occur in two different forms, fluorescence and phosphorescence. Which type of emission is given off by any given molecule is determined by the nature of its excited state. These processes are usually illustrated by the Jablonski diagram (Figure 1.9). The Jablonski diagram describes the excitation of an electron from the ground state ( $S_0$ ) to the first excitation state ( $S_1$ ) due to the absorption of light ( $h\nu_A$ ), followed by the emission of energy in the form of fluorescence ( $h\nu_F$ ) back to  $S_0$  ( $S_1-S_0$ ). Other processes can take place such as the excitation from  $S_0$  to the second excited state ( $S_2$ ). Following this, an internal

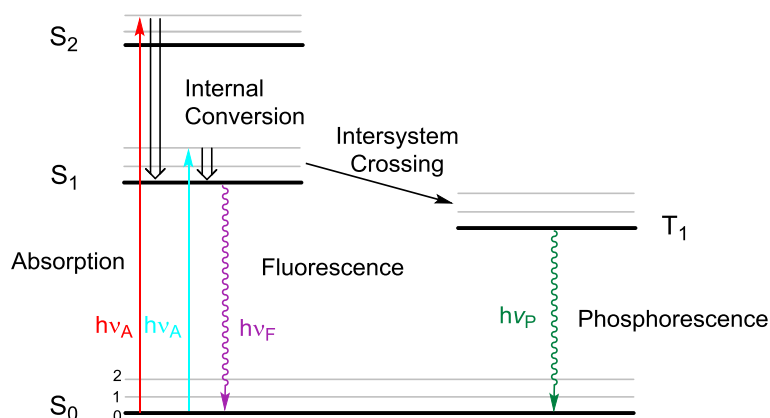
conversion allows the molecule to relax to  $S_1$ . At each of these electronic levels the fluorophores can exist in different vibrational energy levels (0, 1, 2, etc.). Electrons in the  $S_1$  state can also undergo intersystem crossing to the first triplet state  $T_1$ . Emission from  $T_1$  is called phosphorescence ( $h\nu_P$ ) and is usually found at longer wavelengths than fluorescence. An interesting feature of emission is that its energy and its wavelength are extremely related, as Equation 1 shows.<sup>40</sup>  $E$  is the energy of emission,  $h$  is the Planck's constant,  $c$  is the speed of light and  $\lambda$  is the wavelength of the emission.

$$E = \frac{hc}{\lambda}$$

Equation 1

The conversion between  $S_1$  to  $T_1$  is irreversible, since  $T_1$  to  $S_1$  is a spin forbidden transition. Molecules containing heavy atoms like bromine and iodine are more prone to undergo  $S_1$ - $T_1$  transitions. Heavy atoms facilitate intersystem crossing enhancing the phosphorescence quantum yields of the molecules which contain them. A phosphorescent material does not immediately re-emit the radiation it absorbs. The slower time scales of phosphorescence emission are associated with forbidden energy state transitions in quantum mechanics. As these transitions occur extremely slowly in certain materials, absorbed radiation is emitted at a lower intensity for up to several hours after the original excitation. This phenomenon occurs when an electron in  $S_1$  migrates to a separate excited state known as the triplet excited state ( $T_1$ ) by intercrossing system.<sup>40</sup>

The photophysical phenomenon of interest for the purposes of this project is fluorescence, which is the emission of a photon from  $S_1$ - $S_0$ .



**Figure 1.9 Jablonski diagram; internal conversion depicted by thick arrows, excitation by solid arrows, and radiative processes by wavy arrows.**

The emission spectrum of a fluorescent molecule is usually found at higher wavelength (lower energy) than the absorption spectrum due to internal conversions that take place when the excitation leads to an energy level higher than the lowest vibrational level of  $S_1$ . The Stokes shift ( $\Delta\nu_{st}$ ) is the energy gap between the maximum of the first absorption band and the maximum of the fluorescence spectrum.<sup>41</sup> The quantum yield ( $\Phi_F$ ) and lifetime ( $\tau$ ) of fluorescent compounds are important features found in this type of molecule. The value given by  $\Phi_F$  is a measure of the efficiency of a fluorescent molecule comparing the total number of photons emitted to the total number of photons absorbed. The nature of this comparison allows a maximum  $\Phi_F$  value of 1. In terms of an instrument, a  $\Phi_F$  value of 1 would mean that each absorbed photon was emitted back without the occurrence of any side processes, such as heat emission, phosphorescence or increasing the kinetic energy of the sample. Therefore, efficiency would be equal to 1 in a perfect fluorescence system.<sup>41</sup> The fluorescence procedure can be dramatically diminished under certain circumstances, a phenomenon called fluorescence quenching and there are several reasons why it may occur, which are discussed in the next section.

In biological systems, it is possible to find molecules and proteins that are naturally fluorescent. This phenomenon is called autofluorescence or intrinsic fluorescence. Nicotinamide adenine dinucleotide (NAD),<sup>42</sup> tryptophan,<sup>43</sup> chlorophyll<sup>44</sup> and certain proteins are known for being fluorescent.<sup>45</sup>

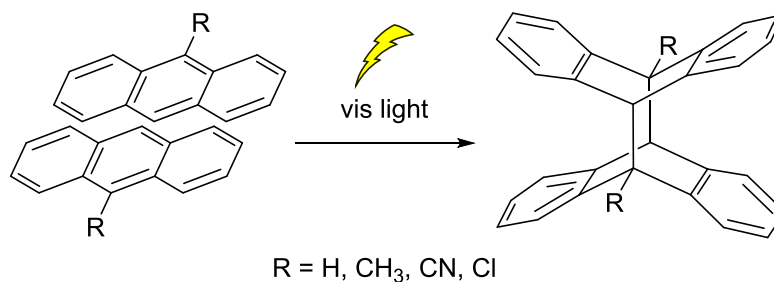
When developing fluorescence compounds with biological activity, it is important to keep in mind the effects that different substituents can exert on fluorescence, such as fluorescence quenching, which is discussed in the next section.

#### **1.4.1 Fluorescence quenching**

Dioxygen has shown the capacity to provoke fluorescence quenching by colliding with the fluorophore – this interaction reduces the emission of photons from  $S_1$ . This has been corroborated by performing fluorescence and absorbance measurements on solutions equilibrated with pressures of oxygen up to 100 atm.<sup>46</sup> In order to avoid this undesirable effect, it is recommended to purge solvents with an inert gas prior to use.

Non-radiative processes can be augmented when increasing the temperature of the sample to be measured – this effect is known as thermal agitation. The formation of excimers<sup>47</sup>,<sup>48</sup> (*i.e.* dimers in the excited state formed by the collision of an excited molecule and an identical unexcited molecule) and exciplexes (*i.e.* excited state complexes formed by

collision of an excited molecule with an unlike unexcited molecule) can also lower fluorescence – it is diffusion controlled and therefore more pronounced in more highly concentrated solutions. This is especially common in concentrated solutions since the possibility of an excited molecule interacting with a molecule in its ground state is statistically higher.<sup>48</sup>



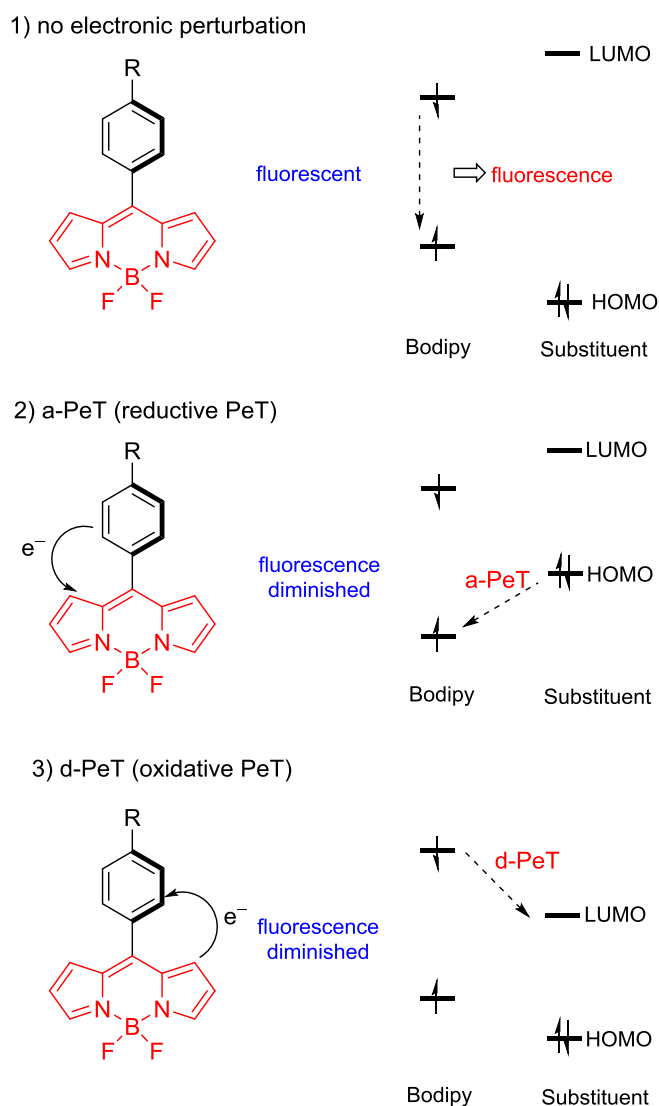
**Figure 1.10 Structures of the anthracene sandwich dimer, and its photodimer 9-substituted anthracenes form photodimers and sandwich dimers in the *trans* conformation.<sup>48</sup>**

Intersystem crossing occurs between isoenergetic vibrational levels belonging to electronic states of different multiplicities *e.g.*  $S_1-T_n$  as shown in Figure 1.9. This process is spin forbidden but occurs due to spin orbit coupling (coupling between the orbital magnetic moment and the spin magnetic moment). Heavy atoms or triplet oxygen molecules promote intersystem crossing and therefore a decrease in fluorescence is often observed.<sup>40, 41</sup>

Another mechanism by which fluorescence quenching can occur is known as Photoinduced Electron Transfer (PeT). This mechanism is caused by the presence of an electron donor or electron acceptor in the vicinity of the fluorophore when the latter has been excited to  $S_1$ . This step is crucial since it allows for the formation of a donor-electron complex ( $D^+A^-$ ) that can return to its ground state by means of a process in which no photons are emitted. Lastly, the added electron in the acceptor can return to the electron donor. The excited fluorophore can act either as the electron donor or the acceptor; this depends on the oxidation and reduction potential of the ground and excited states.<sup>40</sup> The fluorescence of molecules can be modified by the transfer of electrons between nonplanar parts of the molecule.<sup>49</sup> Nagano *et al.* used orbital energy levels calculations and experimental electrochemical data in order to explain quantum yields. They started their investigations with fluorescein<sup>50, 51</sup> systems, and then expanded it in order to also explain BODIPY systems.<sup>52</sup> The oxidation potentials of some substituents in relation to the excited-state of their BODIPY core can make them act as electron donors or acceptors



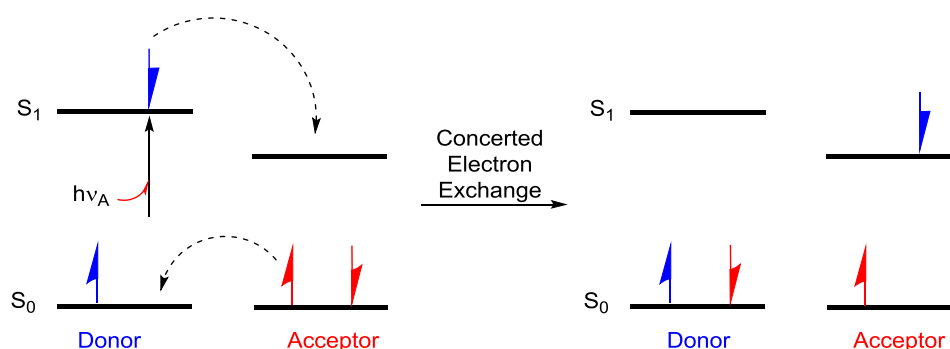
producing Photoinduced Electron Transfer (PeT). This process diminishes fluorescence when the fluorescent group in its excited-state is reduced. In this case, the fluorescent group is an acceptor of electrons, and can thus be called reductive-PeT or a-PeT (“a” for acceptor). On the other hand, if the fluorescent group donates electrons to the substituent LUMO, an oxidative process takes place (oxidative-PeT or d-PeT, “d” for donor).



**Figure 1.11 Molecular orbital schematic for Photoinduced Electron Transfer (PeT). BODIPY, a known fluorophore, is used to exemplify the phenomenon.<sup>40</sup>**

Fluorescence quenching phenomena can be caused by the Dexter electron transfer process. This is a fluorescence quenching mechanism provoked by an excited electron that is transferred from a donor to an acceptor via a non-radiative path.<sup>53, 54</sup> This type of effect requires a wave function overlap between the donor and acceptor, which usually occurs

at short distances. In this process an electron in  $S_1$  is transferred from the donor moiety to the acceptor moiety. In a Dexter electron transfer with an efficiency of 100%, there would be no trace of emission from the donor. Relative short separations between chromophores have shown efficient energy transfer via the Dexter mechanism when the chromophores are orthogonally aligned to avoid an interaction between their electronic systems which would lead them to act as one single fluorophore.<sup>55, 56</sup>



**Figure 1.12 Schematic for Dexter electron transfer process.**

The groups that provide fluorescence in a molecule are known as fluorophores and have different chemical structures. The next section provides a description of the fluorophores used in this research.

## 1.5 Fluorophores

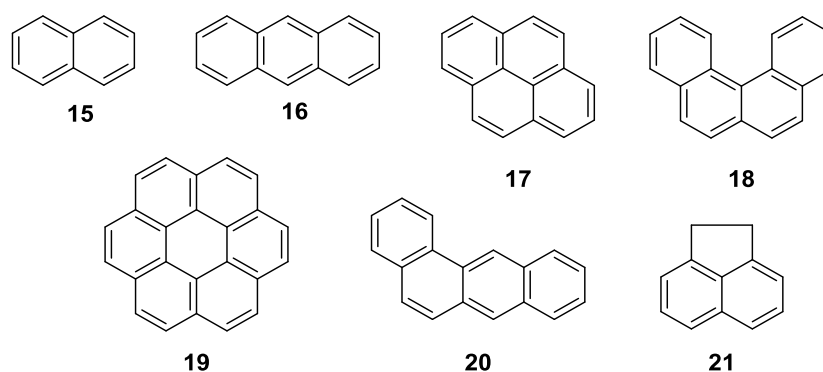
This section will provide an introduction to the specific fluorophore compounds that were used during the development of this project.

### 1.5.1 Polycyclic Aromatic Hydrocarbons (PAH)

Two of the three aforementioned research projects involved the synthesis of compounds containing three important PAHs, naphthalene **15**, anthracene **16** and pyrene **17**.

PAHs are composed of multiple aromatic rings, which means that they have the following characteristics: 1) a delocalized conjugated  $\pi$  system (usually an alternate arrangement of single and double bonds); 2) a coplanar structure, with all the contributing atoms in the same plane; 3) the contributing atoms are arranged in one or more rings; 4) a number of  $\pi$ -delocalized electrons that is even, but not a multiple of 4. That is,  $4n + 2$   $\pi$ -electrons, where  $n = 0, 1, 2, 3$ , and so on, this is known as Hückel's rule.<sup>57</sup> Interestingly, this rule loses its validity for PAH formed by more than 3 fused aromatic rings in a cyclic arrangement. Examples of this behaviour are pyrene **17**, since it contains 16 conjugated

electrons distributed in 8 different double bonds, and coronene **19**, with 24 conjugated electrons in 12 double bonds. Although both PAHs are aromatic, they fail to fulfil the  $4n + 2$  rule;<sup>58</sup> their degree of aromaticity is given by independent rings within the PAH.<sup>59</sup> This kind of compound can be formed during human productive activities via the incomplete combustion of organic materials or other organic substances such as tobacco and plants.<sup>60</sup> PAHs can be also found in fossil fuels such as oil and coal.<sup>61</sup> Their presence in the environment is significant since previous research has shown that they can be related to the development of chemical carcinogenesis due to environmental contaminants.<sup>62</sup>

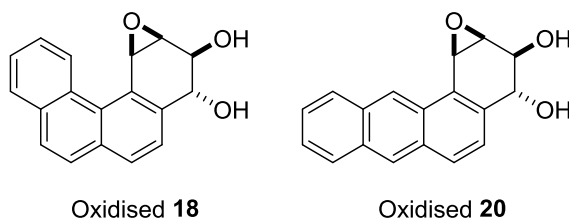


**Figure 1.13** Examples of PAHs: naphthalene **15**, anthracene **16**, pyrene **17**, benzo(*c*)phenanthrene **18**, coronene **19**, benz(*a*)anthracene **20** and acenaphthene **21**.

### 1.5.1.1 PAHs and DNA

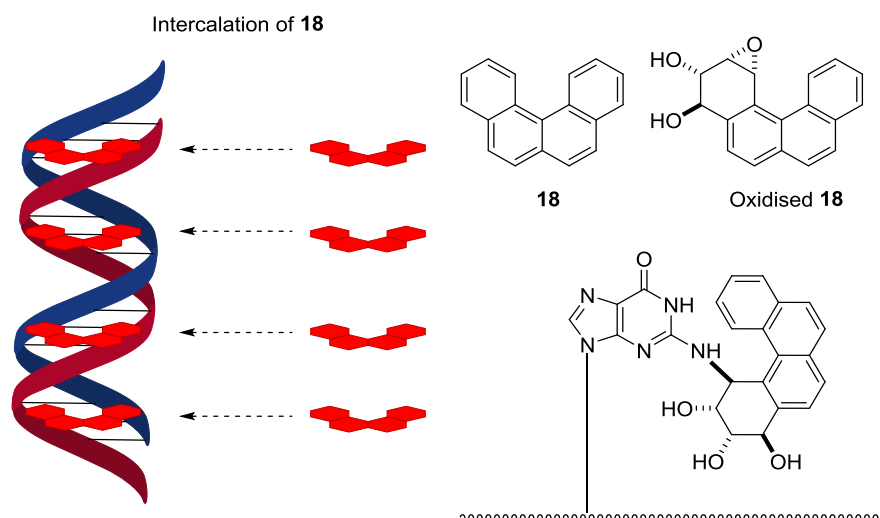
The different structures of PAHs influence the biological effect that they can exert on DNA. This structure-effect relationship can determine whether or not a PAH can be carcinogenic.<sup>63, 64</sup> Interactions between PAHs and DNA can lead to different outcomes since some carcinogenic PAHs are genotoxic and produce DNA lesions that induce cancer; on the other hand, other types are not genotoxic but can affect cancer processes.<sup>63, 64</sup> The compounds that have been shown to positively start carcinogenic processes require activation. This is caused by oxidations catalysed by the P450 enzymes (CYPs) that ultimately produces vicinal diol-epoxides. These compounds are electrophiles capable of binding to DNA, while some of the diol epoxide stereoisomers of PAHs are found to be ultimate carcinogens.<sup>65</sup> These carcinogens are usually PAHs that contain four or more aromatic rings and a “bay region” or a structural pocket where the oxidation will take

place. Mutagenic metabolites of PAHs include diol epoxides, quinones, and radical PAH cations.<sup>65</sup>



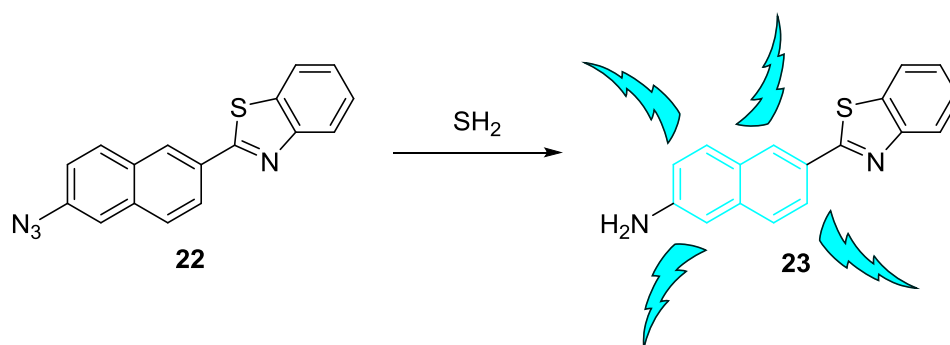
**Figure 1.14** Carcinogenic metabolites of **18** and **20**.

The metabolites produced by CYP have the capacity to bind to DNA in certain sites, creating bulky complexes known as DNA adducts. When the formed adducts are stable, they might provoke DNA replication errors that can transform genes allowing for the production of cancer-causing oncogenes.<sup>63</sup> Another mechanism by which PAHs disrupt normal cell development is the dysregulation of DNA gap junctions, intercellular connections between different cells.<sup>66</sup> This affects intercellular communication with enzymes in charge of activating transcription factors involved in cell proliferation, producing an excessive replication of certain cells.<sup>67</sup> Benzo(c)phenanthrene **18** is an example of the mechanism by which PAHs intercalate with DNA forming DNA adducts. Intercalation is the insertion of molecules between the planar bases of DNA. Intercalation occurs when a molecule with the appropriate size and chemical features puts itself between base pairs of DNA. These molecules are mostly polycyclic, aromatic, and planar. Benzo(c)phenanthrene **18** is oxidized by the CYP enzymes creating a diol epoxide, which undergoes a nucleophilic attack by an exocyclic amino group of deoxyadenosine generating an adduct where the PAH is attached to the major groove edge of DNA.<sup>68</sup> Cosman *et al.*<sup>69</sup> identified that after the amino group of deoxyadenosine became covalently attached to oxidised form of **18**, the PAH intercalates to the helix without disrupting other base pairs. This phenomena is called intercalation. They observed a buckling of the intercalation cavity reflecting the selective overlap of the intercalated PAH **18**. They determined that in spite of the covalent bond formed, the major groove edge of deoxyadenosine can still intercalate into the helix without further disruption of the modified base pair.



**Figure 1.15** Left: Intercalation of oxidised **18** to DNA. Right: Benzo(c)phenanthrene **18**, its oxidised metabolite, and the adduct derived from trans-opening of this epoxide by the exocyclic 2-amino group of deoxyguanosine.

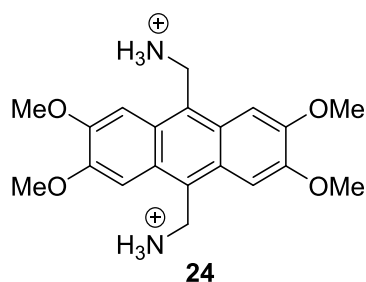
Naphthalene **15** has useful fluorescent features such as a very low self-quenching effect in solutions.<sup>70</sup> These features have a niche in fluorescent microscopy and its applications.<sup>71</sup> The dependence of the fluorescence intensity of naphthalene has been studied, demonstrating that it initially decreases with increasing concentrations. However, above a certain concentration, the fluorescence, surprisingly, remains constant.<sup>72</sup> The photophysical features of naphthalene, such as its fluorescence quantum yield ( $\Phi_F = 0.23$ ) and good photo- and chemo-stability, make it a significant candidate for the development of different fluorescent probes. This PAH has therefore been used in probes to determine the presence of toxic pollutants,<sup>73</sup> the concentration of endogenous compounds of physiological importance,<sup>74, 75</sup> protein tagging<sup>76</sup> and to identify metallic ions in living cells.<sup>77, 78</sup>



**Figure 1.16** Naphthalene-based probe for determining the presence of  $\text{H}_2\text{S}$ , signalling compound involved in different physiological processes in living cells<sup>79,80</sup>.  $\text{H}_2\text{S}$  reduces the azide group and the naphthalene recovers its fluorescence at 320 nm emitting a blue colour.<sup>75</sup>

Naphthalene-based **22** is a probe for developed by Mao *et al.*<sup>79, 80</sup> detecting the cellular presence of  $\text{SH}_2$  exhibiting a wide linear response concentration range (0–5  $\mu\text{M}$ ) with high selectivity. Compound **22** is not fluorescent due to the presence of an electron withdrawing group ( $\text{N}_3$ ), which disrupts the  $\pi$ -conjugation of naphthalene. When the naphthalene-azide **22** as is placed in a solution containing 10 equivalents of  $\text{SH}_2$  in water, the naphthalene derivative is turned into **23** increasing its fluorescence 67-fold after 60 min.

In the same fashion as other PAHs, anthracene is frequently used as a fluorophore for sensors for organic and inorganic analytes and as probes and markers in biological or supramolecular systems<sup>49</sup> due to its quantum yield ( $\Phi_F = 0.36$ ).<sup>81-83</sup> In addition, anthracene can insert itself between the planar bases of DNA (intercalation),<sup>84</sup> which forms the core base of anthracyclines<sup>85, 86</sup> and provides a possible fluorophore core for DNA probes.<sup>87</sup> The anthracene derivative **24** was developed by Ostaszewski *et al.*<sup>88</sup> using calf thymus DNA (ct-DNA) to measure the affinity of this compound for the macromolecule. Using UV-Vis spectroscopy, they determined the affinity of **24** for intercalating with DNA and they established that the complex **24**-ct-DNA is not fluorescent.

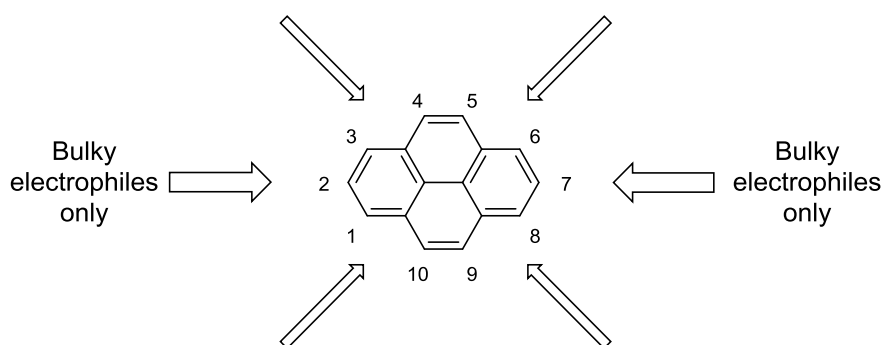


**Figure 1.17 Anthracene derivative 24 developed by Ostaszewski *et al.*<sup>88</sup> 24 is an efficient DNA intercalator agent.**

Pyrene **17** is a PAH that consists of four fused benzene rings, resulting in a flat aromatic system. This colourless solid is the smallest peri-fused PAH, which means that the rings that form its structure are fused through more than one face.

Pyrene **17** is a PAH that is widely exploited for its quantum yield ( $\Phi_F = 0.36$ ),<sup>83</sup> and for its capacity to take part in non-covalent interactions. For example, poly(pyrenebutyric acid) is used as a noncovalent stabilising unit for single-walled carbon nanotubes, preventing the formation of bundles and enabling dispersion in solvents.<sup>89</sup> This fluorophore possesses an outstandingly long fluorescence lifetime, and the vibronic band structure of its emission shows dependence on the polarity in which the solution takes place.<sup>90</sup> These photophysical features have led to the development of pyrene-based oligonucleotides that have been studied in DNA and RNA hybridization assays.<sup>91-94</sup>

While pyrene is now used extensively, its current applications seem to be limited. The main limitation is a lack of reliable procedures for the synthesis of pyrenes with various substitution patterns. Thus, while pyrene is easily appended to a system, the generation of structures with pyrenyl cores is much less straightforward when polysubstituted pyrenes are required.<sup>95</sup>

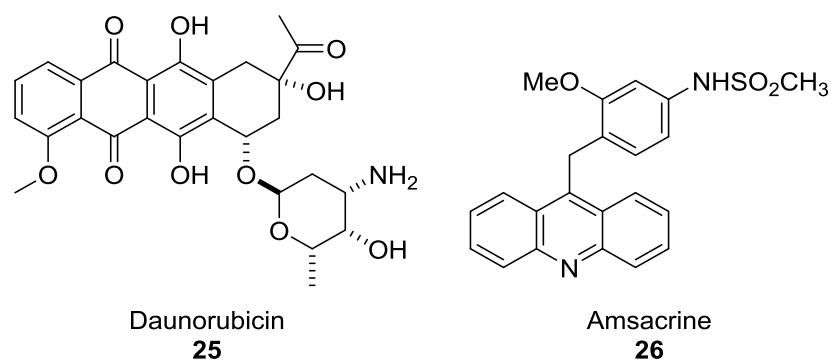


**Figure 1.18** Pyrene is activated towards electrophilic aromatic substitution at the 1, 3, 6 and 8 positions only. Some bulky electrophiles are forced by steric hindrance to react at the 2 and 7 positions.<sup>95</sup>

### 1.5.1.2 Drugs based on PAHs

Drugs have been developed around these PAH characteristics. Topoisomerase inhibitors are compounds used in chemotherapy<sup>96</sup> since they inhibit enzymes that restore the topological integrity of DNA. DNA replication and transcription processes can be stopped due to the presence of molecular torsion lesions. Furthermore, their presence gets intensified ahead of a replication process. In order to repair these types of topological problems caused by double helix spatial distribution, topoisomerases cut the phosphate backbone in DNA strands, which allows the structure to redistribute its spatial arrangement by untangling or unwinding. At the end of this process, the DNA backbone is resealed again. This process does not change the chemical structure or the connectivity of DNA.<sup>97</sup> Topoisomerase inhibitors block the activity of topoisomerases – in this group it is possible to find different structures that are based on the PAHs having a flat moiety made by fused rings. Their mechanism of action is thought to inhibit the step in which the DNA strands are resealed again which leads to single and double stranded breaks undermining the integrity of the genome. These lesions subsequently provoke apoptosis, or cell death.<sup>98</sup> Due to their mechanism of action, this type of compound has been shown to exhibit antibacterial activity.<sup>99</sup>





**Figure 1.19** Daunorubicin **25**<sup>85,86</sup> and Amsacrine **26**<sup>100</sup> are different topoisomerase inhibitors containing PAH moieties.

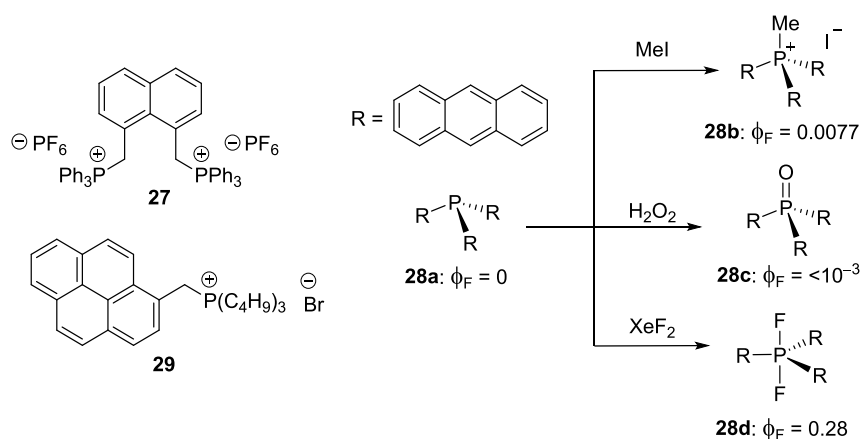
### 1.5.1.3 Phosphorus containing PAHs derivatives

As we have already seen, PAHs offer a versatile tool for developing compounds with useful properties. Their reactivity allows them to add phosphorus atoms to their structures, which adds extra features to the resulting molecules as will be shown in this section.

An interesting type of phosphorus-containing compound is the phosphonium cation. These molecules have the general chemical formula  $PR_4^+$ , they are common intermediate products in the Wittig reaction.<sup>101</sup> In addition, mitochondria is a good target for phosphonium ions with anticancer activity. The electron transport chain contained within the impermeable inner mitochondrial membrane provides a negative membrane potential (ca. 150 mV to 170 mV) in healthy cells.<sup>102</sup> In cancerous and ischaemic heart cells, mitochondrial dysfunction can significantly disrupt the membrane potential,<sup>103</sup> causing a tenfold increase in accumulation of membrane potential-dependent compounds.<sup>102</sup>

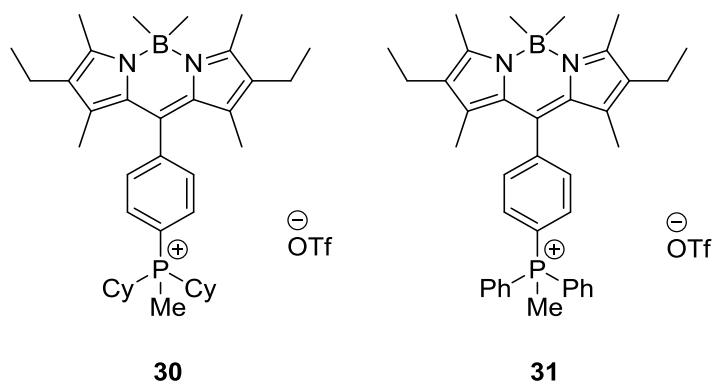
The phosphonium salt **27** is an innovative compound containing a naphthalene moiety, which was synthesised by the reaction of 1,8-dibromomethylnaphthalene with triphenylphosphine. The phosphonium salt **27** exhibits colour in the presence of fluoride ions. Yeo *et al.* attributed the high selectivity for fluoride to the acidity of the methylene protons and the small size of fluoride ions.<sup>104</sup> As discussed, anthracene is a well-known  $\pi$ -electron rich fluorophore whose photophysical properties are frequently used in the fluorescence sensors field.<sup>105</sup> Fascinating work carried out by Yamaguchi *et al.* compared the fluorescence of phosphine **28a** ( $\Phi_F = 0$ ), phosphonium ion **28b** ( $\Phi_F = 0.0077$ ), phosphonium oxide **28c** ( $\Phi_F = <10^{-3}$ ) and fluorophosphine **28d** ( $\Phi_F = 0.28$ ). Interestingly, the fluorophosphine **28d** exerted the highest fluorescence, which was comparable with the fluorescence of the parent anthracene.<sup>105</sup> Compound **29** is a pyrene based

phosphonium ion reported by Real *et al.*<sup>106</sup> whose photophysical measurements proved that the sample did not undergo dimers formation during excitation for measuring fluorescence. This was attributed to the charge of the phosphonium ion which should increase the repulsion forces between each independent molecule in the solution. The positively charged pyrene derivative **29** has the advantage of being water soluble, while avoiding affecting the pyrene fluorescence. The pyrene moiety gives it the capacity to intercalate with DNA. The positive charge and the butyl groups, contribute to a weak binding interaction in the external groove of the double helix. The importance of this compound resides on its capability to discriminate between a double helix and a strand due to its incomplete intercalation originated by the butyl chains.<sup>106</sup>



**Figure 1.20** Different examples of PAHs containing a phosphorus-based functional group. These compounds exert interesting photophysical properties.

PAHs are not the only fluorophores that have been used to take advantage of the high absorption of phosphonium ions in the mitochondria of abnormal cells. Our group has reported the development of BODIPY based agents for mitochondrial imaging. Compounds **30** and **31** were shown to be taken up in a mitochondrial membrane potential-dependent manner in both cancer and heart cells. The BODIPY-cyclohexane **30** derivative demonstrated a better absorption in mitochondria than its phenyl analogue **31**. DFT calculations showed that the positive charge in **30** is mainly held by the P-atom. Since the absorption is regulated by a difference of potentials, this might be the factor that differentiates the absorption of both compounds.<sup>107</sup>



**Figure 1.21** The synthesis of the BODIPY analogues **30** and **31** has shown the importance of the positive charge in relation to mitochondrial absorption.

Therefore, BODIPY is another significant fluorophore when developing compounds with biological activity.

The first project presented in this thesis will describe the synthesis of novel 1,2-azaphosphindoles, which are P-containing heterocycles that include the coupling of either naphthalene or anthracene moieties. The second project describes the synthesis of a pyrene-based tridentate ligand that was used to obtain complexes with possible biological applications. The final project presented here describes the obtaining of a fluorescent BODIPY-based ligand that was used to produce a fluorescent BODIPY-<sup>64</sup>Cu complex intended for use as a fluorescent imaging agent and a radiotracer. This entire project involved fluorophores, which is the reason behind the short overview of this topic.

### 1.5.2 BODIPY

The compound 4,4-difluoro-4-bora-3a,4a-diaza-*s*-indacene (abbreviated to *F*-BODIPY), is a versatile fluorophore. The characteristics that make this a useful fluorophore are: strong UV absorption profile, sharp fluorescence emission peak, high quantum yields, high thermal and photochemical stability, negligible triplet state formation and high solubility in different solvents.<sup>108-110</sup> Although BODIPY derivatives have been known since 1968,<sup>111</sup> BODIPY **13** has not been reported in the literature (Figure 1.22). This might be due to synthetic difficulties since none of the pyrrole carbons on the core are blocked towards an electrophilic attack. The synthesis of the symmetrical tetramethyl-substituted BODIPY **32** established a reference for other alkylated BODIPYs. It also suggests that alkylating the carbon positions on the pyrrole moiety increases the stability of this type of compound.<sup>112</sup> The unsymmetrically substituted systems **33** and **34** suggests

that there are minimal differences in the photophysical behaviour of the different BODIPY systems synthesised.<sup>113</sup>

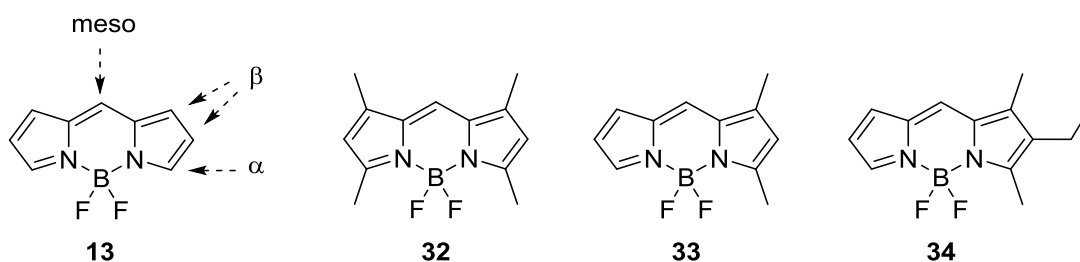


Figure 1.22 Different BODIPY systems and the difference in stability provoked by their alkyl substituents. BODIPY and its different positions.<sup>108</sup>

There are different synthetic routes to produce BODIPY molecules. One of these routes involves a pyrrole condensation; an electrophilic carbonyl forms a bridge between the two pyrrole units forming C–C bonds with this carbon atom in the newly formed *meso* position (Figure 1.22). The newly formed dipyrromethane **35** is then transformed to dipyrromethene **36** by the action of 2,3-dichloro-5,6-dicyano-1,4-benzoquinone (DDQ). The boron atom is then coupled to the molecule creating two N–B bonds, and a base is used, usually a sterically impeded amine, in order to remove a fluorine atom from the boron trifluoride molecule (Figure 1.23).

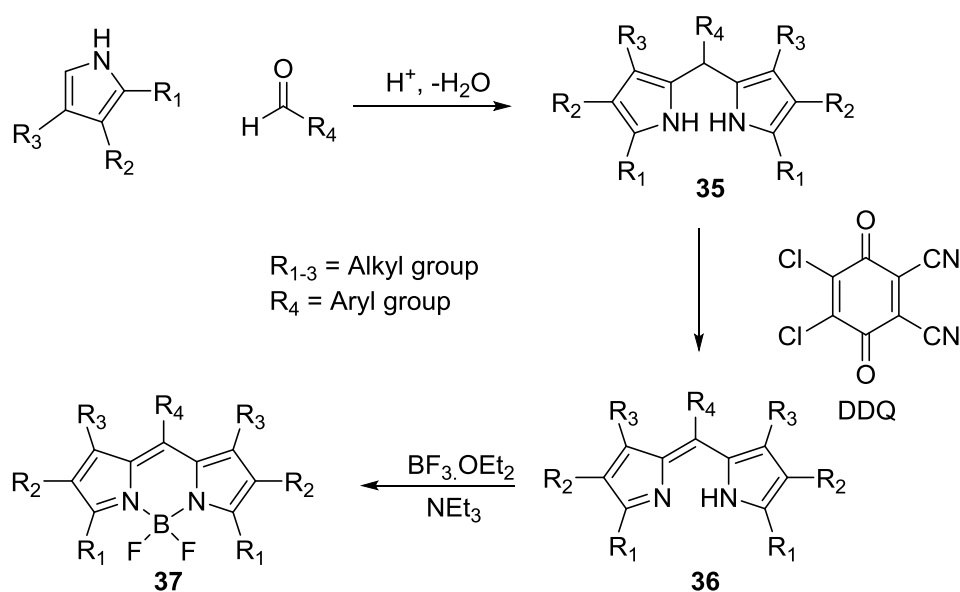
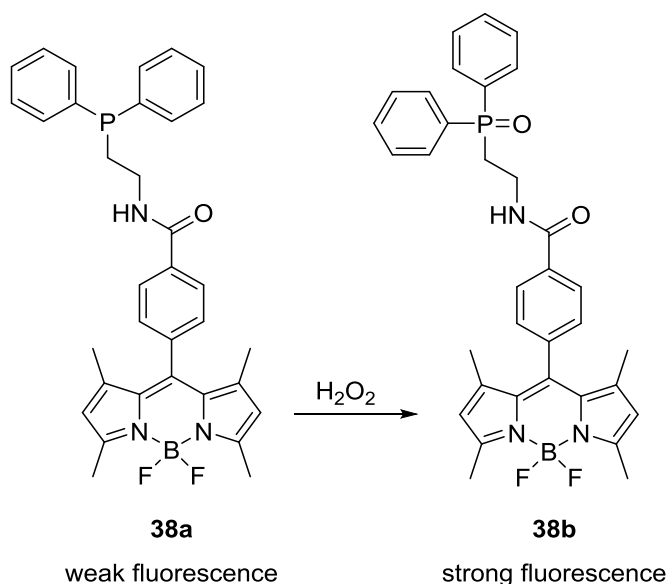


Figure 1.23 A synthetic approach for the production of BODIPY compounds.<sup>109</sup>

The positions adjacent to the nitrogen atom in the pyrrole moiety tend to be substituted to avoid the formation of any undesired side products as a result of the polymerisation of the molecule<sup>109</sup>. Typically, the “8” carbon is the position that is substituted with aryl and alkyl groups. These substitutions do not change the absorption and emission profiles of the molecule. However, in order to maintain high quantum yields, positions “1” and “7” are substituted to prevent the free rotation of the substituent in the *meso*, which would reduce the energy from the excited state *via* non-radiative molecular motion and decrease the quantum yield. The BODIPY core can be modified by a variety of chemical alterations allowing it to accept different groups in the *meso*  $\alpha$  and  $\beta$  positions. This gives chemical versatility to the core, producing several dyes for different applications, including sensors of particular redox active molecules,<sup>114-116</sup> pH probes,<sup>117</sup> metal-chelators<sup>118</sup> and biomolecule conjugating groups.<sup>119</sup>

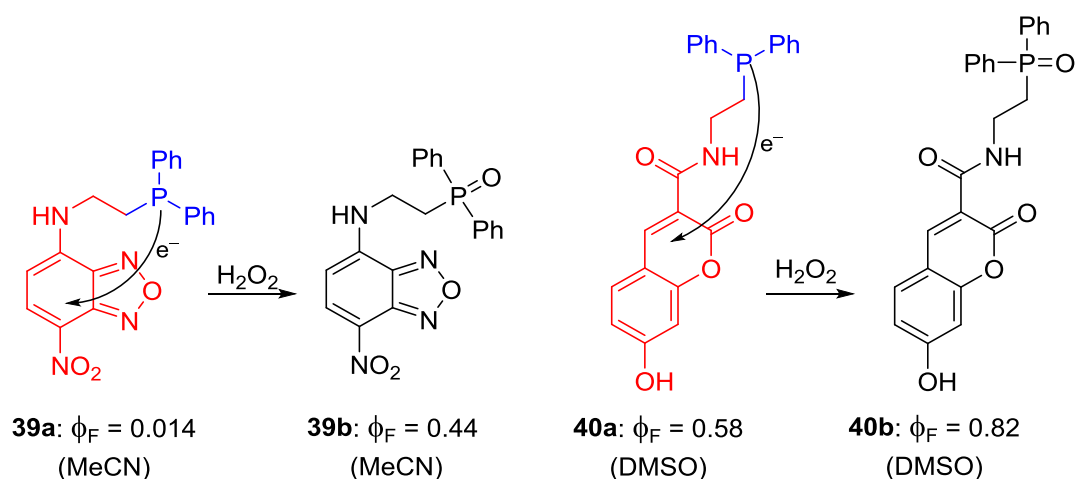
### 1.5.2.1 Phosphorus containing BODIPY derivatives

The number of BODIPY compounds containing phosphorus as a substituent is highly limited to date.<sup>120-123</sup> In 2009, Inoue *et al.* reported the first phosphorus-containing BODIPY compound (**38a**). The importance of this compound is related to its oxidation to the phosphine oxide **38b** in the presence of lipid hydroperoxides, which have been connected to arteriosclerosis, hyperlipidaemia, cancer, and aging.<sup>121</sup>



**Figure 1.24** Probe for lipid peroxides developed by Inoue. The oxidation of the phosphorus atom shows a higher fluorescence.<sup>121</sup>

Different chronic diseases and physiological processes (*i.g.* inflammation and hypoxia-reoxygenation) have proved to be governed by reactive oxygen species such as hydrogen peroxide. However, the mechanism of action involved in this type of process has not been fully elucidated yet.<sup>124</sup> Compound **39a**, in Figure 1.25, produced and increased fluorescence as its phosphine oxide form **39b**, whose existence is dependent on the concentration of hydrogen peroxide.<sup>121</sup> Reductive-PeT is thought to arise from the electron donating phosphine donor whose HOMO energy level is high enough for electron transfer to the excited BODIPY acceptor.<sup>121</sup> Similar mechanisms have been proposed for compounds **40a** and **40a**.<sup>124, 125</sup> As has been shown, fluorescent phosphines can experience PeT, a phenomenon that can be removed upon oxidation of the lone pairs of electrons to the phosphine oxide.



**Figure 1.25** Fluorescent probes for monitoring hydrogen peroxide using.<sup>124, 125</sup>

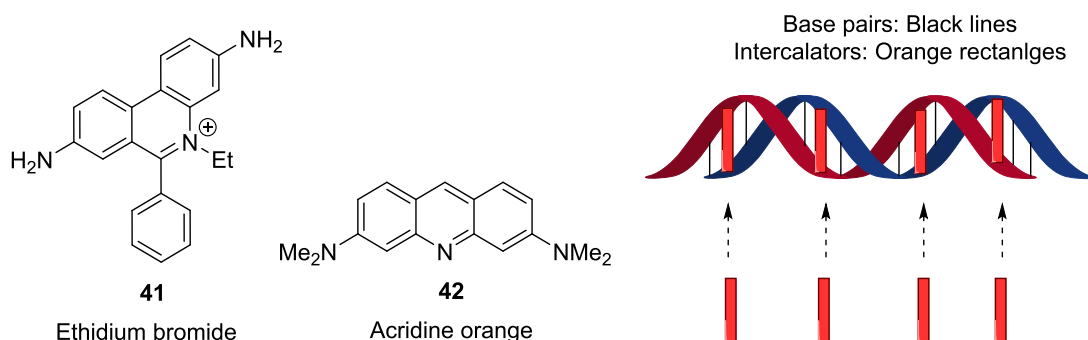
When the HOMO energy of the donor is high enough to provoke electron transfer to the acceptor, quantum yields will be diminished. Therefore, compounds with high quantum yields usually contain electron donors with low HOMO energy levels. Compound **40** is a good example of this, since the values of HOMO energies for methyldiphenylphosphine and methyldiphenylphosphine oxide HOMO were calculated to be  $-8.33$  and  $-9.95$  eV respectively proving that the donor with the lowest HOMO (the phosphine oxide) provides the highest fluorescence.<sup>124</sup>

The BODIPY dyes, mentioned above, were initially developed in order to replace fluorescein and rhodamine compounds. The structure of the specific BODIPY can change its emission wavelength, which is usually set in a range around 510 to 675 nm. Their quantum yields are also an important feature since they are high and tend to approach the

unit. They also possess an important insensitivity to solvent polarity and pH which make them good candidates for biological probes.<sup>40</sup> Therefore, the development of new BODIPY-based compounds offers a niche for the development of compounds with novel applications.

### 1.5.3 DNA probes

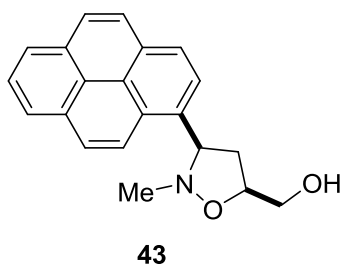
Fluorescence is used as a non-destructive way of tracking or analysing biological processes and molecules. It is possible to label proteins, nucleic acids, lipids or other endogenous compounds with external fluorophores. Usually the molecules of interest in the body are not fluorescent or their fluorescence is not adequate for the particular experiment required. DNA is a target for this kind of probe since unlabelled DNA has shown very weak intrinsic emission. This emission is too weak and out of the UV spectra for practical purposes. However, a wide variety of probes have been developed which have affinity for DNA and, after binding to it, display enhanced emission.<sup>126-128</sup> Ethidium bromide **41** is an intercalating agent, meaning that, since its geometry is flat, it can be inserted between the planar bases of DNA<sup>129</sup> as it has been explained in Section 1.5.1.1. This characteristic turns ethidium bromide **41** into a reagent for an assay known as “Ethidium bromide displacement”, which tests the intercalation of novel compounds with DNA by measuring the concentration of displaced ethidium bromide **41** from a DNA-**41** complex. This complex is placed in a solution with the competitor compound, whose DNA affinity is to be tested – spectrophotometry is used to determine the amount of **41** that was displaced by the tested compound.<sup>130</sup>



**Figure 1.26** Left: Different DNA probes and their excitation and emission wavelengths referred to the DNA-dye complex.<sup>40</sup> Right: Intercalating of DNA and fluorescent probes (orange rectangles).

Acridine orange **42** is a fluorescent dye that is highly nucleic acid-selective. Due to this characteristic, this compound is commonly used for cell cycle determination.<sup>131</sup> This compound permeates the cell and interacts with DNA by intercalation, and with RNA by

electrostatic attractions.<sup>132</sup> Rescifina *et al.*<sup>133</sup> developed an isoxazolidinyl-pyrene molecule with the expectation that the heteroatoms in the isoxazolidinyl moiety would interact electrostatically with the base pairs of DNA. In order to explore the capacity of this compound to bind to DNA, UV spectral analysis of a mixture of the isoxazolidinyl-pyrene **43** and ct-DNA was performed. The red shift of 13 nm for DNA<sup>134</sup> and the binding constant for **43** with ct-DNA ( $6 \times 10^3 \text{ M}^{-1}$ ) were consistent with intercalation. Additionally, preliminary docking studies of compound **43** to the DNA fragment d(CGCAATTGCG)<sub>2</sub> indicated that it preferentially intercalates into the DNA Adenosine-Thymine (AT) region where resulting complex appears to be further stabilized by the formation of a hydrogen bond between the hydroxyl group of the isoxazolidinyl moiety and an oxygen of the phosphate group.<sup>133</sup>



**Figure 1.27** Isoxazolidinyl-pyrene **43** developed by Rescifina *et al.*<sup>133</sup>

As discussed above, intercalation is an important mechanism for DNA-binding agents, such as DNA probes. Intercalators bind by inserting a planar aromatic chromophore between adjacent DNA base pairs causing little perturbation of the DNA structure.<sup>135</sup> This mechanism is usually followed by PAHs. Therefore, it would be possible to develop a PAH as intercalator which includes a second moiety that interacts with DNA in order to increase its efficiency. An example of this hypothetical second moiety is platinum. This metal is the main core of many anticancer treatments currently in use. The main example of this type of compounds is cisplatin “cis-[Pt(NH<sub>3</sub>)<sub>2</sub>Cl<sub>2</sub>]”.<sup>136</sup> Therefore, in this thesis, we present the development of a pyrene-platinum complex. Fluorescent compounds are not the only tool for studying living systems. Radiotracers can be also used for this particular purpose.



## 1.6 Radiotracers

A radioactive tracer is a chemical compound in which one or more atoms have been replaced by a radioisotope which can be monitored using different techniques such as Photon Emission Tomography (PET) and (Single-Photon Emission Tomography).

### 1.6.1 Positron Emission Tomography (PET)

Radiotracers are molecules in which one or more atoms are replaced by a radioactive isotope giving an agent that can be traced via biological systems. In Positron Emission Tomography (PET), certain isotopes with an excess of nuclear energy make them unstable. The excess energy can be released by the emission of a positively charged particle, called a positron, which travels a short distance (known as the positron range) around the tissue before it combines with an electron causing its annihilation.<sup>137</sup> After this process, the mass of both particles is converted into energy producing 511 keV  $\gamma$ -rays which are emitted simultaneously and follow opposite trajectories at  $180^\circ$  to each other. These  $\gamma$ -rays are detected by detectors located in the periphery of the location of the event, which collect and record information about the positron annihilation. Collecting data from a large number of annihilations provides information about the spatial distribution of radioactivity as a function of time that can be reconstructed into an image.<sup>137</sup> The energy of the positron is highly important, since the positron will travel further in the tissue and the spatial resolution will be diminished if the amount of energy is too high.

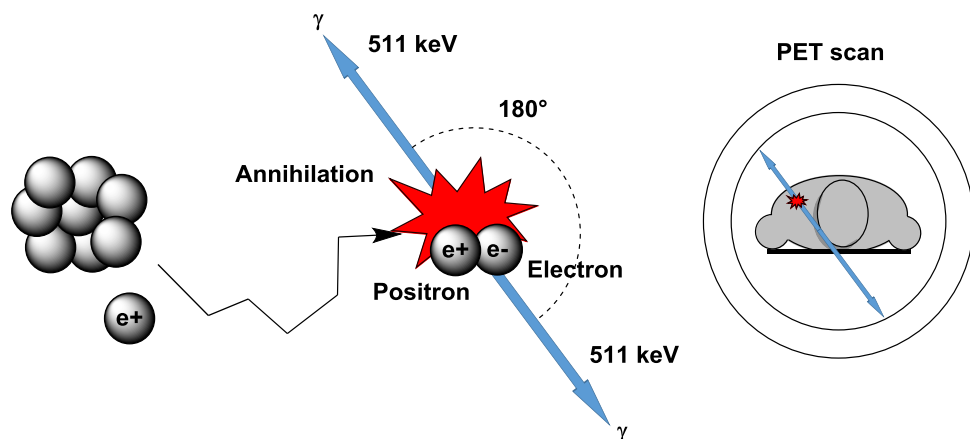


Figure 1.28 Representation of annihilation process used in PET.

Typically PET nuclides are incorporated into molecules with biological activity. Usually, the isotopes used as PET imaging agents have half-lives comparable to the half-time of the imaging process. The main mode of decay used in this technique is positron emission.

However, other decay modes can be accepted as long as their energies do not approach 511 keV. Table 1.1 shows the most commonly used nuclides.

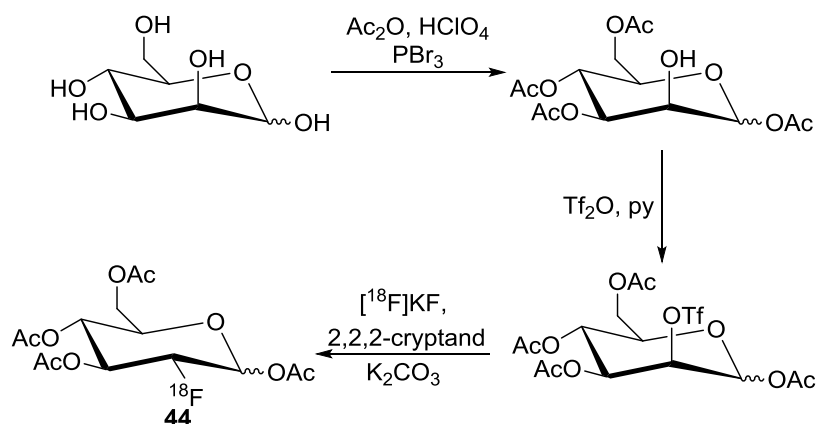
Nuclide	Half-live/min	Mode of Decay	$E_{\beta}$ (max) MeV
$^{11}\text{C}$	20	$\beta^+$ (99%)	0.97
$^{13}\text{N}$	10	$\beta^+$ (100%)	1.20
$^{15}\text{O}$	2	$\beta^+$ (100%)	1.74
$^{18}\text{F}$	110	$\beta^+$ (97%), EC (3%)	0.64
$^{64}\text{Cu}$	762	$\beta^+$ (19%), EC (41%), $\beta^-$ (40%)	0.66
$^{68}\text{Ga}$	68	$\beta^+$ (89%), EC (11%)	1.90
$^{124}\text{I}$	60,192	$\beta^+$ (25%), EC (75%)	2.14
$^{94\text{m}}\text{Tc}$	53	$\beta^+$ (72%), EC (28%)	2.47

EC: Electron Capture

Table 1.1 Radionuclides used for PET imaging.<sup>137</sup>

The development of a radiotracer requires the study of the non-radioactive (or “cold”) molecular analogue and its interaction with the target that it was designed for.<sup>137</sup> Synthetic routes for the preparation of a small library of analogues are then designed which incorporate the isotopic label at a late stage of the synthesis. The ‘cold’ (non-radioactive) compounds are initially tested for affinity with the receptor.

A popular compound used in cancer PET imaging is 2- $^{18}\text{F}$ fluoro-2-deoxyglucose **44**. This compound is transported into the cells by membrane glucose transporters, it then undergoes phosphorylation which traps it irreversibly in the interior of the cell. This confers selectivity to this compound towards the tissue that forms tumours, since many of them have unregulated glucose transport and glycolysis. This selectivity turned **44** into a popular option as a biomarker of many human malignancies.



**Figure 1.29** Synthesis of the radiotracer 2- $^{18}\text{F}$ fluoro-2-deoxyglucose **44** used in PET imaging.<sup>138</sup>

The synthetic cyclic monosaccharide **44** has some limitations as an imaging agent, including high uptake in healthy tissues, such as the brain and bladder, which limits its use for the identification of gliomas and prostate cancers. Additionally, inflammatory conditions can provoke an increase in the uptake of **44**, creating false positives. These limitations have prompted the continuous development of specific biomarkers with higher specificity.<sup>139</sup>

### 1.6.2 Isotopes of copper: $^{64}\text{Cu}$ and $^{62}\text{Cu}$

The utility of PET has not been fully exploited due to the limited availability of relevant isotopes, which require the construction of nuclear reactors or particle accelerators. The invention of different techniques for the development of a wider variety of radionuclides, such as the small biomedical cyclotron, increased the demand of PET for research and clinical purposes.<sup>140</sup>

The isotopes  $^{18}\text{F}$ ,  $^{15}\text{O}$ ,  $^{13}\text{N}$ , and  $^{11}\text{C}$  have been traditionally used for their ability to integrate into small molecules. However, short half-lives, and rapid clearance make them more suited to studies that do not require extended periods of time, which makes it difficult to explore biological phenomena that have a duration of hours or days. Given the development of compounds that have specific biological targets, it was clear that new radionuclides needed to be produced with half-lives that could be appropriate for the challenges faced by biological investigation. There are a few transition metals and post-transition metal elements whose radionuclides have been developed to fulfil these new requirements of biological research. Copper, Gallium, Indium, Yttrium, and Zirconium complexes have been used before for PET imaging.<sup>140</sup> This section will refer mainly to

Copper. Table 1.1 gives an example of some interesting radionuclides that have been studied, as well as providing the long half-life of  $^{64}\text{Cu}$  in comparison with other radionuclides of commercial importance.<sup>137</sup>

Copper nuclides are an important area of research due to the variety of half-lives and decay energies, which can be useful in diagnostic imaging and radiotherapeutic applications.<sup>141</sup> Specifically,  $^{64}\text{Cu}$  has a half-life of 762 minutes and a  $\beta^+$  emission of 18%, ( $E_{\text{max}} = 0.655 \text{ meV}$ ). The low  $\beta^+$  abundance is a deficiency that is compensated by its long half-life, since this makes it easier to be transported, prepared and delivered for clinical applications.<sup>142</sup> The isotope  $^{64}\text{Cu}$  is a plausible alternative to  $^{18}\text{F}$ , maintaining a high sensitivity and high spatial resolution of PET without maintaining expensive radionuclide production facilities. Since  $^{64}\text{Cu}$  is a transition metal, it would be possible to attach it to a myriad of ligand carriers that would not work with  $^{18}\text{F}$  due to its chemistry.  $^{62}\text{Cu}$  is produced in generators. Its short half-life (9.7 minutes), allows the patient to receive consecutive doses without resulting in a dangerous exposure to radiation and allows radiotracers made with this radionuclide to obtain similar imaging results as other radiotracers containing radionuclides produced with more expensive methods.<sup>143</sup> The production of  $^{62}\text{Cu}$  requires the use of a zinc-62/copper-62 radionuclide generator<sup>144</sup> while the production of  $^{64}\text{Cu}$  requires a cyclotron.<sup>145</sup> This radionuclide exerts a  $\beta^+$  emission of 98%, ( $E_{\text{max}} = 2.93 \text{ meV}$ ), which is lower than the  $\beta^+$  emission of  $^{64}\text{Cu}$ . Kobayashi *et al.*<sup>146</sup> compared the performance of  $^{62}\text{Cu}$  and  $^{64}\text{Cu}$  radionuclides for PET. They found that  $^{64}\text{Cu}$  produced images of higher quality and better definition when the 3D acquisition mode was used. The definition of the images produced using  $^{64}\text{Cu}$  was more accurate than for those obtained using  $^{62}\text{Cu}$ , because the latter has a higher maximum  $\beta^+$  emission energy. This results in a longer positron range than  $^{64}\text{Cu}$ .<sup>147</sup>

## 2 Novel 1,2-azaphosphindoles

### 2.1 Introduction

#### 2.1.1 1*H*-indazole

Indazole derivatives display a broad variety of bioactivity. These type of compounds are rare in nature.<sup>148</sup> The plant *Nigella sativa* contains the alkaloids nigellicine **45**, nigeplanine **46**, and nigellidine **47**, which are examples of indazoles produced in nature.



Figure 2.1 *Nigella sativa* (commonly known as black cumin) flowers.

The synthesis of these indazoles has been accomplished by different methods and their biological, chemical and physical properties have been recently studied.<sup>149</sup>

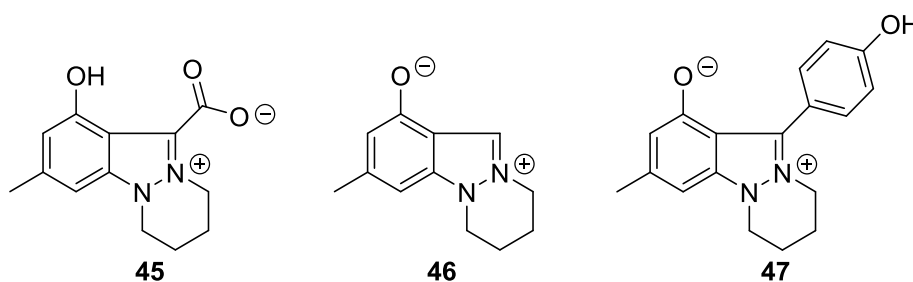
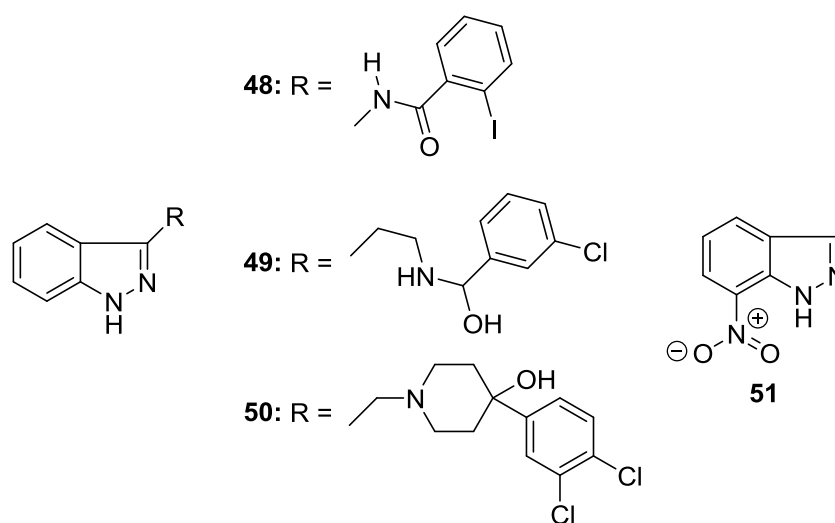


Figure 2.2 The indazole alkaloids nigellicine **45**, nigeplanine **46**, and nigellidine **47**.

There has been recent interest in the pharmacological properties of indazoles.<sup>150</sup> Since the electronic properties and geometry of small molecules play an important role in their interaction with biological receptors, there have been studies on these aspects in a collection of different chemical cores, including indazoles. These studies are aimed to support the development of new drugs.<sup>151</sup> The use of indazole in medicinal chemistry led

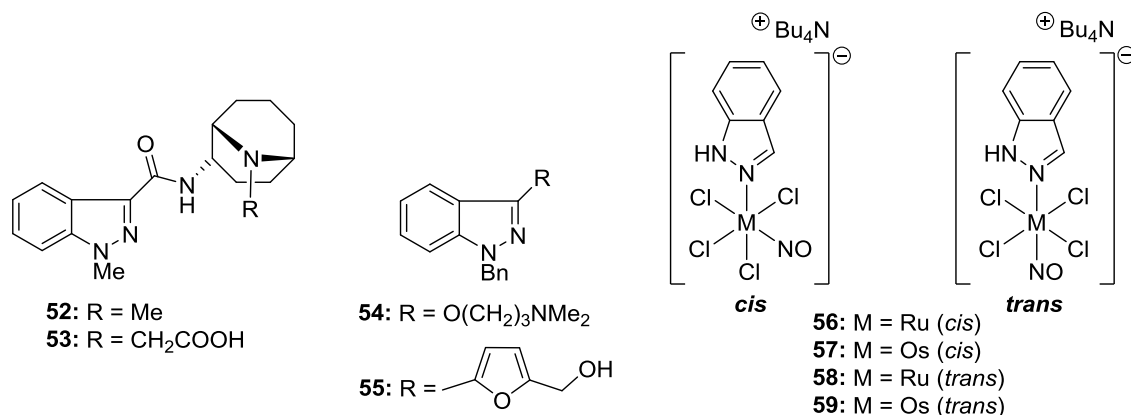
to the development of tumour inhibiting and redox-active antineoplastic ruthenium complexes.<sup>152</sup> There is a broad horizon for the use of derivatives of indazoles. The iodobenzamide derivative **48** has demonstrated antifungal activity<sup>153</sup> and compound **49** has been studied as a  $\beta_3$ -adrenergic receptor agonist in an attempt to treat type II diabetes. Indazole **50** has been studied due to its properties as a dopamine D2 receptor antagonist.<sup>154</sup> The compound 7-nitroindazole **51** is an indirect inhibitor of nitric oxide (NO), since it selectively inhibits the enzyme that produces this compound in the brain.<sup>155</sup> These features led to the research of 7-nitroindazole **51** as a possible protective agent against nerve damage caused by excitotoxicity or neurodegenerative diseases.<sup>156</sup>



**Figure 2.3** Different synthetic indazole analogues with interesting biological properties.

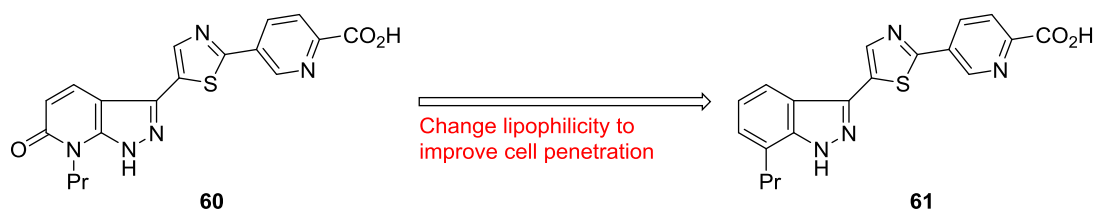
The biological properties of certain disubstituted indazoles have been already reported, suggesting that the biological properties found in the indazole core cannot only be retained but also modified according to the different substituents placed on the core. There are published examples of N(1)–C(3)-disubstituted indazoles showing pharmacological properties. Granisetron **52** is a clinically used antiemetic for treating nausea and emesis provoked by chemotherapy, and works by inhibiting the 5-HT<sub>3</sub> receptor.<sup>157</sup> By changing the methyl group to a carboxylic acid on the amine compound **53** was obtained, which is a gastrointestinal prokinetic and dopamine D2 receptor antagonist.<sup>158</sup> Benzydamine **54** is an anti-inflammatory agent used topically,<sup>159</sup> although, it also exhibits antifungal properties. The indazole derivative **55** has shown to be an activator of the cardiovascular and central nervous system by interacting with specific receptors. Interestingly, it also can inhibit endothelial cell functions that are activated by angiogenic factors *in vitro* and

angiogenesis *in vivo*.<sup>160</sup> The indazole core has also been reported as an interesting ligand. Complexes **56-59** have been reported in a study showing their interconversion between *cis* and *trans* isomers induced by high temperatures.<sup>161</sup>



**Figure 2.4** Examples of disubstituted indazoles that have shown biological activity.

Recently, indazoles have also shown to have antibiotic properties. Zhang *et al.* targeted bacterial DNA gyrase B, which is present in bacterial DNA making it a potent antibiotic target.<sup>162</sup> The crystal structure of the enzyme showed a pocket where a pyrazole moiety could interact electrostatically. Cell penetration was a problem which was resolved by physicochemical property optimization of pyrazolopyridone **60**, leading to the development of indazole **61**. This displayed a considerable improvement in activity against *S. aureus* and *S. pneumoniae*.<sup>162</sup>



**Figure 2.5** Development of the DNA bacterial gyrase B inhibitor indazole **60** from the pyrazolopyridone **61**.

Due to the applications that have been found for indazole analogues, different synthetic approaches for producing a broad variety of these compounds have been developed.

### 2.1.2 Synthetic routes towards indazoles

Indazoles can be prepared using diazo groups in phenyl rings, while *o*-methyl groups are required in order to close the newly formed 5-membered ring. The simplicity of this approach makes it versatile enough to produce different indazole analogues.<sup>163, 164</sup>

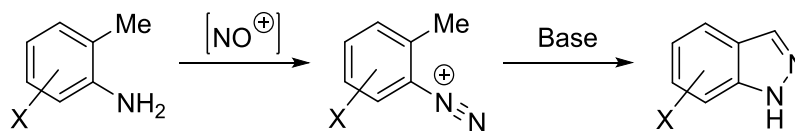


Figure 2.6 General synthesis of indazoles.

Similar syntheses include the diazotation of *o*-alkynylanilines such as **62**, producing the indazole **63**. This is an advance in this field since the benzylic position can have substituents that are not sensitive to basic conditions.<sup>165, 166</sup> The elucidation of the mechanism involved in this reaction led to derivatives such as five-membered pyrazole or six-membered pyridazine.<sup>167, 168</sup>

A recent breakthrough involved the development of a procedure for the synthesis of *2H*-indazoles by virtue of their increasing interest in medicinal chemistry applications, most notably as anticancer agents.<sup>169, 170</sup> This procedure, known as David-Beirut synthesis, is characterised by the formation of an *N,N*-bond to form the heterocycle required for the synthesis of *2H*-indazoles and indazolones.<sup>171, 172</sup> The group that originally developed this procedure made different analogues, with the intention of determining their activity against cystic fibrosis.<sup>173</sup> Figure 2.7 illustrates the Davis-Beirut approach for synthesising compound **63**, and other *N*-substituted indazoles.<sup>174</sup>

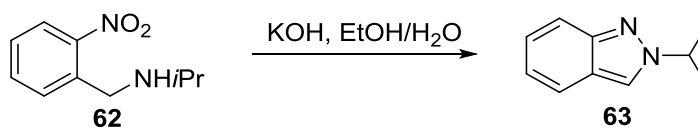


Figure 2.7 Synthesis of an indazole using the Davis-Beirut approach.

The similarity of phosphorus with nitrogen due to their positions in the periodic table had led to the development of different compounds where the nitrogen atom has been substituted with a phosphorus atom. Some of these find applications in the optoelectronic field, such as phospholes.<sup>175, 176</sup> However, some phosphorus analogues of important nitrogen-containing natural products have also displayed interesting biological properties themselves. An example of which can be found in  $\alpha$ -amino acids, being these are the building blocks of life, they are a natural target for developing phosphorus-based analogues.<sup>177</sup>



The field of phosphorus-based analogues of indazoles requires a more resourceful synthetic approach in comparison with its nitrogen counterparts due to the different reactivity of phosphorus. An organometallic approach has been employed to overcome this problem. J. P. Majoral and group<sup>178</sup> used the metallacycles obtained with zirconium in order to synthesise azaphosphindoles. In their methodology, they relied upon the thermolysis of diphenylzirconocene to generate a benzyne intermediate, which in the presence of a wide variety of nitriles, formed the required azazirconacyclopentanes. The zirconocene complex formed was reacted with the nitriles (*i*-Pr<sub>2</sub>N)<sub>2</sub>PCN and (Cy<sub>2</sub>N)<sub>2</sub>PCN, forming azaphosphindoles **64** in high yields (80-90%). Then, they were reacted with phenyldichlorophosphine and *tert*-butylchlorophosphine, leading to elimination of Cp<sub>2</sub>ZrCl<sub>2</sub> in order to produce novel 1,2-azaphosphindoles **65**. Finally, elemental sulfur was added in order to produce the monosulfide **66**.

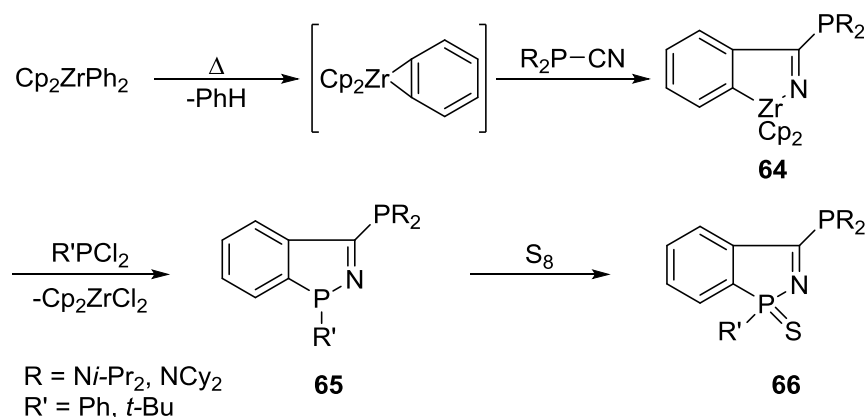


Figure 2.8 Synthesis of Majoral *et al.* by 2H-1,2-Azaphosphindoles.<sup>178</sup>

## 2.2 Synthetic target

The synthesis developed by Majoral and his group<sup>178</sup> allows the incorporation of different aromatic rings in the 3-position of the phosphindole in order to incorporate functionality; the only requirement is that the group that will be added must be a nitrile in order to perform the coupling to achieve the phosphindole ring. The chosen aromatic systems are phenyl, naphthyl and anthracyl, since polyaromatic hydrocarbons are well known for interacting with DNA.<sup>63</sup>

To our knowledge, there are no examples of 1,2-azaphosphindoles with an electron donating group in the phenyl ring; therefore, a methyl group will be added in the *para* position. Sulfur and selenium will be added to oxidize the phosphorus atom to making it

more stable towards oxidation and the electronic differences between the two chalcogen-containing derivatives will be measured.

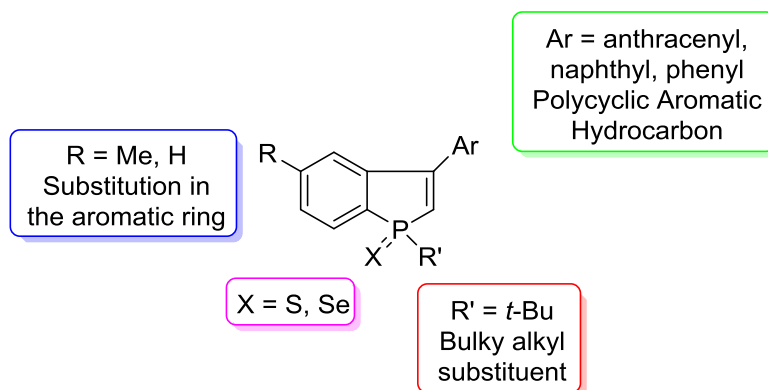
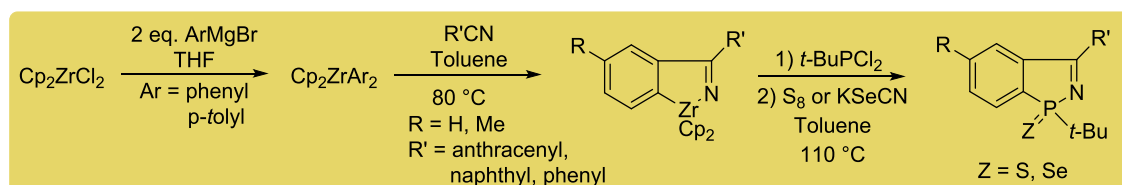
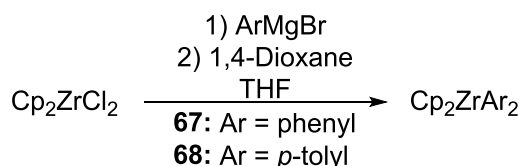


Figure 2.9 Proposed substitutions on 1,2-azaphosphindoles core.

## 2.3 Synthesis of 1,2-azaphosphindoles

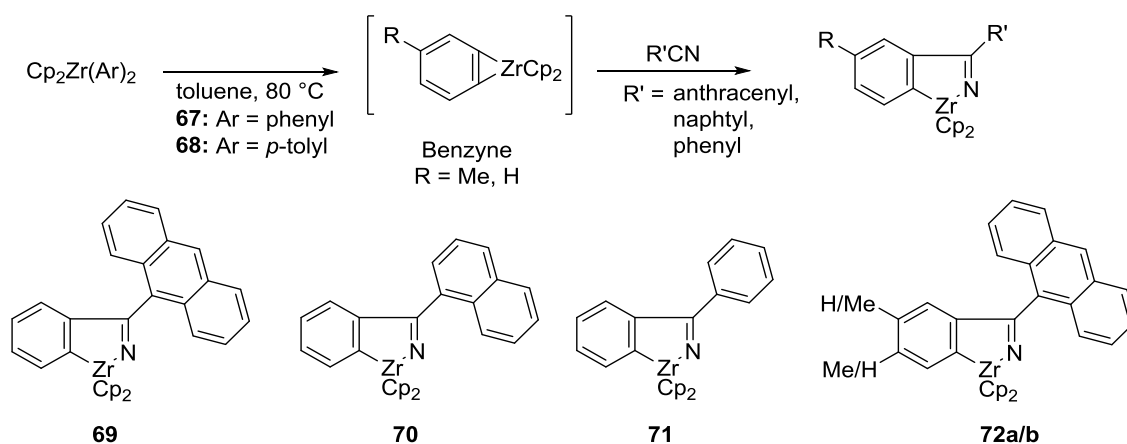


The synthesis of the 1,2-azaphosphindoles began with commercially available zirconocene dichloride. The addition of 2 equivalents of a Grignard reagent to the zirconocene dichloride solution formed the desired disubstituted zirconocene complexes **67** and **68**. The resulting complexes **67** and **68** were handled under dinitrogen to avoid their interaction of the Zr metal centre with oxygen or moisture from the air. The excess Grignard reagent was quenched using 1,4-dioxane since the normal hydrolysis using water would lead to the formation of oxygen-bridged products.<sup>179</sup> In order to remove the salts formed by the reaction of dioxane with the Grignard reagent, THF was evaporated and the resulting mixture was redissolved in toluene, leading to a pale yellow suspension that was then filtered under dinitrogen using a cannula. The solvent from the resulting solution was evaporated and no further form of purification was performed. <sup>1</sup>H and <sup>13</sup>C NMR were obtained and were in agreement with structures **67** and **68**.



**Figure 2.10** Synthesis of zirconocene compounds **67** and **68**.

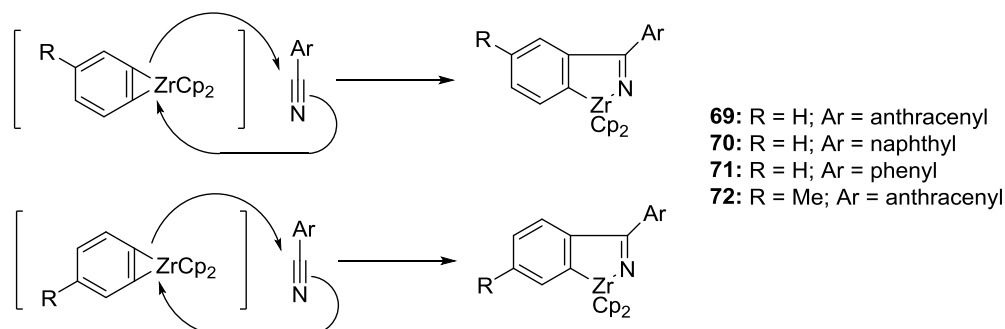
The zirconocenes obtained were heated to 80 °C in toluene in order to induce a thermolysis reaction, obtaining a reactive zirconocene benzyne complex. Our study was focused on the use of anthracene, naphthalene and benzene nitriles in order to successfully form azazirconacyclopentenes. As it can be seen in **Figure 2.11**, this reaction, 4 different products using exactly the same procedure were produced. Diphenyl zirconocene **67** was used as starting material to produce the azaphosphindoles **69-71** and di-*p*-tolyl zirconocene **68** was used to produce the azaphosphindole **72a/b**. Each reaction was allowed to stir at 80 °C overnight, producing a suspension which was filtered under dinitrogen. The resulting mixtures were evaporated under dinitrogen and washed with pentane in order to remove traces of unreacted aromatic nitriles. The resulting compounds contained an imine, which was identified by <sup>13</sup>C and by infrared spectroscopy (Table 2.1).



**Figure 2.11** Synthesis of Azaphosphindoles **69-72**. The resulting products contained different substituents.

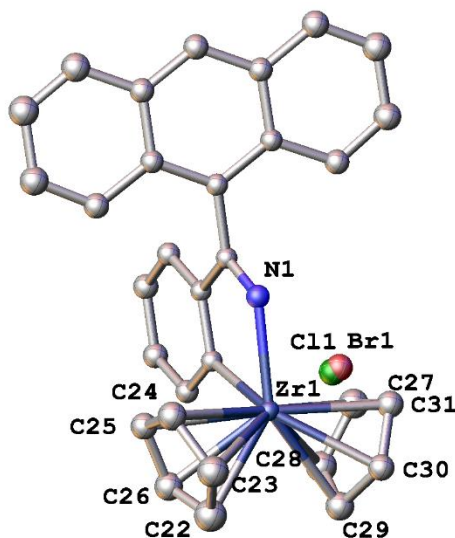
Electron donating groups, such as methyl groups, in benzyne mediated reactions, have previously proven to be poor regioselective substituents,<sup>180</sup> which explains why compound **72a/b** shows two different peaks at  $\delta$  2.31 and 2.27 ppm in <sup>1</sup>H NMR. This is intrinsic of the reaction mechanism, in which the benzyne adduct is trapped by the nitrile.

Due to the electronic environment and the lack of steric hindrance, the nitrile can trap the benzyne intermediate in two different spatial arrangements, as shown in Figure 2.12.<sup>181</sup>



**Figure 2.12** Formation of complexes 69-72. The different positions of the benzene intermediate is not important when R = H.

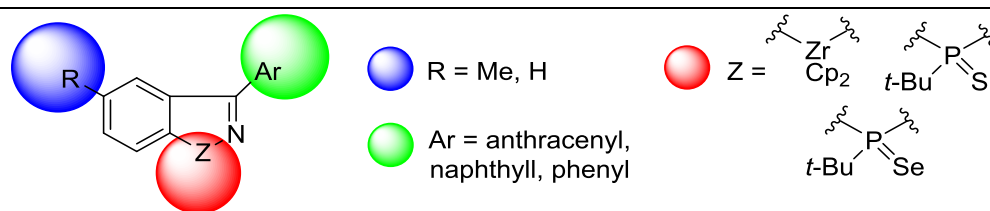
Purifying the compound at this stage proved to be impractical due to the formation of different products in the chromatography column inferring decomposition of the product. However, it was possible to obtain a crystal of **69** suitable for X-ray crystallographic analysis.



**Figure 2.13** X-ray crystal structure view of **69** (50% probability ellipsoids with bromine, carbon, chlorine, nitrogen and zirconium atoms labelled. Carbon atoms in grey). Hydrogen atoms have been omitted for clarity. Selected bond distances [Å] and angles [°]: Zr1–N1 2.2901(17), Zr1–C1 2.3788(18), Zr1–C22 2.524(2), Zr1–C23 2.521(2), Zr1–C24 2.523(2), Zr1–C25 2.5280(19), Zr1–C26 2.503(2), Zr1–C27 2.536(2), Zr1–C28 2.536(2), Zr1–C29 2.541(2), Zr1–C30 2.4984(18), Zr1–C31 2.5067(19), N1–C7 1.291(2); N1–Zr1–C1 68.36(6), N1–Zr1–C22 137.17(7), N1–Zr1–C23 110.21(8).

After reacting the imino zirconocycle with *tert*-butyldichlorophosphine, it was possible to obtain spectroscopic data of the constitutional isomers proposed.

Treatment of compounds **69-72a/b** with *tert*-butyldichlorophosphine led to the elimination of zirconocene dichloride, producing a five-membered phosphole that was immediately oxidized by reaction with a chalcogen. The resulting 1,2-azaphosphindoles were all purified via column chromatography. Table 2.1 contains the IR and  $^{13}\text{C}$  NMR spectroscopic data, showing that the imine function remained intact after displacement of the zirconocene dichloride. This table also contains the general structure of compounds **69-79**, highlighted with different colours to indicate the positions that allow for substitutions to occur.



Compound	$\nu$ C=N (cm <sup>-1</sup> )	$\delta$ C=N (ppm)
<b>HZrAnth 69</b>	1589	191.2
<b>HZrNaph 70</b>	1593	188.9
<b>HZrPh 71</b>	1593	186.2
<b>MeZrAnth 72a/b</b>	1578	179.1
<b>HPSAnth 73</b>	1531	182.2 (d, $^2J_{\text{CP}} = 8.3$ Hz)
<b>HPSNaph 74</b>	1593	181.1 (d, $^2J_{\text{CP}} = 8.3$ Hz)
<b>HPSPh 75</b>	1531	180.0 (d, $^2J_{\text{CP}} = 7.2$ Hz)
<b>MePSAnth 76a/b</b>	1577	182.4 (d, $^2J_{\text{CP}} = 7.7$ Hz), 182.1 (d, $^2J_{\text{CP}} = 8.5$ Hz)
<b>HPSeAnth 77</b>	1537	182.2 (d, $^2J_{\text{CP}} = 11.2$ Hz)
<b>HPSeNaph 78</b>	1532	181.2 (d, $^2J_{\text{CP}} = 10.4$ Hz)
<b>HPSePh 79</b>	1531	179.1 (d, $^2J_{\text{CP}} = 9.8$ Hz)

Table 2.1 IR stretching frequencies and  $^{13}\text{C}\{^1\text{H}\}$  NMR, key data for the imine functional group. PS: P=S, PSe: P=Se, Anth: Anthracenyl, Naph: Naphthyl, Ph: Phenyl.

During the experimental procedure, it was noted that temperature played a key role in attaining the closure of the five membered ring when the phosphorus atom displaces the zirconocene. When this reaction is heated to 110 °C, the target is obtained; however, if the reaction is heated to 80 °C, the isolated compound instead contains a P–Cl bond that is attached to the phenyl ring by a C–C bond with the carbon of the imine. This interesting result shows that the chlorothiophosphonates obtained are the kinetic products of this reaction, which means that the activation energy required to close the ring was not reached and must be higher than the energy barrier at 80 °C. The ring-closed compounds are the thermodynamic products, which means that while they are more thermodynamically stable, they require more energy to be attained. Interestingly, Majoral reported reflux temperatures were used only for the benzyne production step. Substitution of the zirconocene group by the phosphine chloride and its further oxidation with sulfur were performed at room temperature (Section 2.1.2). The different compounds obtained with this procedure are listed in Figure 2.14. The final compounds were purified by column chromatography and traces of zirconocene dichloride were recovered.

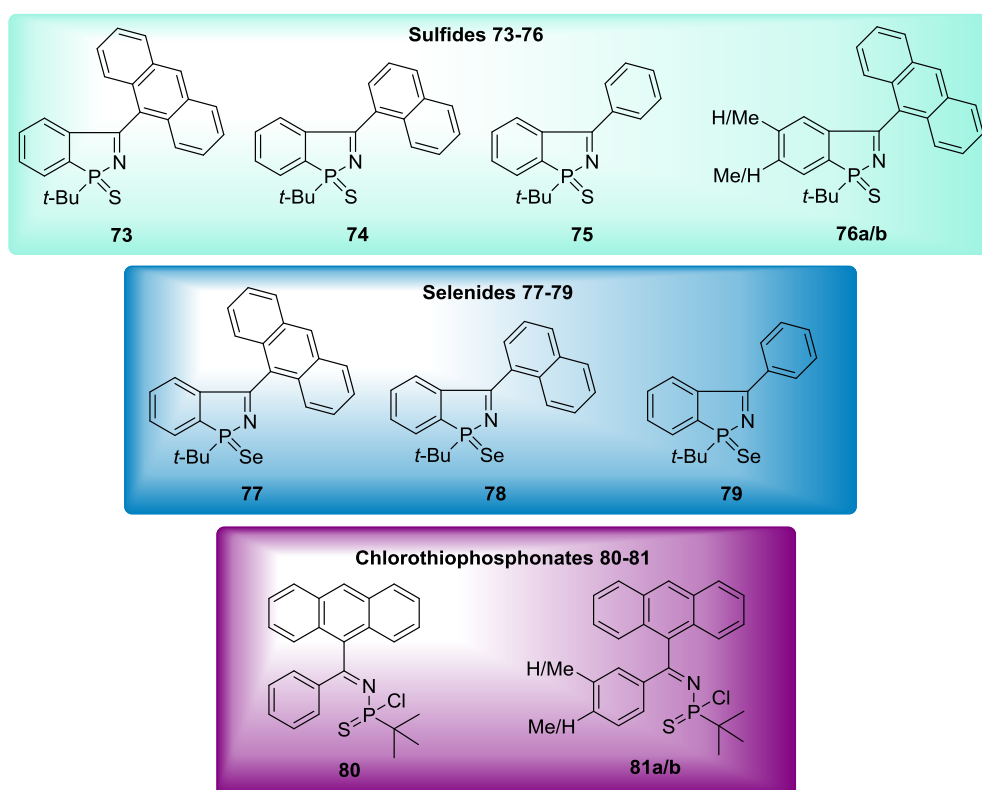


Figure 2.14 Novel 1,2-azaphosphindoles 73-79 and chlorothiophosphonates 80 and 81.

The structure of novel chlorothiophosphonates **80** and **81a/b** was determined by X-ray crystallographic analysis – this will be explained in further detail in Section 2.4.2. There are examples of reported crystal structures of compounds containing N–P–Cl bonds;<sup>182, 183</sup> however, fewer examples exist with the addition of sulfur on the phosphorus atom. Synthesis of chlorothiophosphonates has been already reported, with the intention of developing chiral phosphorus compounds with insecticidal activity.<sup>184</sup>

## 2.4 Structural and electronic properties of 1,2-azaphosphindoles

### 2.4.1 Phosphorus-selenium coupling constants in NMR

The magnitude of  $^1J_{\text{PSe}}$  is highly dependent upon the nature of the organic groups bound to the phosphorus atom; electron-withdrawing groups cause the  $^1J_{\text{PSe}}$  coupling constant to increase whereas electron-donating and bulky groups cause it to decrease. It is well known that coupling constants between directly bonded atoms arise predominantly from the Fermi-contact interaction between nuclear moments and electron spins in *s* orbitals,<sup>185</sup> and there have been a number of postulations in the literature that is a correlation exists between the magnitude of these coupling constants and the lengths of the bonds between adjacent atoms.<sup>186</sup> Sterically demanding substituents can indirectly influence the coupling if the intervalence angles of the phosphorus are widened; the *s*-character of the phosphorus lone pair is therefore reduced, resulting in increased Lewis basicity.<sup>187</sup> This lowers the  $^1J_{\text{PSe}}$  magnitude also. Identifying the isolated effect caused on  $^1J_{\text{PSe}}$  by steric and electronic effects has proven to be a difficult endeavour.<sup>188</sup> Thus, electronic information about the compounds synthesised in this work can be acquired by inspection of the  $^1J_{\text{PSe}}$  magnitude.

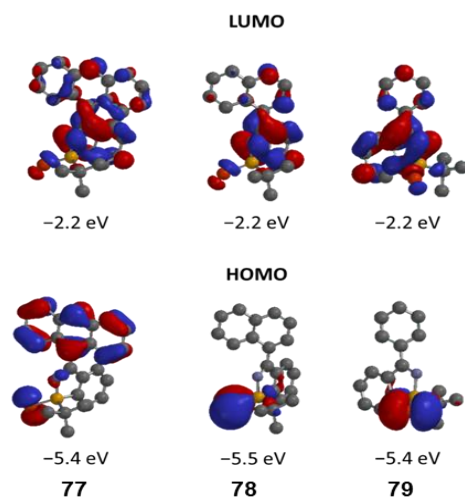


Figure 2.15 HOMO diagrams with accompanying energies of 77-79 (in that order) calculated at the B3LYP/6-31G\* level of theory.

Compounds **77-79** were obtained by adding KSeCN to the corresponding phosphole solution in toluene and heating it to 110 °C. Their  $^1J_{\text{PSe}}$  were measured and contrasted with the values of calculated HOMO energies (calculated at the B3LYP/6-31G\* level of theory) of their respective phosphole parents. The anthracenyl substituent decreases the value of  $^1J_{\text{PSe}}$ . However, this might be related to its size rather than its electronic features, since anthracene is a polyaromatic hydrocarbon. In comparison, the anthracenyl group seems to have a more extended conjugated  $\pi$ -electron system, which gives it more stability than the naphthyl or phenyl substituents. There have been previous attempts to relate theoretical data with the behaviour of tertiary phosphines as ligands using DFT-generated data.<sup>189, 190</sup> It has been found in a set of tertiary phosphines that there is a linear relationship between the activation energy and the energy of the tertiary phosphines' HOMO.<sup>189</sup> The DFT calculations in Figure 2.15 show that the HOMO is more dispersed in **77**, which contains the anthracenyl group. For the naphthyl and phenyl derivatives, we can determine that the HOMO contains a higher selenium character. The calculated energy for the HOMO energies shows that the compound **77** is the highest in energy and gives the lowest  $^1J_{\text{PSe}}$  coupling constant experimentally. The difference in the  $^1J_{\text{PSe}}$  magnitudes of **77-79** must therefore be related to the HOMO distribution.

Magnitude	<b>77</b>	<b>78</b>	<b>79</b>
$^1J_{\text{PSe}}$ (Hz)	749.5	756.9	777.4
HOMO (eV)	-5.4	-5.5	-5.4

**Table 2.2 Values of  $^1J_{\text{PSe}}$  (Hz) and the HOMO energy calculated for the selenides 77-79**

Previous reports of selenides **82a,b**<sup>191</sup> provide an example to contrast these results, since the phosphorus atom forms part of a five-membered ring. The reported  $^1J_{\text{PSe}}$  for phospholanes **82a,b** is 693 Hz, which suggests that these compounds are stronger  $\sigma$ -donors in comparison with the phosphindoles **77-79**.



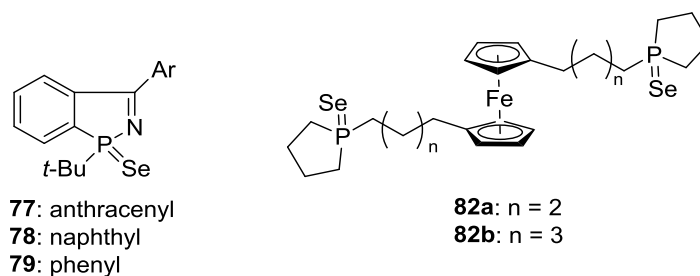
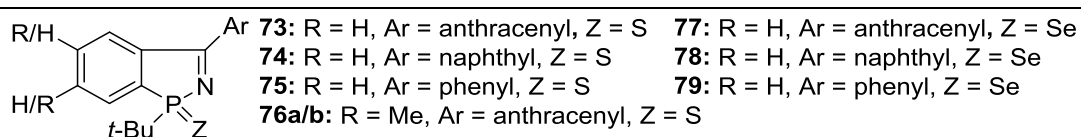


Figure 2.16 Phosphindole 77-79 and phospholanes 82a,b.

## 2.4.2 X-ray crystallographic analysis and molecular structures

Crystal structures were obtained for compounds **73-79**; the measurement of their P=Z and P–N bonds show very little variations. Compound **76a/b** presents an interesting case, since the P=S bond is shorter than in **73-75** and the P–N bond is longer. Compounds **73-75** show very little variation in their P=S and P–N bonds, with the former one being the longest of the two in all the compounds.



Compound	P=Z* (Å)	P–N (Å)
73	1.9425(6)	1.7189(14)
74	1.9401(7)	1.714(1)
75	1.9417(5)	1.715(1)
76a/b	1.9354(7)	1.7259(13)
77	2.0910(5)	1.7193(16)
78	2.0910(5)	1.7142(16)
79	2.0974(10)	1.715(3)

Table 2.3 Selected P=Z and P–N bond lengths of compounds 73-79 (Å).

The methyl group in **76a/b** is exerting an effect that shortens the P–N bond and elongates the P=S bond. Aladzheva *et al.*<sup>192</sup> reported crystallographic data showing the elongation of P=S bonds of Pd(II) and Pt(II) complexes with the sulfur directly coordinated to the metallic core. However, this does not affect the P–N bond. The electron withdrawing

effect of the metal centres does not resemble the effect provided by the methyl group in **76ab**; therefore, the electron donating effect that the methyl group can provide does not satisfactorily explain this effect. For compounds **73-79**, slow diffusion of diethyl ether into a saturated toluene solution yielded crystals suitable for X-ray crystallographic analysis. Compound **76a/b** is an interesting case since the mechanism that produces it allows a mixture of regioisomers. The formation of benzyne allows for two different sites where the addition of 9-anthracenecarbonitrile can occur.

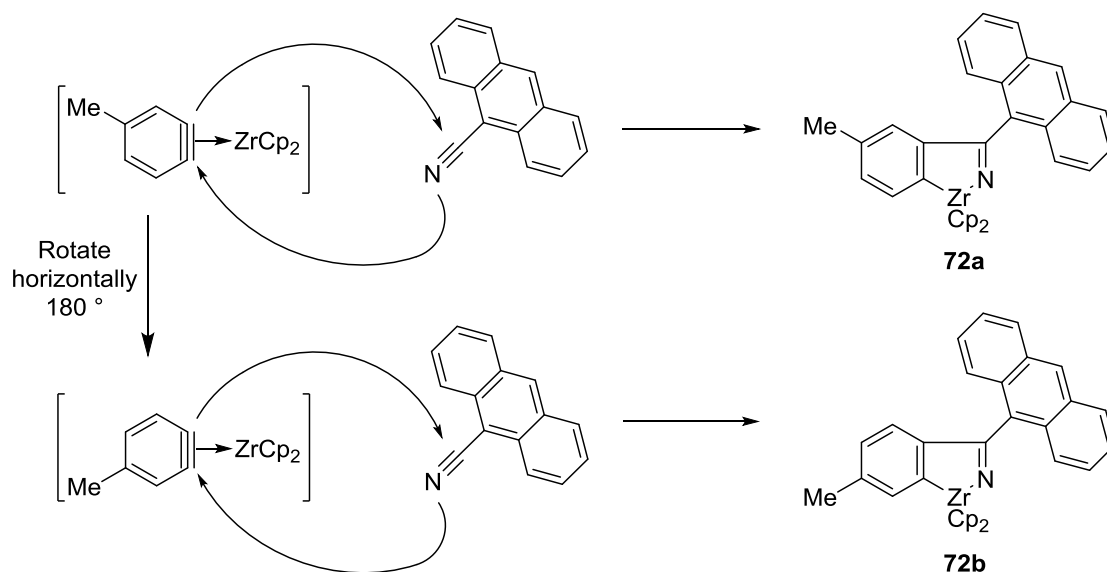
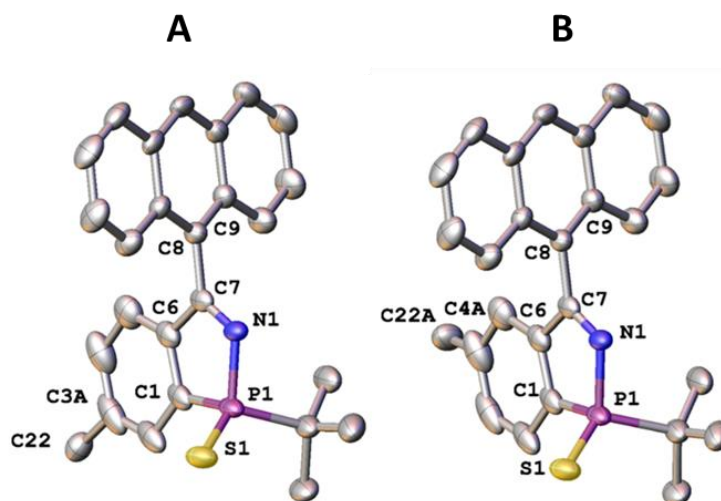


Figure 2.17 Depiction of the formation of regioisomers **72**.

Regioselective reactions using benzyne derivatives have been reported using inductive or steric effects in order to control the selectivity.<sup>193</sup> However, the methyl group in this case was used to prove that it is possible to have different substituents using the zirconocene approach developed by Majoral *et al.*<sup>178</sup> X-ray crystallographic analysis showed the presence of two methyl groups in the phenyl ring of compound **76a/b**. The presence of these two methyl groups was expected since the *p*-tolyl zirconocene used to produce **76a/b** does not possess strong inductive effects, nor is it sterically demanding enough to provide high regioselectivity. Groups providing this character include O-protected groups<sup>193, 194</sup> and fused heterocycles;<sup>195, 196</sup> however, the development of regioselective benzyne derivatives is an ongoing process.

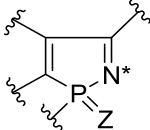
The crystallographic analysis corroborated the NMR data that suggests that the compound **76** exists as a mixture of two regioisomers, with the methyl group (C22, C22A) in the phosphindole ring occupying the *para* or *meta* positions.

The crystal structure provided information on the sulfides **73-76**, the selenides **77-79** and the chlorides **80-81a/b**. It was found that the length of the P–Se bond is larger than those of their P–S analogues. The P=S is shorter than the P=Se bond, which is a normal trend when compared to other crystal structures in the literature.<sup>197, 198</sup> P=Te is the longest bond,<sup>199</sup> which makes sense if one considers the electronegativity and radii.



**Figure 2.18** View of the molecular structures of regioisomers **76a/b** (50% probability ellipsoids with notable carbon, chlorine, nitrogen, phosphorus and sulfur atoms labelled. Carbon atoms are in grey). Hydrogen atoms have been omitted for clarity. Disordered structure in the solid state with major component **A** (C22 occupancy = 0.5452) and minor component **B** (C22A occupancy = 0.4548).

The bond lengths found agree with the data reported in the literature regarding similar systems where the phosphorus atom is in a five membered-ring with different substituents.<sup>200-202</sup> Table 2.4 shows the average P=Z bond lengths found for sulfides **73-76a/b** and selenides **77-79** and those of similar compounds reported in the Cambridge Structural Database (CSD). The average P=Z bond length of **73-76a/b** is quite similar to the average found in the CSD. Considering the standard deviation, the difference between the two values might be regarded as insignificant. On the other hand, the average P=Z bond length for selenides **77-79** differs considerably from the average values from the CSD. This difference might be explained by the presence of the nitrogen atom, since there are no reported examples of phosphindole selenides containing a nitrogen atom in that position. Therefore, the average was calculated using five-membered ring phosphindole selenides containing a carbon atom instead of the nitrogen. The effect exerted by the nitrogen seems to induce the shortening of the P=Se bond when compared with the average P=Se bond length obtained from the CSD.

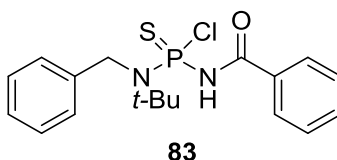
 Searched structure in the Cambridge Structure Database	<b>P=Z bond</b>	<b>Experimental bond length (Average) Å</b>	<b>*Reported bond length (Average) Å</b>
	Z = S	1.940(7) ( <b>73-76</b> )	1.948(5)
Z = Se	2.0931(7) ( <b>77-79</b> )	2.134(17)	

\* There are no reports of crystal structures in CSD of selenides containing a nitrogen in that position, therefore the search was performed with a carbon atom.

**Table 2.4 Comparison of average values of P=Z bond lengths for compounds 73-79 and the average P=Z bond length found in the CSD.**

### 2.4.3 Chlorothiophosphonates 80-81

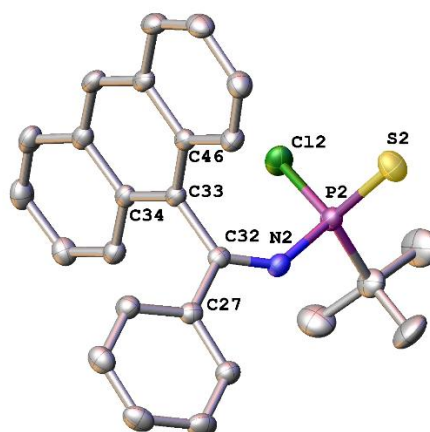
The synthesis of sulfides **73-76a/b** led to the serendipitous synthesis of phosphinothioic chlorides **80** and **81a/b** that were identified after purification. Phosphinothioic chloride systems have been synthesised before because of their interesting synthetic properties.<sup>203-205</sup> Compound **83** was developed by Gholivand *et al.*<sup>206</sup> as an acetylcholinesterase inhibitor, predicting that the chlorine would act as a leaving group. This would result in the phosphorylation of acetylcholinesterase leading to its irreversible inhibition.



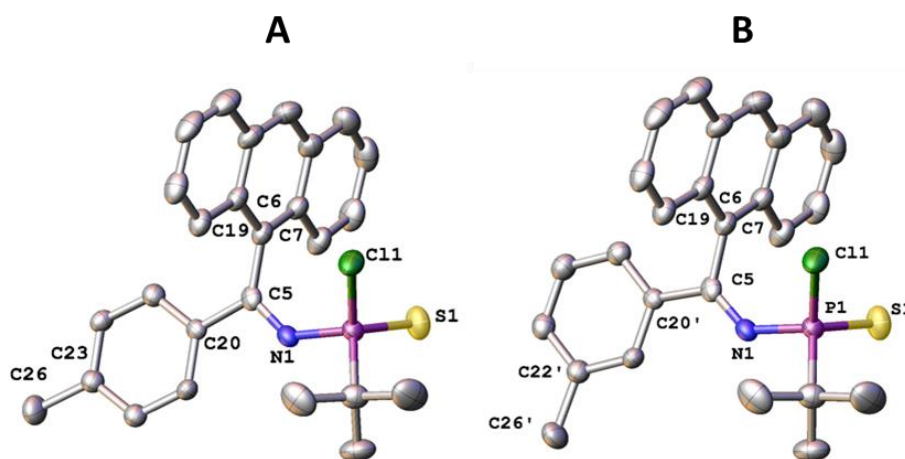
**Figure 2.19 Acetylcholinesterase inhibitor developed by Gholivand.<sup>206</sup>**

<sup>31</sup>P{<sup>1</sup>H} NMR is a useful technique for identifying compounds and monitoring reactions where phosphorus is involved. In this case, the technique was useful in the form of providing information about changes in the starting material, *t*BuPCl<sub>2</sub>. The <sup>31</sup>P{<sup>1</sup>H} NMR spectrum obtained was originally compared to that obtained by Majoral *et al.*<sup>178</sup> Their results showed that the phosphindole sulfide **66** (Figure 2.8) produced a signal at 100 ppm. Compounds **80** and **81a/b** show singlets at 97.4 and 96.7 ppm; therefore, it was thought that the desired phosphindoles had been synthesised, while X-crystallographic data unambiguously assigned the structures of compounds **80** and **81a/b**. <sup>1</sup>H NMR data was similar to their closed ring analogues; although, the integration suggested the presence of one more hydrogen for both compounds. X-ray analysis helped to elucidate that this extra hydrogen came from the loss of the phosphindolic system. As was mentioned in Section

2.3, the temperature at which this reaction takes place seems to be the controlling factor for obtaining the phosphindole or the phosphinothioic chloride. Compound **81a/b** contains the same mixture of regioisomers where the methyl group in the phenyl ring can be found in *para* and *meta* positions in the same way as the phosphindole **76**. This is not surprising, since the information available suggests that the regioisomers are formed during the benzyne formation. Therefore, replacement of the zirconocene moiety by the *tert*-butyl phosphine has no effect.



**Figure 2.20** View of the molecular structure of **80** (50% probability ellipsoids with interesting carbon, chlorine, nitrogen, phosphorus and sulfur atoms labelled. Carbon atoms in grey). Hydrogen atoms have been omitted for clarity.



**Figure 2.21** View of the molecular structure of regioisomers **81** (50% probability ellipsoids with interesting carbon, chlorine, nitrogen, phosphorus and sulfur atoms labelled. Carbon atoms in grey). Hydrogen atoms have been omitted for clarity. Disordered structure in the solid state with major component A (C26 occupancy = 0.511(3)) and minor component B (C26' occupancy = 0.489(3)).

The crystallographic data for compounds **80** and **81a/b** shows that carbons, which serve as a link between the phenyl ring and the anthracenyl group, has retained its  $sp^2$  hybridization. Moreover, the imine also retained the  $\pi$  bond between the nitrogen and the carbon in the benzylic position.

It is interesting to highlight that in the phosphinothioic chlorides **80** and **81a/b**, there are two planes where the phenyl ring and the anthracenyl groups are located. These planes have a perpendicular relationship to each other ( $101.66^\circ$  (19) for **80** and  $99.2^\circ$  (4) for **81a/b**).

#### 2.4.4 An investigation to the torsional angles between the phosphindole backbone and the PAH ancillary group

Phosphindoles **73-79** contain two adjacent aromatic groups linked by the C7–C8 bond. This bond is interesting as it represents the junction of the two adjacent aromatic groups and is affected by the PAH attached to the phosphindole moiety. The results collected in Table 2.5 show that the C7–C8 bond length follows the pattern: **73**>**74**>**75**. This trend suggests that the phenyl ring is shortening the bond. It is not clear why this happens unless the torsional angle formed by the two aromatic rings, the phosphindole and the PAH, is taken into account. As compounds **73-79** contain two aromatic rings attached by a  $\sigma$ -bond, a dihedral angle can be measured between the two planes formed in the solid state.

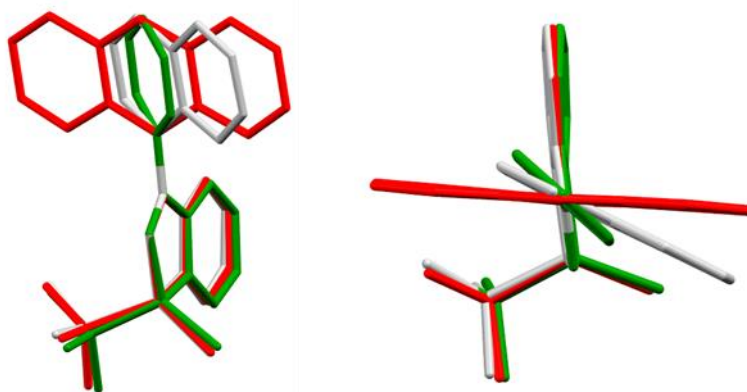


Figure 2.22 An overlay diagram of **73** (red), **74** (grey) and **75** (green) showing the variation in the conformation of the PAH substituent.

Figure 2.22 illustrates the angles  $\theta_a$  and  $\theta_b$  formed by the spatial arrangement of these compounds when measured in their solid state. For all of the derivatives synthesised **73-79**,  $\theta_b$  is larger when the PAH is smaller, suggesting a relationship between the C7–C8 bond length and the PAH attached to the phosphindole. This relationship is also present

for the sulfides **73-75**. A larger value of  $\theta_b$  implies a more parallel relationship between the phosphindole and the corresponding PAH. Therefore, the level of  $\pi$ -conjugation between the two aromatic moieties will increase. This conjugation could be used to rationalise the C7–C8 bond length pattern found for sulfides **73-75**. This trend in the C7–C8 bond length is not followed by the selenides **77-79**, suggesting that the selenium atom is exerting an effect on the  $\pi$ -conjugation or directly on the C7–C8 bond length. On the other hand, the selenides, **77-79**, follow the trend that  $\theta_b$  increases as the PAH gets smaller.

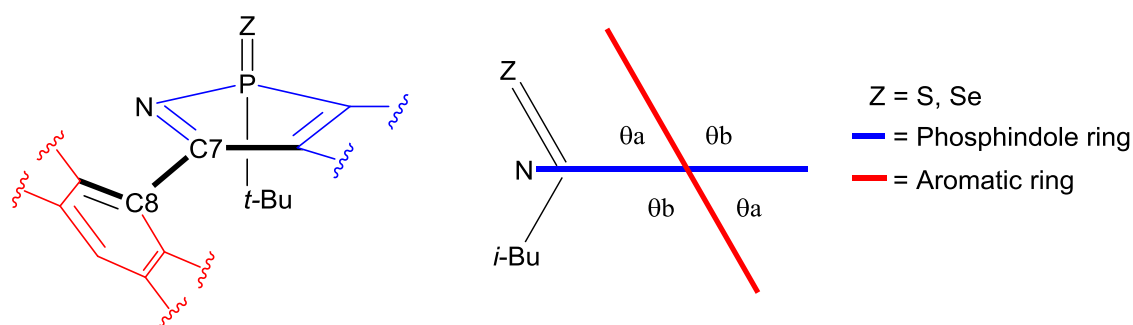


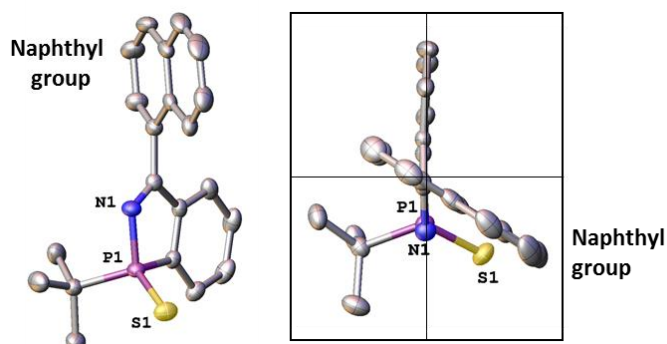
Figure 2.23 Spatial representation of the measured dihedral angles  $\theta_a$  and  $\theta_b$ .

Entry	C7–C8 (Å)	P=Z* (Å)	Experimental (average)		Calculated	
			$\theta_a$ (°)	$\theta_b$ (°)	$\theta_a$ (°)	$\theta_b$ (°)
<b>73</b>	1.495(2)	1.9425(6)	77.9(2)	101.6(2)	82.5	97.5
<b>74</b>	1.488(2)	1.9401(7)	54.7(2)	126.5(2)	56.7	123.3
<b>75</b>	1.482(2)	1.9417(5)	42.9(2)	139.0(2)	35.2	144.8
<b>76</b>	1.4868(5)	1.9354(7)	74.4(2)	103.8(2)	67.9	112.1
<b>77</b>	1.495(5)	2.0910(5)	76.8(2)	103.2(2)	67.2	112.8
<b>78</b>	1.487(4)	2.0910(5)	51.2(5)	128.8(6)	54.2	125.6
<b>79</b>	1.488(7)	2.0974(10)	35.0(5)	145.0(7)	45.3	134.76

\* Z = S for 73-76 and Z = Se for 77-79

Table 2.5 Crystallographic and DFT (B3YLP) calculated data of compounds **73-79**.

At first glance, it seems that the *tert*-butyl group exerts a repulsion effect on the PAH due to steric hindrance, yielding a larger  $\theta_b$  than  $\theta_a$  as a result. However, Figure 2.22 shows that the *tert*-butyl group is too far away from the PAH group. On the other hand, analysis the crystal structure of sulfide **74** shows that most of the asymmetrical naphthyl group is in the quadrant near the S atom, suggesting a repulsion effect exerted by the *tert*-butyl group. This may not be definite evidence because, as it has been mentioned before, the *tert*-butyl and the naphthyl group, are too far away from each other in this molecule (Figure 2.24).



**Figure 2.24** View of the molecular structure of **74** (50% probability ellipsoids with nitrogen, phosphorus and sulfur atoms labelled. Carbon atoms in grey). Hydrogen atoms have been omitted for clarity. The majority of the naphthyl group is located in the same quadrant as the S1 atom.

Comparing angles  $\theta_a$  and  $\theta_b$  from sulfides **73-75** to selenides **77-79**, it is possible to appreciate that there are no changes in the trend. The larger the PAH, the more acute the  $\theta_b$ . Therefore, the phenyl ring produced the biggest values for the angle  $\theta_b$ . The size of the S and Se atoms do not provoke any changes in the trend of the two sets of compounds. DFT calculations obtained via the B3YLP functional (with the 6-31G\* basis set) of the spatial arrangement show the same pattern and similar values.

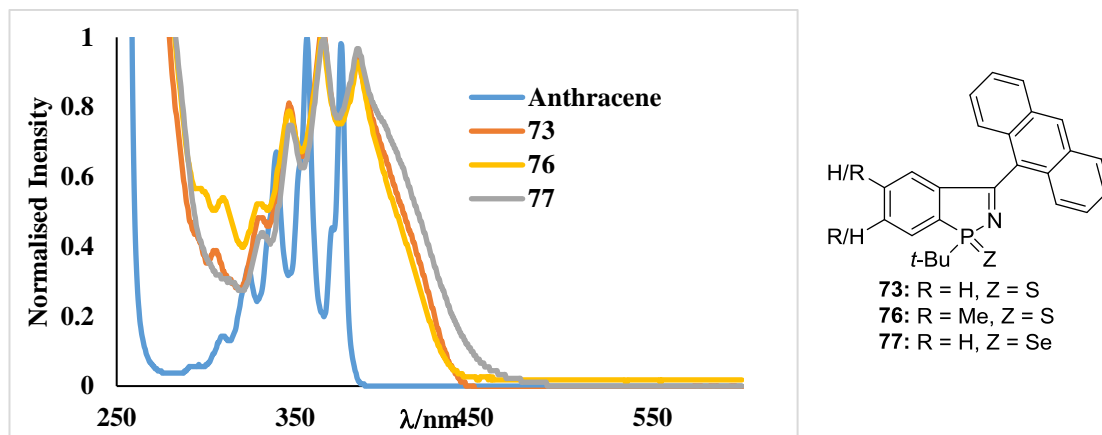
## 2.5 Photophysical data

### 2.5.1 UV-Vis absorption spectroscopy

After characterising the novel synthesised compounds **73-79**, their absorption spectra was measured. The absorption profile of the novel 1,2-azaphosphindoles **73-79** was compared to the absorption profile of the different PAHs contained in them. For ease of viewing, the different absorption spectra obtained will be placed next to their corresponding molecules in the following section. Anthracene produces an absorption spectrum with five sharp bands between 300-400 nm that are attributed to  $\pi \rightarrow \pi^*$  transitions.<sup>40</sup> Sulfides

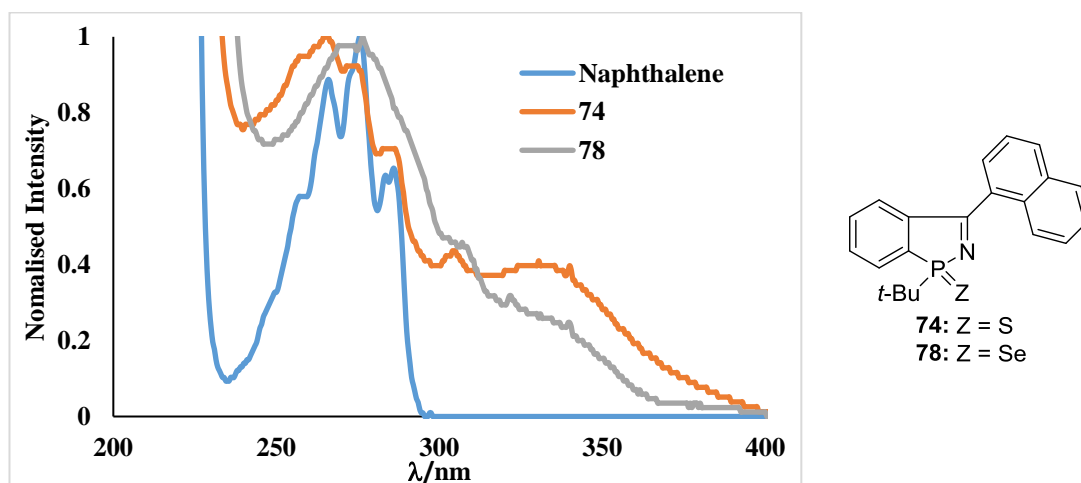


**73**, **76** and selenide **77** produce four visible bands that are slightly redshifted. The three novel compounds show a broad band at around 300 nm with a medium intensity that overlaps one of the bands visible in the anthracene absorption spectrum. Another visible difference is the broad shoulder that is visible at around 400-450 nm (Figure 2.25).



**Figure 2.25** Absorption spectrum of anthracene and anthracene derivatives **73**, **76** and **77**, recorded in cyclohexane at room temperature at a  $7.5 \times 10^{-6}$  M concentration.

The absorption spectrum of naphthalene shows bands corresponding to  $\pi \rightarrow \pi^*$  transitions of the  $\pi$  system in the aromatic molecule between 250-300 nm. The absorption spectra of the sulfide **74** and the selenide **78** show a broad band at around 250-300 nm, as in the case of naphthalene; however, there is a second broad band in both cases. This is located at around 300-350 nm (Figure 2.26).



**Figure 2.26** Absorption spectrum of naphthalene and naphthalene derivatives **74** and **78** recorded in cyclohexane at room temperature at a  $1.3 \times 10^{-5}$  M concentration.

It is important to note that the second band might correspond to the absorption produced in the phosphindole core, since they contain heteroatoms and double bonds that can undergo  $n \rightarrow \pi^*$  and  $\pi \rightarrow \pi^*$  transitions. Figure 2.27 shows a visible shoulder at around 400-450 nm which can be also explained by the presence of the new phosphindole core and its electronic transitions.

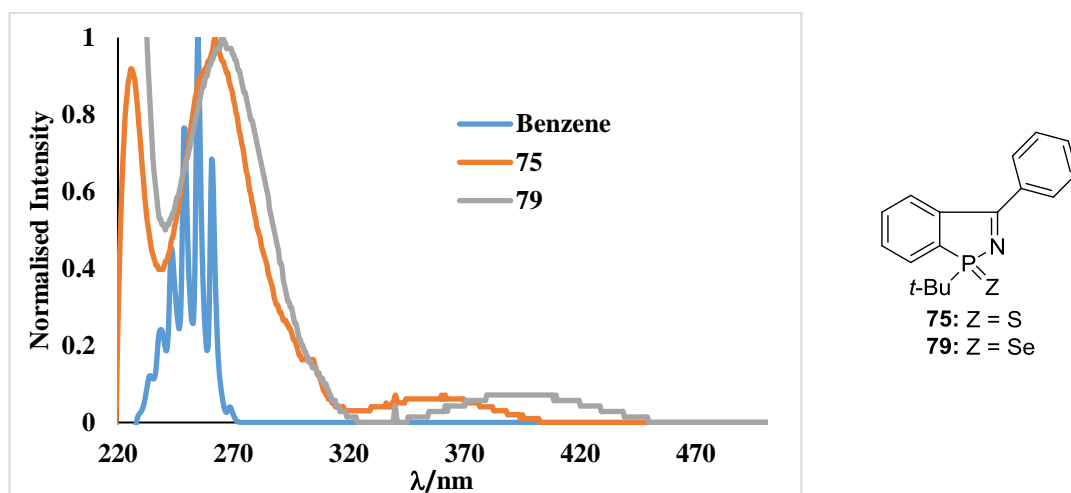


Figure 2.27 Absorption spectrum of benzene and benzene derivatives **75** and **79** recorded in cyclohexane at room temperature at a  $2.8 \times 10^{-4}$  M concentration.

The absorption spectrum of benzene shows well defined bands at around 220-270 nm. The novel compounds **75** and **79** produced broad bands at around 230-320 nm which suggests the absorption produced by the phenyl ring contained in them absorbs at a longer wavelength. As with the other compounds, it is possible to observe a second band that is attributed to the novel phosphindole core. When comparing the different absorption spectra for the compounds **73-79**, it is clear that the band we assumed is produced by the phosphindole absorbs at the same wavelength, around 350-400 nm. Benzene is the PAH with the least extended aromaticity; therefore, its HOMO-LUMO gap is higher which makes it to require more energy to absorb a photon.

Molecule	HOMO (eV)	LUMO (eV)	$\Delta E$ (eV)
Benzene	-6.7	0.1	6.8
Naphthalene	-5.8	-1.0	4.8
Anthracene	-5.2	-1.6	3.6

Table 2.6 HOMO and LUMO energies of anthracene, naphthalene and benzene calculated at the B3LYP/6-31G\* level of theory.

Anthracene is the PAH with the highest extended aromaticity which makes the opposite effect occur, allowing it to absorb photons with a less energetic wavelength. There are no differences in the phosphindole core of the different compounds which suggests that there should not be any difference in its HOMO-LUMO gap and absorption wavelength. Table 2.6 shows the DFT-calculated values for the HOMO-LUMO gaps of the PAHs.

### 2.5.2 Quantum yield

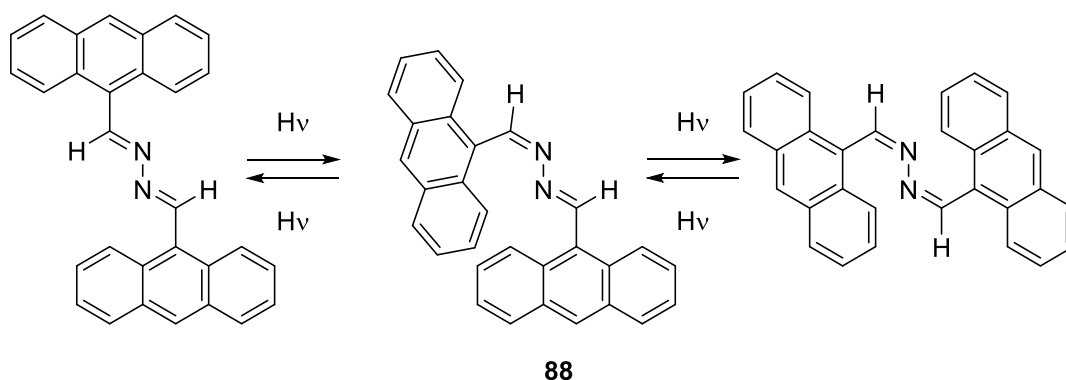
The measurement of the photophysical properties of the novel compounds showed that their fluorescence quantum yields were quenched. The reference used in each case was the fluorophore itself, so for compounds **73**, **76** and **77** the reference used was anthracene. For **74** and **78** naphthalene was used, and benzene was used for **75** and **79**. In order to prove that the quenching was not due to a solvent effect, photophysical measurements were performed in solvents with varying polarities.

Table 2.7 demonstrates that the fluorescence of compounds **73-79** is virtually 0. It is also possible to ascertain that the solvent effect does not improve the quantum yields, even though the solvents used here have a wide range of polarities. This must be related to the fact that the fluorophore group of the molecules synthesised are not polar enough to interact with the molecules of polar solvents. The solvent effect can have a dramatic influence on emission spectra when the fluorophore is highly polar.<sup>207, 208</sup>

Compound	$\Phi_F$ in:			
	Cy	DCM	MeOH	MeCN
<b>73</b>	$54 \times 10^{-5}$	0	$41 \times 10^{-5}$	0
<b>74</b>	0	0	$30 \times 10^{-4}$	$41 \times 10^{-5}$
<b>75</b>	$26 \times 10^{-5}$	0	$14 \times 10^{-5}$	$2 \times 10^{-5}$
<b>76</b>	$45 \times 10^{-3}$	0	$13 \times 10^{-3}$	0
<b>77</b>	$31 \times 10^{-4}$	$96 \times 10^{-5}$	$28 \times 10^{-4}$	$17 \times 10^{-5}$
<b>78</b>	$54 \times 10^{-3}$	$19 \times 10^{-3}$	$23 \times 10^{-3}$	$50 \times 10^{-3}$
<b>79</b>	0	0	$20 \times 10^{-4}$	$23 \times 10^{-5}$

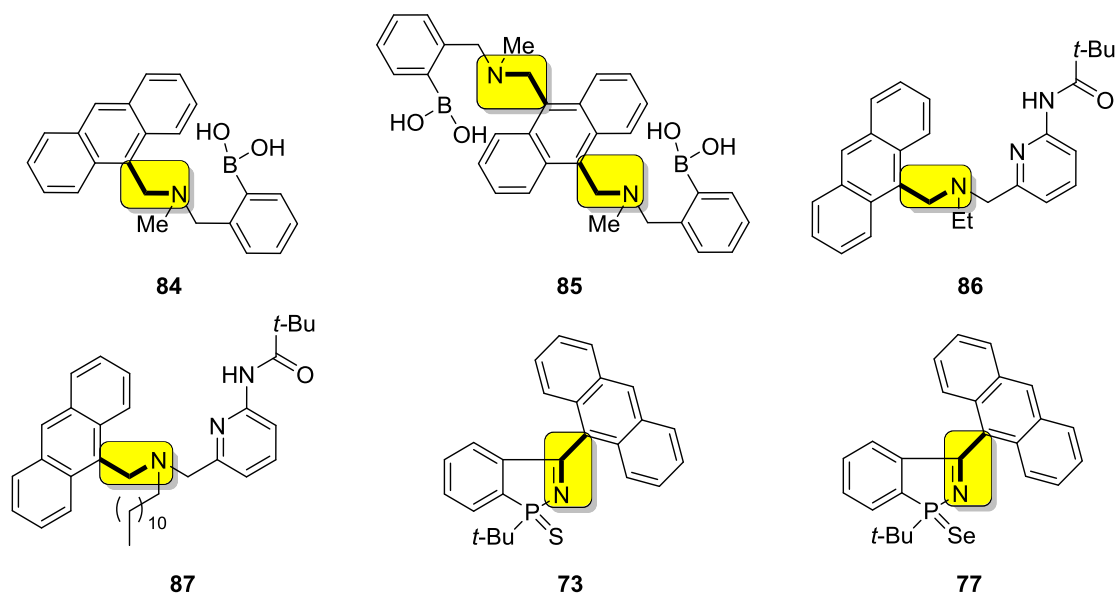
**Table 2.7** The quantum yield values of compounds **73-79** obtained in cyclohexane, dichloromethane, methanol and acetonitrile solvents. Measurements were performed in dry degassed solvents at room temperature.

It has been reported that the interconversion of 9-anthraldehyde azine **88** into its isomers results in low quantum yield (Figure 2.28).<sup>209</sup> The interconversion in the **73-79** systems is not possible due to the fact that the imine group forms part of a five-membered ring. This forms a highly restrained framework where exchange of substituents on the imine double bond is highly unlikely without first breaking the five membered ring of the phosphindole core. Therefore, although the electronic environment is more similar, this explanation does not satisfy this particular system.



**Figure 2.28** 9-Anthraldehyde azine **88** and the isomerization that leads to a decrease in fluorescence.

Compounds **73-79** contain an imine group and a chalcogenide atom. Both groups could act as donors and produce Photoinduced Electron Transfer (PeT), a process that has been detailed in Section 1.4.1. It is proposed that the lack of fluorescence in compounds **73-79** might be due to this phenomena since the PAH moieties can act as acceptors and the lone pair of electrons on the nitrogen atom can act as a donor. Shinkai *et al.*<sup>210</sup> have reported that the fluorescent sensors **84** and **85** whose fluorescence is quenched by the pair of electrons of its benzylamine moiety. Ghosh *et al.*<sup>211</sup> synthesised **86** and **87**, which are anthracenyl-containing compounds that contained a benzylamine which dramatically decreased their quantum yields. The addition of an organic acid to a solution of these compounds increased their quantum yields. The structure is similar to compounds **73** and **77**. However, the main difference is that, in the case of **73** and **77**, the electron donor is an imine, not an amine as shown in Figure 2.29.



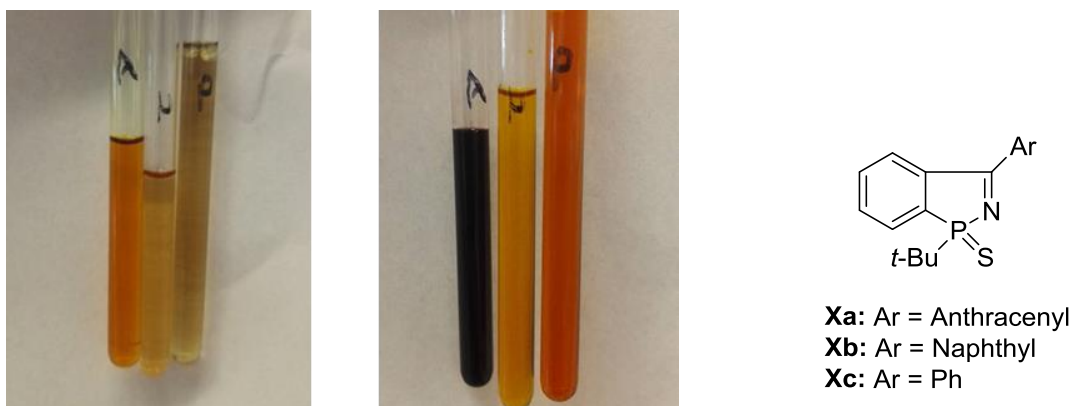
**Figure 2.29** Compounds **73** and **77** compared to previously reported analogous compounds that experience PeT.

The electronic environment of Shinkai and Ghosh's amines and the novel compounds **73-79** reported here are quite different. Compound more similar to **73-79** would better explain the behaviour of their fluorescence.

In the literature there are many examples of molecules containing anthracene with a benzylic amine<sup>212-216</sup> or imine,<sup>217, 218</sup> quenching the fluorescence of the molecule via a PeT effect. These types of molecules are commonly used as sensors that increase their fluorescence when the nitrogen atom in the amine or imine group is no longer able to act as a PeT donor. Therefore, this mechanism could be a candidate to explain the fluorescence quenching suffered by compounds **73-79**.

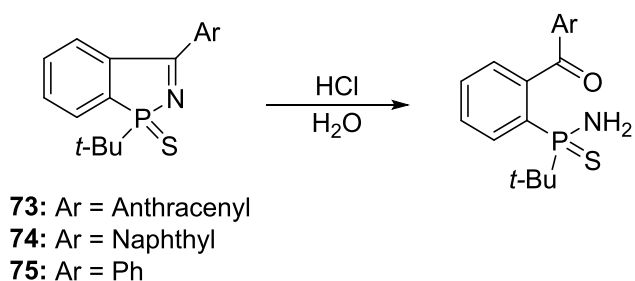
The protonated form of the compounds should be free of PeT effects if they exist. Compounds **73-75** were therefore dissolved in methanol and citric acid was added to the resulting solution. However, the solutions proved to be non-fluorescent under the UV light. This might not necessarily mean that the PeT did not cause this fluorescence quenching, since the citric acid might not have been strong enough to protonate the imine. Therefore, hydrochloric acid was added (The pKa in water of the different protons in citric acid is 3.13, 4.76 and 6.39 whereas for hydrochloric acid the value is -6.13). Unfortunately, the result regarding fluorescence quenching was the same as with citric acid. However, the colour of the solutions did change. It is noticeable that compounds **73** and **74** were more affected than compound **75**. The lack of fluorescence in these solutions

suggests that the lone pair of electrons in the phosphindole core is not producing a quenching effect by PeT. However, the change of colour supports the idea that the imine is involved in the absorption of these compounds providing an  $n \rightarrow \pi^*$  transition.



**Figure 2.30** Left: Compounds 73, 75 and 74 (in that order) in a solution with  $\text{CDCl}_3$ . Right: Compounds 73, 75 and 74 in  $\text{CDCl}_3$  after the addition of 0.1 ml of 2 M solution of HCl in ethereal HCl.

Imines can be hydrolysed in acidic conditions;<sup>219</sup> therefore, it was a concern that the change of colour in the solution was due to a change in the molecular structure of compounds 73-75.



**Figure 2.31** Possible product from hydrolysis of the imine in compounds 73-75.

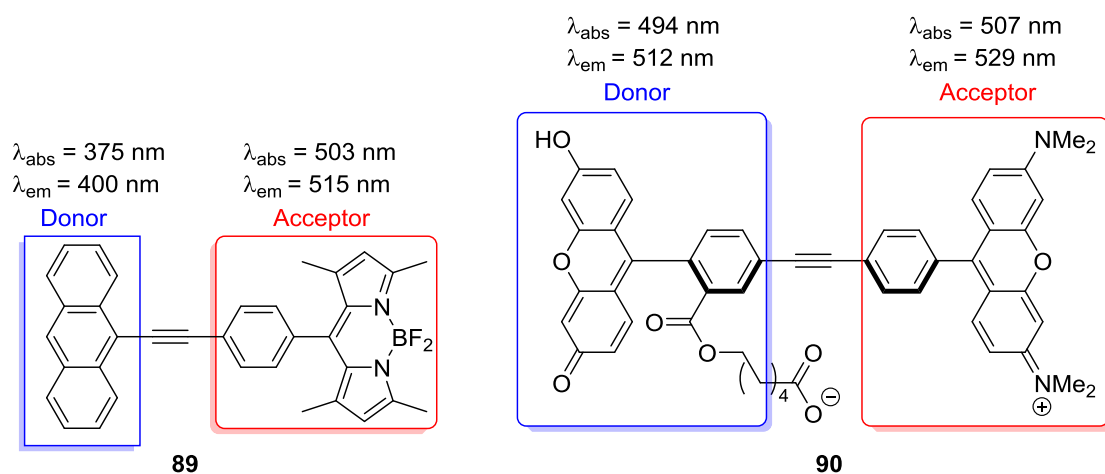
However, this possibility seems unlikely due to the stability provided by the aromaticity of the phosphindole core. NMR spectroscopy demonstrated that there was no formation of a new product. The  $^{31}\text{P}\{^1\text{H}\}$  NMR showed that the compounds retained the same chemical shift for the phosphorus atom as before addition of the acid.  $^{13}\text{C}\{^1\text{H}\}$  NMR spectra of the compounds showed the same signal for the carbonyl of the imine which was definitive proof that the imine was unaffected (Table 2.8).

Compound	$\delta$ C=N (ppm)	$\delta$ P (ppm)
<b>73</b>	182.2 (d, $^2J_{CP} = 8.4$ Hz)	107.8
<b>73 + HCl</b>	181.5 (d, $^2J_{CP} = 7.9$ Hz)	106.7
<b>74</b>	181.1 (d, $^2J_{CP} = 8.3$ Hz)	106.3
<b>74 + HCl</b>	181.3 (d, $^2J_{CP} = 8.3$ Hz)	105.8
<b>75</b>	180.0 (d, $^2J_{CP} = 7.2$ Hz)	104.6
<b>75 + HCl</b>	181.2 (d, $^2J_{CP} = 4.2$ Hz)	101.8

**Table 2.8** C=N signal in  $^{13}\text{C}\{^1\text{H}\}$  NMR and P signal in  $^{31}\text{P}\{^1\text{H}\}$  NMR. The chemical shifts were constant for compounds **73-75** before and after the addition of ethereal HCl.

The presence of the imine is proven by the lack of C=N shift; therefore, the results suggest that the change of colour is a pH-dependant bathochromic shift. This experiment proved that the PeT mechanism seems a weak explanation for the fluorescence quenching of compounds **73-79**.

Another explanation for the fluorescence quenching of compounds **73-79** can be given by the Dexter electron transfer process. As was described in Section 1.4.1, short separations between chromophores and chromophores arranged orthogonally aligned to each other favour this fluorescence quenching process. The X-ray analysis of the crystal structures of compounds **73-79** shows this kind of spatial disposition; however, the crystal structures do not necessarily represent the behaviour of the molecule in solution. In this type of molecules where two fluorophores are attached via covalent bonds, the donor is the fluorophore that absorbs at the shorter wavelength, whereas the acceptor is the moiety that absorbs at higher wavelength. Figure 2.32 depicts examples of compounds with these features. Compound **89** contains anthracene and a BODIPY analogue. In this compound, anthracene donates the energy received when excited to the BODIPY moiety and this releases the energy in the form of photons. This molecule has a large Stokes shift which is necessary to avoid self-quenching.<sup>55</sup> In compound **90** Fluorescein is the donor and Rhodamine 123 is the acceptor.



**Figure 2.32** Anthracene- BODIPY (89)<sup>55</sup> and Fluorescein-Rhodamine 123 (90)<sup>56</sup>. The dye with the shorter  $\lambda_{\text{abs}}$  wavelength works as the donor and the dye with the longest  $\lambda_{\text{abs}}$  works as the acceptor.

Taking in account the Dexter electron transfer effect, DFT calculations (calculated at the B3LYP/6-31G\* level of theory) were carried out in order to compare the HOMO-LUMO orbitals of the PAHs contained in compounds **73-79** with the novel phosphindole cores synthesised (Figure 2.33). The results showed that all of the PAHs have higher LUMO energies than those in the novel phosphindole cores. Therefore, it is sensible to propose that Dexter electron transfer is occurring in compounds **73-79** since the distance separating the two aromatic moieties is one C–C bond. In addition, the LUMO energies suggest that it is possible that after the electronic system of the PAHs become excited, the energy is transferred to the LUMO of the corresponding phosphindole core. However, this energy is not released as photons but in other forms of decay such as vibration of the moiety or heat. Therefore, the fluorescence quenching might occur due to the intrinsic lack of fluorescence in the phosphindole core despite the chalcogen atom contained in it (O, S or Se). Figure 2.33 shows the HOMO and LUMO surfaces calculated using DFT at the B3LYP/6-31G\* level of theory. The phosphindole cores synthesised in this work contained S and Se; however, in order obtain a better explanation, the O analogue was calculated as well.



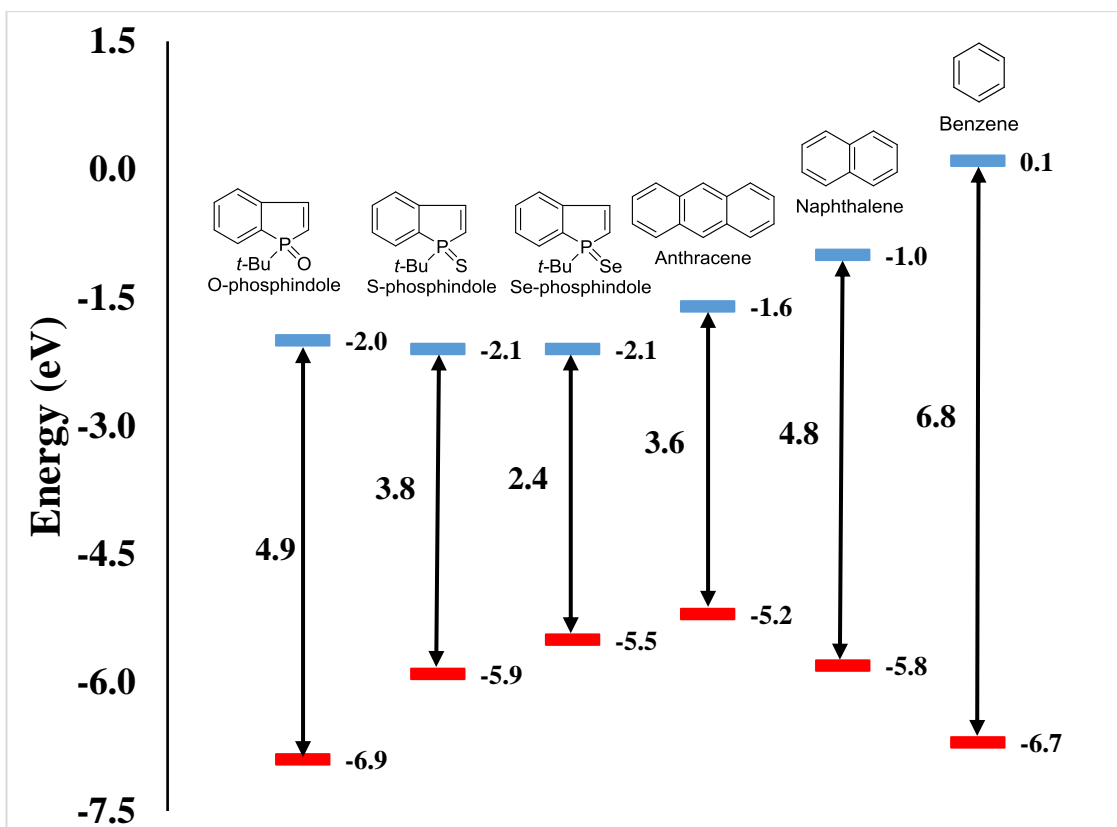
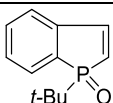
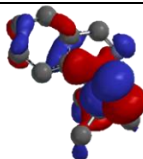
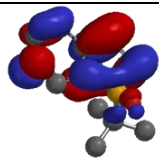
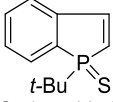
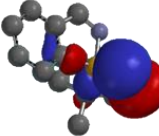
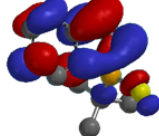
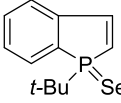
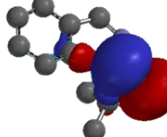
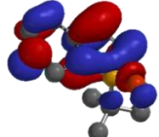
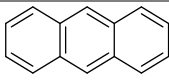
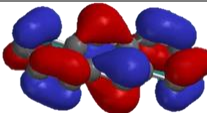
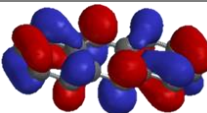
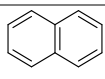
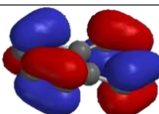
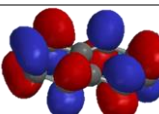
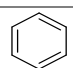

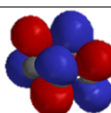
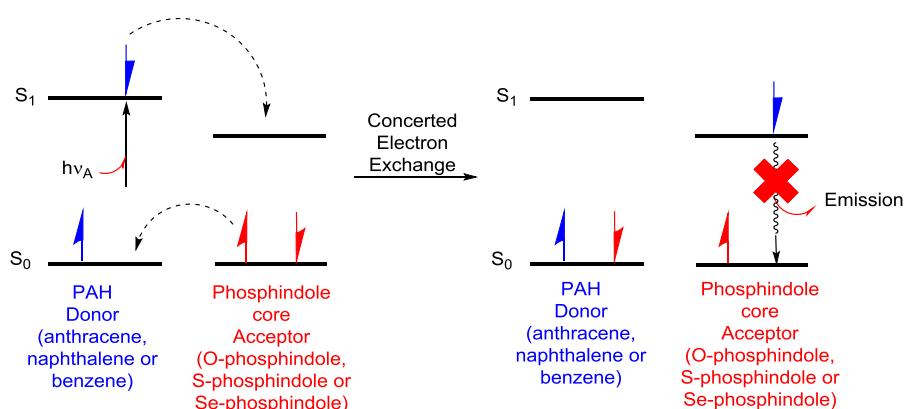


Figure 2.33 HOMO and LUMO energies obtained using DFT calculations (calculated at the B3LYP/6-31G\* level of theory).

Figure 2.33 also shows the effect exerted on the HOMO by the chalcogenides on the phosphindole core. The size of these HOMO energies decreases in the order of O-phosphindole < S-phosphindole < Se-phosphindole. The LUMO energies do not seem to be as affected for the different chalcogenides as the HOMO energies. It is important to highlight that the O-phosphindole core also has lower LUMO than any of the PAHs (anthracene, naphthalene or benzene); therefore, it is highly probable that the oxide version of the novel phosphindoles **73-79** would be non-fluorescent as well since the Dexter electron transfer could also occur, according to the DFT calculations of HOMO energies (Table 2.9). Figure 2.34 depicts the electron exchange proposed for explaining the fluorescence quenching of compounds **73-79** based on the theory of Dexter electron transfer process.

Compound	HOMO	LUMO
 $t\text{-Bu}$ -O-phosphindole		
 $t\text{-Bu}$ -S-phosphindole		
 $t\text{-Bu}$ -Se-phosphindole		
 Anthracene		
 Naphthalene		
 Benzene		

**Table 2.9** HOMO and LUMO surfaces of the different aromatic moieties present in compounds 73-79 (calculated at the B3LYP/6-31G\* level of theory).



**Figure 2.34** Graphical interpretation of the fluorescence quenching provoked by the Dexter electron transfer process.

## 2.6 Biological activity of the novel synthesised phosphindazoles

As mentioned previously in Section 2.1.1 (Figure 2.5), indazole-containing compounds have shown biological activity. The antibiotic activity of the compounds prepared by

Zhang *et al.*<sup>162</sup> gave us impetus to measure the biological activity of the novel phosphindoles presented in this work. Therefore, it was decided to measure the Minimum Inhibitory Concentration (MIC) of these compounds.

### **2.6.1 Determination of Minimum Inhibitory Concentration (MIC)**

In the next section, different procedures for defining the susceptibility of bacterial pathogens to compounds **73**, **76** and **80** are presented. Quantitative *in vitro* determinations are usually expressed as the MIC. This measures the lowest concentration of a compound that inhibits the growth of the microbiological agent being tested.<sup>220</sup> The MIC of compounds **73**, **76** and **80** was determined by the agar diffusion test (Kirby–Bauer antibiotic testing), which tests the antibiotic sensitivity of bacteria. It was performed by impregnating paper wafers with solutions of different concentrations of the compounds of interest, dissolved in DMSO, to test the extent to which the bacteria were affected by them. Impregnated wafers were placed on a blood agar plate onto which bacteria were inoculated, and the plate was left to incubate at 35°C overnight. The aim of this test is to determine the compound concentration that inhibits microbial growth on the plate by measuring the zone that is free of bacteria after incubation – this is called the zone of inhibition.

The concentrations used were 0, 1, 2, 4, 8, 16, 32, 64, 128 and 256 mg/L. The first concentration is used as baseline, in order to assure that the effect seen is not due to the solvent (in this case DMSO which was used to dissolve the compound). A compound with a higher MIC is not as potent against that particular microorganism compared to a compound with a lower MIC value.

<b>Group</b>	<b>Bacteria</b>	<b>73</b>	<b>76</b>	<b>80</b>
<b>Gram-negative Bacteria</b>	<i>Acinetobacter baumannii</i>	>256	>256	>256
	<i>Burkholderia cepacia</i>	>256	>256	>256
	<i>Enterobacter cloacae</i>	>256	>256	>256
	<i>Escherichia coli</i>	>256	>256	>256
	<i>Klebsiella pneumoniae</i>	>256	>256	>256
	<i>Providencia rettgeri</i>	>256	>256	>256
	<i>Pseudomonas aeruginosa</i>	>256	>256	>256
	<i>Salmonella typhimurium</i>	>256	>256	>256
	<i>Serratia marcescens</i>	>256	>256	>256
	<i>Yersinia enterocolitica</i>	>256	>256	>256
<b>Gram-positive Bacteria</b>	<i>Bacillus subtilis</i>	>256	>256	<b>8</b>
	<i>Enterococcus faecalis</i>	>256	>256	<b>128</b>
	<i>Enterococcus faecium</i>	>256	>256	>256
	<i>Listeria monocytogenes</i>	>256	>256	<b>128</b>
	<i>Staphylococci epidermidis</i>	>256	>256	<b>32</b>
	<i>Staphylococcus aureus</i>	>256	>256	<b>16</b>
	<i>Staphylococcus aureus (MRSA)</i>	>256	>256	<b>32</b>
	<i>Streptococcus pyogenes</i>	>256	>256	<b>4</b>
<b>Yeasts</b>	<i>Candida albicans</i>	>256	>256	<b>128</b>
	<i>Candida glabrata</i>	>256	>256	<b>256</b>

**Table 2.10 Results of the Kirby Bauer test to determine MIC of bacteria to compounds 73, 76 and 80. Concentrations given in mg/L.**

Table 2.10 shows that compounds **73** and **76** did not inhibit the growth of any microorganisms; however, compound **80** was effective in this regard. The best result for

**80** was against *Bacillus subtilis* and *Streptococcus pyogenes*, the latter being a pathogenic microorganism<sup>221</sup> that has shown antibiotic resistance to tetracycline in the past.<sup>222</sup>

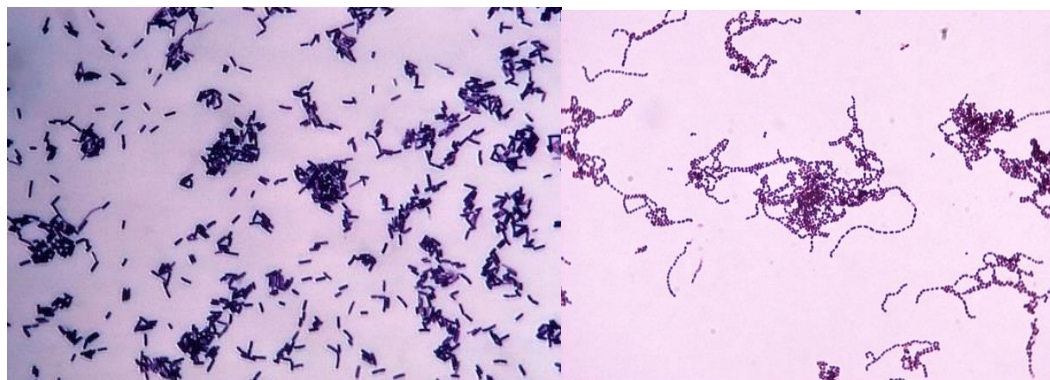
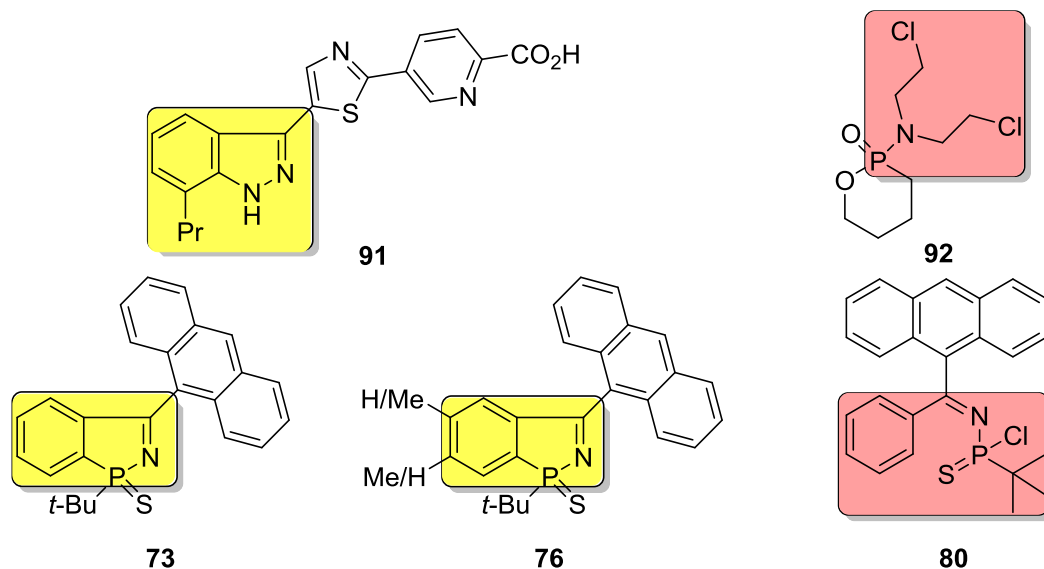


Figure 2.35 Left: *Bacillus subtilis*. Right: *Streptococcus pyogenes*

Zhang<sup>162</sup> synthesised nearly 40 different compounds to obtain the promising bacterial gyrase B inhibitor **91**. This compound was most effective against *Staphylococcus aureus* and *Streptococcus pneumoniae* with a MIC = 0.06  $\mu\text{g/ml}$  (or  $0.06 \text{ mg/mL} \times 10^{-3}$ ) for both. Compound **80** showed activity against *Staphylococcus aureus* with a MIC = 16  $\text{mg/mL}$ ; it is visibly less potent than compound **91**. Their mechanism of action must be different since compound **80** does not contain a similar core to the indazole in **91**. However, the results obtained for compounds **73** and **76** do not necessarily mean that the novel phosphindole core does not have biological activity against microorganisms. As the research carried out by Zhang<sup>162</sup> showed, the absorption of the core inside the bacteria is quite important; therefore, in order to assure that the phosphindole core does not exert any antibiotic activity, it would be necessary to create analogues with different lipophilic values and compare their results. To our knowledge, there are no examples of reported antibiotic activity of similar compounds to phosphonamidothioic chloride **80** containing P–N, P= S and P–Cl bonds as in the compound presented here. It could be argued that its activity might come from the chloride atoms, since Cl is a good leaving group, as in the case of different alkylating agents used in chemotherapy such as cyclophosphamide **92**.<sup>223</sup> However, current alkylating agents contain a C–Cl bond, not a P–Cl bond; therefore, a direct comparison of the biological activity of phosphonamidothioic chlorides reported to **80** is not feasible at this point.



**Figure 2.36** Structure of bacterial gyrase B inhibitor **91** developed by Zhang compared with the novel compounds **73** and **76**. The core phosphindole core in phosphonamidothioic chloride **80** is clearly lost; therefore its antibiotic activity might be related to its P–Cl bond as in the case of the anticancer agent cyclophosphamide **92**.

## 2.7 Summary

Seven novel phosphindoles **73-79** were successfully synthesised. They contain a novel core that resembles the one found in the natural product indazole, with phosphorus in the position of nitrogen in the natural product. The starting material for this synthesis was zirconocene dichloride, which is a metallocene that contains zirconium as the central metal. Using Grignard reagents, it was possible to create two Zr–aryl bonds from which a benzyne intermediate could be formed. Benzyne has a biradical character, demonstrating a highly reactive nature.<sup>224</sup> The benzyne formation, from compounds **67** and **68**, allowed the addition of aromatic rings, anthracene, naphthalene and benzene, in the 3-position of the ring that were later transformed into the azaphosphindole core. Addition of the corresponding nitriles (9-anthracenecarbonitrile, 1-cyanonaphthalene or benzonitrile) led to the formation of the azazirconocycles **69-72**, which were then reacted with *tert*-butyl dichlorophosphine to give the phosphindoles **73-79**.

Phosphindole **76a/b** exists as a mixture of regioisomers that are formed due to the nature of the benzyne adduct, which is a highly reactive transition state. The coupling of the benzyne adduct of the zirconacycle **68** with 9-anthracenecarbonitrile allows for two different spatial rearrangements to be adopted (Figure 2.17), which explains the outcome of two different regioisomers, whose NMR data proved that the formation occurred after

the coupling of the 9-anthracenecarbonitrile. Finally, the substitution of zirconocene in the five-membered ring using the sterically hindered *tert*-butyl dichlorophosphine as the electrophile and its further oxidation with the chalcogenides, sulfur and selenium, led to the synthesis of compounds **73-79**. Temperature was found to be a key variable in the last step since a temperature below 110 °C led to the formation of chlorothiophosphonates **80** and **81a/b** where the  $\sigma$ -bond between the phosphorus atom and the benzene ring never formed.

Furthermore, spectroscopic analysis of compounds **73-79** showed that their quantum yields were virtually zero. Different hypotheses were tested in order to elucidate why the quantum yields of these molecules displayed such a dramatic drop. The distance between the phosphindole core and the corresponding PAH (a C–C bond) in compounds **73-79** suggests that the possible mechanism is Dexter electron transfer. This mechanism usually takes place in compounds containing two different dyes. One dye acts as the donor of an electron and the other one as the acceptor. The LUMO energies calculated using DFT of the PAHs and different phosphindole cores (Figure 2.33) shows that the LUMO energies of the PAHs is higher than those of the phosphindole cores. This suggests that the Dexter electron transfer is energetically possible, and that this data could mean that compounds **73-79** absorb the energy from light in the PAH moiety. The energy promotes an electron in the PAH orbital from a ground state to an excited state, and the electron is then transferred to the excited state of the acceptor phosphindole core, which in turn transfers an electron from its ground state to the ground state of the donor PAH. When the transferred electron returns to the ground state of the phosphindole, there is no emission due to loss of energy in the other routes but by simple emission (such as vibration or heat). This would mean that the phosphindole moiety is intrinsically non-fluorescent.

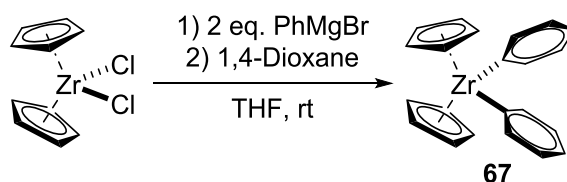
The antibiotic activity demonstrated by the indazole analogues<sup>162</sup> led us to test the antibiotic activity of compounds **73**, **76** and **80** using the Kirby–Bauer antibiotic test. The results showed that the phosphindoles **73** and **76** did not exhibit any antibiotic activity; however, the phosphonamidothioic chloride **80** showed activity against *Bacillus subtilis* and *Streptococcus pyogenes*. Comparison with the reported bacterial gyrase B inhibitor **91** showed that both compounds have activity against *Staphylococcus aureus* but this does not provide a useful comparison for **80** since it is not chemically related to the indazole **91**, whereas **73** and **76** are related by the phosphindole core.

## 2.8 Experimental

### 2.8.1 General Procedure

All air- and/or water-sensitive reactions were performed under a dinitrogen atmosphere using standard Schlenk line techniques. Tetrahydrofuran and toluene were dried over sodium/benzophenone and sodium respectively and distilled prior to use. Toluene and petrol used for column chromatography were used as received from the supplier. All starting materials were purchased from Aldrich, Acros Organics, Alfa Aesar or Strem and used as received. Compound **67**<sup>178</sup> was prepared according to literature procedures. Flash chromatography was performed on silica gel from Fluorochem (silica gel, 40-63u, 60A). Thin-layer chromatography was carried out on Fisher aluminium-based plates with silica gel and fluorescent indicator (254 nm). Melting points were determined in open glass capillary tubes on a Stuart SMP3 melting point apparatus. <sup>1</sup>H, <sup>13</sup>C{<sup>1</sup>H} and <sup>31</sup>P{<sup>1</sup>H} NMR spectra were recorded on a JEOL ECS-400 (<sup>1</sup>H 399.78 MHz) spectrometer at room temperature (21 °C); <sup>1</sup>H and <sup>13</sup>C shifts were relative to tetramethylsilane, <sup>31</sup>P relative to 80% H<sub>3</sub>PO<sub>4</sub>. Infrared spectra were recorded on a Varian 800 FT-IR spectrometer. UV-Vis absorption and emission spectra were recorded on a UV-1800 Shimadzu spectrophotometer and RF-6000 Shimadzu spectrofluorometer respectively. Mass spectrometry was carried out by the EPSRC National Mass Spectrometry Service Centre, Swansea.

### 2.8.2 Diphenyl zirconocene **67**

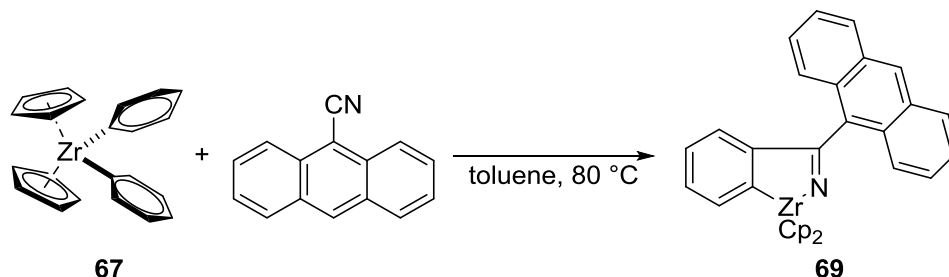


Zirconocene dichloride (1.00 g, 3.42 mmol) was dissolved in THF (10 mL); a solution of phenyl magnesium bromide (2.3 mL, 6.84 mmol) was then added dropwise, giving a transparent brown solution. The reaction was left for 20 minutes and then anhydrous dioxane (1.75 mL, 20.52 mmol) was added dropwise. The solution turned into a suspension containing a white solid in a yellow solution. After 15 hours, the solvent was evaporated and the solid was dissolved again using anhydrous toluene (25 mL). The suspension was then filtered under dinitrogen through a fritted funnel, using a cannula. The yellow obtained solution was then dried under reduced pressure to give a yellow solid (1.02 g, 80%). **MP**: 150.0 °C. **<sup>1</sup>H NMR** (400 MHz, CDCl<sub>3</sub>)  $\delta$  7.31 (d, <sup>3</sup>J<sub>HH</sub> = 7.5 Hz, 4H),



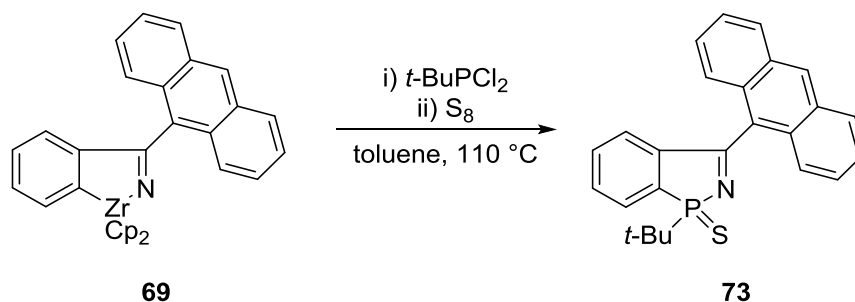
7.18-7.13 (m, 4H), 7.07 (t,  $^3J_{\text{HH}} = 7.8$  Hz, 2H), 6.22 (s, 10H) ppm.  $^{13}\text{C}\{^1\text{H}\}$  NMR (100 MHz,  $\text{CDCl}_3$ )  $\delta$  182.9, 135.8, 126.6, 125.4, 112.3 ppm, **IR** (neat):  $\tilde{\nu} = 3062$  (w), 2214 (s), 1446 (s), 1015 (s), 600 (s), 731 (s)  $\text{cm}^{-1}$ .

### 2.8.3 3-Anthracen-9-yl-(phenyl-azazirconacyclopentene) **69**



Diphenyl zirconocene (2.16 g, 5.73 mmol) was dissolved under dinitrogen in anhydrous toluene (40 mL). The yellow solution then had the corresponding nitrile 9-cyanoanthracene (1.15 g, 5.73 mmol) added to it. The resulting brown suspension was heated to 80 °C and left to react overnight. After that period the reaction was left to cool down to room temperature. The suspension was finally filtered through a fritted funnel using a cannula under dinitrogen, obtaining a brown solid (0.71 g, 25%). **MP**: 147.5 °C.  $^1\text{H}$  NMR (400 MHz,  $\text{CDCl}_3$ )  $\delta$  8.59 (s, 1H), 8.07 (d,  $^3J_{\text{HH}} = 7.6$  Hz, 2H), 7.68 (d,  $^3J_{\text{HH}} = 7.6$  Hz, 1H), 7.59-7.47 (m, 6H), 7.28 (d,  $^3J_{\text{HH}} = 7.1$  Hz, 1H), 6.80 (d,  $^3J_{\text{HH}} = 7.1$  Hz, 1H), 6.76 (d,  $^3J_{\text{HH}} = 7.4$  Hz, 1H), 6.22 (s, 10H) ppm.  $^{13}\text{C}\{^1\text{H}\}$  NMR (75 MHz,  $\text{CDCl}_3$ )  $\delta$  190.8, 144.4, 141.0, 131.2, 131.1, 130.4, 130.3, 129.1, 129.0, 128.9, 128.6, 127.3, 125.8, 124.9, 124.8, 123.9, 111.0, 110.9 ppm. **IR** (neat):  $\tilde{\nu} = 3052$  (w), 2214 (s), 1589 (w), 1446 (s), 1015 (s), 731 (s), 695 (s)  $\text{cm}^{-1}$ .

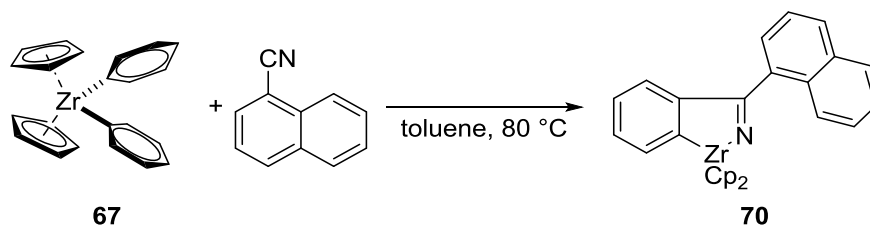
### 2.8.4 3-Anthracen-9-yl-((1-*tert*-butyl)-1-sulfide-1H-1,2-azaphosphindole) **73**



The organophosphorus compound *tert*-butyl dichlorophosphine (0.81 g, 5.13 mmol) was added to a refluxing solution of 3-anthracen-9-yl-(phenyl-azazirconacyclopentene) (**69**) (2.56 g, 5.13 mmol) in anhydrous toluene (50 mL) under dinitrogen. After 3 hours, sulfur (0.32 g, 10.56 mmol) was added to the black mixture which was stirred for another hour

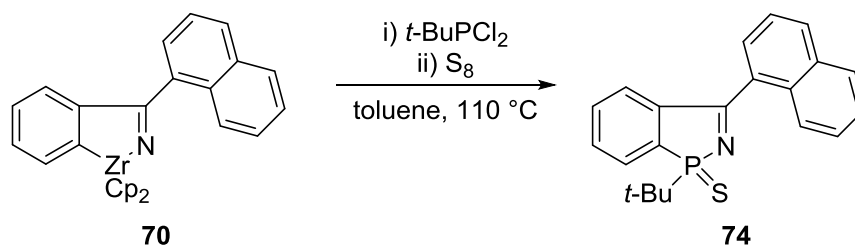
during this time, the reaction was monitored by  $^{31}\text{P}$  NMR. The mixture cooled to room temperature and the solvent evaporated. The resulting mixture was purified using column chromatography (petrol/toluene 1:1,  $R_f = 0.5$ ). The product was a bright yellow solid (0.66 g, 33%). A sample suitable for X-ray crystallographic analysis was obtained from toluene. **MP**: 91.8 °C.  **$^1\text{H}$  NMR** (300 MHz,  $\text{CDCl}_3$ )  $\delta$  8.53 (s, 1H), 8.01 (d,  $^3J_{\text{HH}} = 8.6$  Hz, 1H), 7.98-7.90 (m, 3H), 7.58-7.48 (m, 2H), 7.42-7.35 (m, 3H), 7.32-7.24 (m, 2H), 6.85 (d,  $^3J_{\text{HH}} = 7.8$  Hz, 1H), 1.38 (d,  $^3J_{\text{HP}} = 17.6$  Hz, 9H) ppm.  **$^{13}\text{C}\{^1\text{H}\}$  NMR** (75 MHz,  $\text{CDCl}_3$ )  $\delta$  182.2 (d,  $^2J_{\text{CP}} = 8.4$  Hz), 155.0, 141.7 (d,  $J_{\text{CP}} = 26.5$  Hz), 139.5, 138.9, 131.3, 130.9 (d,  $J_{\text{CP}} = 8.1$  Hz), 129.7, 129.0, 128.3, 128.1, 127.9 (d,  $J_{\text{CP}} = 6.3$  Hz), 127.5, 126.7 (d,  $J_{\text{CP}} = 20.1$  Hz), 126.4, 125.5, 125.3 (d,  $J_{\text{CP}} = 12.1$  Hz), 124.8, 124.2 (d,  $J_{\text{CP}} = 15.9$  Hz), 123.9, 119.0, 34.4 (d,  $^1J_{\text{CP}} = 59.0$  Hz), 23.7 ppm.  **$^{31}\text{P}\{^1\text{H}\}$  NMR** (121 MHz,  $\text{CDCl}_3$ )  $\delta$  107.8 ppm. **IR** (neat):  $\tilde{\nu} = 2972$  (w), 2256 (w), 1980 (w), 1676 (s), 1531 (s), 1286 (s), 1131 (s), 889 (s), 734 (s), 685 (s)  $\text{cm}^{-1}$ . **HRMS** (ESI $^+$ ) exact mass calcd. for  $\text{C}_{25}\text{H}_{23}\text{N}_1\text{P}_1\text{S}_1$   $[\text{M}+\text{H}]^+$  requires  $m/z$  400.1289, found  $m/z$  400.1289 (0.1 ppm).

### 2.8.5 3-Naphthalen-1-yl-(phenyl-azazirconacyclopentene) 70



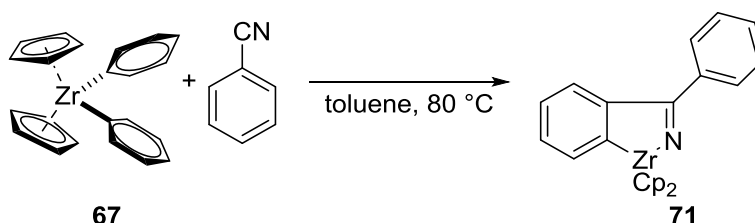
Diphenyl zirconocene (1.93 g, 5.13 mmol) was dissolved under dinitrogen in anhydrous toluene (40 mL) resulting in a yellow transparent solution and 1-cyanonaphthalene (0.78 g, 5.13 mmol) was then added. The resulting brown suspension was heated to 80 °C and left to react overnight. After that period the reaction was left to cool down to room temperature. The suspension was then filtered through a fritted funnel using a cannula under dinitrogen, obtaining a brown solid (0.71 g, 25%). **IR** (neat):  $\tilde{\nu} = 3059$  (w), 2959 (w), 1724 (m), 1593 (m), 1505 (s), 1275 (s), 1017 (s), 795 (s)  $\text{cm}^{-1}$ .

### 2.8.6 3-Naphthalen-1-yl-((1-*tert*-butyl)-1-sulfide-1H-1,2-azaphosphindole) 74



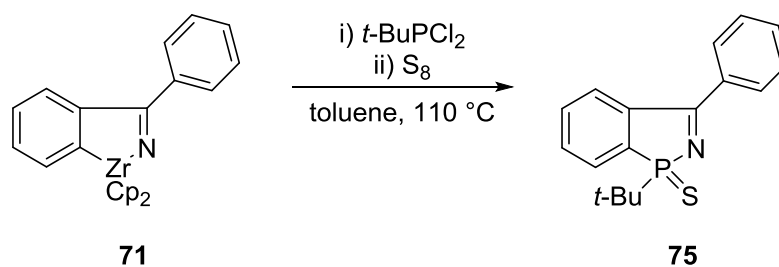
The organophosphorus compound *tert*-butyl dichlorophosphine (0.81 g, 5.13 mmol) was added to a refluxing solution of 3-naphtalen-1-yl-(phenyl-azazirconacyclopentene) (**70**) (2.31 g, 5.13 mmol) in anhydrous toluene (50 mL) under dinitrogen. After 3 hours, sulfur (0.32 g, 10.56 mmol) was added to the black mixture which was stirred for another hour during this period, the reaction was monitored by  $^{31}\text{P}$  NMR spectroscopy. The mixture cooled to room temperature and the solvent evaporated. The resulting mixture was purified using column chromatography (petrol/toluene 3:1,  $R_f = 0.4$ ). The product was a pale yellow solid (0.71 g, 40%). A sample suitable for X-ray crystallographic analysis was obtained from toluene. **MP**: 101.3 °C.  $^1\text{H}$  NMR (300 MHz,  $\text{CDCl}_3$ )  $\delta$  7.59-7.75 (m, 4H), 7.57 (d,  $^3J_{\text{HH}} = 7.1$  Hz, 1H), 7.51-7.29 (m, 5H), 7.21 (d,  $^3J_{\text{HH}} = 7.5$  Hz, 1H), 1.21 (d,  $^3J_{\text{HP}} = 18.0$  Hz, 9H) ppm.  $^{13}\text{C}\{^1\text{H}\}$  NMR (75 MHz,  $\text{CDCl}_3$ )  $\delta$  181.1 (d,  $^2J_{\text{CP}} = 7.9$  Hz), 141.8 (d,  $J_{\text{CP}} = 31.6$  Hz), 140.4 (d,  $J_{\text{CP}} = 69.4$  Hz), 133.8, 132.3, 132.1, 131.8 (d,  $J_{\text{CP}} = 8.5$  Hz), 131.3, 130.9, 129.1 (d,  $J_{\text{CP}} = 8.9$  Hz), 128.7, 127.3, 127.2, 126.7, 126.6, 126.4, 125.3 (d,  $J_{\text{CP}} = 37.7$  Hz), 35.5 (d,  $^1J_{\text{CP}} = 58.1$  Hz), 24.6 ppm.  $^{31}\text{P}\{^1\text{H}\}$  NMR (121 MHz,  $\text{CDCl}_3$ )  $\delta$  106.3 ppm. **IR** (neat):  $\tilde{\nu} = 2968$  (s), 2928 (w), 2864 (s), 2399 (w), 2272 (w), 1538 (s), 1294 (s), 1254 (s), 1205 (s), 1130 (s), 936 (s), 829 (s), 804 (s), 766 (s), 743 (s), 709 (s), 688 (s)  $\text{cm}^{-1}$ . **HRMS** (ESI $^+$ ) exact mass calcd. for  $\text{C}_{21}\text{H}_{21}\text{N}_1\text{P}_1\text{S}_1$   $[\text{M}+\text{H}]^+$  requires  $m/z$  350.1127, found  $m/z$  350.1130 (0.9 ppm).

### 2.8.7 3-Phenyl-(phenyl-azazirconacyclopentene) **71**



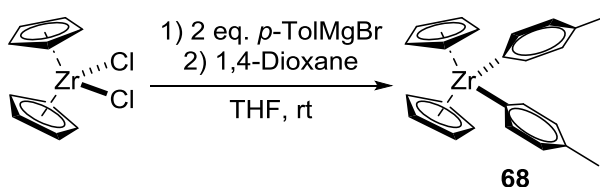
Diphenyl zirconocene (1.93 g, 5.13 mmol) was dissolved under dinitrogen in anhydrous toluene (40 mL) resulting in a yellow transparent solution; 1-cyanonaphthalene (0.53 ml, 5.13 mmol) was then added. The resulting brown suspension was heated to 80 °C and left to react overnight. After that period, the reaction was left to cool down to room temperature. The suspension was then filtered through a fritted funnel using a cannula under dinitrogen, obtaining a yellow solid (0.71 g, 25%). **IR** (neat):  $\tilde{\nu} = 3292$  (w), 1593 (s), 1487 (m), 1280 (m), 1072 (s), 1019 (s), 804 (s), 756 (s), 695 (s)  $\text{cm}^{-1}$

### 2.8.8 3-Phenyl-((1-*tert*-butyl)-1-sulfide-1*H*-1,2-azaphosphindole) 75



The organophosphorus compound *tert*-butyl dichlorophosphine (0.81 g, 5.13 mmol) was added to a refluxing solution of 3-phenyl-(phenyl-azazirconacyclopentene) (**71**) (2.06 g, 5.13 mmol) in anhydrous toluene (50 mL) under dinitrogen. After 3 hours, sulfur (0.32 g, 10.56 mmol) was added to the black mixture which was stirred for another hour during this time, the reaction was monitored by  $^{31}\text{P}$  NMR. The mixture cooled to room temperature and the solvent was evaporated. The resulting mixture was purified using column chromatography (petrol/ethyl acetate 9:1,  $R_f = 0.4$ ). The product was a colourless crystalline solid (0.68 g, 44%). A sample suitable for X-ray crystallographic analysis was obtained from toluene. **MP**: 95.0 °C.  $^1\text{H}$  NMR (300 MHz,  $\text{CDCl}_3$ )  $\delta$  7.89-7.73 (m, 4H), 7.59-7.44 (m, 5H), 1.18 (d,  $^3J_{\text{HP}} = 17.4$  Hz, 9H) ppm.  $^{13}\text{C}\{^1\text{H}\}$  NMR (75 MHz,  $\text{CDCl}_3$ )  $\delta$  180 (d,  $^2J_{\text{CP}} = 7.2$  Hz), 141.5, 140.8, 140.5, 140.2, 134.6 (d,  $J_{\text{CP}} = 20.0$  Hz), 131.9 (d,  $J_{\text{CP}} = 32.5$  Hz), 131.5 (d,  $J_{\text{CP}} = 9.5$  Hz), 129.4 (d,  $J_{\text{CP}} = 8.8$  Hz), 128.9 (d,  $J_{\text{CP}} = 18.3$  Hz), 126.3 (d,  $J_{\text{CP}} = 11.5$  Hz), 35.5 (d,  $^1J_{\text{CP}} = 58.8$  Hz), 24.5 ppm,  $^{31}\text{P}\{^1\text{H}\}$  NMR (121 MHz,  $\text{CDCl}_3$ )  $\delta$  104.6 ppm. **IR** (neat):  $\tilde{\nu} = 2970$  (s), 2955 (s), 2863 (s), 2650 (w), 2399 (w), 1972 (w), 1531 (s), 1489 (s), 1443 (s), 1360 (s), 1328 (s), 1296 (s), 1153 (s), 1132 (s), 957 (s), 806 (s), 792 (s), 717 (s), 686  $\text{cm}^{-1}$ . **HRMS** (ESI $^+$ ) exact mass calcd. for  $\text{C}_{17}\text{H}_{18}\text{N}_1\text{P}_1\text{S}_1$  [ $\text{M}+\text{H}$ ] $^+$  requires  $m/z$  350.1127, found  $m/z$  350.1130 (0.9 ppm).

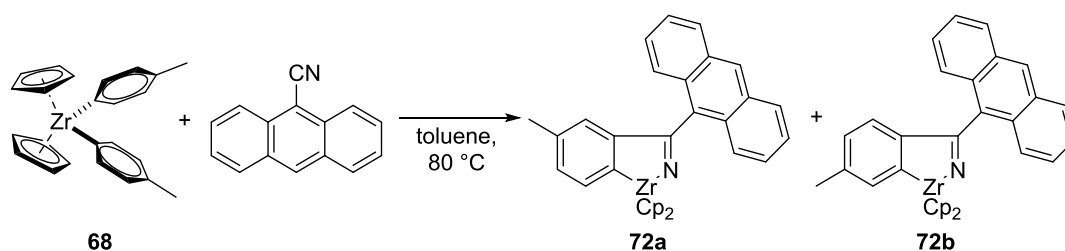
### 2.8.9 Bis(*p*-tolyl) zirconocene 68



Zirconocene dichloride (1.50 g, 5.13 mmol) was dissolved in a Schlenk flask in THF (15 mL); a solution of *p*-tolylmagnesium bromide (3.4 mL, 10.26 mmol) was then added dropwise, resulting in a transparent yellow solution. The solution was left to react for 20 minutes and then anhydrous dioxane (2.6 mL, 30.79 mmol) was added dropwise; the solution turned into a suspension containing a white solid in a yellow solution. After 15

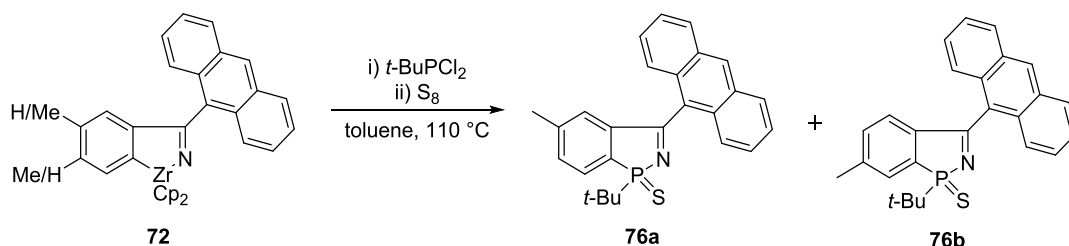
hours, the solvent was evaporated and the resulting solid was dissolved again using anhydrous toluene (40 mL). The resulting suspension was then filtered under dinitrogen through a fritted funnel, using a cannula. The yellow solution was then dried under reduced pressure to give a yellow solid (1.87 g, 90%). **MP**: 150.0 °C. **<sup>1</sup>H NMR** (400 MHz, CDCl<sub>3</sub>) δ 7.21 (d, <sup>3</sup>J<sub>HH</sub> = 7.3 Hz, 4H), 6.98 (d, <sup>3</sup>J<sub>HH</sub> = 7.3 Hz, 4H), 6.20 (s, 10H), 2.29 (s, 6H) ppm. **<sup>13</sup>C{<sup>1</sup>H} NMR** (75 MHz, CDCl<sub>3</sub>) δ 179.0, 135.9, 134.8, 127.3, 112.1, 21.3 ppm. **IR** (neat):  $\tilde{\nu}$  = 2963 (w), 1723 (w), 1599 (m), 1503 (s), 1278 (s), 1017 (m), 800 (s) cm<sup>-1</sup>.

### 2.8.10 3-Anthracen-9-yl-(*p*-tolyl-azazirconocyclopentene) 72a/b



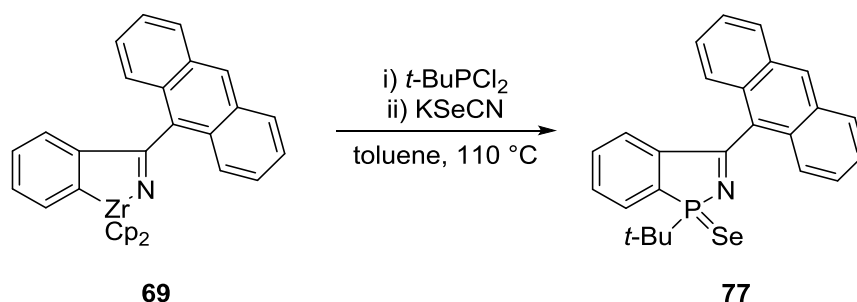
Bis(*p*-tolyl) zirconocene (1.87 g, 4.63 mmol) was dissolved under dinitrogen in anhydrous toluene (30 mL) resulting in a yellow transparent solution; 9-cyanoanthracene (0.94 g, 4.63 mmol) was then added. The resulting brown suspension was heated to 80 °C and left to react overnight. After that time the reaction was left to cool down to room temperature; afterwards, the suspension was filtered through a fritted funnel using a cannula under dinitrogen, obtaining a brown solid. Pentane was added to the resulting black solution, forming a suspension which was filtered under dinitrogen. The solvent of the final yellow solution was evaporated under dinitrogen and the product was a yellow solid (0.25 g, 10%). **MP**: 136.8 °C. **<sup>1</sup>H NMR** (400 MHz, CDCl<sub>3</sub>) δ 8.57 (s, 1H), 8.49 (d, <sup>3</sup>J<sub>HH</sub> = 6.7 Hz, 1H), 8.33 (d, <sup>3</sup>J<sub>HH</sub> = 8.9 Hz, 1H), 8.02-7.94 (m, 6H), 7.61 (d, <sup>3</sup>J<sub>HH</sub> = 8.1 Hz, 2H), 7.53-7.45 (m, 4H), 6.12 (s, 10H) ppm, 2.31 (s, 1.5H), 2.27 (s, 1.5H). **<sup>13</sup>C{<sup>1</sup>H} NMR** (75 MHz, CDCl<sub>3</sub>) δ 179.1, 136.0, 137.8, 134.8, 133.4, 133.2, 132.8, 132.3, 131.3, 130.6, 129.4, 129.0, 128.8, 128.4, 127.4, 127.0, 126.4, 125.9, 125.7, 125.5, 125.3, 112.1, 21.4, 21.3 ppm. **IR** (neat):  $\tilde{\nu}$  = 2956 (w), 2195 (s), 1578 (w), 1436 (s), 1056 (s), 711 (s), 702 (s) cm<sup>-1</sup>.

**2.8.11 3-Anthracen-9-yl-((1-*tert*-butyl)-(4-methyl)-1-sulfide-1*H*-1,2-azaphosphindole) / 3-Anthracen-9-yl-((1-*tert*-butyl)-(5-methyl)-1-sulfide-1*H*-1,2-azaphosphindole) 76a/b**



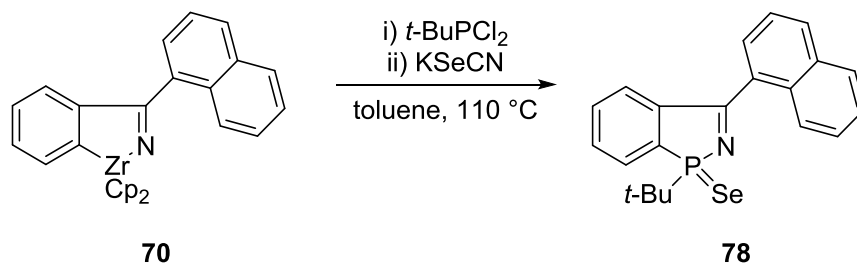
The organophosphorus compound *tert*-butyl dichlorophosphine (0.68 g, 4.27 mmol) was added to a refluxing solution of 3-anthracen-9-yl-(*p*-tolyl-azazirconacyclopentene) (**72**) (2.19 g, 4.27 mmol) in anhydrous toluene (50 mL) under dinitrogen. After 3 hours, sulfur (0.27 g, 8.54 mmol) was added to the black mixture which was stirred for another hour during this time, the reaction was monitored by  $^{31}\text{P}$  NMR. The mixture cooled to room temperature and the solvent was evaporated. The resulting mixture was purified using column chromatography (petrol/toluene 1:2,  $R_f = 0.4$ ). The product was a bright yellow solid (0.65 g, 36%). A sample suitable for X-ray crystallographic analysis was obtained from toluene. **MP**:  $106.0\text{ }^\circ\text{C}$ .  $^1\text{H}$  NMR (300 MHz,  $\text{CDCl}_3$ )  $\delta$  8.56 (d,  $^3J_{\text{HH}} = 6.3\text{ Hz}$ , 1H), 8.07-7.89 (m, 3H), 7.75 (d,  $^3J_{\text{HH}} = 7.3\text{ Hz}$ , 1H), 7.60 (d,  $^3J_{\text{HH}} = 7.7\text{ Hz}$ , 1H), 7.47-7.28 (m, 5H), 7.10 (d,  $^3J_{\text{HH}} = 7.5\text{ Hz}$ , 1H), 2.41 (s, 1.5H), 2.13 (s, 1.5H), 1.43 (d,  $^3J_{\text{HP}} = 3.0\text{ Hz}$ , 4.5H), 1.37 (d,  $^3J_{\text{HP}} = 3.0\text{ Hz}$ , 4.5H) ppm.  $^{13}\text{C}\{^1\text{H}\}$  NMR (75 MHz,  $\text{CDCl}_3$ )  $\delta$  182.4 (d,  $^2J_{\text{CP}} = 7.7\text{ Hz}$ ), 182.1 (d,  $^2J_{\text{CP}} = 8.5\text{ Hz}$ ), 141.2, 140.9, 140.6, 140.5, 137.6, 136.9, 134.2, 133.1, 132.9 (d,  $J_{\text{CP}} = 8.9\text{ Hz}$ ), 131.6, 130.8, 130.0, 129.8 (d,  $^3J_{\text{HP}} = 9.7\text{ Hz}$ ), 129.4 (d,  $J_{\text{HP}} = 3.8\text{ Hz}$ ), 129.1-128.9 (overlapped signals), 128.5, 127.5, 126.8 (d,  $J_{\text{HP}} = 7.4\text{ Hz}$ ), 126.2 (d,  $J_{\text{HP}} = 12.0\text{ Hz}$ ), 125.3-125.1 (overlapped signals), 114.2, 35.4 (d,  $^1J_{\text{CP}} = 53.6\text{ Hz}$ ), 24.8, 21.5 (d,  $^1J_{\text{HP}} = 28.2\text{ Hz}$ ) ppm.  $^{31}\text{P}\{^1\text{H}\}$  NMR (121 MHz,  $\text{CDCl}_3$ )  $\delta$  107.2, 107.1 ppm. **IR** (neat):  $\tilde{\nu} = 2967$  (w), 2376 (w), 1577 (w) 1241 (s), 825 (s), 756 (s), 704 (s)  $\text{cm}^{-1}$ . **HRMS** (ESI<sup>+</sup>) exact mass calcd. for  $\text{C}_{26}\text{H}_{25}\text{N}_1\text{P}_1\text{S}_1$   $[\text{M}+\text{H}]^+$  requires  $m/z$  414.1440, found  $m/z$  400.1439 (0.2 ppm).

### 2.8.12 3-Anthracen-9-yl-((1-*tert*-butyl)-1-selenide-1*H*-1,2-azaphosphindole) 77



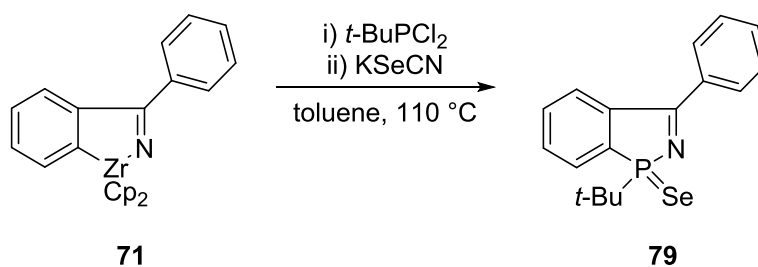
The organophosphorus compound *tert*-butyl dichlorophosphine (0.81 g, 5.13 mmol) was added to a refluxing solution of 3-anthracen-9-yl-(phenyl-azazirconacyclopentene) (**69**) (2.56 g, 5.13 mmol) in anhydrous toluene (50 mL) under dinitrogen. After 3 hours, potassium selenocyanate (1.48 g, 10.56 mmol) was added to the black mixture which was stirred for another hour during this time, the reaction was monitored by <sup>31</sup>P NMR spectroscopy. The mixture cooled to room temperature and the solvent was evaporated. The resulting mixture was purified using column chromatography (petrol/toluene 1:1, *R<sub>f</sub>* = 0.4). The product was a brown solid (0.48 g, 24%). A sample suitable for X-ray crystallographic analysis was obtained from toluene/petrol. **MP**: 110.6 °C. **<sup>1</sup>H NMR** (300 MHz, CDCl<sub>3</sub>) δ 8.57 (s, 1H), 8.05 (d, <sup>3</sup>*J*<sub>HH</sub> = 8.13 Hz, 1H), 8.02-7.89 (m, 3H), 7.61-7.52 (m, 2H), 7.46-7.38 (m, 3H), 7.35-7.27 (m, 2H), 6.90 (d, <sup>3</sup>*J*<sub>HH</sub> = 8.3 Hz, 1H), 1.41 (d, <sup>3</sup>*J*<sub>HP</sub> = 18.1 Hz, 9H) ppm. **<sup>13</sup>C{<sup>1</sup>H} NMR** (75 MHz, CDCl<sub>3</sub>) δ 182.2 (d, <sup>2</sup>*J*<sub>CP</sub> = 11.2 Hz), 142.7, 142.4, 141.1, 132.2, 132.0 (d, *J*<sub>CP</sub> = 7.7 Hz), 131.9, 131.7, 130.8, 130.4, 129.5-129.1 (overlapped signals), 128.5, 127.7, 127.5, 127.2, 126.7, 126.5, 125.9, 125.3 (d, *J*<sub>CP</sub> = 8.9 Hz), 124.9, 35.5 (d, <sup>1</sup>*J*<sub>CP</sub> = 47.4 Hz), 24.8 ppm. **<sup>31</sup>P{<sup>1</sup>H} NMR** (121 MHz, CDCl<sub>3</sub>) δ 103.0 (s with <sup>77</sup>Se satellites, <sup>1</sup>*J*<sub>SeP</sub> = 749.5 Hz) ppm. **IR** (neat):  $\tilde{\nu}$  = 2970 (w), 2394 (w), 2242 (w), 1537 (s), 1359 (s), 1241 (s), 1131 (s), 914 (s), 889 (s), 727 (s) cm<sup>-1</sup>. **HRMS** (ESI<sup>+</sup>) exact mass calcd. for C<sub>25</sub>H<sub>23</sub>N<sub>1</sub>P<sub>1</sub>Se<sub>1</sub> [M+H]<sup>+</sup> requires *m/z* 448.0735, found *m/z* 448.0727 (0.1 ppm).

### 2.8.13 3-Naphth-1-yl-((1-*tert*-butyl)-1-selenide-1*H*-1,2-azaphosphindole) 78



The organophosphorus compound *tert*-butyl dichlorophosphine (0.73 g, 4.56 mmol) was added to a refluxing solution of 3-naphtalen-1-yl-(phenyl-azazirconacyclopentene) (**70**) (2.06 g, 4.56 mmol) in anhydrous toluene (50 mL) under dinitrogen. After 3 hours, potassium selenocyanate (0.32 g, 10.56 mmol) was added to the black mixture which was stirred for another hour during this time, the reaction was monitored by  $^{31}\text{P}$  NMR. The mixture cooled to room temperature and the solvent evaporated. The resulting mixture was purified using column chromatography (petrol/toluene 5:1,  $R_f = 0.6$ ). The product was a pale brown solid (0.76 g, 42%). A sample suitable for X-ray crystallographic analysis was obtained from toluene. **MP**: 105.6 °C.  $^1\text{H}$  NMR (300 MHz,  $\text{CDCl}_3$ )  $\delta$  7.95 (d,  $^3J_{\text{HH}} = 8.5$  Hz, 2H), 7.90-7.84 (m, 2H), 7.64 (d,  $^3J_{\text{HH}} = 7.3$  Hz, 1H), 7.58-7.51 (m, 2H), 7.49-7.37 (m, 3H), 7.30 (d,  $^3J_{\text{HH}} = 7.5$  Hz, 1H), 1.27 (d,  $^3J_{\text{HP}} = 18.2$  Hz, 9H) ppm.  $^{13}\text{C}\{^1\text{H}\}$  NMR (75 MHz,  $\text{CDCl}_3$ )  $\delta$  181.2 (d,  $^2J_{\text{CP}} = 10.4$  Hz), 141.9, 141.5, 141.1, 133.8, 132.0-131.7 (overlapped signals), 131.2, 131.0, 129.3, 129.2, 127.9 (d,  $J_{\text{CP}} = 101.3$  Hz), 127.4, 126.8, 126.7, 125.5, 124.9, 35.6 (d,  $^1J_{\text{CP}} = 48.9$  Hz), 24.7 ppm.  $^{31}\text{P}\{^1\text{H}\}$  NMR (121 MHz,  $\text{CDCl}_3$ )  $\delta$  101.2 (s with  $^{77}\text{Se}$  satellites,  $^1J_{\text{SeP}} = 756.9$  Hz) ppm. **IR** (neat):  $\tilde{\nu} = 3665$  (w), 2969 (w), 2901 (w), 2222 (w), 1953 (w), 1532 (s), 1295 (s), 1254 (s), 1130 (s), 1066 (s), 935 (s), 803 (s), 774 (s)  $\text{cm}^{-1}$ . **HRMS** (ESI $^+$ ) exact mass calcd. for  $\text{C}_{21}\text{H}_{20}\text{N}_1\text{P}_1\text{Se}_1$  [ $\text{M}+\text{H}$ ] $^+$  requires  $m/z$  392.0632, found  $m/z$  392.0636 (0.9 ppm).

#### 2.8.14 3-Phenyl-((1-*tert*-butyl)-1-selenide-1*H*-1,2-azaphosphindole) **79**

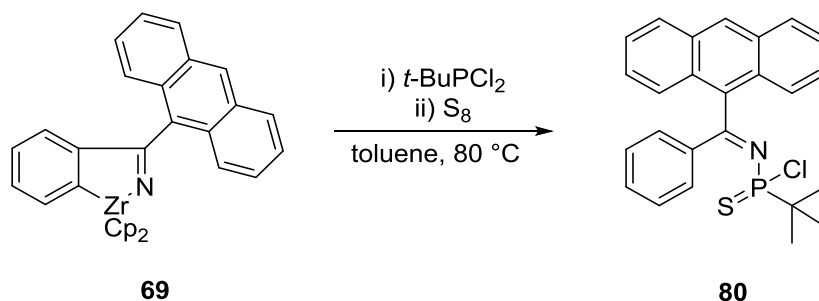


The organophosphorus compound *tert*-butyl dichlorophosphine (0.81 g, 5.13 mmol) was added to a refluxing solution of 3-Phenyl-(phenyl-azazirconacyclopentene) (**71**) (2.06 g, 5.13 mmol) in anhydrous toluene (50 mL) under dinitrogen. After 3 hours, sulfur (0.32 g, 10.56 mmol) was added to the black mixture which was stirred for another hour; during this time, the reaction was monitored by  $^{31}\text{P}$  NMR spectroscopy. The mixture cooled to room temperature and the solvent evaporated. The resulting mixture was purified using column chromatography (petrol/ethyl acetate 9:1,  $R_f = 0.5$ ), and was obtained a colourless crystalline solid (0.68 g, 44%). A sample suitable for X-ray crystallographic analysis was obtained from toluene. **MP**: 95.0 °C.  $^1\text{H}$  NMR (300 MHz,  $\text{CDCl}_3$ )  $\delta$  7.89-7.73 (m, 4H),



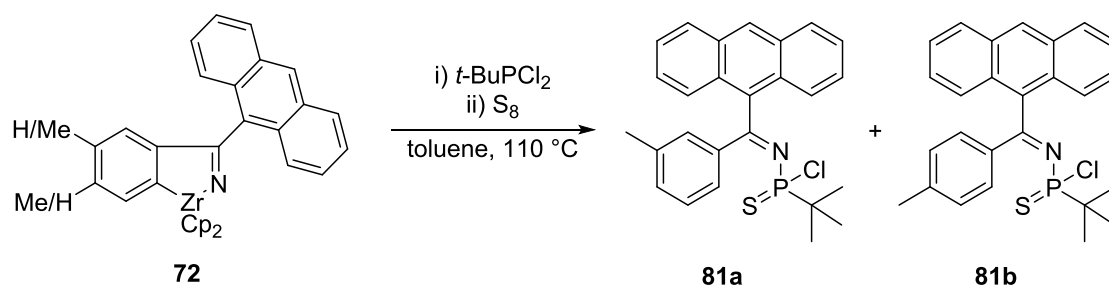
7.59-7.44 (m, 5H), 1.18 (d,  $^3J_{\text{HP}} = 17.4$  Hz, 9H) ppm.  $^{13}\text{C}\{^1\text{H}\}$  NMR (75 MHz,  $\text{CDCl}_3$ )  $\delta$  179.1 (d,  $^2J_{\text{CP}} = 8.4$  Hz), 141.4, 140.8, 139.3, 139.0, 133.5 (d,  $J_{\text{CP}} = 21.7$  Hz), 130.8 (d,  $J_{\text{CP}} = 13.2$  Hz), 130.5 (d,  $J_{\text{CP}} = 9.7$  Hz), 128.5 (d,  $J_{\text{CP}} = 10.5$  Hz), 127.9 (d,  $J_{\text{CP}} = 30.0$  Hz), 125.5 (d,  $J_{\text{CP}} = 11.9$  Hz), 34.6 (d,  $^1J_{\text{CP}} = 50.5$  Hz), 23.5 ppm.  $^{31}\text{P}\{^1\text{H}\}$  NMR (121 MHz,  $\text{CDCl}_3$ )  $\delta$  104.6 (s with  $^{77}\text{Se}$  satellites,  $^1J_{\text{SeP}} = 777.4$  Hz) ppm. IR (neat):  $\tilde{\nu} = 2970$  (s), 2955 (s), 2863 (s), 2650 (w), 2399 (w), 1972 (w), 1531 (s), 1489 (s), 1443 (s), 1360 (s), 1328 (s), 1296 (s), 1153 (s), 1132 (s), 957 (s), 806 (s), 792 (s), 717 (s), 686  $\text{cm}^{-1}$ . HRMS (ESI $^+$ ) exact mass calcd. for  $\text{C}_{21}\text{H}_{21}\text{N}_1\text{P}_1\text{S}_1$   $[\text{M}+\text{H}]^+$  requires  $m/z$  350.1127, found  $m/z$  350.1130 (0.9 ppm).

### 2.8.15 *N*-(Anthracen-9-yl(phenyl)methylene)-*P*-(*tert*-butyl)phosphonamidithioic chloride **80**



The organophosphorus compound *tert*-butyl dichlorophosphine (0.81 g, 5.13 mmol) was added to a solution of 3-anthracen-9-yl-(phenyl-azazirconacyclopentene) (**69**) (2.56 g, 5.13 mmol) heated at 80 °C in anhydrous toluene (50 mL) under dinitrogen. After 3 hours, sulfur (0.32 g, 10.56 mmol) was added to the black mixture which was stirred for another hour; during this time, the reaction was monitored by  $^{31}\text{P}$  NMR. The mixture cooled to room temperature and the solvent was evaporated. The resulting mixture was purified using column chromatography (petrol/toluene 1:1,  $R_f = 0.6$ ). The product was a bright yellow solid (0.63 g, 29%). A sample suitable for X-ray crystallographic analysis was obtained from toluene.  $^1\text{H}$  NMR (300 MHz,  $\text{CDCl}_3$ )  $\delta$  8.58 (s, 1H), 8.07-8.02 (overlapping signals, 2H), 7.80 (d,  $^3J_{\text{HH}} = 8.6$  Hz, 1H), 7.74 (d,  $^3J_{\text{HH}} = 8.4$ , 2H), 7.59-7.42 (m, 5H), 7.36 (m, 3H), 1.44 (d,  $^3J_{\text{HP}} = 21.6$  Hz, 9H) ppm.  $^{13}\text{C}\{^1\text{H}\}$  NMR (75 MHz,  $\text{CDCl}_3$ )  $\delta$  181.2 (d,  $^2J_{\text{CP}} = 8.2$  Hz), 138.9, 138.6, 133.7, 131.2, 131.0, 130.7, 130.1, 129.8, 129.0, 128.9, 128.8-128.7 (overlapping signals), 128.4, 127.6, 127.0, 126.6, 126.4, 126.1, 125.5, 125.3, 43.3 (d,  $^1J_{\text{CP}} = 85.9$  Hz), 24.9 ppm.  $^{31}\text{P}\{^1\text{H}\}$  NMR (121 MHz,  $\text{CDCl}_3$ )  $\delta$  97.4 ppm.

**2.8.16 *N*-(Anthracen-9-yl(*p*-tolyl)methylene)-*P*-(*tert*-butyl)phosphonamidothioic chloride / *N*-(anthracen-9-yl(*m*-tolyl)methylene)-*P*-(*tert*-butyl)phosphonamidothioic chloride **81a/b****



The tertiary phosphine *tert*-butyl dichlorophosphine (0.68 g, 4.27 mmol) was added to a solution of 3-anthracen-9-yl-(*p*-tolyl-azazirconacyclopentene) (**72**) (2.19 g, 4.27 mmol) heated at 80 °C in anhydrous toluene (50 mL) under dinitrogen. After 3 hours, sulfur (0.27 g, 8.54 mmol) was added to the black mixture which was stirred for another hour, during this time, the reaction was monitored by <sup>31</sup>P NMR. The mixture cooled to room temperature and the solvent was evaporated. The resulting mixture was purified using column chromatography (petrol/toluene 1:2, *R<sub>f</sub>* = 0.4), which gave a bright yellow solid (0.65 g, 36%). A sample suitable for X-ray crystallographic analysis was obtained from toluene. <sup>1</sup>H NMR (300 MHz, CDCl<sub>3</sub>) δ 8.33-8.31 (m, 2H), 7.98-7.93 (m, 3H), 7.71 (d, <sup>3</sup>*J*<sub>HH</sub> = 8.4 Hz, 1H), 7.64-7.60 (m, 1H), 7.54 (d, <sup>3</sup>*J*<sub>HH</sub> = 8.4 Hz, 1H), 7.50-7.46 (m, 2H), 7.41-7.37 (m, 2H), 7.06 (d, <sup>3</sup>*J*<sub>HH</sub> = 8.0 Hz, 1H), 2.28-2.20 (m, 3H), 1.35 (d, <sup>3</sup>*J*<sub>HP</sub> = 22.0 Hz, 9H). <sup>13</sup>C{<sup>1</sup>H} NMR (100 MHz, CDCl<sub>3</sub>) δ 178.3, 143.8, 133.6, 135.07, 133.1, 132.3, 131.7, 130.1, 129.7, 129.7, 129.1, 128.6, 127.9, 127.7, 127.6, 127.4, 127.3, 126.6, 126.0, 125.4, 125.3, 124.9, 42.1 (d, <sup>1</sup>*J*<sub>CP</sub> = 90.0 Hz), 23.7, 20.7, 20.4 ppm. <sup>31</sup>P{<sup>1</sup>H} NMR (121 MHz, CDCl<sub>3</sub>) δ 96.7 ppm.

### 3 Synthesis of a pyrene-based tridentate phosphine and its coordination chemistry in complexes of biological interest

#### 3.1 Primary phosphines on aromatic backbones

The synthesis of primary phosphines is a task that requires an elevated technical effort due to their high reactivity towards oxidation in the presence of atmospheric oxygen (Section 1.3). Our research group has developed different air-stable phosphines, which has allowed the further synthesis of ligands with interesting properties.

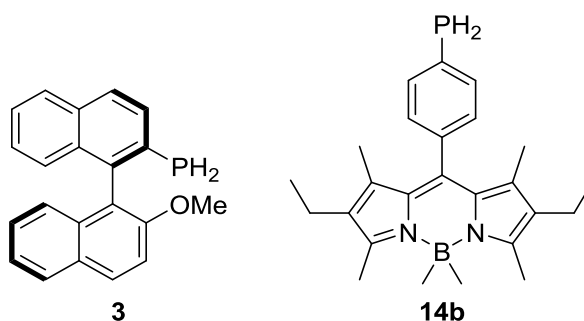
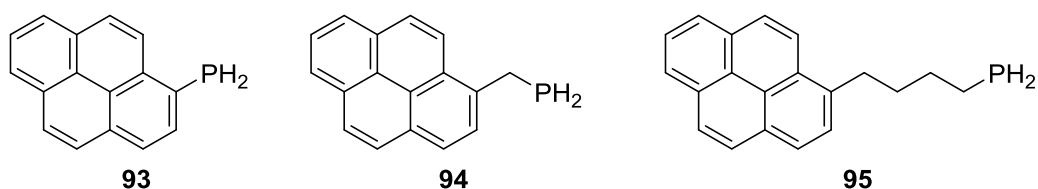


Figure 3.1 Primary phosphines previously reported by this group.

The chiral primary phosphine **3**<sup>188</sup> and the fluorescent air-stable phosphine **14b**<sup>225</sup> were developed as required intermediates to develop different phosphine analogues. This type of compound are underdeveloped despite their importance in catalytic and biomedical applications. An example of these applications is the use of by the fluorescent phosphine **14b** to develop imaging probes containing Re and <sup>99m</sup>Tc as radionuclides.<sup>152</sup> The phosphines presented in Figure 3.1 have something in common, both functional groups are bonded directly to the aryl group. This is important because the effect provided by the extended  $\pi$  conjugation of the aromatic rings stabilizes the  $-\text{PH}_2$  group towards air-oxidation. Our group decided that it would be interesting to use this knowledge on a different fluorescent core. As it was mention in Section 1.5.1.1, Polycyclic Aromatic Hydrocarbons (PAHs) are not only fluorescent but are also capable of intercalating with DNA giving them biological activity. Therefore, it was decided to use pyrene as the aromatic backbone of a novel phosphine. In order to keep the intercalating activity of the pyrene core, it was necessary to add an alkyl chain as a spacer to avoid any interference of the new moieties attached to the PAH.



**Figure 3.2 Possible primary phosphines containing pyrene as backbone.**

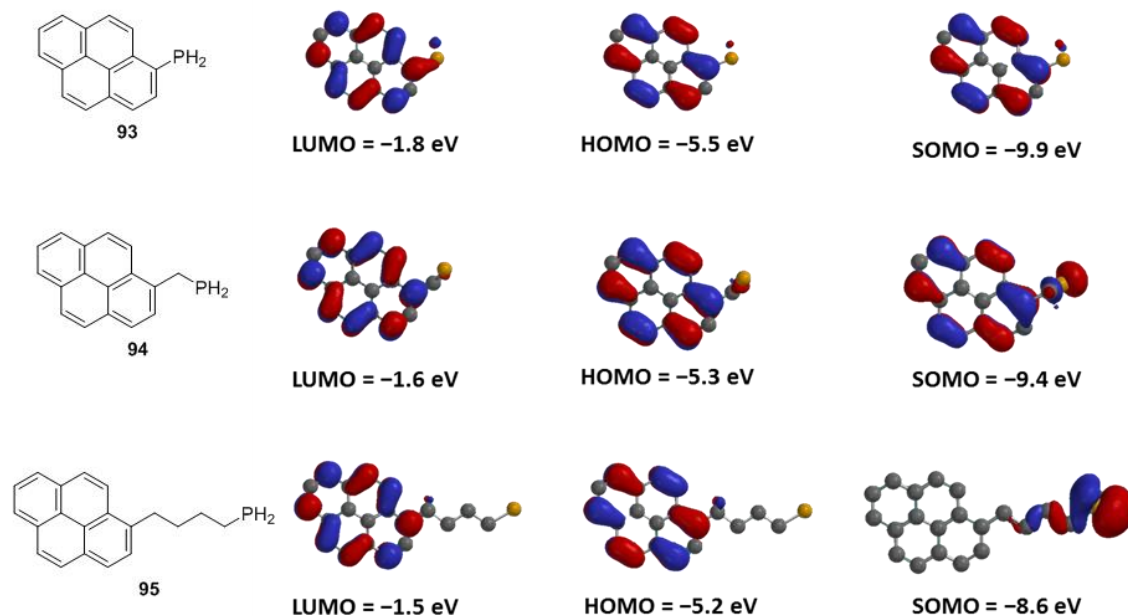
Figure 3.2 contains the structures of interest for our research. Following the success with BODIPY- $\text{PH}_2$ , we were interested in primary phosphines containing an R group with other potential biological roles. We also know that  $\pi$  conjugation gives stability on the  $-\text{PH}_2$  group. Therefore, knowing that pyrene intercalates DNA, we decided to synthesise a primary phosphine containing a pyrenyl group as backbone. The parent compound  $\text{PyrPH}_2$  **93** is of interest as another aryl bound  $-\text{PH}_2$  molecule, but the commercial availability of starting materials, favoured the synthesis of the alkyl-chain  $\text{PyrCH}_2\text{PH}_2$  **94** and  $\text{Pyr}(\text{CH}_2)_4\text{PH}_2$  **95**. This allowed us to investigate the effect of having a remote  $\pi$ -stabilising group on the phosphine air-sensitivity. For compound  $\text{Pyr}(\text{CH}_2)_4\text{PH}_2$  **95** the relatively large separation between the aryl and the phosphine group may facilitate DNA intercalation. This feature might be important when incorporating a transition metal of biomedical importance/significance.

### 3.2 Quantum chemical calculations

Initial calculations predict that the incorporation of the phosphino group onto a pyrene backbone would lead to a SOMO above  $-10$  eV, which is an indicator of a stable primary phosphine.

In order to establish the electronic nature of **93**, **94** and **95** in comparison to other phosphines, a series of DFT calculations using the B3LYP function with a 6-31G\* basis set were employed (theoretical groups have used the same level of theory for modelling phenylphosphine<sup>226</sup>). This showed that phosphines that have an extended  $\pi$ -electron structural motif possess a HOMO with no significant phosphorus character, they also demonstrate stability to air oxidation.<sup>37</sup> It was anticipated from initial quantum chemical calculations that the incorporation of a phosphino functional group onto a pyrenyl skeleton would produce air-stable primary phosphines. The molecular structure of **95** does not indicate a crowded environment in the vicinity of the P-atom since the pyrene structure is flat and it is four carbon atoms away from the primary phosphine, thus ruling

out steric hindrance as a contributor to any air-stability and isolating electronics as the key controlling factor.

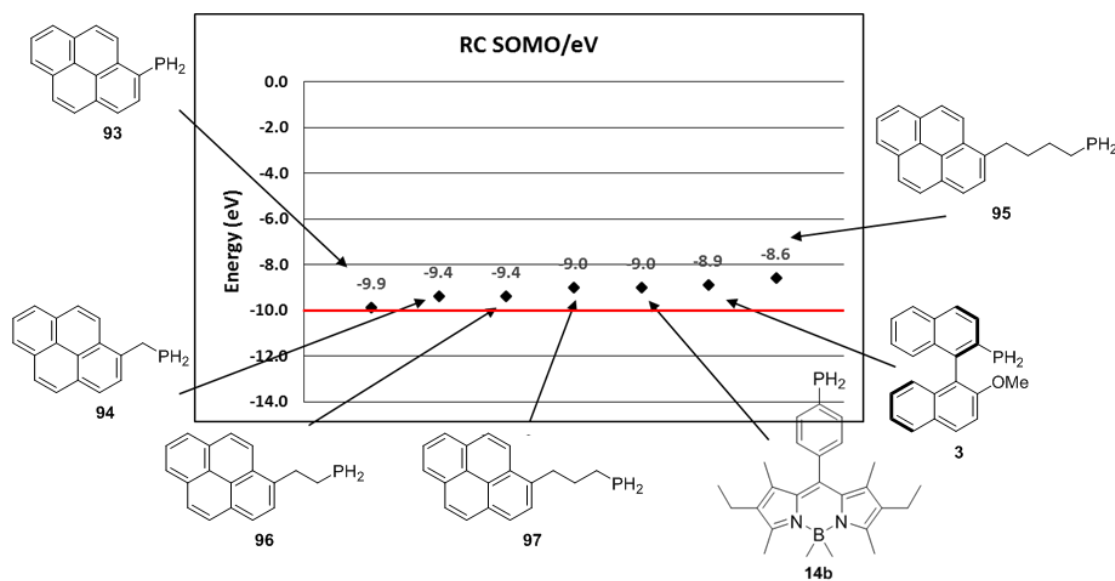


**Figure 3.3** Calculated molecular orbital surfaces from the LUMO, HOMO and SOMO of the primary phosphines **93-95**.

The HOMOs of the neutral molecules of **93**, **94** and **95** are shown in Figure 3.3. The compound PyrPH<sub>2</sub> **93** shows a weak phosphorus character in the HOMO and its SOMO energy is too near to the proposed stability threshold  $-10$  eV. The methylene group used as a linker in PyrMePH<sub>2</sub> **94** does not efficiently isolate phosphorus from the HOMO that is on the pyrene system. On the other hand, the HOMO of Pyr(CH<sub>2</sub>)<sub>4</sub>PH<sub>2</sub> **95** do not incorporate the phosphorus atom and is predominately on the pyrene skeleton. It is possible to infer from this result that long aliphatic chains attached to a PAH such as pyrene could lead to more stable phosphines. In the three compounds, **93**, **94** and **95**, the SOMO energy is above the stability threshold. Following the pattern discovered in previous findings,<sup>37</sup> it is possible to predict that the phosphines PyrPH<sub>2</sub> **93**, PyrCH<sub>2</sub>PH<sub>2</sub> **94** and Pyr(CH<sub>2</sub>)<sub>4</sub>PH<sub>2</sub> **95** will be resistant to air oxidation. However, it would be interesting to compare their stabilities since the differences shown in their HOMO and SOMO energies might also lead to stability differences.

In order to have a better understanding of the effect exerted by the alkyl chain, the SOMO energies of a series of pyrenyl-alkyl phosphines using the B3LYP function with a 6-31G\*

basis set were obtained. The results show that long alkyl chains increase the SOMO energy of the corresponding primary phosphine (Figure 3.4).



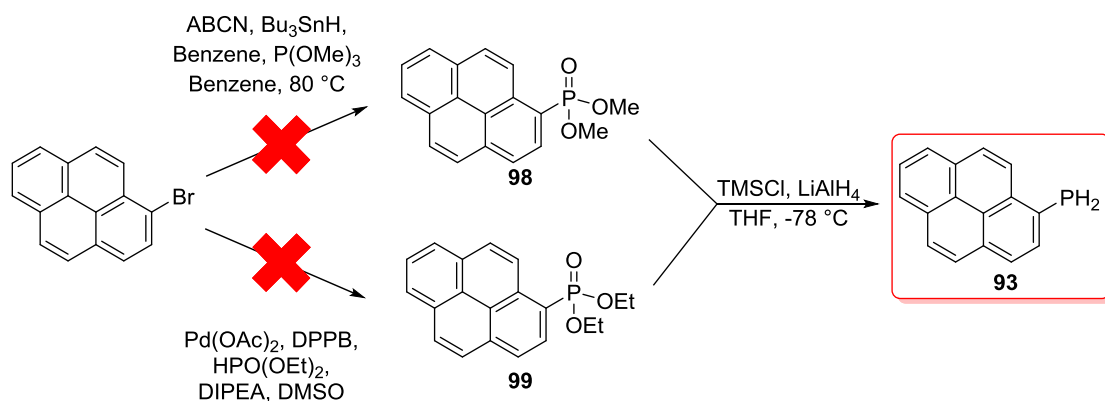
**Figure 3.4** Plot of the SOMO energy of the radical cations for the pyrene derivatives **93-97** and the primary phosphines **3** and **14b**. The line indicates an apparent “air stability” threshold value of  $-10$  eV; phosphines above or on this line are found to be air-stable.

The calculated SOMO energies of the radical cations for PyrPH<sub>2</sub> **93**, PyrCH<sub>2</sub>PH<sub>2</sub> **94** Pyr(CH<sub>2</sub>)<sub>4</sub>PH<sub>2</sub> **95** are  $-9.9$ ,  $-9.4$   $-8.6$  eV and respectively, which is above the  $-10$  eV threshold. The HOMO of PyrPH<sub>2</sub> **93** and PyrCH<sub>2</sub>PH<sub>2</sub> **94** shows weak phosphorus character. On the other hand, the HOMO of Pyr(CH<sub>2</sub>)<sub>4</sub>PH<sub>2</sub> **95** has no phosphorus character in it. These results could predict a comparatively lower stability towards air-oxidation for PyrPH<sub>2</sub> **93** and PyrCH<sub>2</sub>PH<sub>2</sub> **94** than for Pyr(CH<sub>2</sub>)<sub>4</sub>PH<sub>2</sub> **95** (Section 1.3.1). It is also important to highlight that comparing the SOMO energy of the reported MOPH<sub>2</sub> **3** and BODPH<sub>2</sub> **14b** shows that the novel Pyr(CH<sub>2</sub>)<sub>4</sub>PH<sub>2</sub> **95** has a higher value, which would imply a higher degree of stability towards air-oxidation.

### 3.3 Synthesis of air-stable phosphines pyrene-based **93-95**

After calculating the SOMO for different phosphines with a pyrene backbone, it was clear that the three proposed phosphines would be air-stable. The synthesis of PyrPH<sub>2</sub> **93** started with the commercially available 1-bromopyrene. This approach involves the substitution of bromine for a source of phosphorus to produce the corresponding primary phosphine.

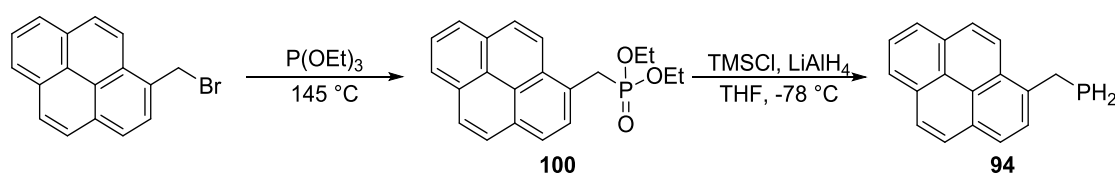
Aryl radicals, which have a  $sp^2$  hybridization, have been generated from aryl bromide precursors under standard thermal azobisisobutyronitrile (AIBN)/ $n\text{-Bu}_3\text{SnH}$  conditions.<sup>227</sup> When trapped by trimethyl phosphite, these aryl radicals give dimethyl arylphosphonates in good yields.<sup>227</sup> Therefore, we decided to react 1-bromopyrene with trimethyl phosphite in the presence of 1,1'-azobis(cyclohexanecarbonitrile) (ABCN)/  $n\text{-Bu}_3\text{SnH}$  in benzene at 80 °C. After leaving the reaction overnight (the original procedure reported by Yun was 6 hours<sup>227</sup>), the reaction was stopped and purified using column chromatography on silica gel. Unfortunately, the starting material was recovered proving that there was no reaction. A second attempt was carried out with the catalyst palladium(II) acetate with the ligand 1,4-bis(diphenylphosphinobutane) (DPPB), these conditions have been proven to produce aryl phosphonates from aryl bromides.<sup>228</sup> The result was the same; after purification using column chromatography, the starting material was recovered.



**Figure 3.5** Attempted synthesis of pyrene phosphine **93**.

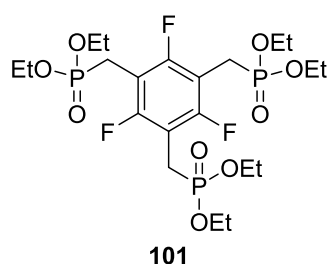
In order to compare the effect exerted by the alkyl chain, a novel primary phosphine was synthesised, with a methylene group linking the phosphine to the pyrene moiety. Commercially available 1-(bromomethylene)pyrene was used as the starting material. The first reaction was the synthesis of the phosphonate **100**. The  $^1\text{H}$  NMR spectrum integrates to 9 protons in the aromatic region corresponding to the pyrene backbone. In addition, a multiplet signal with a chemical shift between  $\delta$  3.86-3.64 ppm indicates the presence of the three methylene groups in this molecule. Finally, a triplet at  $\delta$  1.42 ppm proves that the molecule contains two methyl groups corresponding to the ethyl groups on the phosphonate. The  $^{31}\text{P}$  NMR spectrum shows a singlet at  $\delta$  25.9 ppm which is characteristic of phosphonates. The phosphonate **100** was finally reduced in order to produce the primary phosphine **94**. The  $^1\text{H}$  NMR spectrum shows that the signals

corresponding to the ethyl groups of phosphonate **100** had disappeared. In addition, they show a multiplet at  $\delta$  3.54 ppm that belongs to the methylene group. It is also possible to observe a doublet of multiplets that integrates to 2 protons and resembles a doublet of triplets with a  $^1J_{\text{HP}}$  value of 194.0 Hz. These signals must belong to the protons of the phosphine group. The  $^{13}\text{C}$  NMR spectrum shows a doublet at  $\delta$  19.0 ppm, the alkyl region, with a  $J_{\text{CP}}$  value of 12.3 Hz. The only alkyl carbon in phosphine **94** is the one in the methylene carbon; therefore, it is reasonable to assume that this signal belongs to the methylene carbon and its multiplicity is due to its position next to the P-atom.



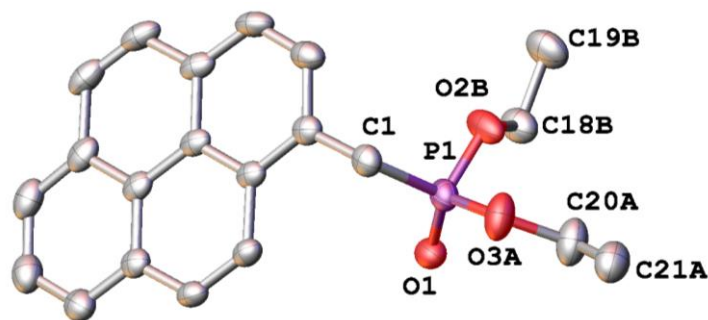
**Figure 3.6** Synthetic route followed to obtain the primary phosphine **94**, which contains a methylene group as spacer.

Crystal structures appropriate for X-ray crystallography were obtained for compounds **94** and **100**. The P1–C1 bond in PyrCH<sub>2</sub>Phos **100** has a 1.7937(18) Å bond length, whereas the P1–C1 bond in PyrCH<sub>2</sub>PH<sub>2 **94** has a P1–C1 1.847(3) Å bond length. There are examples of phosphonates in benzylic positions, for instance, Vilela *et al.*<sup>229</sup> reported the compound hexaethyl ((2,4,6-trifluorobenzene-1,3,5-triyl)tris(methylene))tris(phosphonate) (**101**) whose P–C bond lengths are 1.790 Å, 1.793 Å and 1.788 Å. The Cambridge Structural Database (CSD) does not contain any records of benzylic primary phosphines to our knowledge.</sub>

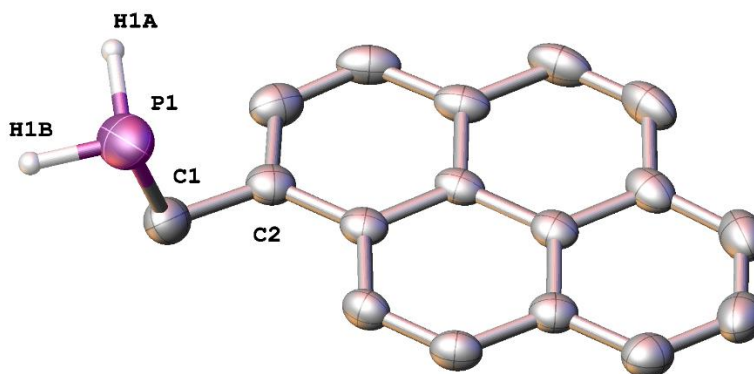


**Figure 3.7** ((2,4,6-trifluorobenzene-1,3,5-triyl)tris(methylene))tris(phosphonate) (**101**), phosphonate reported by Vilela *et al.*<sup>229</sup>





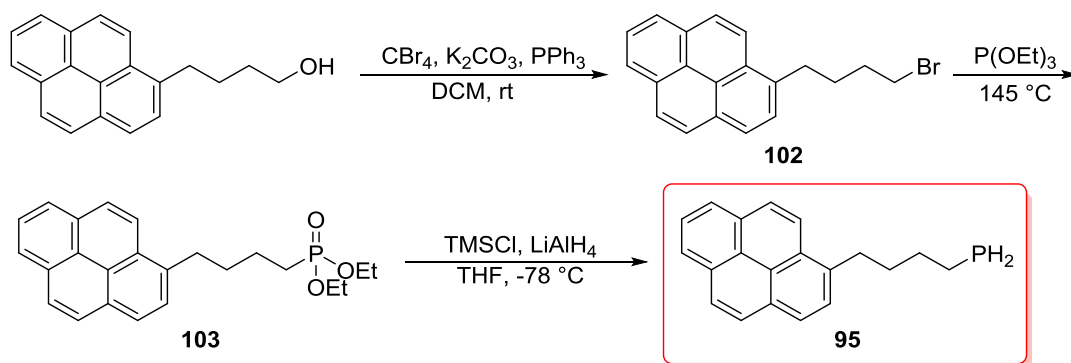
**Figure 3.8** X-ray crystal structure view of **100** (50% probability ellipsoids with interesting phosphorus, oxygen and carbon atoms labelled. Carbon atoms in grey). Hydrogen atoms have been omitted for clarity. Selected bond distances [Å] and angles [°]: P1–O1 1.4630(13), P1–C1 1.7937(18), P1–O3A 1.579(9), P1–O2B 1.563(11), O3A–C20A 1.460(10), C20A–C21A 1.471(7), O2B–C18B 1.438(12), C18B–C19B 1.500(13); O1–P1–C1 117.47(8), O1–P1–O2A 114.0(9), O1–P1–O3A 114.3(11), O1–P1–O2B 114.8(12), O3A–P1–C1 102.8(5), O2B–P1–C1 106.6(10), C20A–O3A–P1 116.6(10), O3A–C20A–C21A 106.7(6), C18B–O2B–P1 122.9(18), O2B–C18B–C19B 106.3(14).



**Figure 3.9** X-ray crystal structure view of **94** (50% probability ellipsoids with interesting phosphorus, oxygen and carbon atoms labelled. Carbon atoms in grey). Hydrogen atoms have been omitted for clarity. Selected bond distances [Å] and angles [°]: P1–C1 1.847(3), C1–C2 1.499(4); C2–C1–P1 109.66(19).

For compound **95**, the butyl group between the pyrene function and the phosphine group gave SOMO higher than  $-10$  eV, which, as previously demonstrated by our group, suggests a threshold for air-stability.

The starting material for the synthetic route was commercially available 1-pyrenebutanol, which undergoes a bromination reaction, resulting in the synthesis of bromide **102**. An Arbuzov reaction<sup>230</sup> with triethyl phosphite gave the ethyl phosphonate **103**, which was reduced in order to obtain the final primary phosphine **95**.

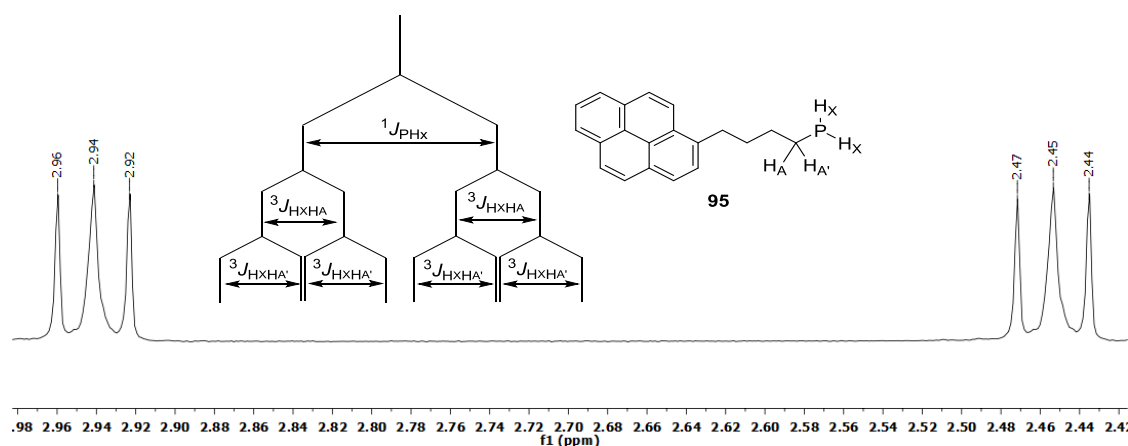


**Figure 3.10** Synthesis of the primary phosphines **95**.

Following bromination, the NMR spectra showed that the typical singlet around 2 ppm for a proton in an  $\alpha$  position, respect to an alcohol, was no longer visible and a further analysis by  $^{13}\text{C}\{^1\text{H}\}$  NMR showed that there were no singlets around 60 ppm, the usual chemical shift for a carbon bound to a terminal alcohol.<sup>231</sup> Electrospray mass spectrometry confirmed the presence of bromide **102** showing an ion,  $[\text{M}+\text{H}]^+$  at  $m/z$  337.0586.

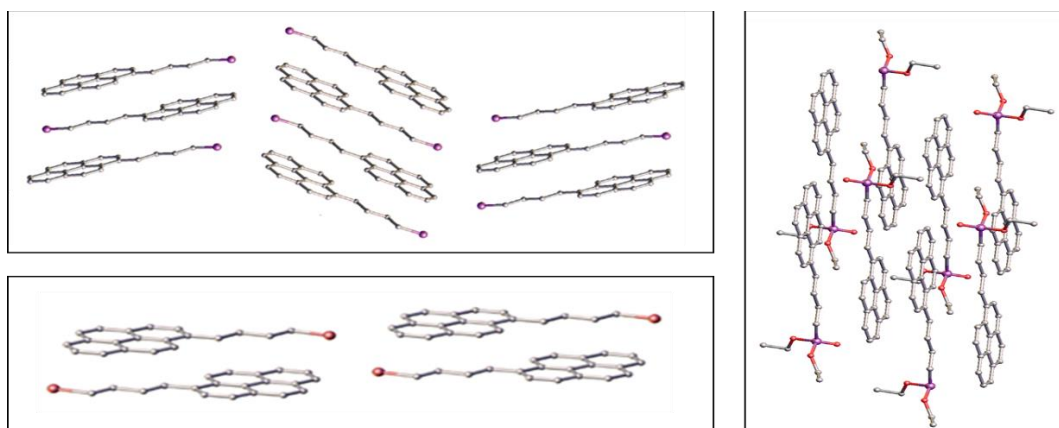
The bromine atom in compound **102** is an excellent leaving group, and was replaced by a phosphonate group using triethyl phosphite as the nucleophile. The  $^{13}\text{C}\{^1\text{H}\}$  NMR data of phosphonate **103** showed a doublet at 25.7 ppm, for which the magnitude of  $J$  was 140.9 Hz. Previous reports in the literature show that this is indicative of carbon atoms in an alpha position relative to the phosphorus atom,<sup>232</sup> proving the formation of a C–P bond. Finally,  $^{31}\text{P}\{^1\text{H}\}$  NMR spectra and showed a singlet with a shift of 32.8 ppm, which is also characteristic for phosphonates.

The reduction of phosphonate **103** was carried out in the presence of lithium aluminium hydride and chlorotrimethylsilane, which yielded the primary phosphine **95**. The work-up of this reaction was performed in air and the compound proved to be air stable. The  $^1\text{H}$  NMR spectrum shows a doublet of doublets of doublets, in the range of 2.96–2.43 ppm, with a  $^1J_{\text{PH}} = 194.3$  Hz. This suggests that there is a  $^1J_{\text{PH}}$  type coupling, as this  $^1J_{\text{PH}}$  value is very similar to those obtained for the binaphthalene phosphine **3** ( $^1J_{\text{PHa}} = 203.9$  Hz and  $^1J_{\text{PHa}'} = 203.9$  Hz = 204.8 Hz) reported by our group.<sup>233</sup> The additional splitting is given by the magnetically inequivalent protons  $\text{H}_a$  and  $\text{H}_{a'}$ . The similar  $J$  values of primary phosphine **95** ( $^1J_{\text{HxHa}} = 7.3$  Hz and  $^1J_{\text{HxHa}'} = 7.4$  Hz) causes the doublets to be close enough to overlap, resembling a triplet (Figure 3.11). The  $^{31}\text{P}\{^1\text{H}\}$  NMR shows a singlet with a shift of  $-138.1$  ppm proving the presence of a primary phosphine.



**Figure 3.11**  $^1\text{H}$  NMR spectrum of primary phosphine **95** showing the doublet of doublet of doublets produced by  $\text{H}_x$ . The pascal triangle depicts how the similarity between  $^3J_{\text{HxHA}}$  and the  $^3J_{\text{HxHA}'}$  merges the two peaks.

Samples of compounds **95**, **102** and **103** suitable for X-ray crystallographic analysis were obtained from the slow evaporation of their dichloromethane solutions. The compounds allow for the  $\pi$ - $\pi$  stacking, sandwich type, interactions of pyrene<sup>234</sup> to be maintained thanks to their flat structures and electronic interactions. Compounds **95**, **102** and **103** seem to have a flat spatial disposition that could favour  $\pi$ - $\pi$  stacking. However, their unit cell packing reveals that they have a head to tail “arrangement of which **95** has a herring bone”-type orientation. Compounds **102** and **103** are coplanar in a staggered configuration (Figure 3.12). The distances for the planes formed by the pyrene moieties are 3.505(1) Å for **95**, 3.497(1) Å for **102** and 3.605(1) Å for **103**. The highest value for **103** makes sense since the phosphonate group is the bulkier than the phosphino and the bromide creating greater repulsion between the two planes.



**Figure 3.12** Left-up: Pack diagram of **95**. Left-down: Pack diagram of **102**. Right: Pack diagram of **103**. Colour legend: grey, carbon; purple, phosphorus; red, bromine.

Many alkyl bromide crystal structures<sup>235-239</sup> show that the C–Br bond length tends to have a distance of 1.9 Å, which correlates to the value found in the structure of bromide **102**, 1.9545 Å. This trend is also seen in other long-chain alkyl bromides. For instance, the aliphatic C–Br bond length in the indole **104** is 1.949 Å<sup>240</sup>, in the alcohol **105** is 1.995 Å<sup>241</sup> and the carboxylic acid **106** is 1.995 Å.<sup>242</sup> It is also interesting to highlight the C–C bond  $\alpha$  to the carbon bearing the halide atom, because it is shorter than the rest of the aliphatic C–C bonds in the butyl chain (Figure 3.13). This must be induced by the bromine atom since it attracts the electron density from carbon adjacent to it; this creates polarity in the C–C bond, which makes it shorter than the rest.

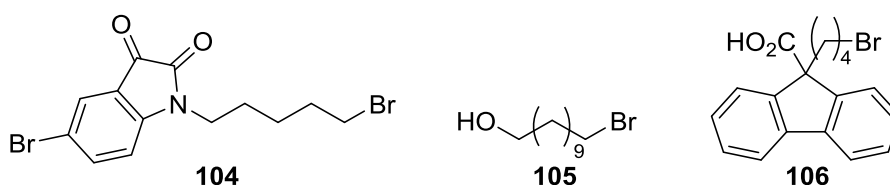


Figure 3.13 Examples of bromides reported in the Cambridge Structural Database.

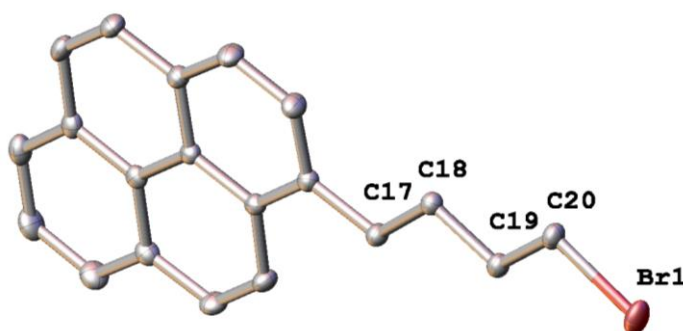


Figure 3.14 X-ray crystal structure view of **102** (50% probability ellipsoids with interesting bromine and carbon atoms labelled. Carbon atoms in grey). Hydrogen atoms have been omitted for clarity. Selected bond distances [Å] and angles [°]: Br1–C20 1.9545(14), C19–C20 1.5087(19), C18–C19 1.5271(18), C17–C18 1.5258(19); Br1–C20–C19 110.32(10), C20–C19–C18 111.95(11), C19–C18–C17 110.48(11).

The analysis of the phosphonate **103** crystal structure shows that the C–P bond has a 1.7803 Å bond length. This distance is typical for this type of pentavalent organophosphorus compound where the phosphonate is in the terminal position of an alkyl chain,<sup>243-248</sup> for example, Bichlmaier reported ethyl phosphonate **107** whose C–P bond length is 1.790 Å<sup>249</sup>. The electronegativity of phosphorus, 2.2, and carbon, 2.5, is

not notably different. This means that the C–C bond adjacent to the C–P bond does not change in length relative to the C–C bond length in other alkyl bromides such as bromide **102**. This is also seen in other alkyl phosphonates that do not contain other functional groups on the aliphatic chain.<sup>245-248</sup> For instance, the C–P bond length in the ethyl phosphonate **108** is 1.795 Å, whereas C7–C8 bond length is 1.525 Å, C8–C9 bond length is 1.554 Å and C8–C12 bond length is 1.531 Å<sup>250</sup>

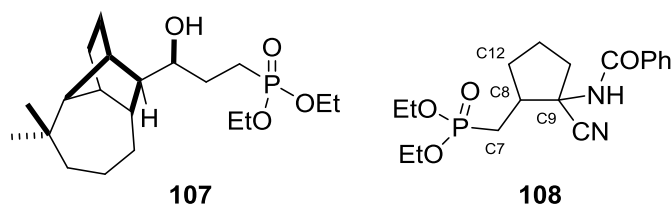


Figure 3.15 Examples of phosphonates reported in the Cambridge Structural Database.

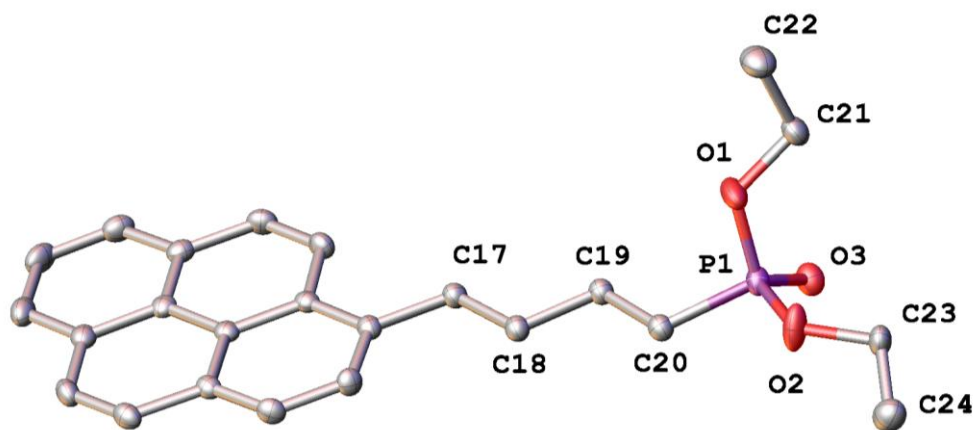


Figure 3.16 X-ray crystal structure view of **103** (50% probability ellipsoids with interesting phosphorus, oxygen and carbon atoms labelled. Carbon atoms in grey). Hydrogen atoms have been omitted for clarity. Selected bond distances [Å] and angles [°]: P1–O1 1.5843(12), P1–O2 1.5758(13), P1–O3 1.4646(12), C20–P1 1.7803(15), O1–C21 1.4487(19), O2–C23 1.4381(19), C17–C18 1.519(2), C18–C19 1.524(2), C19–C20 1.529(2), C21–C22 1.496(2), C23–C24 1.496(2); O1–P1–C20 101.03(7), O2–P1–O1 105.58(7), O2–P1–C20 100.76(7), O3–P1–O1 113.93(7), O3–P1–O2 114.30(7), O3–P1–C20 119.28(7), C21–O1–P1 120.01(10), C23–O2–P1 124.62(11), C17–C18–C19 113.13(12), C18–C19–C20 110.27(12), C19–C20–P1 116.74(11), O1–C21–C22 107.24(13), O2–C23–C24 107.87(14).

The crystal structure of primary phosphine **95** is a rare example of a crystal structure of a primary phosphine containing an alkyl group bound to the phosphino –(PH<sub>2</sub>) function–. Very few examples of these exist as they are often oily compounds with a low molecular weight.<sup>7, 11, 13, 14, 251, 252</sup> The C–P bond length in compound **95** is 1.850 Å, this value is similar to the few other reported crystal structures.<sup>11, 13, 14, 251, 252</sup> For instance, in compound (2-phosphanylethyl)ferrocene **6** (Figure 1.3) the C–P bond length is 1.884 Å.<sup>253</sup>

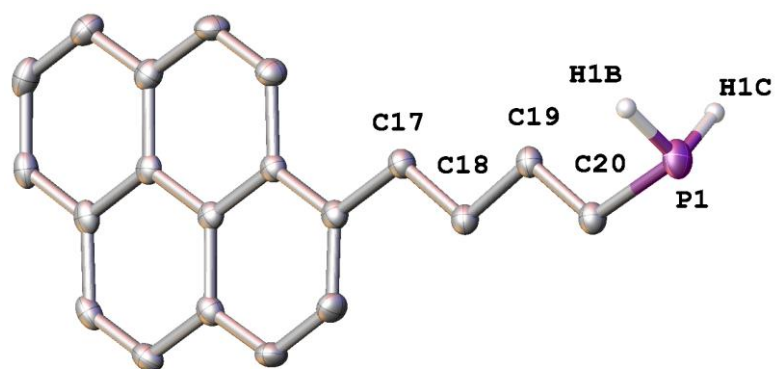


Figure 3.17 X-ray crystal structure view of **95** (50% probability ellipsoids with interesting phosphorus and carbon atoms labelled. Carbon atoms in grey). Hydrogen atoms have been omitted for clarity. Selected bond distances [Å] and angles [°]: C20–P1 1.8500(17), C17–C18 1.522(2), C18–C19 1.526(2), C19–C20 1.523(2); C17–C18–C19 112.26(14), C20–C19–C18 112.02(14), C19–C20–P1 117.65(12).

The X-ray structures shown make it possible to compare the C–P bond length of the organophosphorus compounds **94**, **95**, **100** and **103**, showing that this bond is longer in the phosphines **94** and **95** than in the phosphonates **100** and **103**. They also show that for the compounds in which the linker is a methylene group, a dihedral angle is created between the pyrene plane and the C–P plane (Figure 3.18).

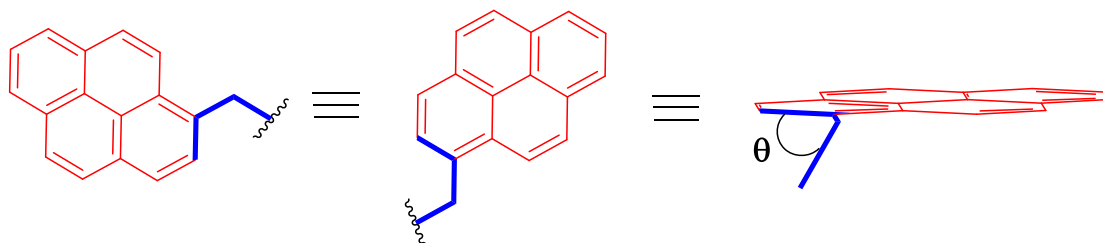


Figure 3.18 Spatial representation of the measured dihedral angle  $\theta$  formed in **94** and **100**.

Compound	Experimental	Calculated	Experimental	Calculated
	C–P (Å)	C–P (Å)	$\theta$ (°)	$\theta$ (°)
<b>PyrCH<sub>2</sub>Phos 100</b>	1.7937(18)	1.832	92.7(2)	100.1
<b>PyrCH<sub>2</sub>PH<sub>2</sub> 94</b>	1.847(3)	1.901	87.7(3)	99.7
<b>Pyr(CH<sub>2</sub>)<sub>4</sub>Phos 103</b>	1.7803(15)	1.818	1.4(2)	0.62
<b>Pyr(CH<sub>2</sub>)<sub>4</sub>PH<sub>2</sub> 95</b>	1.8500(17)	1.880	1.2(2)	0.0

Table 3.1 Crystallographic and B3YLP calculated data of compounds **94**, **95**, **100** and **103**.

The DFT calculations obtained through B3YLP (with the 6-31G\* basis) of the C–P bond length and the dihedral angle show similar values. The difference might be because the P-atom does not allow a *gauche* configuration for the methylene analogues **94** and **100** whereas the butyl analogues have an *anti* configuration.

### 3.3.1 NMR experiments to determine the air stability of PyrCH<sub>2</sub>PH<sub>2</sub> **94** and Pyr(CH<sub>2</sub>)<sub>4</sub>PH<sub>2</sub> **95**

The air stability of novel primary phosphines PyrCH<sub>2</sub>PH<sub>2</sub> **94** and Pyr(CH<sub>2</sub>)<sub>4</sub>PH<sub>2</sub> **95** was examined by dissolving a sample (20 mg) of each phosphine in *d*-chloroform. The resulting solution was placed into an NMR tube without a cap, exposing the solution to atmospheric oxygen and was left in the dark for seven days. In order to allow integration of the different phosphorus signals within the spectrum, the <sup>31</sup>P NMR spectrum was obtained in proton coupled mode, less NOE effects and with a relaxation time of three seconds between pulses.

The oxidation of primary phosphines leads to different oxidised forms of phosphorus whose chemical shifts are more downfield than the phosphine parent. Therefore, it is possible to obtain the remaining percentage of phosphine in the solution by removing the integration value of the P-oxide formed signals around 0-40 ppm from the integration value of the primary phosphine signal. The primary phosphine PyrCH<sub>2</sub>PH<sub>2</sub> **94** was comparatively less stable towards oxidation as is shown in Figure 3.19. On day seven, there was 55.1% of the original sample of PyrCH<sub>2</sub>PH<sub>2</sub> **95**. The results of the integration show that, for compound Pyr(CH<sub>2</sub>)<sub>4</sub>PH<sub>2</sub> **95**, 98.2% of the original amount of phosphine was still present at the end of the seven days.

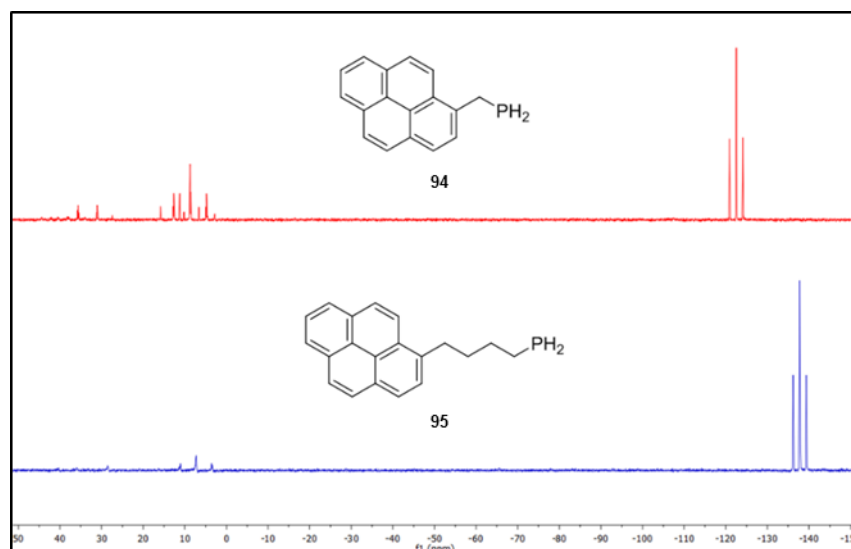


Figure 3.19  $^{31}\text{P}$ - $^1\text{H}$  NMR spectrum of  $\text{PyrCH}_2\text{PH}_2$  **94** and  $\text{Pyr}(\text{CH}_2)_4\text{PH}_2$  **95** after seven days in a solution in *d*-chloroform.

As was estimated, the butyl derivative **95** is more resistant to oxidation than the methyl analogue **94**. Benzylic species are often unstable so perhaps this explains why  $\text{PyrCH}_2\text{PH}_2$  **94** is more unstable than its butyl analogue. This benzylic position in PAH has shown to form highly stable radicals that are stabilised by low resonance stabilization energies as described by McMillen *et al.*<sup>254</sup> Figure 3.20 shows the percentage of phosphines **94** and **95** remaining in solution over the seven days the air oxidation stability test was conducted.

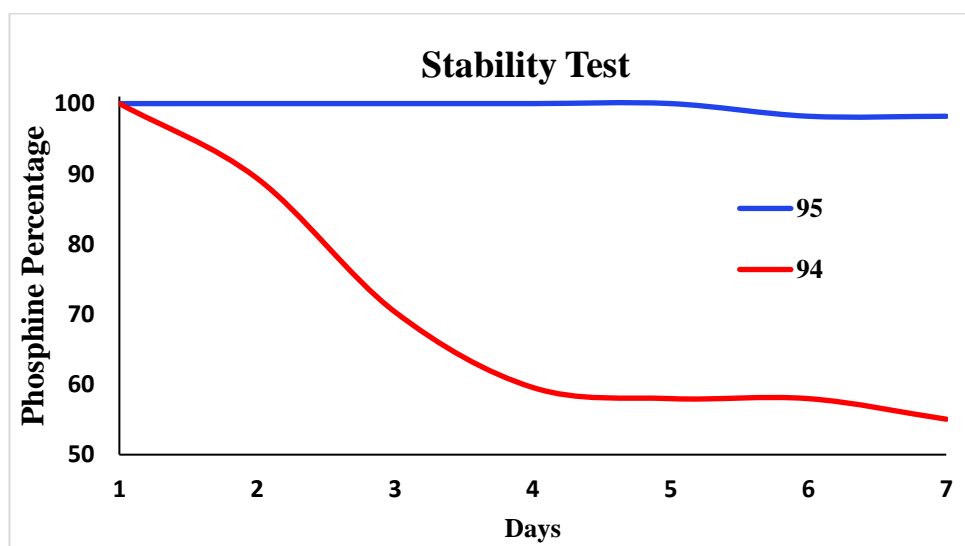


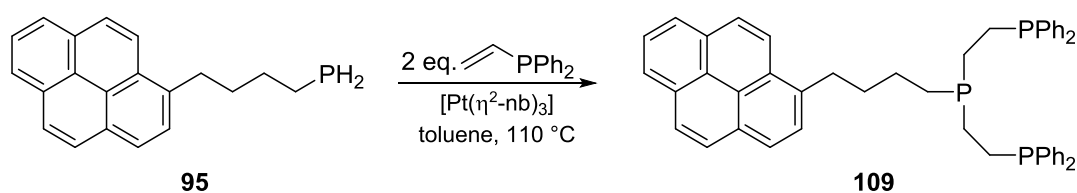
Figure 3.20 Graph showing the percentage of phosphines  $\text{PyrCH}_2\text{PH}_2$  **94** and  $\text{Pyr}(\text{CH}_2)_4\text{PH}_2$  **95** remaining over seven days.



This experiment proved that  $\text{PyrCH}_2\text{PH}_2$  **94** is less stable towards air-oxidation than  $\text{Pyr}(\text{CH}_2)_4\text{PH}_2$  **95** corroborating the calculations and the model presented in Section 3.2. These results indicated how stable these primary phosphines are. This opens a new starting material for the development of compounds with biological activity, not only to our group but also to other research groups interested in developing biological probes with pyrene.

### 3.4 Synthesis of the pyrene-based ligand **109**

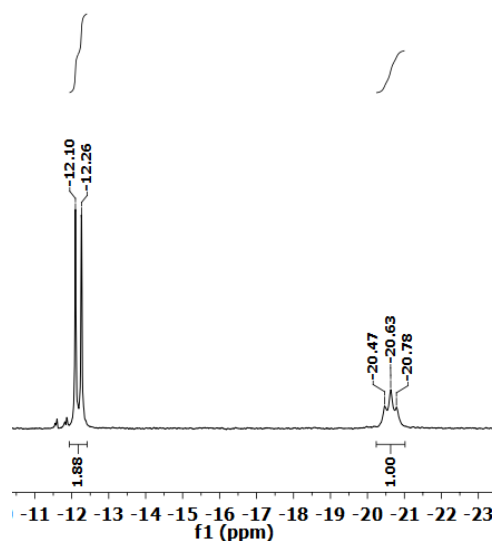
The novel phosphine **95** contains two P–H bonds which can undergo a hydrophosphination for the development of a tridentate phosphine derivative.<sup>255</sup> Such double addition will yield target tridentate phosphine **109**. This was to confirm that the resistance to air oxidation does not interfere with the behaviour of the normally reactive P–H bonds. A common reaction of a primary phosphine is the hydrophosphination reaction across a C=C double bond creating a tridentate ligand. This type of compound is important in coordination chemistry and homogeneous catalysis<sup>256</sup> because they do not readily dissociate from the metal centre due to their chelating ability and hence confer kinetic stability on the resulting transition metal complexes. Therefore, it was decided to treat primary phosphine **95** with two equivalents of diphenylvinylphosphine, using  $[\text{Pt}(\eta^2\text{-nb})_3]$  as a catalyst, to generate the tridentate ligand **109** with a 55% yield (Figure 3.21). No starting material was recovered from this reaction which suggests that 45% of the starting material was turned into different unwanted side products. The reaction required a temperature of 110 °C and was left overnight, in contrast with previous reports from this group, for which the backbone of the phosphine was the BODIPY primary phosphine **14b**, in that case the required reaction time was five days.<sup>39</sup>



**Figure 3.21** The hydrophosphination of primary phosphine **95** and 2 equivalents of vinyl diphenyl phosphine.

If the reaction is carried out without any catalyst, after three days of heating unwanted side products start to form but no presence of the tridentate phosphine can be detected using  $^{31}\text{P}\{^1\text{H}\}$  NMR. This means that the double bond of the vinyl diphenyl phosphine

cannot interact with the phosphorus atom under these conditions. Hydrophosphination of primary phosphines can occur in the presence of a radical initiator, base or metal catalyst.<sup>257-261</sup> This result correlates with Pringle's work, showing the effectiveness of the  $[\text{Pt}(\eta^2\text{-nb})_3]$  catalyst in hydrophosphination reactions.<sup>262, 263</sup> Future work could investigate new metal based catalysts to improve the rate of conversion whilst maintaining high selectivity.



**Figure 3.22** The  $^{31}\text{P}\{^1\text{H}\}$  NMR spectrum of tridentate phosphine **109** in *d*-chloroform, showing a characteristic doublet and triplet.

The  $^{31}\text{P}\{^1\text{H}\}$  NMR spectrum of **109** exhibited a typical  $\text{AX}_2$  system, producing a doublet at  $\delta -12.1$  ppm for the two equivalent terminal phosphines and a triplet at  $\delta -20.6$  ppm for the central phosphine. These signals are, in a 2:1 ratio, with a  $^3J_{\text{PP}}$  coupling constant of 26.5 Hz (Figure 3.22). In the aromatic region of the  $^1\text{H}$  NMR spectrum, the 9 protons of the pyrene moiety plus 20 protons that belong to the four phenyl rings of the tridentate ligand are visible. The multiplicity of these protons is complex; therefore, their identification was made mainly by comparison of their integrals. The results of the HRMS analysis of tridentate ligand **109** also corroborates the molecular formula of the structure proposed for this compound. Ligand **109** was stored under atmospheric conditions showing no further oxidation proving that it is more stable than its parent, primary phosphine **95**.

### 3.4.1 Group 10 coordination chemistry of tridentate phosphine 109

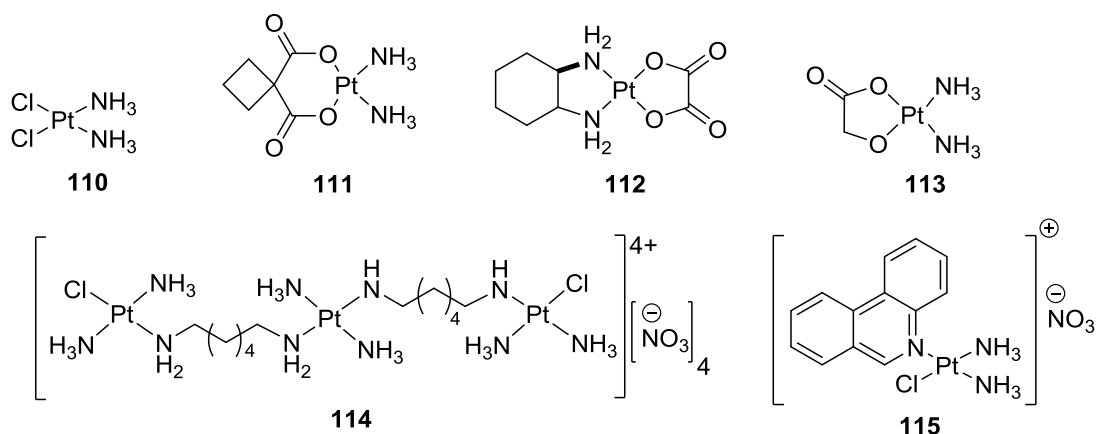
Cis-platin ( $\text{cis-Pt}(\text{NH}_3)_2\text{Cl}_2$ ) is known to have DNA-modifying properties with strong anticancer potency.<sup>264</sup> This compound is widely used despite its side effects, such as nephrotoxicity, ototoxicity and allergy.<sup>265</sup> The limitations of cis-platin opens the possibility for the development of platinum complexes that overcome those limitations. Palladium complexes have been also investigated in order to compare their biological activity with that of their platinum analogues. This improves the understanding of the mechanism of action of these complexes.<sup>266</sup> The success of cis-platin, led researchers to investigate and synthesise new metal-based drugs for experimental oncology. In recent years new metal-complexes have been identified as a very promising class of antitumor active compounds.<sup>267, 268</sup> Nickel has been tested in complexes with ligands that have shown previous biological activity in order to modulate their interaction with cancer cells.<sup>269</sup>

The aforementioned background knowledge about the transition metals of group 10, makes them important for research. Therefore, we decided to make group 10 metal complexes our novel ligand **109**.

#### 3.4.1.1 Platinum

Platinum complexes have been widely used as versatile catalysts and anticancer drugs.<sup>270-272</sup> In 1965, it was discovered that electrolysis of platinum electrodes generated a soluble platinum complex which inhibited binary fission in *Escherichia coli* bacteria.<sup>273</sup> The octahedral platinum(IV) complex  $\text{cis-}[\text{PtCl}_4(\text{NH}_3)_2]$ , but not the *trans* isomer, was found to be effective at producing this effect in the microorganism. Further tests showed that the square planar platinum(II) complex,  $\text{cis-}[\text{PtCl}_2(\text{NH}_3)_2]$  **110** turned out to be even more effective.<sup>273</sup> This finding led to the observation that **110** was indeed highly effective at reducing the mass of sarcomas in rats, which allow for the development of one of the most popular anticancer drugs used today.<sup>136</sup> Cisplatin interferes with DNA replication since, in cellular conditions, a chloride ligand is slowly displaced by water giving the a complex  $\text{cis-}[\text{PtCl}(\text{NH}_3)_2(\text{H}_2\text{O})]^+$ .<sup>274, 275</sup> The newly added  $\text{H}_2\text{O}$  ligand in  $\text{cis-}[\text{PtCl}(\text{NH}_3)_2(\text{H}_2\text{O})]^+$  is itself easily displaced by the *N*-heterocyclic bases on DNA, which forms a crosslinked adduct when another *N*-heterocyclic base displaces the remaining chloride ligand.<sup>274, 275</sup> This process interferes with cell division by mitosis, which finally leads to apoptosis, in some tissues, by a cascade of cell signalling.<sup>276</sup>

Different platinum(II) complexes have been tested, which shows that there is a strong relationship between the structural differences and the anticancer activity that the compounds can exert. This knowledge led to the synthesis of new interesting platinum(II) complexes that are available on the market, or that are still undergoing trials, as alternative anticancer drugs, such as carboplatin **111**, oxaliplatin **112**, nedaplatin **113**, triplatin tetranitrate **114**, among others.<sup>277-279</sup>



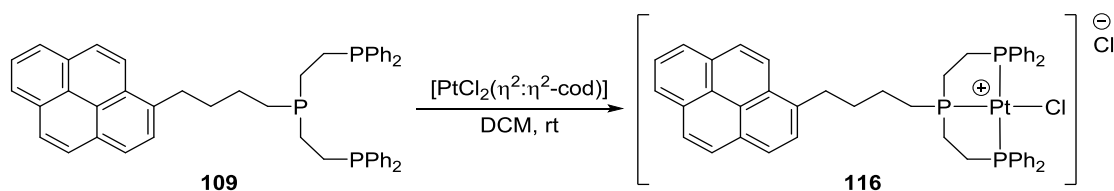
**Figure 3.23** Platinum based anticancer drugs, compounds **110-113** are currently in clinical use. Research on compounds **114** and **115** show promising biological properties.

Although platinum(II) complexes are the basis of treatment for many cancers, initial positive results have been achieved in clinical use. However, it is possible for patients to develop resistance, reducing the effect of the drug.<sup>280</sup> This has been explained by different mechanisms including changes in cellular uptake and efflux of the drug, increased detoxification of the drug, inhibition of apoptosis and increased DNA repair.<sup>281</sup> The resistance mechanism opens a niche for the development of new complexes aimed at improving the efficacy of this kind of drug. Among the variety of platinum(II) complexes that have been investigated for antitumor activity, it was found that, in general, neutral complexes exhibit activity while charged species tend to be inactive and relatively nontoxic.<sup>282</sup> This is not always the case, however, since there are examples of positively charged platinum(II) complexes that exhibit unusual potency as anticancer drugs. That is the case of triplatin tetranitrate **114**<sup>279</sup> and phenanthriplatin **115** (Figure 3.23).<sup>283</sup>

The novel tridentate ligand **109**, developed by this group, contains a pyrene moiety which is an example of PAH. PAHs are soluble in lipids, and are capable, when metabolically activated, of interacting with cellular molecules, such as proteins and nucleic acids. This leads them to be considered as indirect-acting carcinogens.<sup>284</sup> PAHs can also act as DNA

intercalators, as was stated in Section 1.5.1.1 – they are characterized by the insertion of planar aromatic or heteroaromatic rings between DNA base pairs.<sup>285, 286</sup> This kind of interaction leads to the inhibition of topoisomerases I and II, which would eventually inhibiting the activity of the DNA or RNA polymerases involved in the processes of DNA replication.<sup>287, 288</sup> Therefore, PAHs offer a different approach to developing interesting chemotherapeutic DNA intercalators.<sup>85, 289, 290</sup>

In an effort to make a platinum(II) complex similar to the cisplatin analogues presented above, **109** and  $[\text{PtCl}_2(\eta^2:\eta^2\text{-cod})]$  were reacted in dichloromethane at room temperature. After being washed with hexane to remove the remaining cyclooctadiene,  $[\text{PtCl}(\mathbf{109})][\text{Cl}]$  (**116**) was produced as a white solid with an excellent yield of 76% (Figure 3.24).

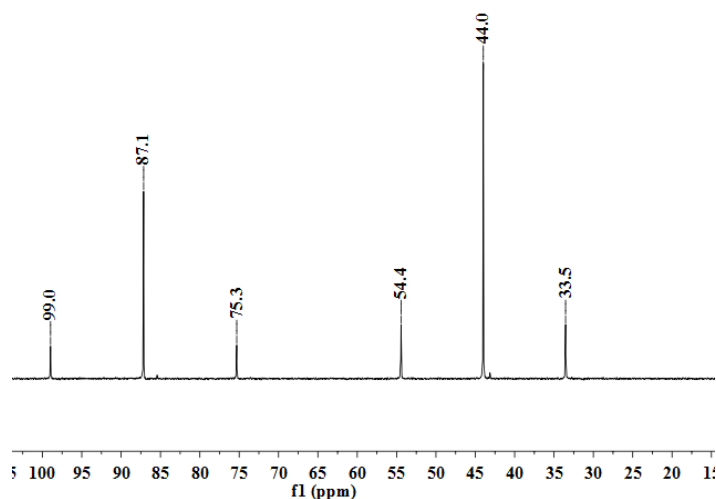


**Figure 3.24** Synthesis of the square planar platinum(II) complex  $[\text{PtCl}(\mathbf{109})][\text{Cl}]$  **116**.

The  $^{31}\text{P}\{^1\text{H}\}$  NMR spectrum of complex  $[\text{PtCl}(\mathbf{109})][\text{Cl}]$  **116** displayed signals at  $\delta$  87.1 ppm for the central phosphorus atom and at  $\delta$  44.0 ppm for the terminal phosphorus atoms, with  $^1J_{\text{PPt}}$  values of 2883 and 2538 Hz. These values are common for a phosphorus atom *trans* to a chloride and a phosphorus atom *trans* to another phosphorus atom respectively.<sup>291-293</sup>

No phosphorus-phosphorus coupling was observed, but this is not unexpected for complexes of this type. Meek *et al.* worked on a series of platinum-polyphosphine complexes, which showed coupling constants of  $<0.8$  Hz.<sup>294</sup> The  $^{31}\text{P}\{^1\text{H}\}$  NMR signals for the coordinated phosphine are significantly shifted downfield in comparison to the free ligand, a phenomenon also found for related chelating ligand complexes.<sup>294-296</sup> The magnitude of the change in chemical shift ( $\Delta\delta$ ) for chelated phosphines is dependent on the size and number of chelate rings containing the phosphorus atom.<sup>294-296</sup> For example, the  $^{31}\text{P}\{^1\text{H}\}$  NMR spectrum of the reported compound  $[\text{PtCl}(\text{triphos-Ph})][\text{SnPh}_2\text{Cl}_3]$  showed a signal for the terminal P-atoms at  $\delta$  39.8 ppm, for the central P-atom at  $\delta$  83.7 ppm, and the  $^1J_{\text{PPt}}$  values found were 3015 and 2484 Hz respectively.<sup>295</sup> For the central phosphorus atom the observed  $\Delta\delta$  from unchelated ligand to complex is 107.7 ppm, which

is extremely large compared to those of the terminal phosphorus atoms, where  $\Delta\delta = 44.0$  ppm. The substantial difference in  $\Delta\delta$  values for the central compared to the terminal phosphorus is due to the central phosphorus being part of two five-membered chelate rings.<sup>297</sup>



**Figure 3.25**  $^{31}\text{P}\{^1\text{H}\}$  NMR spectrum of  $[\text{PtCl}(\mathbf{109})][\text{Cl}]$  **116**; the peak at  $\delta$  87.1 ppm is assigned to the central phosphorus atom and the peak at  $\delta$  44.0 ppm is assigned to the terminal phosphorus atoms.

The satellites shouldering the main peaks in the  $^{31}\text{P}\{^1\text{H}\}$  NMR spectrum of  $[\text{PtCl}(\mathbf{109})][\text{Cl}]$  **116** occur due to the coupling of  $^{31}\text{P}$  with the platinum nucleus. The isotope  $^{195}\text{Pt}$  consists of about 33.8% of the atomic content of platinum, with the rest of the platinum isotopes being NMR inactive. This means that 66.2% of the  $^{31}\text{P}$  nuclei in the sample do not couple to any nuclei; whereas 33.8% do couple to  $^{195}\text{Pt}$ , creating the satellite signals which can be seen around the main peak.

Crystals of  $[\text{PtCl}(\mathbf{109})][\text{Cl}]$  **116** suitable for X-ray crystallographic analysis were obtained from slow diffusion (hexane/dichloromethane). The Pt–P bond lengths (Figure 3.26) are in the expected range for platinum complexes and compare well to  $[\text{PtCl}(\text{triphos-Ph})][\text{Cl}]$ , where the Pt–P<sub>terminal</sub> bond lengths were 2.312(2), 2.315(2) Å and the Pt–P<sub>central</sub> bond length was 2.207(2) Å.<sup>297</sup> The Pt–P<sub>central</sub> bond length is found to be shorter than the Pt–P<sub>terminal</sub> due to the double chelate effect and to the lower *trans* influence of the chloride compared to the phosphorus atom. The complex has a distorted square planar geometry at the platinum, which is shown by the P–Pt–Cl bond angles of 93.71(5)° (P1–Pt–Cl1), 175.78(6)° (P2–Pt–Cl1) and 95.80(5)° (P3–Pt–Cl1) and the P–Pt–P bond angles of 84.93(5)° (P1–Pt–P2), 169.46(5)° (P1–Pt–P3) and 85.26(5) (4)° (P2–Pt–P3). However,

[PtCl(109)][Cl] **116** is less distorted relative to the ideal square planar geometry than similar nickel and palladium complexes.<sup>298</sup>

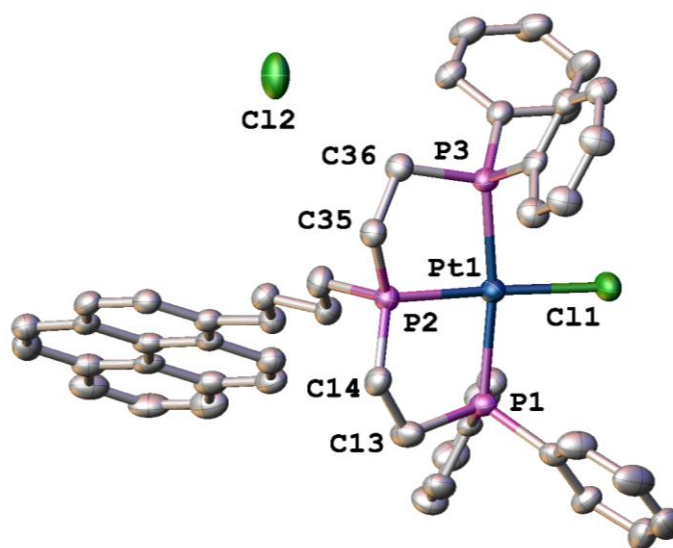


Figure 3.26 X-ray crystal structure view of [PtCl(109)]Cl **116** (50% probability ellipsoids with interesting chloride, platinum, phosphorus and carbon atoms labelled. Carbon atoms in grey).

Hydrogen atoms have been omitted for clarity: Pt1–P1 2.3090(12), Pt–P2 2.312(2), Pt–P3 2.3057(11), Pt–Cl1 2.3613(10), P1–C13 1.850(5), P2–C35 1.820(5), P2–C14 1.811(5), P3–C36 1.857(5); P1–Pt–P2 84.93(5), P1–Pt–P3 169.46(5), P2–Pt–P3 85.26(5), P1–Pt–Cl1 93.71(5), P2–Pt–Cl1 175.78(6), P3–Pt–Cl1 95.80(5).

### 3.4.1.2 Palladium

Palladium phosphine complexes are well known to be a useful resource for catalytic processes which utilise alkenes as substrates. For example, Pd(PPh<sub>3</sub>)<sub>4</sub> **117** has been used for creating a C–C bonds for synthesising caparratrien, a compound that shows considerable growth inhibition in CEM leukemia cells.<sup>299</sup> These type of palladium complexes are widely used for coupling reactions. That is the case for the complexes (1,1'-bis(diphenylphosphino)ferrocene) palladium(II) dichloride **118**,<sup>300</sup> and the butyl-containing complex [1,4-bis-(diphenylphosphine)butane] palladium(II) dichloride **119**.<sup>301</sup>

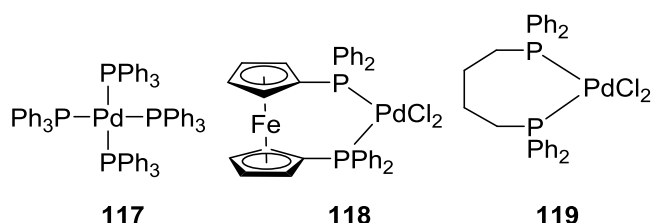
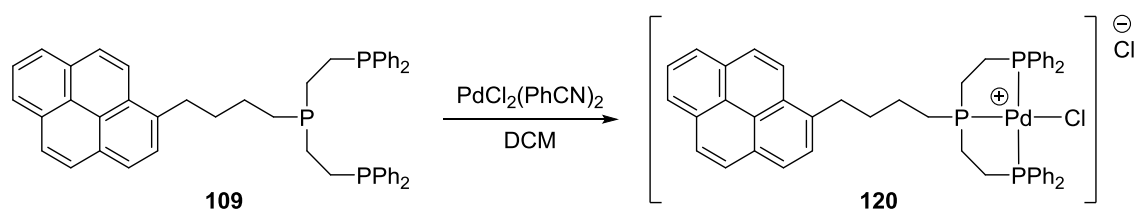


Figure 3.27 Examples of palladium phosphine complexes used in the catalysis of coupling reactions.

The similarity between the coordination chemistry of palladium(II) and platinum(II) compounds has encouraged studies of Pd(II) complexes as antitumor drugs, giving promising results due to the lanthanide contraction.<sup>302-305</sup> It is worth noting that several Pd complexes have been reported to display favourable cytotoxicity at pH 6.8, a predominant condition in tumour cells (the pH of normal cells is 7.4).<sup>305</sup> Furthermore, hydrolytic and DNA-binding studies on the Pd(II) and Pt(II) complexes with anticancer activities showed that the palladium complexes are kinetically labile, produce new charged species to interact with DNA and bind at a faster rate than the platinum complexes.<sup>303</sup> However, Pt(II) complexes are more stable than those of Pd(II), since Pd(II) compounds exchange ligands  $10^4$ – $10^5$  times faster than analogous Pt(II) compounds, which means that Pd(II) complexes do not reach the targeted tissue.<sup>266, 306</sup> This might be modified using ligands that provide more stability to the complex.

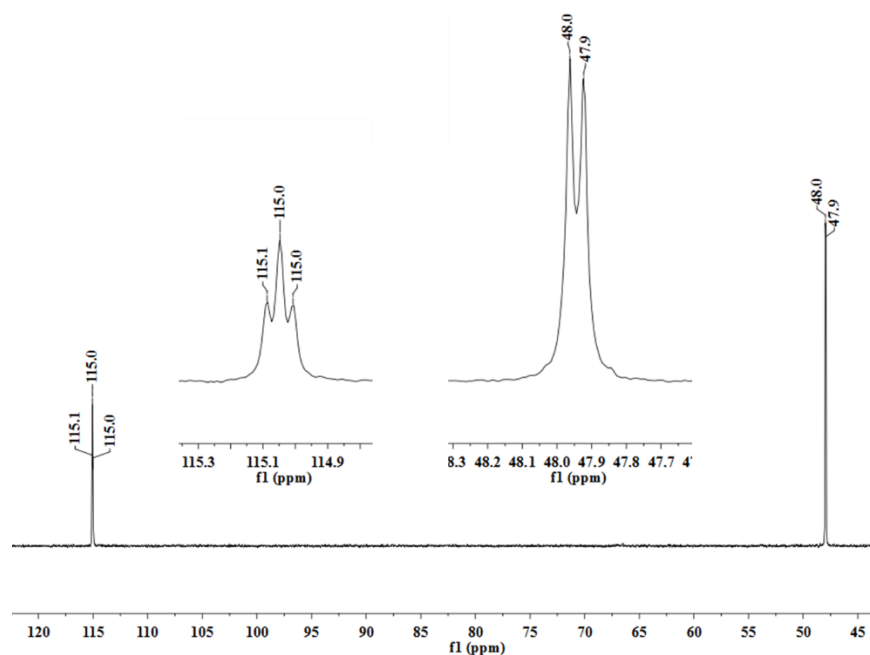
One equivalent of the novel tripodal ligand **109** was reacted with the palladium(II) precursor  $[\text{PdCl}_2(\text{PhCN})_2]$  in dichloromethane for 2 hours,<sup>307</sup> which afforded the palladium(II) complex  $[\text{PdCl}(\mathbf{109})]\text{Cl}$  **120** (Figure 3.28).



**Figure 3.28** Synthesis of the palladium(II) complex,  $[\text{PdCl}(\mathbf{109})]\text{Cl}$  **120**.

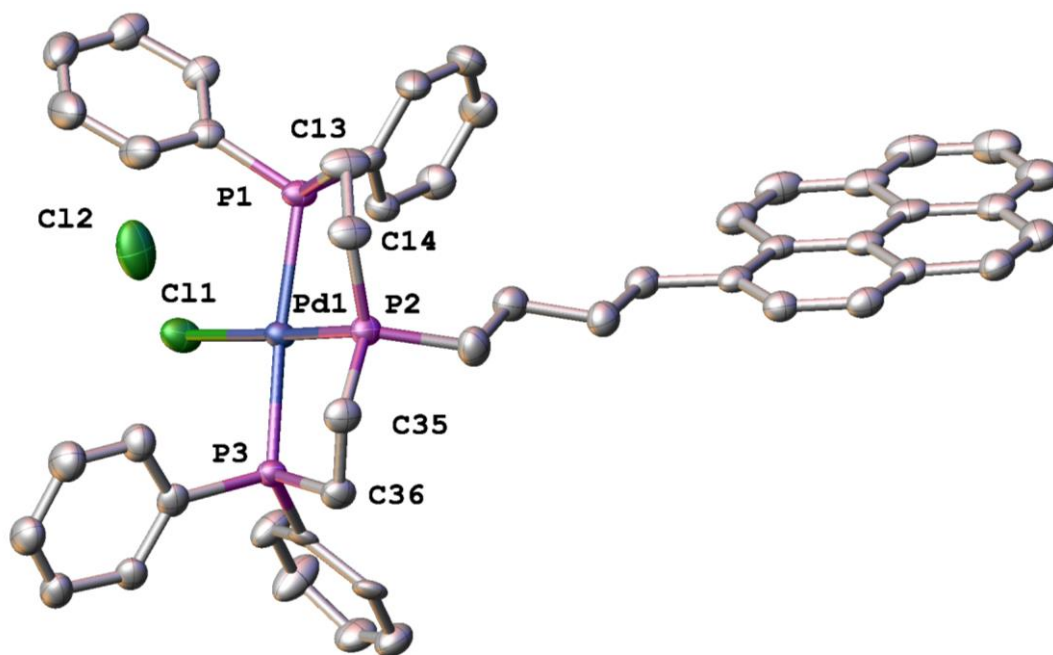
As depicted in Figure 3.28; the three phosphino in ligand **109** coordinate to the palladium, replacing the labile benzonitrile ligands and a chloride atom. Coordination of the phosphine groups caused a downfield shift of their  $^{31}\text{P}\{^1\text{H}\}$ NMR signals. The two terminal phosphines in the free tridentate ligand **109** produce a doublet at  $\delta$  –12.2 ppm and the phosphine in the central position produces a triplet at  $\delta$  –20.6 ppm, the  $^3J_{\text{PP}}$  coupling value for these signals is 26.5 Hz. On the other hand, the  $^{31}\text{P}\{^1\text{H}\}$ NMR spectrum of complex  $[\text{PdCl}(\mathbf{109})]\text{Cl}$  **120** shows a triplet at 115.1 ppm and a doublet at 47.9 ppm, whose  $^3J_{\text{PP}}$  coupling value is 6.3 Hz.





**Figure 3.29**  $^{31}\text{P}\{^1\text{H}\}$  NMR spectrum of the reaction of  $\text{PdCl}_2(\text{PhCN})_2$  and **109** in dichloromethane.

Previous reports of phosphines with a palladium(II) centre indicate a difference in the bond length in P–Pd bond;<sup>308-310</sup> the central tridentate phosphorus tends to form a shorter P–Pd bond than the ones located on the sides of the metallic centre. This trend is also observed on the novel complex  $[\text{PdCl}(\mathbf{109})]\text{Cl}$  **120**. A sample suitable for X-ray crystallographic analysis was achieved from a saturated solution of  $[\text{PdCl}(\mathbf{109})]\text{Cl}$  **120** in dichloromethane and hexane. The complex shows a square planar palladium(II) coordination geometry with the following bond lengths: Pd1–Cl1 2.3593(7), Pd1–P1 2.3188(7), Pd1–P2 2.2175(7) and Pd1–P3 2.3143(7). The angles of the palladium centre are: P1–Pd1–Cl1 94.77(2), P3–Pd1–Cl1 96.60(2), P2–Pd1–P1 84.06(2) and P2–Pd1–P3 84.06(2). It is noticeable that the angles containing the Cl1 atom are slightly wider than the other two contained in the same plane. The chlorine atom is not significantly bigger than the phosphorus atom<sup>311</sup>; therefore, the increased angles are not due to steric interactions. The phenyl groups in P1 and P3 take a spatial arrangement that approach the vicinity of chlorine. Hence, they are more likely to be the factor that increases these angles (Figure 3.30).



**Figure 3.30** X-ray crystal structure view of  $[\text{PdCl}(109)]\text{Cl}$  120 (50% probability ellipsoids with interesting carbon, chlorine, palladium and phosphorus atoms labelled. Carbon atoms in grey). Hydrogen atoms have been omitted for clarity. Selected bond distances [ $\text{\AA}$ ] and angles [ $^\circ$ ]: Pd1–Cl1 2.3593(7), Pd1–P1 2.3188(7), Pd1–P2 2.2175(7), Pd1–P3 2.3143(7); P1–Pd1–Cl1 94.77(2), P2–Pd1–Cl1 175.80(3), P2–Pd1–P1 84.06(2), P3–Pd1–Cl1 96.60(2), P3–Pd1–P1 167.74(2), P2–Pd1–P3 84.06(2).

### 3.4.1.3 Nickel

Nickel complexes have mainly been studied for their application in catalysis.<sup>312-316</sup> The most common example of the use of nickel in catalysis is the Raney nickel alloy, which is used as a catalyst in organic chemistry for the hydrogenation double bonds.<sup>317</sup> Previous studies in prokaryotic and eukaryotic cells have shown that nickel is required to produce certain vital enzymatic activities. For example, the enzyme urease, used for converting urea in ammonia, requires the presence of nickel in order for the cell to function correctly.<sup>318</sup> On the other hand, nickel is known to be a toxic metal when found in the human body in high concentrations.<sup>319, 320</sup> Various studies show that nickel complexes have interesting biological properties.<sup>269, 321</sup> Ferrari *et al.* developed a nickel complex using a *p*-fluorobenzaldehyde thiosemicarbazone as a ligand, which produced a cell inhibiting effect in very resistant human cell lines. No cytotoxic effects were observed during this procedure.<sup>322</sup> Notably, most biological studies on this element have been performed in its complexed form using different thiocarbazonates as ligands.<sup>269, 321-324</sup>

To our knowledge, there are no examples of nickel(II) phosphine complexes with a fluorescent polyaromatic hydrocarbon moiety. Therefore, one equivalent of **109** was reacted with the nickel(II) precursor  $[\text{NiCl}_2(\text{py})_4]$  in dichloromethane for 2 hours, which afforded the nickel(II) complex  $[\text{NiCl}_2(\text{py})(\mathbf{109})]$  **121**.

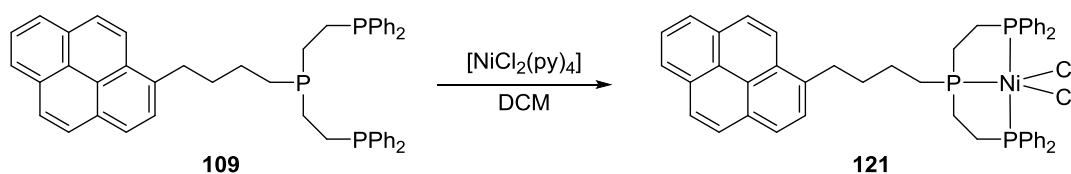


Figure 3.31 Synthesis of the nickel(II) complex,  $[\text{NiCl}_2(\mathbf{109})]$  **121**.

The  $^{31}\text{P}\{^1\text{H}\}$  NMR spectrum of the compound showed a triplet at  $\delta$  115.9 ppm, and a doublet at  $\delta$  50.0 ppm with  $^3J_{\text{PP}} = 42.5$  Hz. Both signals are significantly shifted downfield in comparison with the uncoordinated ligand **109**, whose doublet comes at  $-12.2$  and triplet at  $-20.6$  ppm, proving that there was a change in the chemical environment of the phosphorus atoms. In addition, the presence of no more than two signals indicates that there was no formation of different structural isomers.

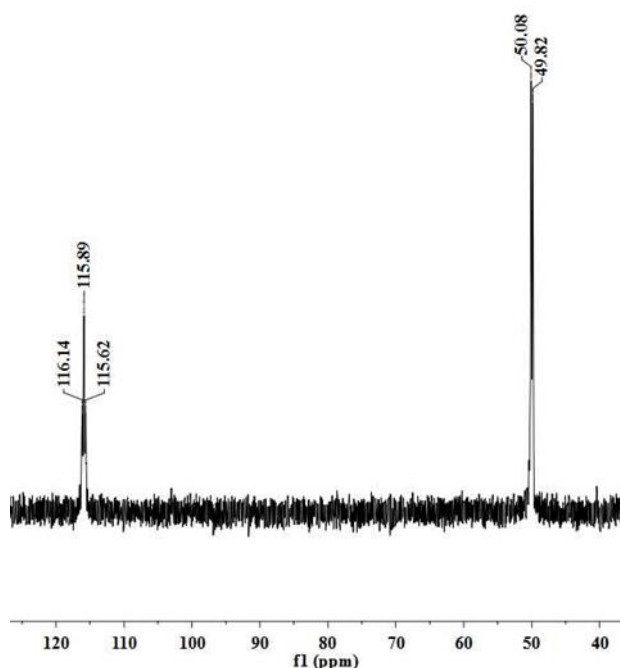
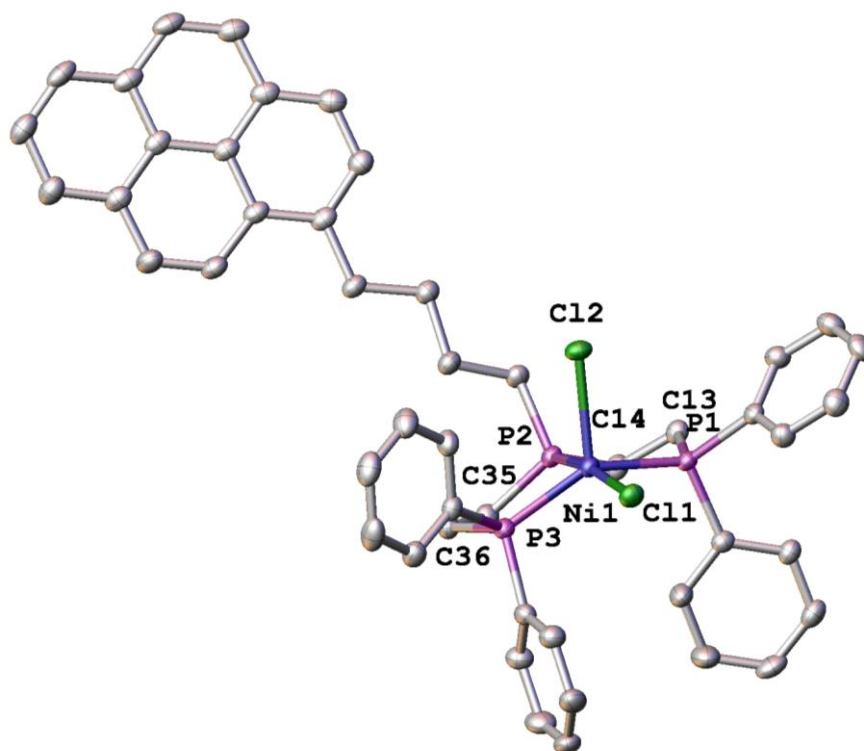


Figure 3.32  $^{31}\text{P}\{^1\text{H}\}$  NMR spectrum of the reaction of  $[\text{NiCl}_2(\text{py})_4]$  and **109** in dichloromethane to give the proposed complex **121**.

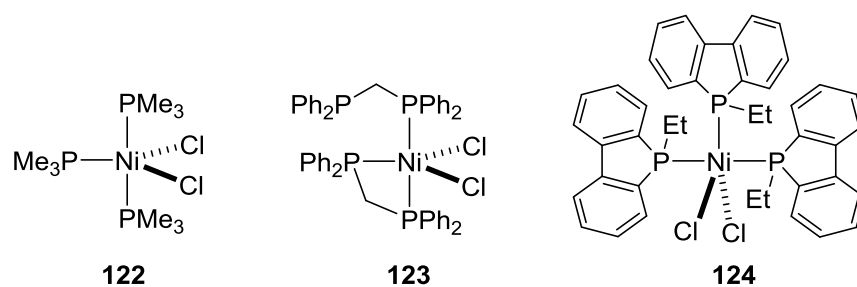
The X-ray analysis confirmed that the tridentate ligand displaced three pyridine molecules as expected. However, a fourth pyridine molecule was also eliminated, which

resulted in the coordination geometry around the nickel atom to be intermediate between trigonal bipyramidal (with C11 and P2 atoms at the axial sites) and square pyramidal (with a Cl2 atom at the axial site). The Ni–Cl2 bond, 2.7749 Å, is 0.2238 Å longer than the Ni–Cl1 bond. A previous report about a similar phosphine with an unusually long Ni–Cl bond, 2.669 Å, indicates that this can be attributed to electronic effects.<sup>325, 326</sup> Another interesting feature of this analysis is that Ni–P2 and Ni–P3 bonds are longer than Ni–P(1) due to the higher trans influence of the phosphine ligands compared to chloride.



**Figure 3.33** X-ray crystal structure view of [NiCl<sub>2</sub>(109)] **121** (50% probability ellipsoids with interesting carbon, chlorine, phosphorus and nickel atoms labelled. Carbon atoms in grey). Hydrogen atoms have been omitted for clarity. Selected bond distances [Å] and angles [°]: Ni1–Cl1 2.2510(7) Ni1–Cl2 2.4749(7), Ni1–P1 2.2176(8), Ni1–P2 2.1577(7), Ni1–P3 2.1856(9), P1–C13 1.843(2), P2–C14 1.829(3), P2–C35 1.825(3), P3–C36 1.843(2); Cl1–Ni1–Cl2 93.71(2), P1–Ni1–Cl1 92.51(2), P1–Ni1–Cl2 97.70(2), P2–Ni1–Cl1 170.24(3), P3–Ni1–Cl2 116.04(2), P2–Ni1–Cl2 96.03(2), P2–Ni1–P1 85.61(2), P2–Ni1–P3 86.51(2), P3–Ni1–Cl1 89.76(2), P3–Ni1–P1 145.97(3).

The CSD contains three examples of pentacoordinated nickel (II) complexes containing three phosphines and two chlorines as ligands, complexes **122–124** (Figure 3.34).<sup>327, 328</sup> These complexes also displayed intermediate geometry between trigonal bipyramidal with a Cl atom in the axial position and square pyramidal.



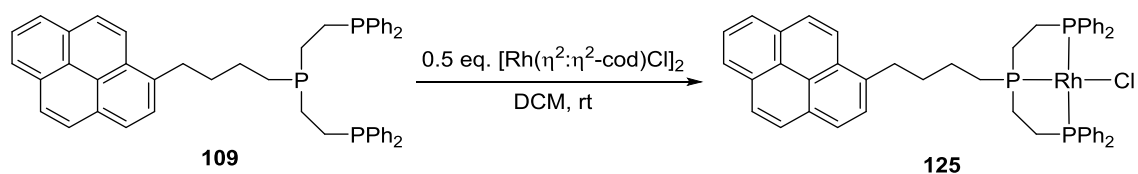
**Figure 3.34 Ni(II) complexes containing phosphines as ligands, the three complexes display an intermediate geometry between trigonal bipyramidal and square pyramidal.**

### 3.4.2 Group 9 coordination chemistry of tridentate phosphine **109**

#### 3.4.2.1 Rhodium

Four-coordinate polydentate phosphine complexes of rhodium have been investigated for use in catalysis<sup>329</sup> and medicine. This is because the  $d^8$  electronic configuration mimics that of the cytotoxic complex cisplatin.<sup>27</sup> Therefore we were interested in the coordination chemistry of ligand **109** with the group 9 metal.

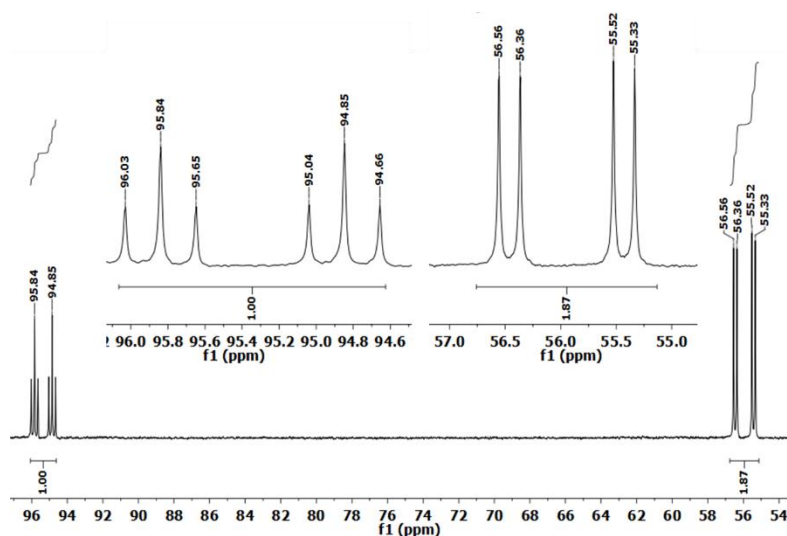
This reaction was tried using  $[\text{Rh}(\text{nbd})_2]\text{BF}_4$  and  $[\text{Rh}(\eta^2:\eta^2\text{-cod})_2]\text{BF}_4$  as the source of Rh and reacting them, separately, with the tridentate ligand **109**. However, the  $^{31}\text{P}\{^1\text{H}\}$  NMR analysis of both samples showed a mixture of different products, probably due to the formation of different isomers. Finally,  $[\text{Rh}(\eta^2:\eta^2\text{-cod})\text{Cl}]_2$  was used. The reaction of two equivalents of **109** with one equivalent of  $[\text{Rh}(\eta^2:\eta^2\text{-cod})\text{Cl}]_2$  in dichloromethane at ambient temperature produced the rhodium(I) species  $[\text{Rh}(\text{Cl})(\mathbf{109})]$  **125**, as depicted below.



**Figure 3.35 Preparation of rhodium(I) complex  $[\text{Rh}(\text{cod})](\mathbf{109})$  **125**.**

The  $^{31}\text{P}\{^1\text{H}\}$  NMR spectrum of the Rh-Triphos complex  $[\text{RhCl}(\text{PhP}(\text{CH}_2\text{CH}_2\text{PPh}_2)_2)]$  in  $\text{CD}_2\text{Cl}_2$  consists of a simple first-order  $\text{AM}_2\text{X}$  splitting pattern producing a doublet of triplets for the central phosphorus atom and a doublet of doublets for the two magnetically equivalent terminal P atoms of the  $\text{PhP}(\text{CH}_2\text{CH}_2\text{PPh}_2)_2$  ligand.<sup>330</sup> This is the same pattern displayed by the  $^{31}\text{P}\{^1\text{H}\}$  NMR spectrum of **125** where the central phosphorus atom shows a triplet and the two terminal phosphorus atoms display a doublet that resembles

an  $AM_2X$  system. The  $^{31}P\{^1H\}$  NMR spectrum of **125** shows a doublet of triplets at  $\delta$  93.4 ppm with a  $^1J_{PRh} = 120.2$  Hz, proving the formation of a P–Rh bond with the central P atom, and a  $^2J_{PP} = 23.0$  Hz. This value of  $^1J_{PRh}$  correlates to the one reported for the central P atom in the  $[RhCl(PhP(CH_2CH_2PPh_2)_2)]$  complex,  $^1J_{PRh} = 163$  Hz.<sup>330</sup> The spectrum also shows a doublet of doublets at  $\delta$  55.9 ppm with a  $^1J_{PRh} = 124.5$  Hz. This value proves the formation of a P–Rh bond with the terminal P atoms of the ligand. Unfortunately it was not possible to obtain crystalline material suitable for X-ray crystallography in order to get more information about the structural arrangement of this compound.



**Figure 3.36** The  $^{31}P\{^1H\}$  NMR spectrum of  $[RhCl(109)]$  **125** showing a  $AM_2X$  multiplicity pattern.

The  $^1H$  NMR spectrum of  $[RhCl(109)]$  **125** does not show the peaks reported for  $\eta^2:\eta^2$ -cod protons in  $[Rh(\eta^2:\eta^2\text{-cod})Cl]_2$ ,<sup>331</sup> which suggests that the final product does not contain that moiety. This spectrum was measured in a Bruker machine model Ascend with a 700 MHz magnet in order to improve the definition of the sample since the spectrometer JEOL ECS with a 400 MHz magnet provided poor definition.

The NMR analysis suggests that the structure of the resulting product is the one depicted in Figure 3.35 for the complex  $[RhCl(109)]$  **125** where the tridentate ligand **109** is tricoordinated to the Rh atom which holds a chlorine ligand.

### 3.4.2.2 Iridium

Iridium organometallic complexes have recently shown promising potential in medicinal imaging with particular emphasis in fluorescence confocal microscopy using 2-phenylpyridine based ligands.<sup>332-334</sup> Complex **126** was developed by Murphy *et al.*<sup>332</sup> as an agent which emission can be reversibly red-shifted when protonated. Complex **127** has been developed as a luminescent compound that shows interesting cytotoxic properties toward HeLa cell lines.<sup>333</sup> Research carried out by Meggers *et al.* afforded the iridium complex **128**, which shows dual anticancer activity, (I) it contains a structural scaffold for molecular recognition of protein kinases, which results in antiangiogenic properties, and (II) it shows visible-light induced anticancer activity through the initiation of cellular apoptosis (Figure 3.37).<sup>335</sup>

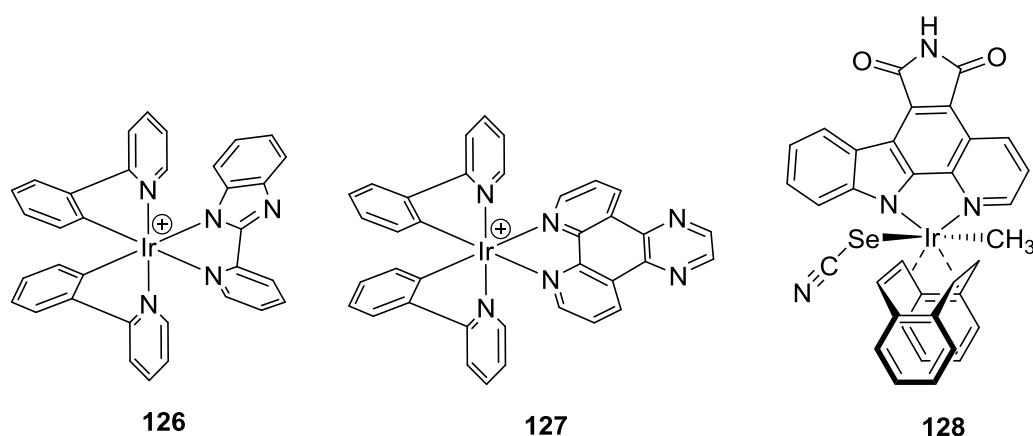
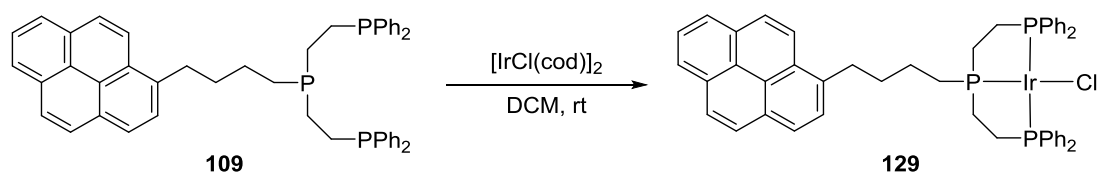


Figure 3.37 Iridium complexes 126-128 that have shown interesting biological properties.<sup>335</sup>

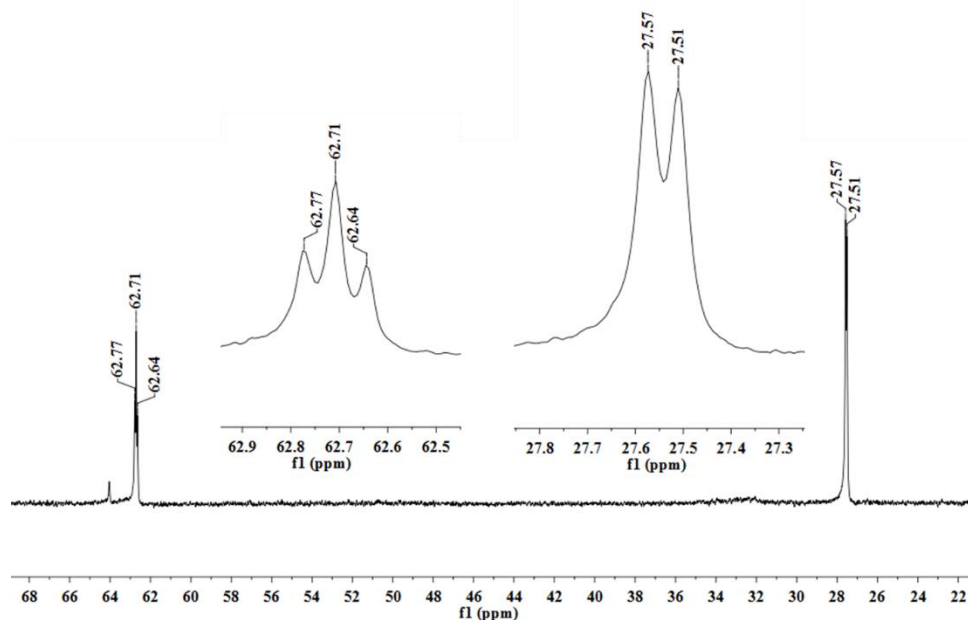
Following the interesting results with rhodium, and the aforementioned background knowledge about the biological applications of iridium(I) complexes, we attempted the preparation of a fluorescent iridium(I) complex, which may have therapeutic and cell imaging applications parallel to the complexes introduced previously. Kubiak and co-workers showed that the complex  $[\text{Ir}(\text{cod})(\text{triphos-Ph})][\text{Cl}]$  is formed from reacting triphos-Ph and  $[\text{Ir}(\text{cod})\text{Cl}]_2$ . Therefore, two equivalents of **109** were therefore reacted with a DCM solution of  $[\text{Ir}(\text{cod})\text{Cl}]_2$ , which led to the formation of  $[\text{IrCl}(\mathbf{109})]$  **129** (Figure 3.38), whose structure was corroborated through the molecular formula found by HRMS.



**Figure 3.38** Synthesis of the iridium(I) complex  $[\text{IrCl}(\text{109})][\text{Cl}]$  **129**.

The  $^3\text{1P}\{^1\text{H}\}$  NMR spectrum gave an  $\text{AX}_2$  spin system:  $\delta$  62.7 (t), 27.5 (d) ppm (1:2) with a small  $^3J_{\text{PP}}$  coupling constant of 10.6 Hz, these values match those of the iridium(I) complex  $[\text{Ir}(\text{cod})(\text{triphos-Ph})][\text{Cl}]$ <sup>336</sup> well. Unlike the iridium(I)-triphos complex reported, the complex we obtained retained the chloride ligand at the expense of the cyclooctadiene ligand. Unfortunately, it was not possible to obtain a crystal structure suitable for X-ray analysis. However, characterisation using HRMS allowed us to determine the mass of the sample. The observed mass for this compound matches the mass of the theoretical isotope pattern of proposed structure **129**. The mass  $m/z$  value found in the sample was 943.2125 which is the same mass of the protonated form of complex **129**. The  $^1\text{H}$  NMR analysis of complex **129** was too broad for accurate interpretation.

As mentioned previously, iridium complexes have shown interesting features as confocal microscopy agents. Therefore, complex **129** could be tested in this area.



**Figure 3.39**  $^3\text{1P}\{^1\text{H}\}$  NMR spectrum of  $[\text{IrCl}(\text{109})][\text{Cl}]$  **129** in  $d$ -chloroform, showing the expected doublet and triplet splitting.



### 3.5 Photophysical data

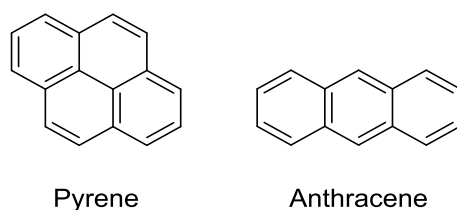
After the effective synthesis of the tridentate phosphine **109** and several transition metal complexes, it was imperative to determine their photophysical properties in order to understand how the different metals change the properties of the pyrene moiety in the different analogues. Our initial concern was whether the heavy metals or would quench the fluorescence of the PAH fluorophore, a phenomenon which is well documented, including in systems where pyrene is the fluorophore.<sup>337-340</sup> The three phosphorus atoms of the tridentate ligand **109** could provoke a similar effect. Table 3.2 shows the absorption maxima ( $\lambda_{\text{abs}}$ ) and emission maxima ( $\lambda_{\text{em}}$ ) of the series of interest showing similar values to the ones recorded for other propargyl pyrene derivatives.<sup>341</sup> It is possible to observe that the Stokes shift ( $\Delta\nu_{\text{st}}$ ) in the different compounds did not experience a considerable change. The most common cause of  $\Delta\nu_{\text{st}}$  is the rapid photon decay from  $S_1$  to  $S_0$ . In addition, fluorophores can decay through vibrational levels, resulting in an additional loss of excitation energy in the form of heat.<sup>40</sup> Therefore, the lack of variation in the reported  $\Delta\nu_{\text{st}}$  values indicates that the different functional groups and metals do not increase vibrational effects.

Compound	$\lambda_{\text{abs}}$ (nm)	$\lambda_{\text{em}}$ (nm)	$\epsilon$ (cm <sup>-1</sup> /M)	$\Delta\nu_{\text{st}}$ (nm)
<b>Pyr(CH<sub>2</sub>)<sub>4</sub>Br 102</b>	342	376	49,000	34
<b>P(O)(OEt)<sub>2</sub> 103</b>	343	376	51,000	33
<b>Pyr(CH<sub>2</sub>)<sub>4</sub>PH<sub>2</sub> 95</b>	344	377	64,000	33
<b>Pyr(CH<sub>2</sub>)<sub>4</sub>P<sub>3</sub> 109</b>	344	377	30,000	33
<b>[RhCl(109)] 125</b>	342	376	64,000	34
<b>[NiCl<sub>2</sub>(109)] 121</b>	342	376	10,000	34
<b>[PdCl(109)]Cl 120</b>	342	376	10,000	34
<b>[PtCl(109)]Cl 116</b>	344	377	43,000	33

**Table 3.2 Photophysical data for the tridentate phosphine 109, its parent compounds and the complexes formed with it. Measured in degassed tetrahydrofuran at room temperature; dyes were excited at 350 nm.**

Pyrene is a compound that, in solution, forms species known as excimers.<sup>48</sup> An excimer is a short-lived dimeric or heterodimeric molecule formed from two molecules, at least

one of which has electrons that can be promoted to the excited state. This is key, because the formation of dimeric molecules takes place when the electrons are in the excited state.<sup>47</sup> This kind of phenomenon is quite common for pyrene, and results in fluorescence quenching of the sample.<sup>342</sup> Therefore, using pyrene as a reference to determine the  $\Phi_F$  of the synthesised compounds could lead to inconsistent results, due to the fluorescence quenching caused by excimer formation. There are studies in which the anthracene derivative 9,10-diphenylanthracene was used as a standard to measure  $\Phi_F$  of pyrene containing compounds.<sup>343</sup> Therefore, it was decided to use both pyrene and anthracene as fluorescence standards in order to compare the results. In order to avoid excimer formation, it was decided that all the samples should be prepared with an absorption of 0.04 at 317 nm when using pyrene as the fluorescence standard, since it is known that the formation of pyrene excimers takes place in solutions with higher concentrations than this.<sup>48</sup>



**Figure 3.40** Compounds used as fluorescence standards to measure the  $\Phi_F$  of the synthesised compounds.<sup>83</sup>

The resulting  $\Phi_F$  values are presented in the Table 3.3. They show that using pyrene as the fluorescence standard resulted in higher  $\Phi_F$  values than those obtained when using anthracene. The formation of pyrene excimers could explain this trend, since they produce a self-quenching effect, reducing the emission of the sample. Since the values obtained for the  $\Phi_F$  were higher when using pyrene as the standard, we can infer that the formation of excimers in the synthesised compounds is less prevalent than in pyrene. The results show that the phosphonate  $P(O)(OEt)_2$  **103** has the highest  $\Phi_F$  of all the compounds synthesised in the series. When using THF as the solvent it is possible to find a general trend of the  $\Phi_F$  regardless the fluorescent standard used:  $\Phi_F$  Pyr $P(O)(OEt)_2$  **103** >  $\Phi_F$  Pyr $(CH_2)_4P_3$  **109** >  $\Phi_F$  Pyr $(CH_2)_4Br$  **102** >  $\Phi_F$  Pyr $(CH_2)_4PH_2$  **95** >  $\Phi_F$ [NiCl $_2$ (**109**)] **121** >  $\Phi_F$ [RhCl(**109**)] **125** >  $\Phi_F$ [PtCl(**109**)]Cl **116** >  $\Phi_F$ [PdCl(**109**)]Cl **120**. On the other hand, there is no obvious trend when using chloroform as a solvent since it shows an

inconsistency for compounds  $\text{Pyr}(\text{CH}_2)_4\text{Br}$  **102** and  $\text{Pyr}(\text{CH}_2)_4\text{P}_3$  **109**. Another interesting feature is the fact that tetrahydrofuran appears to show the highest  $\Phi_F$ .

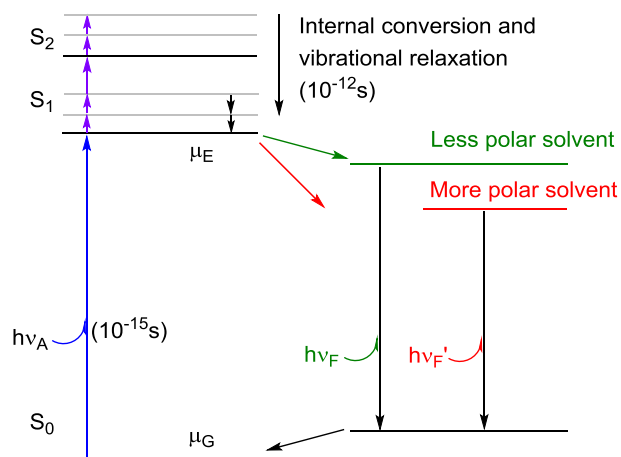
Compound	$\Phi_F^{\text{a,b}}$	$\Phi_F^{\text{a,c}}$	$\Phi_F^{\text{d,b}}$	$\Phi_F^{\text{d,c}}$
<b><math>\text{Pyr}(\text{CH}_2)_4\text{Br}</math> 102</b>	0.39	0.23	0.65	0.45
<b><math>\text{P}(\text{O})(\text{OEt})_2</math> 103</b>	0.43	0.27	0.73	0.61
<b><math>\text{Pyr}(\text{CH}_2)_4\text{PH}_2</math> 95</b>	0.39	0.26	0.49	0.27
<b><math>\text{Pyr}(\text{CH}_2)_4\text{P}_3</math> 109</b>	0.42	0.21	0.72	0.49
<b><math>[\text{RhCl}(\text{109})]</math> 125</b>	0.11	0.06	0.19	0.11
<b><math>[\text{NiCl}_2(\text{109})]</math> 121</b>	0.12	0.09	0.33	0.27
<b><math>[\text{PdCl}(\text{109})]\text{Cl}</math> 120</b>	0.01	0.01	0.13	0.09
<b><math>[\text{PtCl}(\text{109})]\text{Cl}</math> 116</b>	0.02	0.02	0.17	0.12

<sup>a</sup> Measured in degassed chloroform at room temperature. <sup>b</sup> Measured with respect to pyrene; dyes were excited at 317 nm. <sup>c</sup> Measured with respect to anthracene; dyes were excited at 350 nm <sup>d</sup> Measured in degassed tetrahydrofuran at room temperature.

**Table 3.3  $\Phi_F$  values using different fluorescence standards (pyrene and anthracene) to investigate the excimer formation effect of pyrene when using it as fluorescence standard.**

Typically, the fluorophore has a larger dipole moment in the excited state ( $\mu_E$ ) than in the ground state ( $\mu_G$ ). Following excitation the solvent dipoles reorient or relax around  $\mu_E$  reducing the energy of the excited state. The effects of solvent polarity are shown in the diagram below. Less polar solvents contribute to the vibrational relaxation to a lesser extent in comparison with more polar solvents. This causes the emission in less polar solvent to be higher.<sup>40</sup>

Tetrahydrofuran and chloroform have similar polarities, 4.0 and 4.1. Therefore, the results shown in Table 3.3 cannot be fully explained by this solvent relaxation effect. Another possible explanation would be the heavy atom effect. Since the magnitude of the nuclear magnetic field is directly proportional to the nuclear charge and to the atomic number, spin-orbit coupling increases with a higher atomic number. This results in an increase in the rate of radiationless transitions for molecules in the presence of atoms with high atomic numbers.



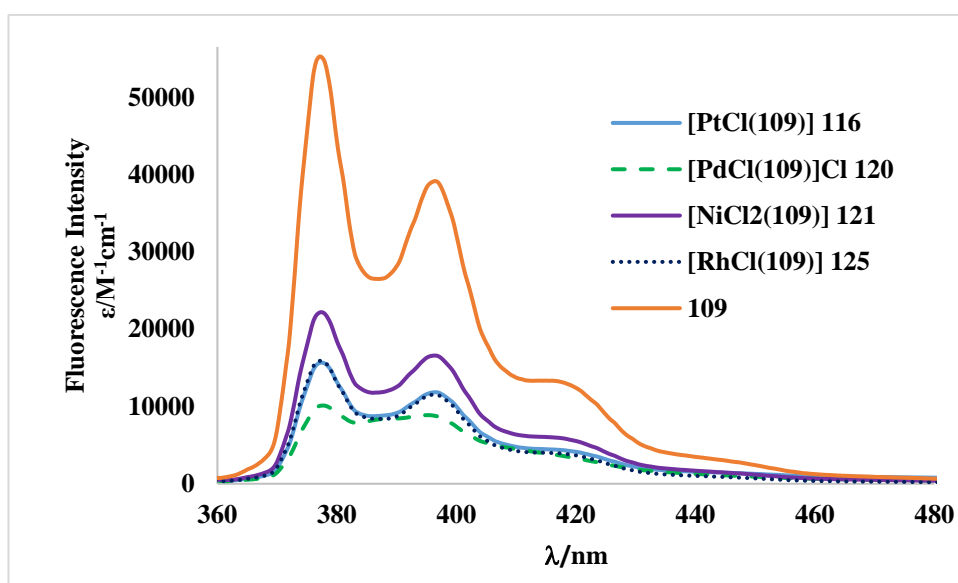
**Figure 3.41 Jablonski diagram for fluorescence with solvent relaxation effects included.**

When heavy atoms get in close contact to the fluorophore, the rate of intersystem crossing increases by a spin-orbit coupling.<sup>344</sup> Thus, the decrease of fluorescence ( $S_1$ - $S_0$ ) can be explained by an increase in the population of the competing triplet state ( $S_1$ - $T_n$ ), which is a radiationless transition of the fluorophore.<sup>345</sup> In addition, Kasha found that fluorescence quenching of aromatic compounds in solution in the presence of alkyl halides was due to an increase in spin-orbit coupling resulting from collisional or external perturbation due to interactions with molecules whose atoms have high atomic numbers.<sup>346</sup> The nature of the solvent can explain the  $\Phi_F$  obtained, since chloroform might exert the same quenching effect as that observed by Kasha. Therefore, the lower  $\Phi_F$  in the solutions prepared in chloroform could be due to the presence of chlorine atoms, with an atomic number, of 17, higher than any atom in tetrahydrofuran. A similar explanation can be used to rationalise the  $\Phi_F$  in the transition metal complexes. Previous comparisons have been made of the luminescent properties of first-row transition-metals in macrocycles, which showed that the nature of the central metal ion influences the ground-state absorption spectra of the macrocycle's excited singlet and triplet states.<sup>347, 348</sup>

The heavy atom effect suggests that high atomic numbers of metals in complexes would reduce their  $\Phi_F$  values. Therefore, the atomic numbers of the metals used for synthesising the complexes presented in this work (Ni = 28, Rh = 45, Pd = 46, Pt = 78) would suggest the following  $\Phi_F$  trend:  $\Phi_F[\text{NiCl}_2(\mathbf{109})] \mathbf{21} > \Phi_F[\text{RhCl}(\mathbf{109})] \mathbf{125} > \Phi_F[\text{PdCl}(\mathbf{109})]\text{Cl} \mathbf{120} > \Phi_F[\text{PtCl}(\mathbf{109})]\text{Cl} \mathbf{116}$ . This trend is correct for Ni and Rh based metals. However, for Pd and Pt the trend is reversed. The same trend is observed regardless the solvent or the fluorescent standard used for measuring the different  $\Phi_F$  of the synthesised complexes.

This experimentally found trend can be observed in the emission spectra in Figure 3.42. It is possible to observe the reduction in fluorescence from the tridentate ligand **109** to  $[\text{NiCl}_2(\mathbf{109})]$  **121**. Then  $[\text{RhCl}(\mathbf{109})]$  **125** and  $[\text{PtCl}(\mathbf{109})]\text{Cl}$  **116** show quite similar fluorescence intensities, albeit the fluorescence of the Rh complex is slightly higher than that of Pt complex. Finally, the fluorescence intensity of  $[\text{PdCl}(\mathbf{109})]\text{Cl}$  **120** is the lowest one of the whole set of complexes.

Another explanation for this lower fluorescence in the metal complexes in comparison with the free ligand **109** might be the solubility. The free ligand **109** is extremely soluble in THF and chloroform. However, in order to solubilise the different complexes, it was necessary to use a sonicator bath to dissolve them thoroughly. The sonication process might have dispersed small particles that might have reduced the fluorescence due a self-quenching effect.<sup>349</sup> This could explain the fact that the Pd complex had a lower fluorescence than the Pt complex despite their atomic numbers.



**Figure 3.42** Emission spectra of the tridentate phosphine **109** and complexes  $[\text{RhCl}(\mathbf{109})]$  **125**,  $[\text{NiCl}_2(\mathbf{109})]$  **121**,  $[\text{PdCl}(\mathbf{109})]\text{Cl}$  **120** and  $[\text{PtCl}(\mathbf{109})]\text{Cl}$  **116** in tetrahydrofuran (excitation at 350 nm) at 25 °C.

The  $\pi^*$ - $\pi$  emission spectrum of monomer pyrene<sup>350</sup> and propargyl pyrene derivatives<sup>341</sup> show two well-defined major bands between 370 and 400 nm and two shoulders with lower intensity between 410 nm and 450 nm. These bands and shoulders can be seen in the emission spectra of the free ligand **109** and its related metal complexes. There is no sign of hypsochromic or bathochromic shifts; which means that the bands are visible at the same wavelengths as in the pyrene emission spectrum.<sup>350</sup> The monomeric version of

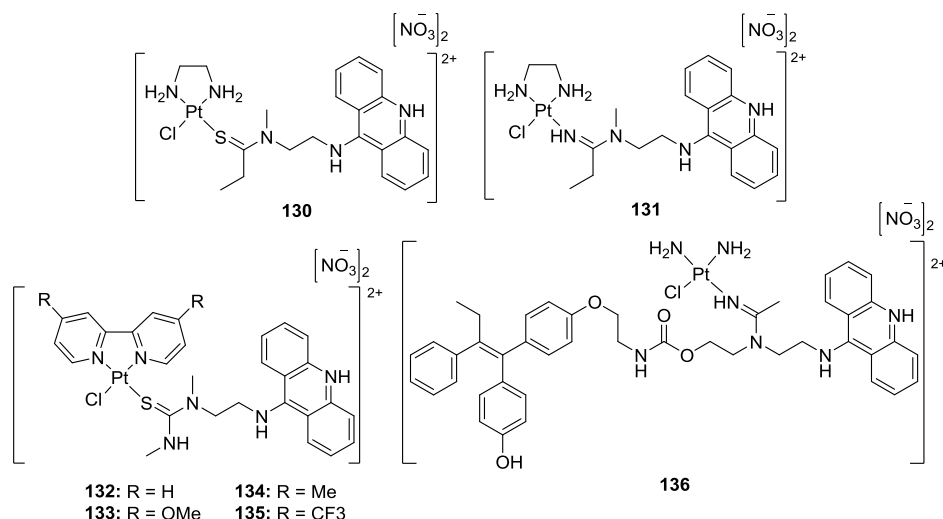
pyrene in ethanol shows  $\lambda_{em}$  at 393 nm.<sup>351</sup> Birks has reported that excimers of pyrene usually show a signal around 500 nm,<sup>342</sup> which is not visible in Figure 3.42. This suggests that there was no formation of excimers during the excitation of the complexes.

If these novel complexes are to be used as fluorescent probes, it is important for them to display fluorescence. These studies have shown that the complexes are fluorescent, so next their biological properties can be tested.

### 3.6 Cell studies with [PtCl(109)][Cl] 116

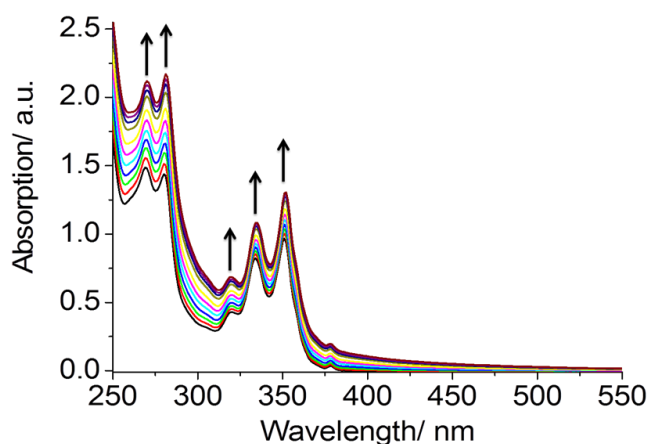
*This section was done in collaboration with the research group of Dr Kogularamanan (Rama) Suntharalingam at King's College London.*

Given the similarity in structure of [PtCl(109)][Cl] (116) and platinum-acridine agents<sup>352-358</sup> capable of intercalating between DNA base pairs and forming monofunctional-DNA adducts, the interaction of [PtCl(109)][Cl] (116) with double-stranded DNA was investigated.



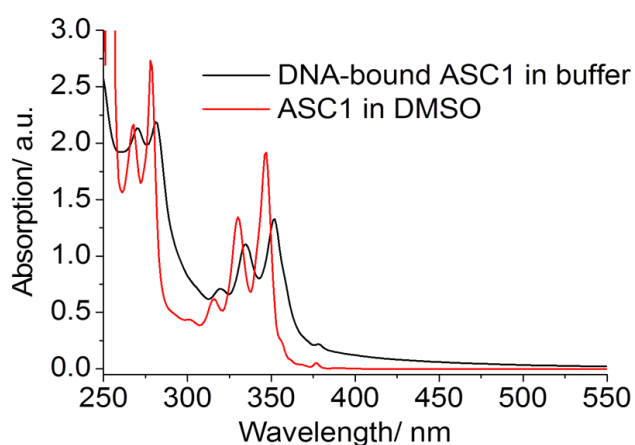
**Figure 3.43** Examples of different platinum-acridine agents developed as anticancer agents.

In order to determine the DNA affinity constant of [PtCl(109)][Cl] (116), UV-Vis spectroscopic studies were carried out with calf thymus DNA (ct-DNA).<sup>359</sup> Upon addition of aliquots of DNA (in the mM range) to an aqueous solution of [PtCl(109)][Cl] (116) (50  $\mu\text{M}$ ), significant spectral changes (hyperchromicity) were observed indicative of strong DNA interactions (Figure 3.44).



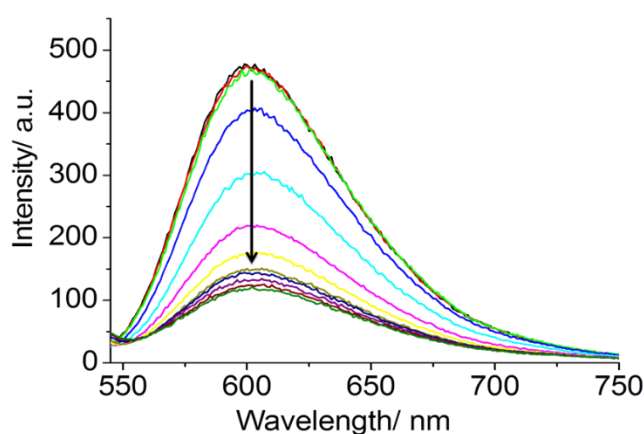
**Figure 3.44** UV-Vis spectra of [PtCl(**109**)]Cl (**116**) (50 μM) upon addition of aliquots of ct-DNA. The arrows show the hyperchromicity, indicator of strong DNA interactions.

From the change in absorption intensity, the concentrations of the bound and unbound metal complex were calculated and extrapolated to determine the apparent binding constant. The binding affinity of [PtCl(**109**)]Cl (**116**) for ct-DNA was  $6.1 \times 10^5 \text{ M}^{-1}$ . The planarity of the pyrene moiety suggests that the mode of interaction ought to be intercalative – such interactions result in hypochromicity upon DNA binding. However, in this case a large hyperchromic effect was observed upon addition of DNA to [PtCl(**109**)]Cl (**116**). In contrast, comparison of the UV-Vis spectrum of [PtCl(**109**)]Cl (**116**) (50 μM) in DMSO and [PtCl(**109**)]Cl (**116**) (50 μM) with ct-DNA (10 equivalents) in aqueous buffer, revealed a hypochromic effect accompanied by a red shift, indicative of intercalation (Figure 3.45).



**Figure 3.45** UV-Vis spectra of [PtCl(**109**)]Cl (**116**) or ASC1 (50 μM) in DMSO (red) and [PtCl(**109**)]Cl (**116**) or ASC1 (50 μM) with ct-DNA (10 equivalents) in aqueous buffer (black).

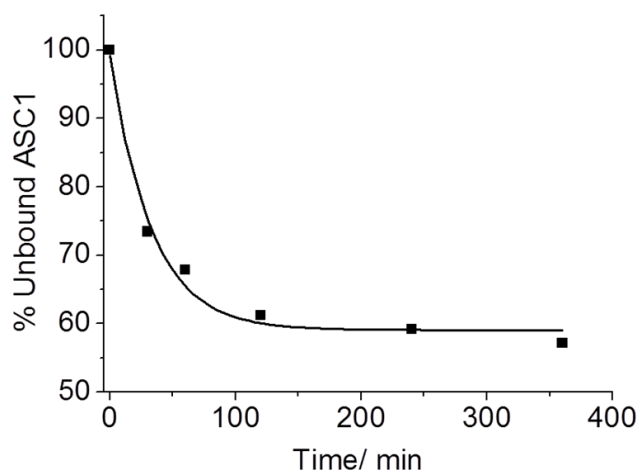
Collectively, the data implies that the complex self-aggregates in aqueous solutions, yielding a lower absorbance of the complex in the absence of DNA – this explains the hyperchromicity observed in Figure 3.44. Upon DNA binding, the  $[\text{PtCl}(\mathbf{109})][\text{Cl}]$  (**116**) aggregates are thought to disperse (increases absorption) before binding to DNA intercalatively. To confirm intercalation, the ethidium bromide displacement assay<sup>130</sup> was performed. Upon addition of  $[\text{PtCl}(\mathbf{109})][\text{Cl}]$  (**116**) to a solution of ct-DNA and ethidium bromide (1:20 ratio), the emission associated to the ethidium bromide-DNA complex (originating from the intercalation of ethidium bromide between DNA base pairs) decreased (Figure 3.46), showing that  $[\text{PtCl}(\mathbf{109})][\text{Cl}]$  (**116**) is able to displace ethidium bromide from DNA.



**Figure 3.46** Emission spectra for ethidium bromide (20  $\mu\text{M}$ ) bound to ct-DNA (1:20 ratio) upon addition of aliquots of ct-DNA.

This result confirms that  $[\text{PtCl}(\mathbf{109})][\text{Cl}]$  (**116**) is able to interact with DNA in an intercalative manner (most likely via the pyrene moiety). To assess the ability of  $[\text{PtCl}(\mathbf{109})][\text{Cl}]$  (**116**) to form irreversible covalent interactions with DNA (via the platinum-phosphine moiety), the ct-DNA precipitation assay was carried out. ct-DNA and  $[\text{PtCl}(\mathbf{109})][\text{Cl}]$  (**116**) were incubated (5:1 ratio) at 37 °C in aqueous buffer and, at certain time-points, ct-DNA was selectively precipitated. The amount of unbound complex was determined by measuring the UV-Vis absorption of the supernatant (Figure 3.47).

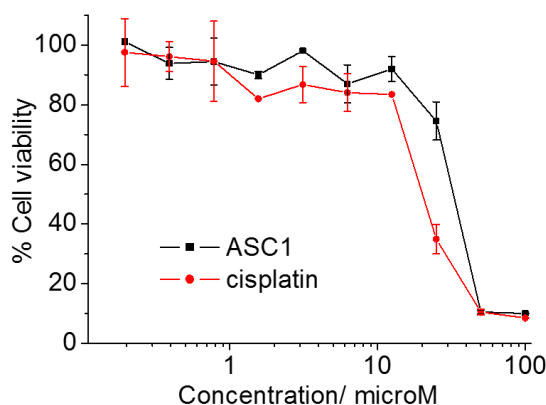




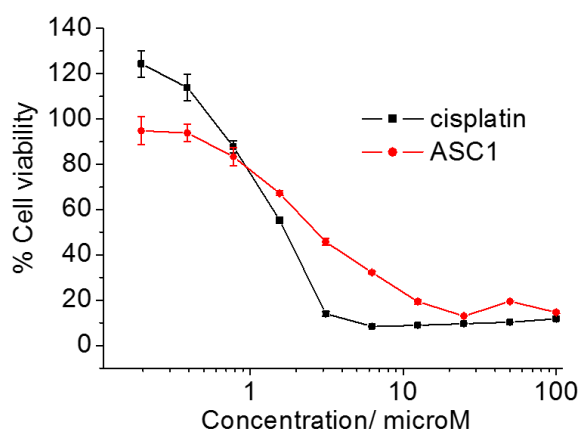
**Figure 3.47** Percentage unbound [PtCl(109)][Cl] (116) or ASC1 (25  $\mu$ M) at various time points after exposure of ct-DNA (250  $\mu$ M).

The absorption intensity of the supernatant decreased exponentially with time, suggestive of covalent binding to DNA. Around half of the available [PtCl(109)][Cl] (116) bound to DNA within 90 min. Overall, the biophysical data suggests that [PtCl(109)][Cl] (116) binds to DNA in dual-mode manner, intercalatively (via the pyrene moiety) and covalently (via the platinum-phosphine unit).

Metal complexes that show high affinity for DNA, often display promising antiproliferative properties. Thus, the cytotoxicity of [PtCl(109)][Cl] (116) toward bone osteosarcoma (U2OS) and transformed mammary cancer (HMLER) cells was determined using the colourimetric MTT assay. Cisplatin, a clinically administered platinum-containing anticancer drug, was used as a positive control. The  $IC_{50}$  values (the concentration required to reduce cell viability by 50%) were derived from dose-response curves (Figure 3.48 and Figure 3.49) and are summarised in Table 3.4.



**Figure 3.48** Average dose-response curves for the treatment of bone osteosarcoma (U2OS) cells with [PtCl(109)][Cl] (116) or ASC1 (n = 18 for each point).



**Figure 3.49** Average dose-response curves for the treatment of transformed mammary cancer (HMLER) cells with [PtCl(109)][Cl] (**116**) or ASC1 (n = 18 for each point).

The novel platinum(II) complex **116**, displayed micromolar potency towards both cell lines, to a similar or better degree than cisplatin. Given the promising antiproliferative data, further in vitro studies are now planned to decipher the mechanism of action of [PtCl(**109**)]Cl (**116**). The intercalating ability of the fluorescent pyrene function of complex **116**, should call into question its cell cytotoxic mechanism. The mechanism for [PtCl(**109**)]Cl (**116**) could be different from the mechanism of cisplatin since the popular anticancer drug cannot undergo DNA intercalation. Furthermore, via modifications to the pyrene and/or platinum-phosphine backbones, we hope to develop more potent agents.

Compound	U20S IC <sub>50</sub> [ $\mu$ M] <sup>[a]</sup>	HMLER IC <sub>50</sub> [ $\mu$ M] <sup>[a]</sup>
<b>116</b>	29.97 $\pm$ 3.09	1.62 $\pm$ 0.18
<b>Cisplatin</b>	20.35 $\pm$ 0.11	2.79 $\pm$ 0.18

**Table 3.4** IC<sub>50</sub> values of the complex **116** and cisplatin against bone osteosarcoma (U20S) and transformed mammary cancer (HMLER) cells. <sup>[a]</sup> Determined after 72 h incubation (mean of three independent experiments  $\pm$  SD).

### 3.7 Summary

By employing pyrene as a remote stability function, the novel air-stable primary phosphines PyrCH<sub>2</sub>PH<sub>2</sub> **94** and Pyr(CH<sub>2</sub>)<sub>4</sub>PH<sub>2</sub> **95** was prepared. This air-stability is consistent with that predicted theoretically by a DFT-based model. According to the calculations obtained, the addition of an alkyl linker group between the pyrene group and the phosphine group would provide a SOMO energy above -10 eV, which is the apparent threshold for air-stable phosphines, in line with our previous reports.<sup>37</sup> Once attained, the stability of the primary phosphines **95** was compared to that of the primary pyrene methylene phosphine, **94**. The stability of the phosphine containing a butyl group as the alkyl linker, **95**, was higher than its pyrene methylene analogue **94**, when left in a solution in chloroform under atmospheric conditions. The result showed that after 7 days in solution, 1.8% of a sample of Pyr(CH<sub>2</sub>)<sub>4</sub>PH<sub>2</sub> **95** was oxidized, compared to 44.9% for PyrCH<sub>2</sub>PH<sub>2</sub> **93**. DFT calculations based on the B3LYP function with a 6-31G\* basis set showed that the SOMO value of the pyrene methylene phosphine **94** is -9.4 eV, closer to the threshold value of -10 eV, than the SOMO value calculated for pyrene butyl phosphine **95** (-8.6 eV). As explained earlier in Section 1.3.1, a radical cation generated from a more stable orbital will be more reactive than an analogue with a higher HOMO/LUMO, and is therefore more likely to oxidize. However, with a value of -9.4 eV we would – according to the model – expect air-stability for **94** which is not observed under the used conditions. This requires further investigation. The air stability of primary phosphine Pyr(CH<sub>2</sub>)<sub>4</sub>PH<sub>2</sub> **95** does not interfere with its reactivity; the tridentate ligand **109** was thus fruitfully synthesised via a double hydrophosphination reaction of the primary phosphine **95** with vinyl diphenylphosphine in the presence of [Pt(η<sup>2</sup>-nb)<sub>3</sub>] as a catalyst. This suggests that the novel primary phosphine **95** can be used as the starting material for a range of different compounds, as the P-H bonds are highly reactive and can be easily functionalised.<sup>34</sup> Subsequent complexation reactions of **109** with group 9 and 10 metals produced interesting complexes, whose photophysical properties were tested proving that the fluorescence of these complexes is not quenched. The Φ<sub>F</sub> values of the complexes obtained were lower in comparison with the free ligand **109**, mostly likely due to the heavy atom effect. It is also possible to see that the atomic number did not determine the Φ<sub>F</sub> trend of the complexes since the Pd complex has a lower Φ<sub>F</sub> than the Pt complex. Ni and Rh complexes followed the expected trend. One of the complexes obtained from the group 10 metals study has particularly interesting properties. Complex [PtCl(**109**)]Cl

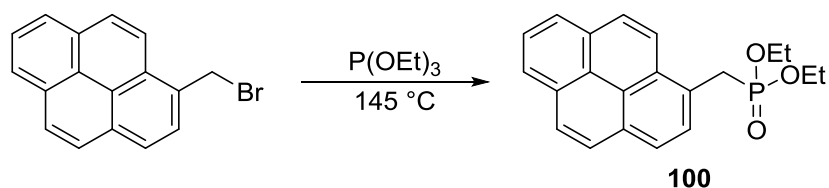
**116** is an interesting alternative to the well-known *cis*-[PtCl<sub>2</sub>(NH<sub>3</sub>)<sub>2</sub>] **110**, a compound commonly used for treating various types of cancer.<sup>360</sup> The DNA affinity of the novel platinum(II) complex **116** has been tested due to its similarity to different platinum-acridine compounds, these agents have shown interesting biological activity.<sup>352-357</sup> The UV-Vis spectrum of a solution of the novel platinum(II) complex **116** with DNA showed that the complex interacted with DNA. The reduction of the  $\pi^*$ - $\pi$  absorption bands of its spectrum provided the main proof of an interaction. Further tests in cells made it possible to compare the potency of our complex against the drug *cis*-[PtCl<sub>2</sub>(NH<sub>3</sub>)<sub>2</sub>] **110**. The novel platinum(II) complex proved potent against bone osteosarcoma (U2OS) and transformed mammary cancer (HMLER) cells to a similar or higher degree than cisplatin. Further research on the mechanism of action of compound **116** on these cancer cells may allow us to improve upon its biological activity.

## 3.8 Experimental

### 3.8.1 General Procedure

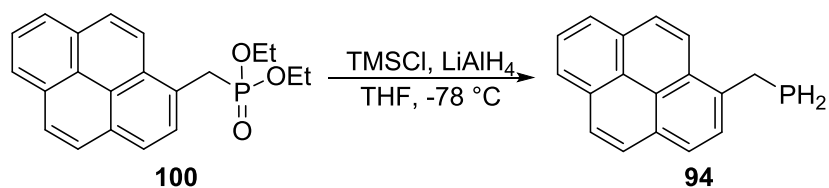
All air- and/or water-sensitive reactions were performed under a dinitrogen atmosphere using standard Schlenk line techniques. Tetrahydrofuran and toluene were dried over sodium/benzophenone and sodium respectively, dichloromethane was dried over calcium hydride; all solvents were distilled prior to use. All starting materials were purchased from Aldrich, Acros Organics, Alfa Aesar or Strem and used as received. Compounds PyrCH<sub>2</sub>Phos **100**,<sup>361</sup> Pyr(CH<sub>2</sub>)<sub>4</sub>Br **102**,<sup>362</sup> and Pyr(CH<sub>2</sub>)<sub>4</sub>Phos **103**<sup>363</sup> were prepared according to literature procedures. Flash chromatography was performed on silica gel from Fluorochem (silica gel, 40-63u, 60A). Thin-layer chromatography was carried out on Fisher aluminium-based plates with silica gel and fluorescent indicator (254 nm). Melting points were determined in open glass capillary tubes on a Stuart SMP3 melting point apparatus. <sup>1</sup>H, <sup>13</sup>C{<sup>1</sup>H} and <sup>31</sup>P{<sup>1</sup>H} NMR spectra were recorded on a JEOL Lambda 500 (<sup>1</sup>H 500.16 MHz) or JEOL ECS-400 (<sup>1</sup>H 399.78 MHz) spectrometer at room temperature (21°C); <sup>1</sup>H and <sup>13</sup>C shifts were relative to tetramethylsilane, <sup>31</sup>P relative to 80% H<sub>3</sub>PO<sub>4</sub>. Infrared spectra were recorded on a Varian 800 FT-IR spectrometer. UV-Vis absorption and emission spectra were recorded on a UV-1800 Shimadzu spectrophotometer and RF-6000 Shimadzu spectrofluorometer respectively. Mass spectrometry was carried out by the EPSRC National Mass Spectrometry Service Centre, Swansea.

### 3.8.2 Diethyl 1-pyrenylmethylene phosphonate **100**



1-(Bromomethyl)pyrene (0.33 g, 1.12 mmol) was placed in a Schlenk flask, then dissolved in P(OEt)<sub>3</sub> (3 mL) under dinitrogen. The mixture was heated to 145 °C and was left to react for 1.5 hours. The reaction was monitored by TLC and, once complete, the reaction was left to cool room temperature and the solvent was then evaporated. The resulting crude material was purified using column chromatography (ethyl acetate/petroleum ether 1:1, R<sub>f</sub> = 0.3). The product was a light brown solid (0.25 g, 63%). A sample suitable for X-ray crystallographic analysis was obtained from chloroform. **MP**: 76.1 °C. **<sup>1</sup>H NMR** (300 MHz, CDCl<sub>3</sub>) δ 8.12 (d, <sup>3</sup>J<sub>HH</sub> = 9.3 Hz, 1H), 7.99 (d, <sup>3</sup>J<sub>HH</sub> = 2.3 Hz, 1H), 7.97 (d, <sup>3</sup>J<sub>HH</sub> = 2.3 Hz, 1H), 7.95-7.90 (m, 2H), 7.87-7.77 (m, 4H), 3.86-3.64 (m, 6H), 1.00 (t, <sup>3</sup>J<sub>HH</sub> = 7.0 Hz, 6H) ppm, **<sup>13</sup>C{<sup>1</sup>H} NMR** (75 MHz, CDCl<sub>3</sub>) δ 131.3, 130.8, 130.5, 129.3 (d, J<sub>CP</sub> = 6.5 Hz), 128.8 (d, J<sub>CP</sub> = 6.5 Hz), 127.6, 127.4, 127.2, 126.0, 125.8, 125.7 (d, J<sub>CP</sub> = 6.5 Hz), 125.2, 125.0, 124.8, 124.7, 123.8, 62.3 (d, <sup>2</sup>J<sub>CP</sub> = 7.1 Hz), 31.5 (d, <sup>1</sup>J<sub>CP</sub> = 138.5 Hz), 16.4 (d, <sup>3</sup>J<sub>CP</sub> = 5.8 Hz) ppm, **<sup>31</sup>P{<sup>1</sup>H} NMR** (121 MHz, CDCl<sub>3</sub>) δ 25.9 ppm.

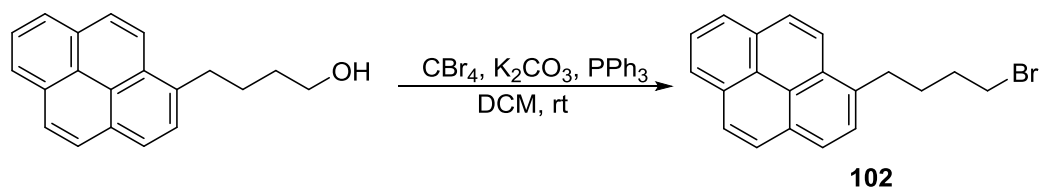
### 3.8.3 1-Pyrenylmethylene phosphine **94**



Chlorotrimethylsilane (0.23 g, 2.13 mmol) was placed in a flask and dissolved in anhydrous THF (6 mL). The solution was cooled in a dry ice bath. A suspension of LiAlH<sub>4</sub> (0.08 g, 2.13 mmol) in anhydrous THF (2 mL) was then added dropwise. The solution was taken out of the dry ice bath. In another flask, diethyl 1-pyrenylmethylene phosphonate (**100**) (0.25 g, 0.71 mmol) was dissolved in anhydrous THF (5 mL), giving a transparent solution. The phosphonate **100** solution, in the second flask, was added dropwise into the flask containing the reducing solution, using a dry ice bath to reduce the temperature to -78 °C. The reaction was then left stirring at room temperature for 3 hours and was quenched by adding water dropwise (1 mL). The mixture was then

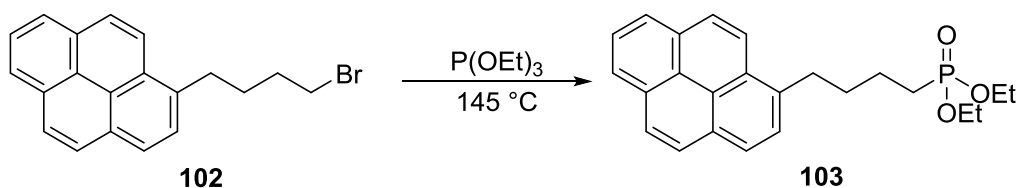
extracted with DCM (20 mL x 3). Purification using column chromatography on silica gel (petrol,  $R_f = 0.8$ ) yielded a white-yellowish solid (0.11 g, 62%). A sample suitable for X-ray crystallographic analysis was obtained from the saturated solution of the compound dissolved in dichloromethane cooled in an ice bath. **MP**: 95.6 °C.  **$^1\text{H NMR}$**  (300 MHz,  $\text{CDCl}_3$ )  $\delta$  8.14 (d,  $^3J_{\text{HH}} = 9.4$  Hz, 1H), 8.10 (d,  $^3J_{\text{HH}} = 2.7$  Hz, 1H), 8.08 (d,  $^3J_{\text{HH}} = 2.7$  Hz, 1H), 8.05 (d,  $^3J_{\text{HH}} = 7.2$  Hz, 1H), 8.02 (d,  $^3J_{\text{HH}} = 5.7$  Hz, 1H), 7.96-7.88 (m, 3H), 7.79 (d,  $^3J_{\text{HH}} = 8.3$  Hz, 1H), 3.54 (m, 2H), 3.12 (m, 2H) ppm,  **$^{13}\text{C}\{^1\text{H}\}$  NMR** (100 MHz,  $\text{CDCl}_3$ )  $\delta$  137.1, 131.5, 131.0, 129.9, 127.6, 127.4, 126.8, 126.6, 126.5, 126.0, 125.4, 125.3, 125.1, 125.0, 124.8, 123.2, 19.0 (d,  $^1J_{\text{CP}} = 12.3$  Hz)  **$^{31}\text{P}\{^1\text{H}\}$  NMR** (121 MHz,  $\text{CDCl}_3$ )  $\delta$  -121.3 ppm.

### 3.8.4 1-(4-Bromobutyl)-pyrene 102



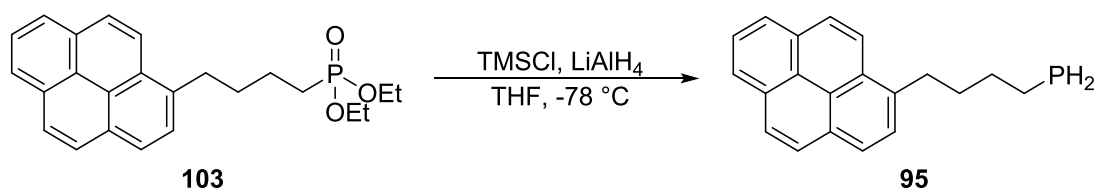
1-(Butan-4-ol)-pyrene (0.20 g, 0.73 mmol, 1 eq.) was dissolved in DCM (15 mL) forming a yellow suspension which was placed in an ice bath; tetrabromomethane (0.32 g, 0.91 mmol, 1.25 eq.) and  $\text{K}_2\text{CO}_3$  (0.15 g, 1.5 eq.) were then added to the solution forming a white suspension.  $\text{PPh}_3$  (0.24 g, 0.91 mmol, 1.25 eq.) was dissolved in DCM (5 mL). The resulting transparent solution was then added dropwise to the suspension containing the mixture with 1-(butan-4-ol)-pyrene while this was still in the ice bath. The mixture was then left to warm to room temperature and reacted over 12 hours. After that period the solvent was evaporated under reduced pressure. The compound was purified using column chromatography on silica gel (hexane/ethyl acetate 8:1,  $R_f = 0.5$ ) resulting in a pale yellow solid (0.18 g, 75%). A sample suitable for X-ray crystallographic analysis was obtained from dichloromethane. **MP** : 77-80 °C.  **$^1\text{H NMR}$**  (400 MHz,  $\text{CDCl}_3$ )  $\delta$  8.26 (d,  $^3J_{\text{HH}} = 9.0$  Hz, 1H), 8.17 (d,  $^3J_{\text{HH}} = 2.7$  Hz, 1H), 8.15 (d,  $^3J_{\text{HH}} = 2.7$  Hz, 1H), 8.11 (d,  $^3J_{\text{HH}} = 9.0$  Hz, 2H), 8.05-7.96 (m, 3H), 7.85 (d,  $^3J_{\text{HH}} = 7.9$  Hz, 1H), 3.46 (t,  $^3J_{\text{HH}} = 6.3$  Hz, 2H), 3.37 (t,  $^3J_{\text{HH}} = 7.1$  Hz, 2H), 2.02 (m, 4H) ppm.  **$^{13}\text{C}\{^1\text{H}\}$  NMR** (100 MHz,  $\text{CDCl}_3$ )  $\delta$  136.1, 131.5, 131.0, 130.0, 128.7, 127.6, 127.5, 127.3, 126.8, 125.9, 125.2, 125.1, 125.0, 124.9, 124.8, 123.3, 33.7, 32.8, 32.7, 30.3 ppm. **IR** (neat):  $\tilde{\nu} = 3044$  (w), 2941 (w), 2868 (w), 1464 (s), 1193 (s), 838 (s), 709 (s), 652 (s)  $\text{cm}^{-1}$ . **HRMS** (ESI<sup>+</sup>) exact mass calcd. for  $\text{C}_{20}\text{H}_{18}\text{Br}_1$   $[\text{M}+\text{H}]^+$  requires  $m/z$  337.0586, found  $m/z$  337.0582 (1.2 ppm).

### 3.8.5 Diethyl (4-(pyren-1-yl)butyl)phosphonate **103**



1-(4-Bromobutyl)-pyrene **102** (0.34 g, 1.01 mmol) was placed in a Schlenk flask, was then dissolved in  $\text{P(OEt)}_3$  (4 mL) under dinitrogen. The mixture was heated to  $145\text{ }^\circ\text{C}$  and was left to react for 1.5 hours. The reaction was monitored by TLC and, once complete, the reaction was left to cool to room temperature; the solvent was then evaporated. The resulting crude material was purified using column chromatography (ethyl acetate,  $R_f = 0.4$ ). The product was a pale yellow solid (0.25 g, 63%). A sample suitable for X-ray crystallographic analysis was obtained from dichloromethane. **MP**:  $79\text{--}82\text{ }^\circ\text{C}$ .  **$^1\text{H NMR}$**  (400 MHz,  $\text{CDCl}_3$ )  $\delta$  8.08 (d,  $^3J_{\text{HH}} = 9.0\text{ Hz}$ , 1H), 8.04 (d,  $^3J_{\text{HH}} = 2.5\text{ Hz}$ , 1H), 8.02 (d,  $^3J_{\text{HH}} = 2.5\text{ Hz}$ , 1H), 7.96 (d,  $^3J_{\text{HH}} = 4.5\text{ Hz}$ , 1H), 7.94 (d,  $^3J_{\text{HH}} = 5.6\text{ Hz}$ , 1H), 7.91-7.85 (m, 3H), 7.68 (d,  $^3J_{\text{HH}} = 8.0\text{ Hz}$ , 1H), 4.08-3.97 (m, 4H), 3.19 (t,  $^3J_{\text{HH}} = 7.5\text{ Hz}$ , 2H), 1.85-1.66 (m, 6H), 1.25 (t,  $^3J_{\text{HH}} = 6.5\text{ Hz}$ , 6H) ppm.  **$^{13}\text{C}\{^1\text{H}\}\text{NMR}$**  (100 MHz,  $\text{CDCl}_3$ )  $\delta$  136.3, 131.5, 131.0, 129.9, 128.6, 127.6, 127.3, 127.3, 126.7, 125.9, 125.2, 125.1, 125.0, 124.9, 124.8, 123.3, 61.5 (d,  $^2J_{\text{CP}} = 6.2\text{ Hz}$ ), 33.2, 32.8 (d,  $^2J_{\text{CP}} = 16.3\text{ Hz}$ ), 25.7 (d,  $^1J_{\text{CP}} = 140.9\text{ Hz}$ ), 22.7 (d,  $^2J_{\text{CP}} = 5.1\text{ Hz}$ ), 16.6 (d,  $^3J_{\text{CP}} = 6.3\text{ Hz}$ ) ppm.  **$^{31}\text{P}\{^1\text{H}\}\text{NMR}$**  (162 MHz,  $\text{CDCl}_3$ )  $\delta$  32.8 ppm. **IR** (neat):  $\tilde{\nu} = 3045\text{ (w)}$ ,  $2981\text{ (w)}$ ,  $2883\text{ (w)}$ ,  $2360\text{ (w)}$ ,  $1602\text{ (s)}$ ,  $1253\text{ (s)}$ ,  $1229\text{ (s)}$ ,  $1058\text{ (s)}$ ,  $1018\text{ (s)}$ ,  $955\text{ (s)}$ ,  $842\text{ (s)}$ ,  $708\text{ (s)}$   $\text{cm}^{-1}$ . **HRMS** ( $\text{ESI}^+$ ) exact mass calcd. for  $\text{C}_{24}\text{H}_{28}\text{O}_3\text{P}_1$   $[\text{M}+\text{H}]^+$  requires  $m/z$  395.1771, found  $m/z$  395.1768 (1.5 ppm).

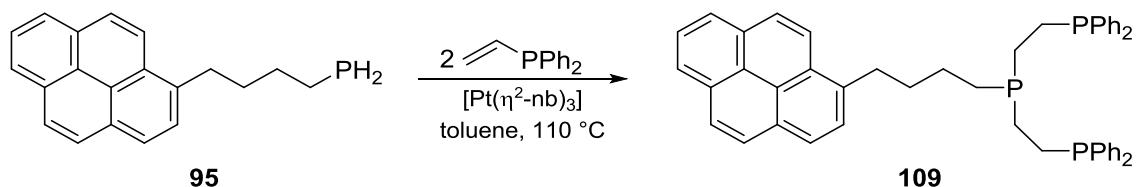
### 3.8.6 4-(Pyren-1-yl)butylphosphine **95**



Chlorotrimethylsilane (0.17 g, 1.59 mmol) was placed in a Schlenk flask and dissolved in anhydrous THF (6 mL). The Schlenk flask was cooled in a dry ice bath to  $-78\text{ }^\circ\text{C}$ . A suspension of  $\text{LiAlH}_4$  (0.06 g, 1.59 mmol) in anhydrous THF (2 mL) was then added dropwise. The solution was taken out of the dry ice bath and allowed to warm to room temperature. In another flask, diethyl (4-(pyren-1-yl)butyl)phosphonate (**103**) (0.21 g, 0.53 mmol) was dissolved in anhydrous THF (5 mL), giving a transparent solution. The

phosphonate **103** solution, in the second flask, was added dropwise into the flask containing the chlorotrimethylsilane solution using a dry ice bath to reduce the temperature to  $-78\text{ }^{\circ}\text{C}$ . The reaction then left stirring at room temperature for 3 hours and was quenched by adding water dropwise (1 mL). The mixture was then extracted with DCM (20 mL x 3). Purification using column chromatography on silica gel (ethyl acetate/petroleum ether 1:7,  $R_f = 0.6$ ) yielded a white solid (0.13 g, 70%). A sample suitable for X-ray crystallographic analysis was obtained from dichloromethane. **MP**:  $89.9\text{ }^{\circ}\text{C}$ .  **$^1\text{H NMR}$**  (400 MHz,  $\text{CDCl}_3$ )  $\delta$  8.26 (d,  $^3J_{\text{HH}} = 9.3\text{ Hz}$ , 1H), 8.16 (d,  $^3J_{\text{HH}} = 2.5\text{ Hz}$ , 1H), 8.14 (d,  $^3J_{\text{HH}} = 2.5\text{ Hz}$ , 1H), 8.11 (d,  $^3J_{\text{HH}} = 1.8\text{ Hz}$ , 1H), 8.09 (d,  $^3J_{\text{HH}} = 3.5\text{ Hz}$ , 1H), 8.04-7.96 (m, 3H), 7.85 (d,  $^3J_{\text{HH}} = 8.0\text{ Hz}$ , 1H), 3.33 (d,  $^3J_{\text{HH}} = 7.9\text{ Hz}$ , 2H), 2.69 (ddd,  $^3J_{\text{HaHx}} = 7.4\text{ Hz}$ ,  $^3J_{\text{Ha'Hx}} = 7.3\text{ Hz}$ ,  $^1J_{\text{HP}} = 194.3\text{ Hz}$ , 2H), 1.96-1.88 (m, 2H), 1.75-1.65 (m, 2H), 1.63-1.52 (m, 2H) ppm.  **$^{13}\text{C}\{^1\text{H}\}$  NMR** (100 MHz,  $\text{CDCl}_3$ )  $\delta$  136.8, 131.5, 131.0, 129.9, 128.7, 127.6, 127.3, 126.9, 126.7, 125.9, 125.2, 125.1, 125.0, 124.9, 124.8, 123.5, 33.3, 33.1, 33.8 (d,  $J_{\text{CP}} = 5.8\text{ Hz}$ ), 13.8 (d,  $J_{\text{CP}} = 7.5\text{ Hz}$ ) ppm.  **$^{31}\text{P}\{^1\text{H}\}$  NMR** (162 MHz,  $\text{CDCl}_3$ )  $\delta$   $-138.1\text{ ppm}$ . **IR** (neat):  $\tilde{\nu} = 3044\text{ (w)}$ ,  $2923\text{ (w)}$ ,  $2855\text{ (w)}$ ,  $2298\text{ (s)}$ ,  $840\text{ (s)}$ ,  $710\text{ (s)}\text{ cm}^{-1}$ . **HRMS** (ESI<sup>+</sup>) exact mass calcd. for  $\text{C}_{20}\text{H}_{20}\text{P}_1$   $[\text{M}+\text{H}]^+$  requires  $m/z$  291.1297, found  $m/z$  291.1298 (0.3 ppm).

### 3.8.7 4-(Pyren-1-yl)butyl-P-bis-(2-ethyldiphenylphosphino)phosphine **109**



4-(Pyren-1-yl)butylphosphine **95** (0.42 g, 1.45 mmol) was dissolved in anhydrous toluene (20 mL). To this vinylidiphenylphosphine (0.58 mL, 2.90 mmol) and  $[\text{Pt}(\eta^2\text{-nb})_3]$  (0.07 g, 0.15 mmol) were added, in that order. The reaction was stirred at reflux for 24 hours under dinitrogen. On completion of the reaction, the volatiles were removed *in vacuo* leaving a brown solid. Purification was performed by column chromatography on silica gel (hexane/dichloromethane 1:1,  $R_f = 0.6$ ) to produce a white powder (0.56 g, 55%). **MP**:  $94.9\text{ }^{\circ}\text{C}$ .  **$^1\text{H NMR}$**  (400 MHz,  $\text{CDCl}_3$ )  $\delta$  8.15 (d,  $^3J_{\text{HH}} = 9.3\text{ Hz}$ , 1H), 8.09 (d,  $^3J_{\text{HH}} = 7.6\text{ Hz}$ , 2H), 8.01 (d,  $^3J_{\text{HH}} = 4.4\text{ Hz}$ , 1H), 7.99 (d,  $^3J_{\text{HH}} = 3.0\text{ Hz}$ , 1H), 7.96-7.88 (m, 3H), 7.74 (d,  $^3J_{\text{HH}} = 7.6\text{ Hz}$ , 1H), 7.32-7.19 (m, 20H), 3.21 (t,  $^3J_{\text{HH}} = 7.5\text{ Hz}$ , 2H), 2.02-1.90 (m, 4H), 1.85-1.73 (m, 2H), 1.48-1.34 (m, 8H) ppm.  **$^{13}\text{C}\{^1\text{H}\}$  NMR** (100 MHz,  $\text{CDCl}_3$ )  $\delta$  138.4 (d,  $J_{\text{CP}} = 3.0\text{ Hz}$ ), 138.2 (d,  $J_{\text{CP}} = 3.0\text{ Hz}$ ), 136.7, 132.9 (d,  $J_{\text{CP}} = 5.0\text{ Hz}$ ), 132.6 (d,  $J_{\text{CP}} = 5.0$



Hz), 131.5, 130.9, 128.7, 128.6-128.3 (overlapping signals), 127.6, 127.2, 126.6, 125.8, 125.1, 125.0, (d,  $J_{CP} = 3.6$  Hz), 124.9, 124.8, 124.7, 123.4, 33.5 (d,  $J_{CP} = 10.6$  Hz), 33.3, 26.3, 26.1, 25.9 (d,  $J_{CP} = 13.0$  Hz), 22.8 (d,  $J_{CP} = 134.0$  Hz) ppm.  $^{31}\text{P}\{^1\text{H}\}$  NMR (162 MHz,  $\text{CDCl}_3$ )  $\delta$  -12.2 (d,  $^3J_{PP} = 26.5$  Hz), -20.6 (t,  $^3J_{PP} = 26.5$  Hz) ppm. IR (neat):  $\tilde{\nu} = 3044$  (w), 2933 (w), 2360 (w), 1434 (s), 836 (s), 736 (s), 693 (s)  $\text{cm}^{-1}$ . HRMS (ESI<sup>+</sup>) exact mass calcd. for  $\text{C}_{48}\text{H}_{46}\text{P}_1$   $[\text{M}+\text{H}]^+$  requires  $m/z$  715.2807, found  $m/z$  715.2806 (1.5 ppm).

### 3.8.8 [PtCl(109)][Cl] 116

4-(Pyren-1-yl)butyl-P-bis-(2-ethyldiphenylphosphino)phosphine (**109**) (0.13 g, 0.18 mmol) was dissolved in anhydrous dichloromethane (1.5 mL) and added to a stirred solution of  $[\text{PtCl}_2(\eta^2:\eta^2\text{-cod})]$  (0.07 g, 0.18 mmol) in anhydrous dichloromethane (1.5 mL). The mixture was stirred at room temperature for 2 hours and the solvent removed. The solid was washed with hexane (3 x 5 mL) and dried *in vacuo* (0.13 g, 72%). A sample suitable for X-ray crystallographic analysis was obtained from hexane/dichloromethane.  $^1\text{H}$  NMR (400 MHz,  $\text{CDCl}_3$ )  $\delta$  8.10 (d,  $^3J_{\text{HH}} = 2.3$  Hz, 1H), 8.07 (d,  $^3J_{\text{HH}} = 2.3$  Hz, 1H), 8.05-7.88 (m, 7H), 7.73-7.63 (m, 4H), 7.61-7.51 (m, 4H), 7.45-7.18 (m, 12H), 3.62-3.37 (m, 2H), 3.05 (t,  $^3J_{\text{HH}} = 7.3$  Hz, 2H), 2.62-2.24 (m, 6H), 2.05-1.72 (m, 4H), 1.60-1.47 (m, 2H) ppm.  $^{13}\text{C}\{^1\text{H}\}$  NMR (126 MHz,  $\text{CDCl}_3$ )  $\delta$  135.4, 133.2, 132.8, 132.3, 132.0, 131.4, 130.9, 129.9, 129.5, 129.4, 129.3, 129.2, 128.5, 127.5, 127.2, 126.8, 125.9, 125.0, 124.9, 123.2, 32.6, 32.5, 29.7, 27.0, 26.9, 25.9 ppm.  $^{31}\text{P}\{^1\text{H}\}$  NMR (121 MHz,  $\text{CDCl}_3$ )  $\delta$  87.1 ( $^1J_{\text{PPt}} = 2883.8$  Hz, 1P), 44.0 ( $^1J_{\text{PPt}} = 2538.1$  Hz, 2P) ppm. IR (neat):  $\tilde{\nu} = 3049$  (w), 2914 (w), 2360 (w), 1596 (m), 1433 (s), 1103 (m), 838 (m), 756 (s)  $\text{cm}^{-1}$ . HRMS (ESI<sup>+</sup>) calcd. for  $\text{C}_{48}\text{H}_{45}\text{Cl}_1\text{P}_3\text{Pt}_1$   $[\text{M}]^+$  requires  $m/z$  939.2016, found  $m/z$  939.2002 (0.1 ppm).

### 3.8.9 [PdCl(109)][Cl] 120

4-(Pyren-1-yl)butyl-P-bis-(2-ethyldiphenylphosphino)phosphine (**109**) (0.05 g, 0.07 mmol) was dissolved in anhydrous dichloromethane (1.5 mL) and added to a stirred solution of  $[\text{PdCl}_2(\text{PhCN})_2]$  (0.03 g, 0.07 mmol) in anhydrous dichloromethane (1.5 mL). The mixture was stirred at room temperature for 2 hours and the solvent removed. The solid was washed with hexane (3 x 5 mL) and dried *in vacuo* (0.04 g, 64%). A sample suitable for X-ray crystallographic analysis was obtained from hexane/dichloromethane.  $^1\text{H}$  NMR (400 MHz,  $\text{CDCl}_3$ )  $\delta$  8.09 (d,  $^3J_{\text{HH}} = 3.4$  Hz, 1H), 8.07 (d,  $^3J_{\text{HH}} = 3.4$  Hz, 1H), 8.03 (d,  $^3J_{\text{HH}} = 9.5$  Hz, 1H), 7.98 (d,  $^3J_{\text{HH}} = 9.5$  Hz, 1H), 7.95-7.89 (m, 5H), 7.71-7.64 (m, 4H), 7.63-7.57 (m, 4H), 7.42-7.37 (m, 2H), 7.34-7.27 (m, 6H), 7.26-7.20 (m, 4H), 3.68-

3.46 (m, 2H), 3.07 (t,  $^3J_{\text{HH}} = 7.2$  Hz, 2H), 2.65-2.54 (m, 2H), 2.50-2.37 (m, 4H), 1.88-1.77 (m, 2H), 1.64-1.51 (m, 2H) 0.84-0.75 (m, 2H) ppm.  $^{13}\text{C}\{\text{H}\}$  NMR (126 MHz,  $\text{CDCl}_3$ )  $\delta$  134.3, 132.0-131.8 (overlapping signals), 131.1, 130.4, 129.9, 128.9, 128.4-128.3 (overlapping signals), 127.7, 127.5, 127.2, 127.0, 126.5, 126.2, 125.7, 124.9, 124.0-123.9 (overlapping signals), 122.2, 31.6, 30.9, 28.3, 25.2, 24.9, 21.7 ppm.  $^{31}\text{P}\{\text{H}\}$  NMR (121 MHz,  $\text{CDCl}_3$ )  $\delta$  115.1 (t,  $^3J_{\text{PP}} = 6.3$  Hz), 47.9 (d,  $^3J_{\text{PP}} = 6.3$  Hz) ppm. IR (neat):  $\tilde{\nu} = 2961$  (w), 2917 (w), 2849 (m), 2363 (w), 1435 (w), 1260 (m), 1095 (s), 1016 (s), 795 (m), 689 (m)  $\text{cm}^{-1}$ .

### 3.8.10 $[\text{NiCl}_2(\mathbf{109})]$ 121

4-(Pyren-1-yl)butyl-P-bis-(2-ethyldiphenylphosphino)phosphine (**109**) (0.05 g, 0.07 mmol) was dissolved in anhydrous dichloromethane (2 mL) and added to a stirred solution of  $[\text{NiCl}_2(\text{py})_4]$  (0.05 g, 0.07 mmol) in degassed ethanol (1 mL). The mixture was stirred at room temperature for 2 hours and the solvent removed. The solid was washed with hexane (3 x 5 mL) and dried *in vacuo* (0.03 g, 51%). A sample suitable for X-ray crystallographic analysis was obtained from dichloromethane.  $^{31}\text{P}\{\text{H}\}$  NMR (121 MHz,  $\text{CDCl}_3$ )  $\delta$  115.9 (t,  $^3J_{\text{PP}} = 42.5$  Hz), 50.0 (d,  $J_{\text{PP}} = 42.5$  Hz) ppm, IR (neat):  $\tilde{\nu} = 2915$  (w), 2358 (w), 2343 (w), 1436 (m), 1260 (m), 1096 (m), 1026 (m), 801 (m), 739 (s), 692 (s)  $\text{cm}^{-1}$ .

### 3.8.11 $[\text{RhCl}(\mathbf{109})]$ 125

4-(Pyren-1-yl)butyl-P-bis-(2-ethyldiphenylphosphino)phosphine (**109**) (0.05 g, 0.07 mmol) was dissolved in anhydrous dichloromethane (2 mL) and added to a stirred solution of  $[\text{Rh}(\eta^2:\eta^2\text{-cod})\text{Cl}]_2$  (0.02 g, 0.04 mmol) in anhydrous dichloromethane (2 mL). The mixture was stirred at room temperature for 2 hours and the solvent removed. The solid was washed with hexane (3 x 5 mL) and dried *in vacuo* (0.03 g, 58%).  $^1\text{H}$  NMR (700 MHz,  $\text{CDCl}_3$ )  $\delta$  8.21 (d,  $^3J_{\text{HH}} = 9.1$  Hz, 1H), 8.18 (d,  $^3J_{\text{HH}} = 8.0$  Hz, 1H), 8.11 (d,  $^3J_{\text{HH}} = 9.1$  Hz, 1H), 8.07, (d,  $^3J_{\text{HH}} = 7.5$  Hz, 1H), 8.04-7.99 (m, 4H), 7.81 (d,  $^3J_{\text{HH}} = 7.5$  Hz, 1H), 7.75-7.70 (m, 6H), 7.56-7.53 (m, 3H), 7.51-7.46 (m, 5H), 7.45-7.41 (m, 4H), 7.27 (d,  $^3J_{\text{HH}} = 8.0$  Hz, 1H), 7.20 (d,  $^3J_{\text{HH}} = 7.8$  Hz, 1H), 3.31 (t,  $^3J_{\text{HH}} = 7.7$  Hz, 2H), 2.51-2.40 (m, 4H), 1.98-1.87 (m, 6H), 1.81-1.74 (m, 2H), 1.68-1.62 (m, 2H) ppm,  $^{13}\text{C}\{\text{H}\}$  NMR (176 MHz,  $\text{CDCl}_3$ )  $\delta$  132.5, 132.2, 131.9, 131.4, 131.3, 131.0, 130.9-130.8 (overlapping signals), 129.9, 129.0, 128.9-128.8 (overlapping signals), 128.5, 128.3, 127.5, 126.3, 125.3, 125.1, 124.9-124.8 (overlapping signals), 33.0, 30.4, 28.9, 23.8, 23.0,

21.5 ppm;  $^{31}\text{P}\{^1\text{H}\}$  NMR (121 MHz,  $\text{CDCl}_3$ )  $\delta$  93.4 (dt,  $^3J_{\text{RHP}} = 120.2$  Hz,  $^3J_{\text{PP}} = 23.0$  Hz), 55.9 (dd,  $^3J_{\text{PP}} = 124.5$  Hz,  $^3J_{\text{PP}} = 23.0$  Hz) ppm.

### 3.8.12 [IrCl(109)] 129

4-(Pyren-1-yl)butyl-P-bis-(2-ethyldiphenylphosphino)phosphine (**109**) (0.08 g, 0.18 mmol) was dissolved in anhydrous dichloromethane (3 mL) and added to a stirred solution of  $[\text{Ir}(\eta^2:\eta^2\text{-cod})\text{Cl}]_2$  (0.04 g, 0.09 mmol) in anhydrous dichloromethane (3 mL). The mixture was stirred at 40 °C for 2 hours and the solvent removed. The solid was washed with hexane (3 x 5 mL) and dried *in vacuo* (0.06 g, 57%).  $^{31}\text{P}\{^1\text{H}\}$  NMR (121 MHz,  $\text{CDCl}_3$ )  $\delta$  62.7 (t,  $J_{\text{PP}} = 10.6$  Hz), 27.5 (d,  $^3J_{\text{PP}} = 10.6$  Hz) ppm. IR (neat):  $\tilde{\nu} = 3051$  (w), 2911 (w), 2342 (w), 1557 (s), 1434 (m), 1183 (m), 1070 (w), 845 (m), 752 (s), 694 (s)  $\text{cm}^{-1}$ . HRMS (ESI<sup>+</sup>) calcd. for  $\text{C}_{48}\text{H}_{46}\text{Cl}_1\text{Ir}_1\text{P}_3$   $[\text{M}]^+$  requires  $m/z$  943.2125, found  $m/z$  943.2125(0.1 ppm).

### 3.8.13 Absorption and Emission Spectroscopy

Absorption spectra were recorded with a Shimadzu Model UV-1800 spectrophotometer while fluorescence studies were recorded with a Shimadzu RF-6000 fluorophotometer. Solvents used for spectroscopic experiments were spectrophotometric grade. Absorption and emission spectra were recorded in dry degassed tetrahydrofuran and chloroform solutions at room temperature. Fluorescence quantum yields were measured with respect to pyrene ( $\Phi_{\text{F}} = 0.32$ ,  $\lambda_{\text{abs}} = 335$  nm,  $\lambda_{\text{em}} = 381$  nm,  $\epsilon = 54,000 \text{ cm}^{-1} \text{ M}^{-1}$ , cyclohexane) and anthracene ( $\Phi_{\text{F}} = 0.36$ ,  $\lambda_{\text{abs}} = 356$  nm,  $\lambda_{\text{em}} = 396$  nm,  $\epsilon = 9,700 \text{ cm}^{-1} \text{ M}^{-1}$ , cyclohexane).<sup>83</sup> Dyes were excited at 317 nm, when compared with pyrene, and at 350 nm, when compared with anthracene; excitation and emission slits were both set to 5 nm.

### 3.8.14 Quantum Yield Method

The fluorescence quantum yield ( $\Phi_{\text{F}}$ ) can be defined as the ratio of emitted photons relative to the number of absorbed photons.<sup>41</sup> All quantum yields were measured in solution at room temperature. In order to define the fluorescence quantum yield appropriate fluorescence standard reference compounds were selected, which absorb and emit over ranges comparable to those of the studied samples. The excitation wavelength, slit widths and the emission range were kept constant for both the reference and the sample. Dilute solutions were prepared, possessing the same absorbance at the excitation wavelength ( $A < 0.09$  at the excitation wavelength, with an error limit of  $\pm 0.005$  between the reference and sample). The following formulae were used to correct the relative emission areas for minor differences in absorbance:

$$A = \log\left(\frac{I_0}{I_T}\right)$$

$$I_a + I_T = I_0 = 1$$

$$QY_{REL} = \frac{area}{I_a}$$

A is the absorbance,  $I_0$  is the intensity of incident light,  $I_T$  is the intensity of the transmitted light,  $I_a$  is the intensity of absorbed light and  $QY_{REL}$  is the relative quantum yield.<sup>17</sup>

Where necessary the quantum yields were corrected for the differences in the refractive index of the solvent:

$$QY_A = \frac{\eta_A^2}{\eta_B^2} QY_B$$

The subscripts A and B denote two difference solvents and  $\eta$  is the refractive index.<sup>17</sup>

The quantum yield of the sample can now be determined using the following equation:

$$QY^{Sl} = \frac{QY_{Rel}^{Sl}}{QY_{Rel}^{Ref}} QY^{Ref}$$

Superscript Sl and Ref denote sample and reference respectively.<sup>40</sup>

### 3.8.15 UV/Vis titration

The UV/Vis spectra were recorded on a Cary 100 spectrometer. To determine the binding constants of the complexes with ct-DNA, [PtCl(**109**)]Cl (**116**) (50  $\mu$ M) was titrated with concentrated solutions of ct-DNA (2.9 mM, nucleotide) in Tris-HCl (50 mM, pH 7.4) buffer. A quartz cuvette (1 cm path length) was used to carry out the measurements. The binding constants were obtained by fitting the data to a reciprocal plot of  $D/\Delta\epsilon_{ap}$  versus D by using the following equation:  $D/\Delta\epsilon_{ap} = D/\Delta\epsilon + 1 / (\Delta\epsilon \times K)$ , in which the concentration of DNA is expressed in terms of base pairs (determined by measuring the absorption at  $\lambda = 260$  nm and the appropriate extinction coefficients), the apparent molar extinction coefficient  $\epsilon_a = A_{observed}/[complex]$ ,  $\Delta\epsilon_{ap} = [\epsilon_a - \epsilon_f]$ ,  $\Delta\epsilon = [\epsilon_b - \epsilon_f]$ , in which  $\epsilon_b$  is the extinction coefficient of the DNA-bound complex,  $\epsilon_f$  is the extinction coefficient of the free complex and  $\Delta\epsilon_{ap} = |\epsilon_a - \epsilon_f|$ .

### 3.8.16 Ethidium bromide displacement assay

To a solution of ct-DNA (20  $\mu$ M) in Tris-HCl (50 mM, pH 7.4) buffer, ethidium bromide (1  $\mu$ M) was added and the resulting solution was incubated at room temperature for 10

min. After this period, the emission spectrum was recorded between 530 and 750 nm with an excitation wavelength of 520 nm. Aliquots of **116** were added to the resultant solution and the emission spectrum was recorded after 10 min incubation. This was repeated until the emission spectrum remained constant.

### **3.8.17 ct-DNA precipitation assay**

The amount of **116** covalently bound to ct-DNA was determined by modification of a previously reported protocol. A solution of ct-DNA (0.25 mM, nucleotide) was incubated with **116** at a base pair:metal complex ratio of 5:1 at 37 °C in Tris-HCl (50 mM, pH 7.4) buffer. At certain time points, a 250 µL aliquot was removed and the DNA was precipitated by adding 10 µL of KCl (5 M) and 1.0 mL of EtOH (stored at 4 °C). The solution was centrifuged to remove DNA, and the concentration of covalently unbound **116** was determined by measuring the UV-Vis absorption of the supernatant.

### **3.8.18 Cell lines and cell culture conditions**

U2OS bone osteosarcoma cells were maintained in Dulbecco's Modified Eagle's Medium (DMEM-low glucose) supplemented with 10% fetal bovine serum and 1% penicillin/streptomycin. HMLER transformed mammary cancer cells were maintained in Mammary Epithelial Cell Growth Medium (MEGM) with supplements and growth factors (BPE, hydrocortisone, hEGF, insulin, and gentamicin/amphotericin-B). All cells were grown at 310 K in a humidified atmosphere containing 5% CO<sub>2</sub>.

### **3.8.19 Cytotoxicity MTT assay**

The colorimetric MTT assay was used to determine the toxicity of **116** and cisplatin. Cells ( $3 \times 10^3$ ) were seeded in each well of a 96-well plate. After incubating the cells overnight, various concentrations of test compound (0.3-100 µM) were added and incubated for 72 h (total volume 200 µL). **116** was prepared as 10 mM solutions in DMSO and diluted using media. The final concentration of DMSO in each well was 0.5% and this amount was present in the untreated control as well. Cisplatin was prepared as a 5 mM solution in PBS and diluted further using media. After 72 h, the medium was removed, 200 µL of a 0.4 mg/mL solution of MTT in DMEM or MEGM was added, and the plate was incubated for an additional 1-2 h. The DMEM/MTT or MEGM/MTT mixture was aspirated and 200 µL of DMSO was added to dissolve the resulting purple formazan crystals. The absorbance of the solution wells was read at 550 nm. Absorbance values were normalized to DMSO-containing control wells and plotted as concentration of test compound versus % cell viability. IC<sub>50</sub> values were interpolated from the resulting dose

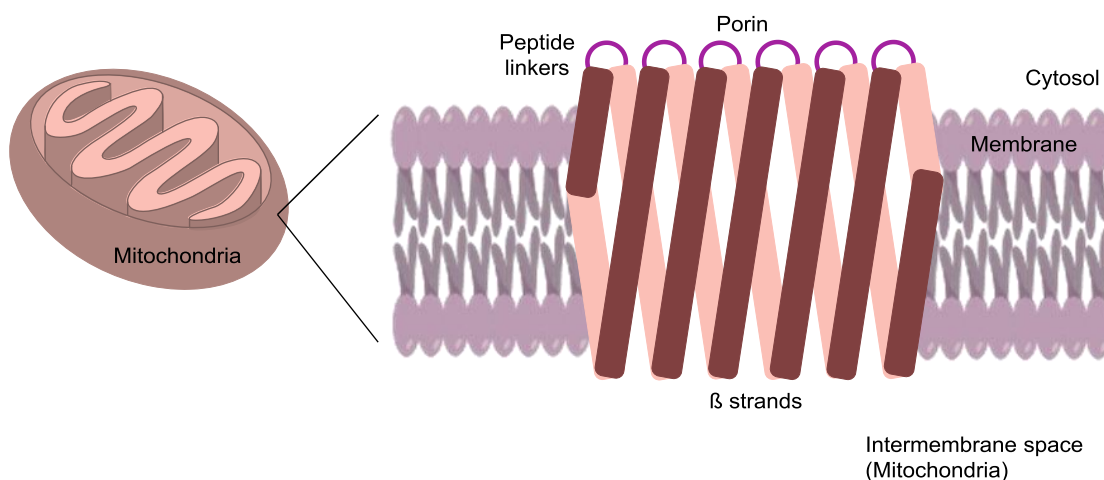
dependent curves. The reported IC50 values were averaged from three independent experiments, each of which consisted of six replicates per concentration level.

## **4 Synthesis of a fluorescent chelator ligand derived from 8-((4-dicyclohexylphosphino)phenyl)-4,4-diphenyl-1,3,5,7-tetramethyl-2,6-diethyl-4-bora-3a,4a-diaza-s-indacene**

This part of the thesis describes the development of a compound with the aim of creating a novel probe specific for targeting the mitochondrion of cells. The chemical features of this novel probe make it a fluorescent PET carrier, turning the compound into a useful agent for *in vivo* and *in vitro* imaging techniques. The introduction will include key information about the biological importance to these types of compounds.

### **4.1 Mitochondria**

Mitochondria generate most of the adenosine triphosphate (ATP) supply in cells; this compound is used as a source of chemical energy for the different processes required in living systems.<sup>364</sup> Energy production is not the only task that this organelle carries out, it is also a keystone in cellular signalling and differentiation, as well as cell death and cell growth.<sup>365</sup> The procedures this organelle is involved with make it an important target for drugs.<sup>366</sup> Mitochondria can be found in all eukaryotic organisms and vary widely depending on the living system, tissue and cell type. For example, red blood cells do not contain any mitochondria, whereas liver cells contain one of the highest densities of mitochondria in the human body.<sup>366</sup> The outer membrane of mitochondria has a high density of a specific trans-membrane protein called porin.<sup>367</sup> These proteins are mainly shaped by  $\beta$  strands, arrangements of amino acids that keep a specific 2-dimensional rectangular motif, linked together by peptide chains that are located in the cytosol. The spatial disposition of the protein makes it look like a cylindrical tube, hence its name,  $\beta$  barrel.<sup>368</sup> The nonpolar residues of the protein are folded outwards, allowing them to interact with the lipids that are situated in the outer membrane. On the other hand, the polar residues face inwards towards the centre of the barrel, producing a chemical environment attractive to molecules of water that form an aqueous channel.<sup>368</sup> The channel found in the porin is partially blocked by a loop, called an eyelet. This loop is placed in the cavity formed by the barrel; its morphology can be variable, which controls the affinity of the channel for certain solutes according to their size. The surface of the inner walls of the channel mainly contains charged amino acids, creating a transversal electric field along the inner pore. However, the eyelet has an excess of negative charges given by the side chains of the amino acids that form it.<sup>369</sup>



**Figure 4.1 Representation of mitochondria and its outer membrane containing the transport protein porin.**

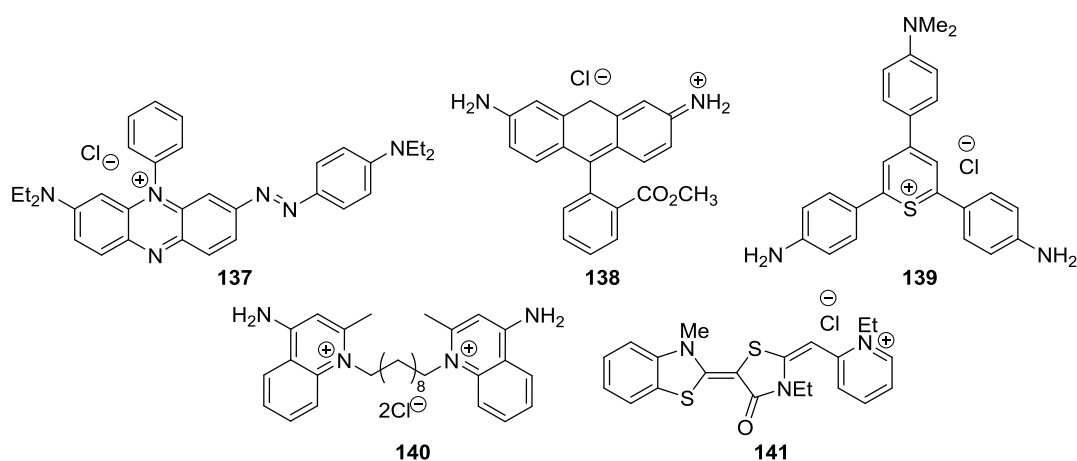
It is thought that a combination of the features mentioned above provide selectivity allowing certain compounds to diffuse through the channel. As mentioned above, a key characteristic of mitochondria is the utilization of a proton electrochemical gradient potential, or electrochemical proton motive force, to generate ATP. This procedure requires different specialized proteins, whose main function is to transport protons against their concentration gradient across the inner mitochondrial membrane.<sup>370</sup> This transmembrane potential ( $\Delta\psi_m$ ) is altered in processes involving cancer caused directly by mitochondrial dysfunction produced by DNA mutation or oxidative stress.<sup>371</sup> As such, probes that can give information on the state of mitochondrial function are sought after.

#### **4.1.1 Mitochondria as a drug target**

Mitochondria has been studied for many years principally because of their functional importance. Janus green B **137** (Figure 4.2) was the first dye to be used to stain mitochondria in cells that are not alive.<sup>372</sup> This dye specifically stains mitochondria as it gets oxidised in the non-mitochondrial parts of the cell. This reduction does not affect the compound absorbed in the mitochondria, which maintains the stain.<sup>372</sup> The nature of the mitochondrial membrane means that it possesses an electric potential,  $\Delta\psi_m$  – it has been shown that this potential is higher in carcinoma cells than in healthy epithelial cells.<sup>103, 373, 374</sup> An example of this is found in the  $\Delta\psi_m$  difference between the colon carcinoma cell line CX-1 and the control green monkey kidney epithelial cell line CV-1. This has been reported at nearly 60 mV ( $163 \pm 7$  mV for cell line CX-1 vs.  $104 \pm 9$  mV for cell line CV-1).<sup>103</sup> Positively charged cations with lipophilic structures or delocalised lipophilic cations (DLCs) can diffuse into the barriers of the plasma and mitochondrial



membranes, and accumulate in the organelle, due to the negative inner transmembrane potentials – this does not require the use of any transporter protein that needs energy to function. They use proteins, such as porins, where diffusion is allowed for positively charged compounds.<sup>375-377</sup> According to the Nernst equation, a difference of 60 mV between the membrane potential of the carcinoma cell and the control epithelial cell; is enough to obtain a 10-fold greater concentration in the carcinoma mitochondria in comparison with the control cell. Therefore, the concentration of DLC found in carcinoma mitochondria is directly proportional to the  $\Delta\psi_m$ : the higher this magnitude, the higher the concentration of DLC in the mitochondria.<sup>293</sup> Most DLCs tend to exert toxic activity on mitochondria at high concentrations. The mechanisms used by this type of compound to provoke toxic effects in the mitochondria are quite diverse. Rhodamine 123 **138**, a probe for membrane polarization in live cell assays within mitochondria and bacteria,<sup>375</sup> and thiopyrylium AA-1 **139**, an antitumor agent,<sup>378</sup> both inhibit the regular synthesis of ATP, which leads to the depletion of an energy source for the affected cell.<sup>103, 377, 379</sup> The quaternary ammonium compound, dequalinium chloride **140**, a salt with mild antibiotic activity,<sup>380</sup> inhibits mitochondrial respiration by inhibiting NADH-ubiquinone, a vital enzyme for respiration in the system that transports electrons in the mitochondria.<sup>381</sup> Rhodacyanine MKT-077, **141**, is a compound that degrades mitochondrial membranes – a non-specific inhibition of the enzymes in charge of mitochondrial respiration is produced as a result. Additionally, this cyanine exerts a slightly disruptive effect on the mitochondrial DNA.<sup>382</sup>



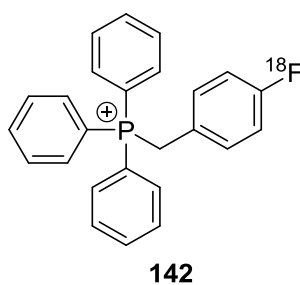
**Figure 4.2 Delocalised lipophilic cations (DLCs) that have shown to possess a high distribution in the mitochondria.**

Despite the various mechanisms used by DLCs to exert cytotoxicity, they nonetheless have something in common: they provoke a significant decrease in ATP production when their accumulation in mitochondria is sufficiently high. A recent study compared the effect of dequalinium chloride **140** in control epithelial CV-1 cells against its effect on DU-145 prostate carcinoma cells.<sup>381</sup> The data revealed that, after 3 hours of exposure to 5  $\mu$ M of dequalinium chloride **140**, the number of viable DU-145 prostate carcinoma cells was reduced by 50% and the ATP content in the viable cells was reduced by 62%. In addition, it was found that the longer the exposure, the higher the effect exerted by the chosen DLC. Control epithelial CV-1 cells did not show any change on their viability or ATP concentrations. This supports the idea that the diffusion of the DLCs is caused by  $\Delta\psi_m$ , resulting in a selective cytotoxic effect and the inhibition of metabolic activity by DLCs in carcinoma.<sup>381</sup>

The information above suggests that mitochondrion is an excellent target for the development of highly selective cytotoxic compounds or probes for diagnoses.

## **4.2 Phosphonium cations capable of binding Cu(II)**

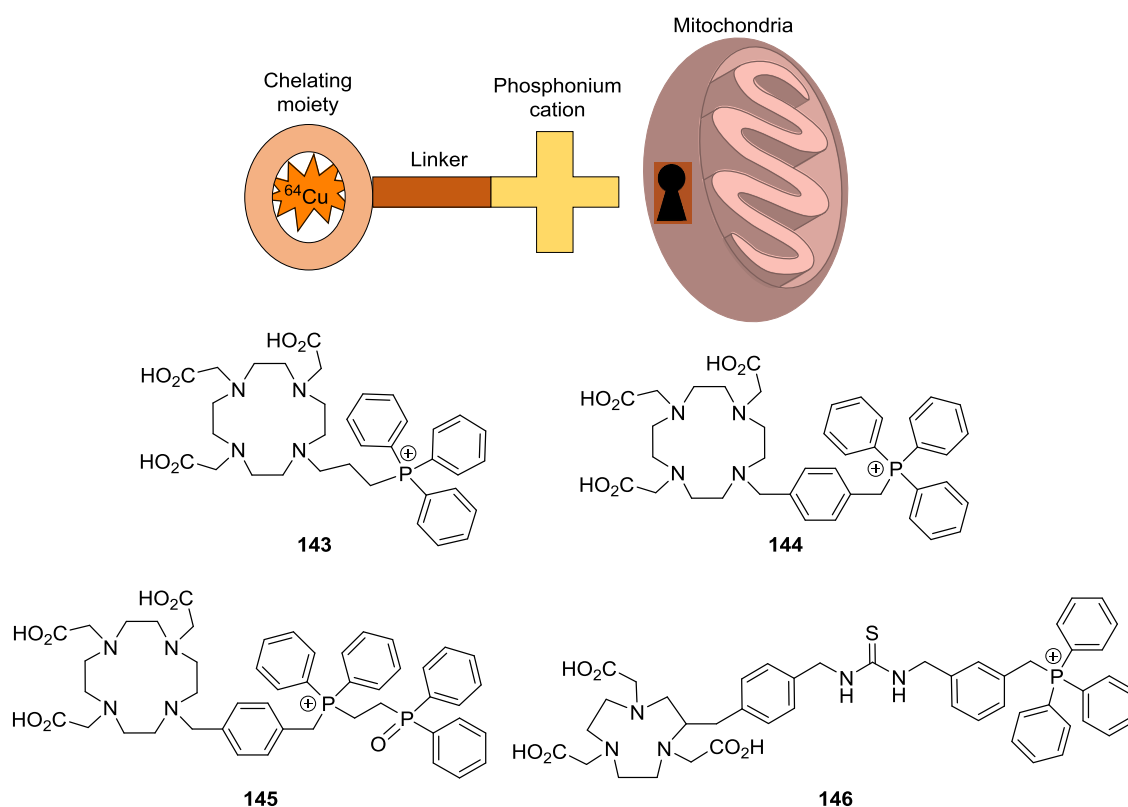
As introduced above, mitochondria can be used as a target for the development of compounds with biological activity, because they undergo certain changes during cancerous processes, such as the change in the transmembrane potential  $\Delta\psi_m$ .<sup>103, 373, 374</sup> The increase in this potential in cancerous cells<sup>103, 373, 374</sup> creates a negative charge increment in the mitochondria that selectively increases the diffusion of cations inside the organelle in cancerous cells. This feature has been exploited during the development of radiotracers, and led to the study of radiolabelled quaternary ammonium, phosphonium and arsonium cations, whose phosphine charge will cause them to accumulate in the mitochondria. The compound 4-(<sup>18</sup>F-benzyl) triphenylphosphonium **142** was developed by taking advantage of the mitochondrial distribution of phosphonium cations. This compound is a targeted PET radiotracer for determining myocardial perfusion and for tumour imaging. However, it showed a high uptake in the heart and liver, which represents a considerable shortcoming for its potential use as a diagnostic agent of cancer in chest and abdominal regions.<sup>383-388</sup>



**Figure 4.3 The cationic PET radiotracer 4-(<sup>18</sup>F-benzyl)triphenylphosphonium 142.**

Other triphenylphosphonium cations had proved to fulfil both the required biodistribution profile for a selective radiotracer and their imaging properties in small animals<sup>388</sup> and dogs.<sup>383, 386</sup> Despite these findings, the radionuclides used to radiolabel the phosphonium cations, <sup>11</sup>C and <sup>18</sup>F, limit their utility due to their short half-lives. The high cost of the infrastructure required to produce these radionuclides is itself another notable shortcoming. In addition, the chemistry of <sup>62</sup>Cu and <sup>64</sup>Cu allows them to form complexes with a broad variety of ligand carriers in the very last step of the synthesis. Therefore, the development of new PET radiotracers based on phosphonium cations with radionuclides that fulfil time, cost and chemistry flexibility requirements is important. The development of more versatile radiolabelled phosphonium ions will provide new tools in non-invasive cancer diagnosis.

Important research in the field of PET radiotracers incorporating on phosphonium cations was carried out by Zhou *et al.*<sup>389</sup> This team used Cu(II) as a source of the <sup>64</sup>Cu radionuclide in order to radiolabel the final phosphonium cation. The d<sup>9</sup> configuration of Cu(II) makes its complexes kinetically labile; they thus used different bifunctional chelators to create complexes with high thermodynamic stability and kinetic inertness to counter this property. This approach has been taken before to create stable <sup>62/64</sup>Cu labelled complexes.<sup>390-393</sup> Their findings showed that more than one positive charge in the radiotracer can provoke a high absorption in hepatocytes which diminishes absorption in any other part of the body. The general structure of their radiotracers contained the chelating ligand attached to the phosphonium moiety via a linker group. In general, the radiotracers made by this group were useful for imaging multidrug resistant (MDR) negative tumours by PET, because the compounds had a high tumour selectivity.

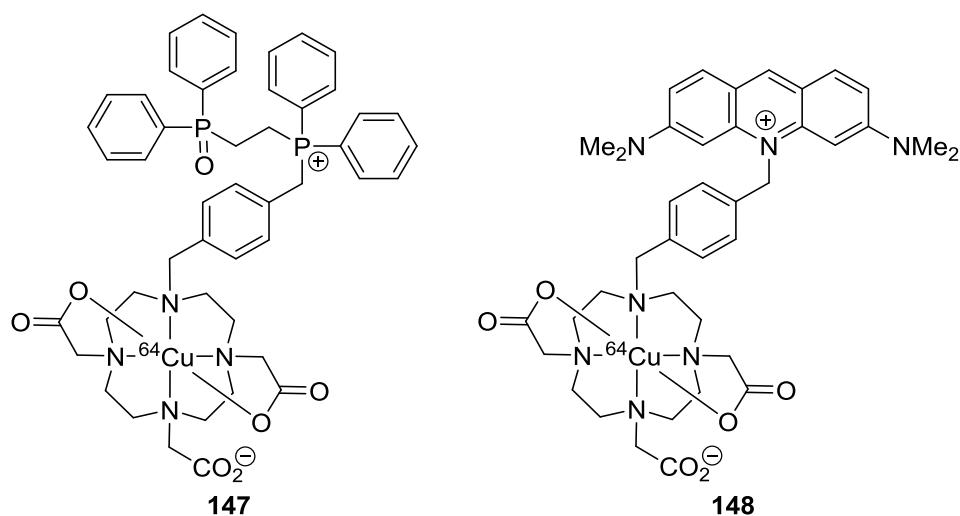


**Figure 4.4** Depiction of the general concept of the development of the compounds developed by Zhou.<sup>389</sup>

Figure 4.4 includes a representation of the importance of the phosphonium cation in the development of these radiotracers – it renders the compounds specific for mitochondria/cancer tissue. It also contains some examples of the phosphonium salt macrocyclic ligands created by that group.

Comparisons between phosphonium and ammonium cations have been reported.<sup>394</sup> In this particular study the phosphonium cation was sacrificed in order to couple the bifunctional chelator to an acridine moiety, a well-known dye that interacts with DNA by intercalation.<sup>132</sup> The phosphonium cation **147** was synthesised and its tumour intake was better than one reported for the pharmaceutical agent  $^{99\text{m}}\text{Tc}$ -Sestamibi, used for myocardial imaging studies.<sup>393</sup> The biodistribution of phosphonium cation **147** was compared to the acridinium cation **148**. The evaluation showed that acridinium **148** made tumours clearly visible in the athymic nude mice bearing U87MG human glioma xenografts. It was possible to assure acridinium **148** absorption by mitochondrion U87MG glioma cells using fluorescent microscopic technique.<sup>394</sup> This makes it possible to visualise the compound of interest directly in the cell, whereas PET allows the

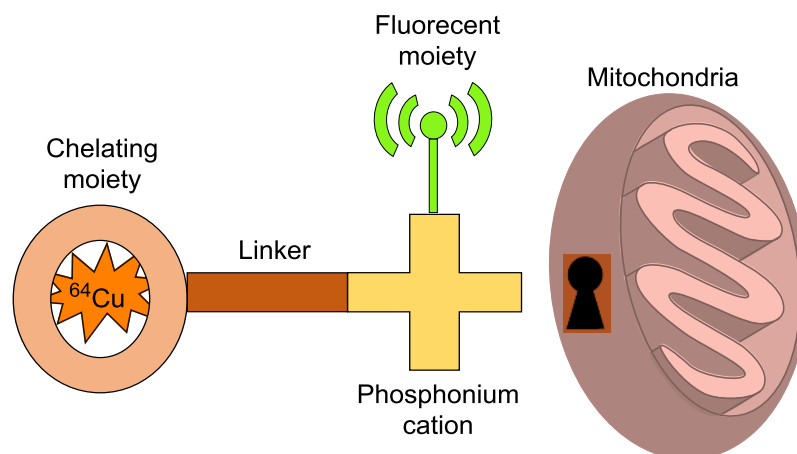
radiotracer in tissue to be visualised. Additionally, it makes it possible to visualise the ‘cold’ compound without the need of a cyclotron. This shows that combining PET and fluorescence imaging techniques ensures the appropriate biodistribution of a PET imaging candidate. However, acridinium **148** showed a higher liver uptake than the phosphonium cation **147**. This feature makes acridinium **148** a bad PET imaging agent in comparison with phosphonium **147** despite the fact that phosphonium **147** does not contain the DNA-intercalating feature that the acridine moiety in **148** has. An intercalating agent with a high selectivity for mitochondria in cells affected by cancer could be a useful tool for the development of anticancer therapies.



**Figure 4.5** Structures of complexes **147** and **148** proposed by Zhou<sup>394</sup> developed in order to compare their properties as PET agents.

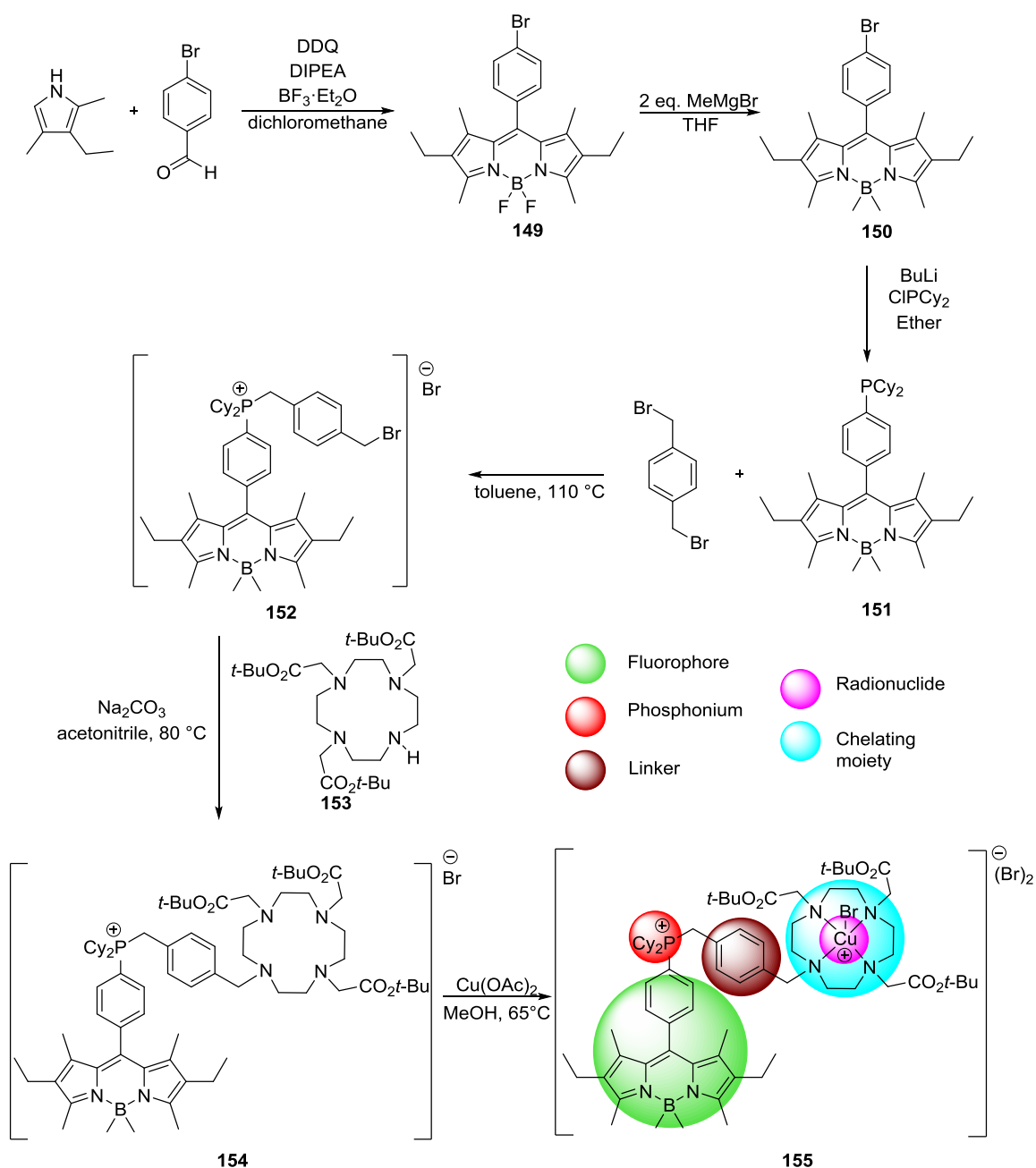
### 4.3 BODIPY-derived ligand target

The LJH research group has experience in the field of phosphines and phosphonium salts;<sup>107</sup> the findings reported by Zhou<sup>389, 394</sup> were therefore of interest.<sup>395</sup> As explained above, radiotracers based on phosphonium cations display a high selectivity for mitochondria in cancer cells. In addition, these compounds seem to have different selectivity according to their physicochemical features. The radiotracers reported included either fluorescence or a phosphonium moiety but not both. The natural next step was for our group to develop a molecule which could contain the useful fluorescent moiety without sacrificing the highly selective phosphonium moiety (Figure 4.6).



**Figure 4.6** General depiction of the radiotracer proposed by the LJH group. This molecule contains the radionuclide  $^{64}\text{Cu}$  and a fluorescent moiety to exploit both techniques, PET and fluorescence imaging, using the same agent.

The synthesis of this proposed radiotracer will include a BODIPY core that will act as the fluorescent moiety. The fluorescent moiety creates the possibility of determining the presence of the radiotracer even when the cold analogue is used in cells, using fluorescence microscopy techniques. Developing a phosphonium salt based on a BODIPY core is a synthetic challenge that can be overcome using previous methodologies developed by our group. A tertiary phosphine in the *meso* position of the BODIPY core will be synthesised and a linker will be attached to it to form the required phosphonium cation. The chosen linker is the commercially available  $\alpha,\alpha'$ -dibromo-*p*-xylene. The addition of this phenyl ring to the radiotracer decreases its tumour uptake more than an alkyl chain. However, there are radiotracer tests of phosphonium cations bearing this linker.<sup>389, 390, 394, 396</sup> Using this commercial linker in the proposed radiotracer **155** will allow us to contrast it with other cations reported in the literature.



**Figure 4.7** Synthesis of the proposed radiotracer **155**. The colours show the different functions that each part of the molecule exerts.

The coupling of 1,4-bis(bromomethyl)benzene with the tertiary phosphine **151** produces the phosphonium salt **152** which will couple with the chelator agent **153** in order to add the chelating moiety that will interact with the metal of interest. Finally,  $[\text{Cu}(\text{OAc})_2]$  will be reacted with the chelating agent **154** to generate the novel radiotracer **155**.

#### 4.4 Synthesis of BODIPY-Cu(II) complex derived from a phosphonium cation

The first reaction required to achieve the proposed novel radiotracer **155** is the one pot condensation of the aryl bromide BODIPY derivative **149**. Commercially available 3-ethyl-2,4-dimethyl-1*H*-pyrrole was dissolved with 4-bromobenzaldehyde in dichloromethane in the presence of trifluoroacetic acid, yielding the bromide **149** in a 55% yield. Then an oxidation took place by the addition of BF<sub>2</sub>. This procedure has been previously reported by the LJH group.<sup>397</sup>

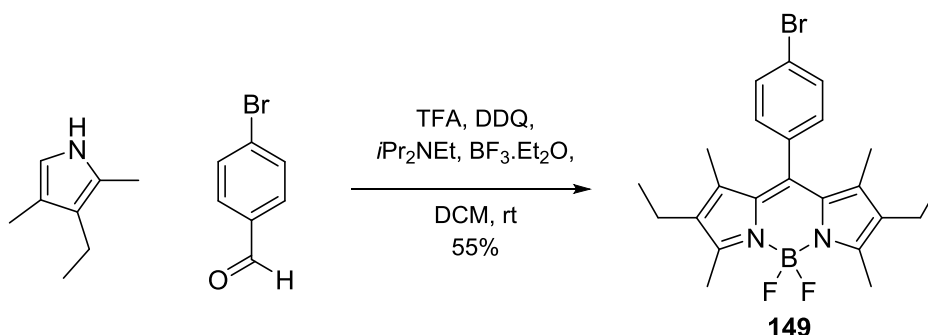


Figure 4.8 Synthesis of bromide **149** by pyrrole condensation.

Research on substitution of the fluorine atoms of the BODIPY core for alkyl and aryl groups has been accomplished using organolithium and Grignard reagents producing BODIPY dyes with alkyl and aryl groups on the boron atom,<sup>398,399</sup> subsequently allowing more versatile chemistry to be carried out on the *meso* position of the BODIPY core.<sup>108-110</sup> The difluorine-BODIPY **149** was reacted with MeMgBr in order to produce the dimethylated BODIPY **150**. C–Boron bonds are less likely to undergo an attack by nucleophiles or reducing agents, in comparison to boron-fluoride bonds.

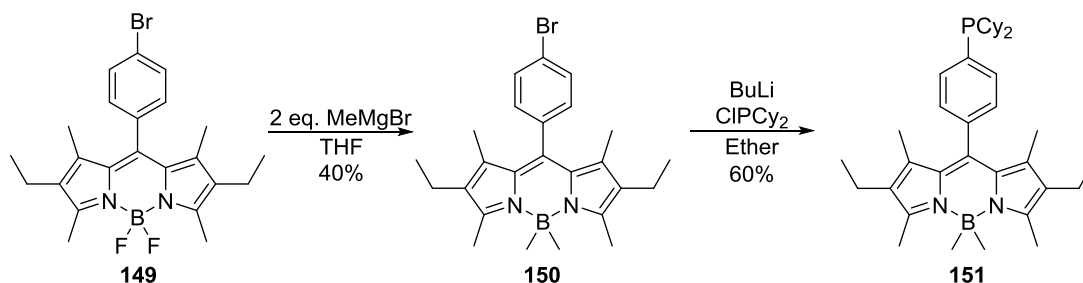


Figure 4.9 Synthesis of the tertiary phosphine **151**.<sup>395</sup>



This step locks down the BODIPY core, allowing a bromine-lithium exchange reaction to be performed in the next step with buthyl lithium, obtaining a nucleophilic species that attacks  $\text{ClPCy}_2$ , displacing the chloride atom and yielding the tertiary phosphine **151**.

The reaction to obtain the tertiary phosphine was shown to have some technical difficulties. Tertiary phosphines can be oxidised to their phosphine oxide form. The oxidation seems to be facilitated when the phosphine is in solution.<sup>35, 36</sup> The first attempts to synthesise this molecule led to the phosphine oxide **156**. The reaction was carefully monitored using the  $^{31}\text{P}\{^1\text{H}\}$  NMR technique. It was found that after 8 hours the desired tertiary phosphine was formed and the formation of the oxide was minimal. It was possible to separate the oxide using column chromatography. The  $^{31}\text{P}\{^1\text{H}\}$  NMR analysis of other reported phosphine oxides had shown values of around 50 ppm for this kind of compound ( $(\text{CH}_3)_3\text{PO}$  and  $(\text{C}_2\text{H}_5)_3\text{PO}$ ).<sup>400</sup> Therefore, at this point it was sensible to infer that the compound producing a singlet at 45.7 ppm in  $^{31}\text{P}\{^1\text{H}\}$  NMR belongs to an phosphine oxide.

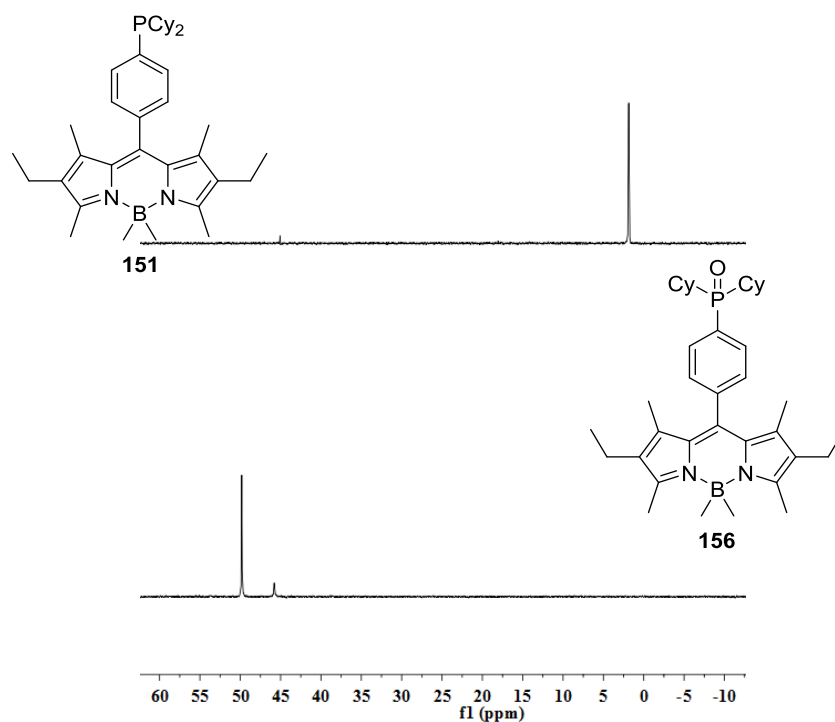
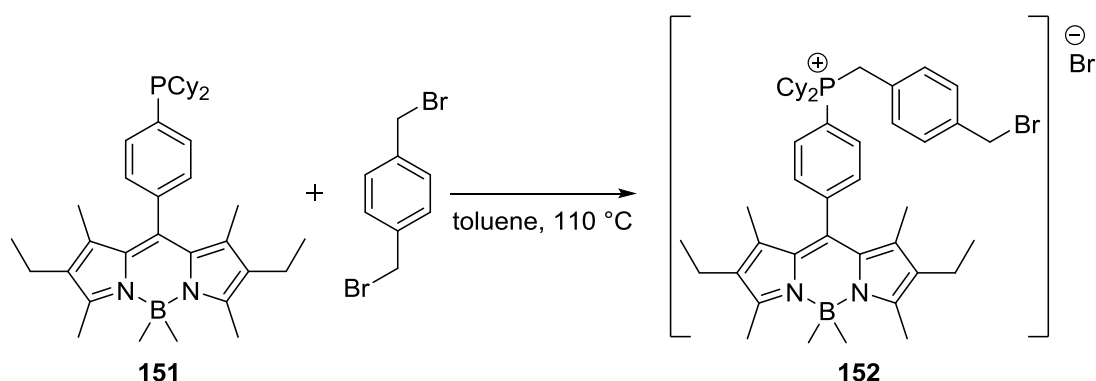


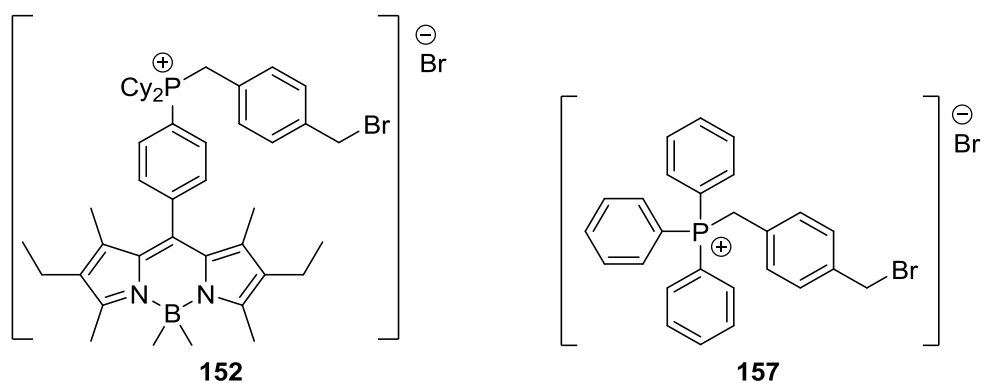
Figure 4.10  $^{31}\text{P}\{^1\text{H}\}$  NMR of the desired tertiary phosphine **151** (2.2 ppm) and the side product phosphine oxide **156** (45.7 ppm).

Tertiary phosphine **151** can act as a nucleophile due to its lone pair of electrons. This is highly significant since it will be useful when adding a linker group to the phosphine functional group, as has been shown by Zhou to synthesise the different ligands made by his group.<sup>389</sup>



**Figure 4.11** Synthesis of phosphonium **152**.

The linker added was 1,4-bis(bromomethyl)benzene. This molecule has 2 bromide atoms which can act as leaving groups. However, the symmetry of the molecule makes both bromide atoms equivalent. In order to avoid the addition of two tertiary phosphines to the same linker molecule, it is important to control the number of equivalents of tertiary phosphine **151** that will be reacted. This reaction has been extensively reported using triphenylphosphine<sup>390, 401-403</sup> and is usually carried out in toluene since its polarity is quite low. The low polarity of this solvent forces the triphenyl phosphonium ion to precipitate from the solution which avoids the reaction of 2 molecules of triphenylphosphine with 1 molecule of 1,4-bis(bromomethyl)benzene. The synthesis of BODIPY phosphonium **152** was performed in toluene following the procedure reported for its triphenylphosphine analogue. However, no solid precipitated from the solution which might explain the low yield obtained for compound **152** (55%) in comparison with the reported triphenyl phosphonium **157** (approximately 80%<sup>218</sup>).

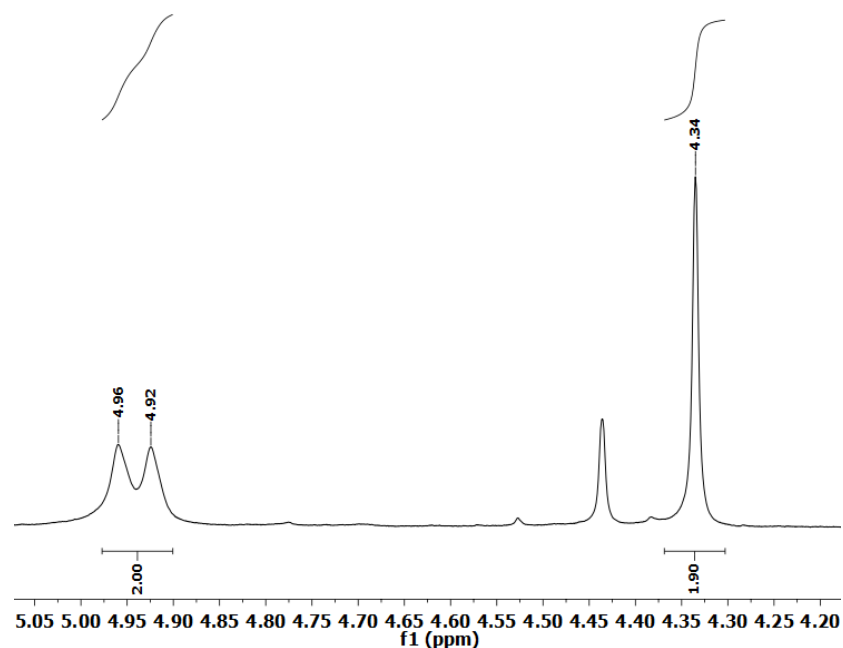


**Figure 4.12 Novel BODIPY phosphonium 152 and the reported triphenyl phosphonium salt 157.**

Figure 4.12 shows the greater degree of non-polar substituent in the novel BODIPY phosphonium **152** in comparison with triphenyl phosphonium **157**. This difference is likely to explain their different solubility in toluene.

This reaction was monitored by  $^{31}\text{P}\{^1\text{H}\}$  NMR until completion. The main proof that the compound proposed was obtained was provided by this NMR technique since there was a shift in the signal of the reaction. The  $^{31}\text{P}\{^1\text{H}\}$  NMR signal corresponding to the tertiary phosphine is detected at 2.8 ppm; the presence of a new signal at 30.2 ppm indicated that the starting material had been consumed. In addition, it suggests that the product obtained is not the phosphine oxide **156**, which was a significant concern since the tertiary phosphine **151** had proved to be readily oxidised in solution.

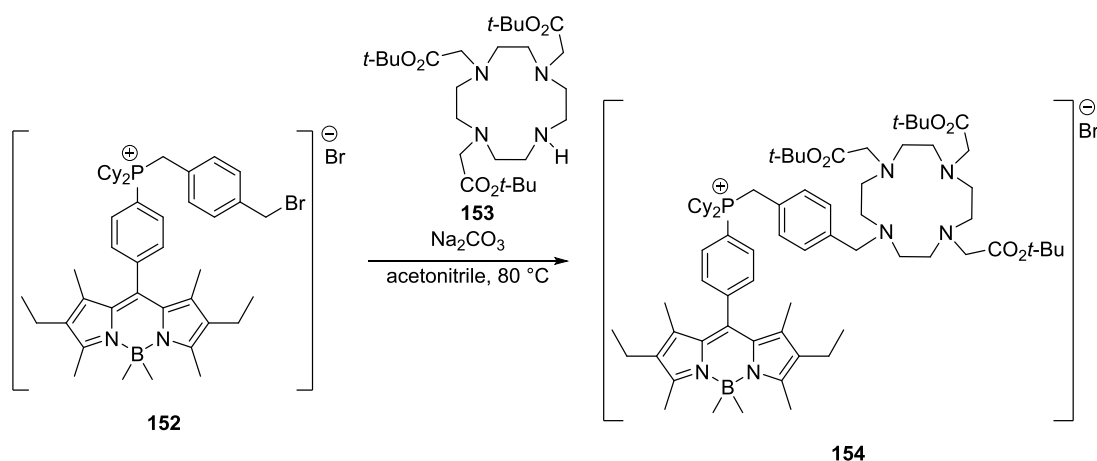
The  $^1\text{H}$  NMR analysis of **152** shows that there is a new set of two aryl doublets that integrate for two protons each. In addition, the protons on the methylene groups of the starting material 1,4-bis(bromomethyl)benzene are a good indicator for determining a coupling of a nucleophile to this molecule. In the starting material, both methylene groups are equivalent; therefore, the  $^1\text{H}$  NMR spectroscopy of both sets of protons produce a singlet with a chemical shift of 4.4 ppm.<sup>404</sup> The  $^1\text{H}$  NMR spectrum of the BODIPY phosphonium salt **152** suggests that the two sets of methylene protons are different in this molecule.



**Figure 4.13**  $^1\text{H}$  NMR of BODIPY-phosphonium salt **152** showing the two different sets of aryl doublets.

The two signals, 4.92 (d,  $^2J_{\text{HP}} = 8.1$  Hz, 2H) ppm and 4.34 (s, 2H) ppm, differ not only in chemical shift but also in multiplicity. This must be due to the effect exerted by phosphorus. The signal at 4.92 ppm belongs to protons on a methylene group that are coupling to the phosphorus atom and the singlet at 4.34 ppm belongs to the methylene that bears the bromide atom. This correlates with the reported spectrum for triphenylphosphonium **157**.<sup>405</sup> The presence of phosphonium **152** was also corroborated by HRMS.

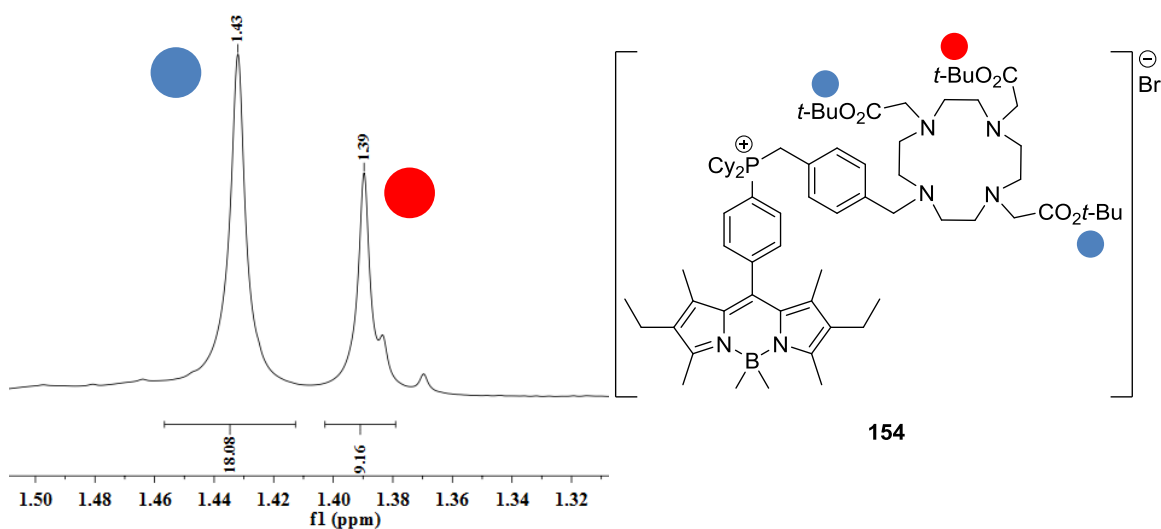
Tri-*tert*-butyl-1,4,7,10-tetraazacyclododecane-1,4,7-triacetate **153** was synthesised using the procedure described by Zhou.<sup>389</sup> Once prepared, the chelating agent **153** was coupled to the BODIPY phosphonium salt **152**. The free amine in **153** act as a nucleophile and attacks the benzylic carbon that bears the bromide atom that will act as a leaving group, producing the BODIPY-substituted macrocycle ligand **154**.



**Figure 4.14** Synthesis of BODIPY-substituted macrocyclic ligand **154**.

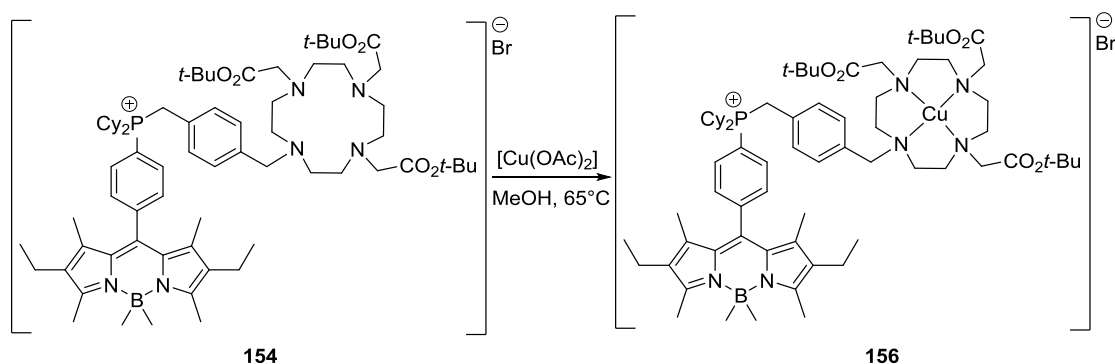
This reaction could not be monitored using  $^{31}\text{P}\{^1\text{H}\}$  NMR spectroscopy, since the coupling of the macrocyclic ligand **154** did not produce a major impact on the chemical environment of the phosphorus atom. The phosphonium **152** produces a signal at 30.2 ppm, whereas the phosphonium ligand **154** produces a signal at 30.3 ppm – the compound was thus initially identified primarily by its  $^1\text{H}$  NMR spectrum. In the novel ligand **154**, the methylene group that bears the nitrogen atom underwent a change in its chemical environment, since the bromide atom has been displaced and substituted for the macrocycle ligand. Similar compounds report the signal of the expected singlet as part of the multiplet produced by the ethyl protons that form the macrocycle.<sup>402</sup> The same displacement occurred with the novel ligand **154**. The protons on the methylene group that couple to the phosphorus atom suffer no change in their chemical shift. Therefore, they were not particularly useful for identifying the newly formed ligand **154**. The *tert*-butyl groups were important for identifying the coupling of macrocycle **153** and the BODIPY-phosphonium salt **152**. The *tert*-butyl groups attached to the nitrogen atoms, which are two bonds away from the nitrogen in the benzylic position, are equivalent. The remaining *tert*-butyl group in the macrocycle is in a different environment. Therefore, the  $^1\text{H}$  NMR spectrum of this molecule would be expected to present 2 singlets in the alkyl NMR region. The integration ratio of the singlets should be 2:1 due to the total amount of proton atoms on these groups, 18:9. This was obtained in the  $^1\text{H}$  NMR spectrum of compound **154** confirming the formation of the expected compound. The *tert*-butyl groups of the free macrocyclic ligand **153** are also different. However, they are similar enough to form a multiplet that integrates 27 protons at 1.47 ppm as was reported by Cao *et al.*<sup>406</sup> The formation of two identifiable singlets was led us to think that the coupling

took place as expected. In addition, the formation of phosphonium ligand **154** was also corroborated by HRMS.



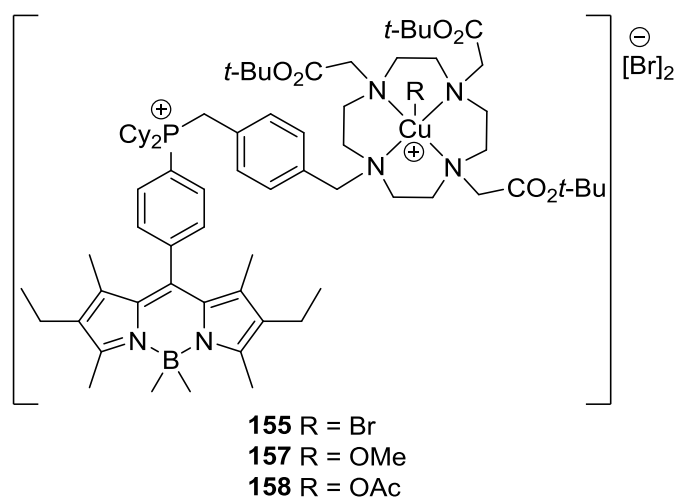
**Figure 4.15**  $^1\text{H}$  NMR showing the types of *tert*-butyl groups in the macrocycle of the BODIPY-substituted ligand **154**.

Once it was established that the ligand **154** had been synthesised, it was decided that a Cu-complex analogous to those reported by Zhou<sup>389</sup> should be prepared. Following the procedure carried out by his group, the fluorescent ligand **154** was reacted with  $[\text{Cu}(\text{OAc})_2]$ . Since  $^{63}\text{Cu}$  and  $^{65}\text{Cu}$ , the most abundant Cu isotopes, have large nuclear quadrupole moments, the reaction could not be monitored by NMR techniques. Therefore, the proof that a product had been formed at this point was provided by the lack of  $^1\text{H}$  NMR signals of the starting material. This proved that the starting material was consumed but it provided no evidence regarding the nature of the complex formed.



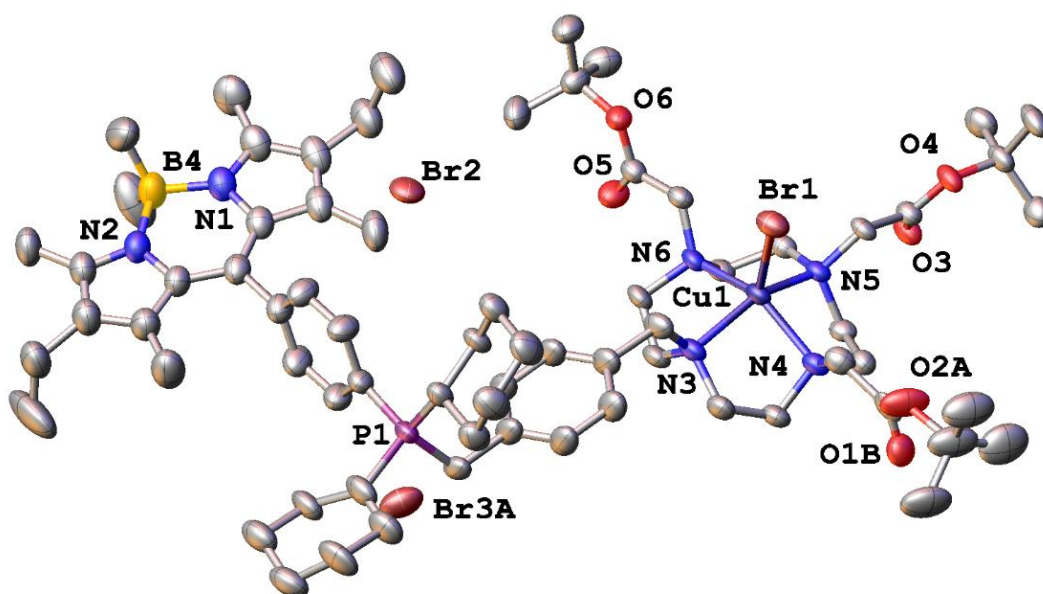
**Figure 4.16** Synthesis of Cu(II) complex **156**. The ethyl acetate groups of  $[\text{Cu}(\text{OAc})_2]$  are displaced by the nitrogen atoms of the BODIPY-substituted macrocyclic ligand **154**.

The TLC showed different fractions that were separated via column chromatography. The HRMS analysis of these fractions suggested complexes with different R groups to acetate on the copper centre. Figure 4.17 shows the structures that correlate with the HRMS findings of the fractions analysed. The M/Z value of the expected complex **156** is 1248.77; but HRMS showed at 664.8417, 639.8755 and 653.8908. In addition, the mass fragmentation patterns observed corresponded to those produced by compounds containing Cu isotopes ( $^{63}\text{Cu}$  with an abundance of 69.17% and  $^{65}\text{Cu}$  with an abundance of 30.83%). Those values M/Z are approximately half of the value expected for the complex **156**. This result led us to assume that there was another positive charge on the complexes, with the Cu the most plausible atom to have this charge. The structures that fit best to the M/Z value are shown in Figure 4.17. The possible substituents on the metallic core that we proposed are bromide (664.8417 M/Z), methoxy (639.8755 M/Z) and acetate (653.8908 M/Z). Zhou *et al.*<sup>389</sup> identified their Cu complexes by comparing their HPLC retention times against Gd and In complexes with their ligands **143-146** (Figure 4.4). They did not report any extra ligands attached to their metallic core besides the main chelating agent. They proposed that the free carboxylate groups would stabilise the Cu atom avoiding the positive charge we saw in the HRMS of our sample. This might be due to the fact that the BODIPY ligand **154** has the *tert*-butyl groups. Therefore, the carboxylate groups are not available to interact in the same fashion as proposed by Zhou. The bromide anion in complex **155** must have been obtained from other molecules of the ligand **154**, since this phosphonium cation has bromide as its counter ion. In complex **157**, a methoxide group occupies a position on the metallic core. This group likely originates from the methanol used during the reaction as solvent. Since the starting material was  $[\text{Cu}(\text{OAc})_2]$ , it is not surprising that in complex **158**, an acetate group is found attached to metallic core as was suggested by the HRMS data.



**Figure 4.17** Probable structure, suggested by HRMS analysis, of complexes **155**, **156** and **158**, obtained from reacting ligand **154** with  $[\text{Cu}(\text{OAc})_2]$ .

Different fractions were separated using column chromatography. Several attempts to recrystallize the purified fractions were set-up until success was achieved. This revealed the structure **155** where the geometry of the metallic centre is a distorted square pyramidal molecular geometry (Figure 4.18).

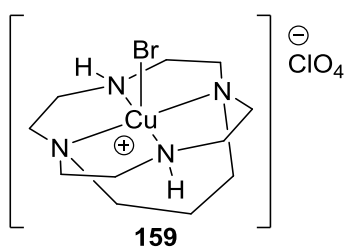


**Figure 4.18** X-ray crystal structure view of  $[\text{CuBr}(\mathbf{154})][\text{Br}]_2$  **155** (50% probability ellipsoids with interesting copper, phosphorus, boron, nitrogen, oxygen and carbon atoms labelled. Carbon atoms in grey). Hydrogen atoms have been omitted for clarity Br1–Cu1 2.4744(7), Cu1–N3 2.073(3), Cu1–N4 2.098(3), Cu1–N5 2.085(3), Cu1–N6 2.085(3), P1–C22 1.796(4), P1–C27 1.832(4), P1–C39 1.800(4), P1–C33A 1.856(7); N3–Cu1–Br1 104.38(10), N3–Cu1–N4 85.72(12), N3–Cu1–N5 148.96(13), N3–Cu1–N6 85.04(12), N4–Cu1–Br1 104.75(9), N5–Cu1–Br1 106.65(8), N5–Cu1–N4 85.66(11), N5–Cu1–N6 86.50(11), N6–Cu1–Br1 107.55(8), N6–Cu1–N4 147.66(12).



The different groups that are suggested by the HRMS indicate that different products are produced in this reaction. This would explain why the yield of complex **155** does not seem to be high (44%).

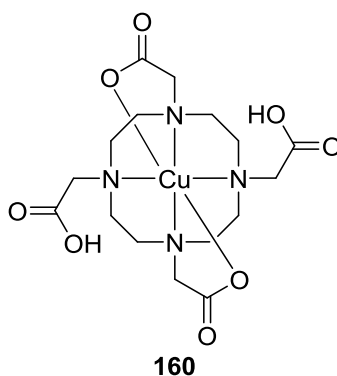
Springborg *et al.*<sup>407</sup> reported the complex **159** which is an example of a Cu(II) complex that is similar to the BODIPY-Cu(II) complex **155**. This complex contains the same macrocycle, a bromine atom and a penta-coordinated geometry, as our BODIPY-complex **155**. The bromine atom is not in the axial position in the complex **159** (Br1–Cu1–N2 153.3(3)). This is different in our complex **155** where the bromine atom is in the axial position (N5–Cu1–Br1 106.65(8)). This difference might be due to the effect exerted by the ethyl group that connects the two nitrogen atoms in the complex **159**. The Cu–N bond lengths are similar in both molecules, having a length of  $2.09 \pm 0.03$  Å. The nitrogen atoms that are attached to the ethyl chain have Cu–N bond lengths below 2.00 Å (Cu1–N1 1.985(6) Å and Cu1–N3 1.995(9)).



**Figure 4.19** Cu(II) complex **159** reported by Springborg *et al.*<sup>407</sup> The ethyl group connecting two nitrogen atoms in this ligand creates some differences in terms of some angles and bond lengths found for the BODIPY-Cu(II) complex **155**

The phosphonium-Cu(II) complexes reported by Zhou<sup>394</sup> were not identified using X-ray crystal analysis. On the other hand, the BODIPY-Cu(II) complex **155** was identified using that technique, which allowed us to determine its molecular geometry. The complexes reported by Zhou<sup>394</sup> contain *tert*-butyl groups protecting the carboxylate functions; therefore, the molecular geometry might be different. Riesen *et al.*<sup>408</sup> synthesised the macrocyclic-Cu(II) complex **160** whose ligand resembles the chelating moiety of BODIPY-Cu(II) complex **155** with one principal difference: the *tert*-butyl groups are not present in the ligand used by Riesen. This allows them to interact with the metallic core resulting in octahedral molecular geometry around the central metallic core. This suggests that the distorted square pyramidal molecular geometry observed in the BODIPY-Cu(II) complex **155** is given by the lack of interaction between the carboxylate groups with the metallic core. Since these groups cannot stabilise the metallic core, the chelating effect of

the bromine, acetate and methoxide groups must be facilitated. Unprotecting the carboxylate groups would possibly decrease the formation of side products.

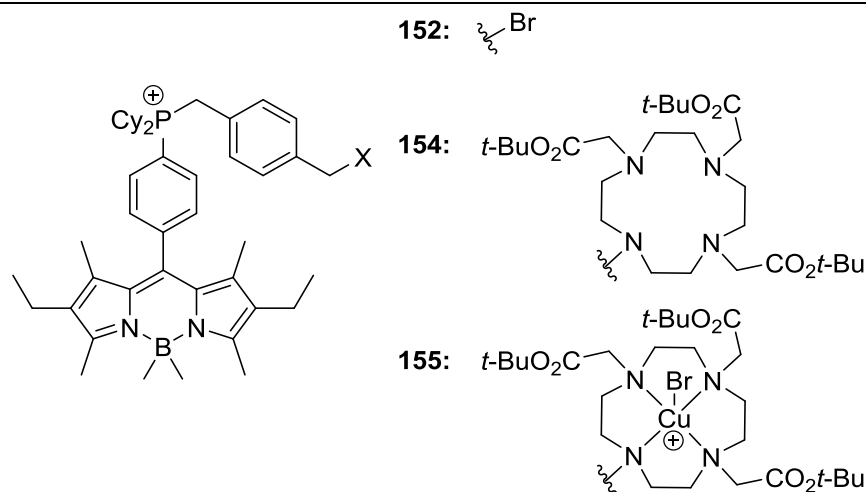


**Figure 4.20** Macrocyclic-Cu(II) complex **160** synthesised by Riesen *et al.*<sup>408</sup>

Complexes of Co and Zn have also shown interesting biological properties,<sup>409, 410</sup> synthesising complexes with these metals and ligand **154** has thus been attempted. However, it has not been possible to properly identify or obtain a crystal for X-ray analysis of the obtained compounds at the time of writing.

#### **4.5 Photophysical Data**

Once the synthesis of complex **155** was accomplished, it was necessary to determine the photophysical properties of this compound to verify whether it can be a candidate for fluorescent cell imaging. It is interesting to investigate the photophysical properties of the different functional groups added during the synthesis of the ligand **154**. The phosphonium cation **152** does not possess the lone pair of electrons that the tertiary phosphine **151** contains.<sup>395</sup>



Compound	$\lambda_{\text{abs}}$ (nm) <sup>a</sup>	$\lambda_{\text{em}}$ (nm) <sup>a</sup>	$\epsilon$ (cm <sup>-1</sup> /M) <sup>a</sup>	$\Delta\nu_{\text{st}}$ (nm) <sup>a</sup>
<b>152</b>	519	545	24,000	26
<b>154</b>	518	544	50,000	26
<b>155</b>	518	545	40,000	27

<sup>a</sup> Measured in dry degassed tetrahydrofuran at room temperature. Dyes were excited at 485 nm.

**Table 4.1** Photophysical data for the Cu(II) complex **155** and its precursors.

The chelating moiety also contains pairs of electrons on the nitrogen atoms that form the main 12-membered macrocycle. Lone pair of electrons from both nitrogen or phosphorus atoms and heavy atoms, such as copper, have shown to have a quenching effect in fluorophores.<sup>121, 124, 125, 337-339, 411, 412</sup> Photophysical data were collected for the Cu(II) complex **155** and its precursors in dry degassed tetrahydrofuran to minimise photobleaching (Table 4.1).

The Stokes shifts in compounds **152**, **154** and **155** do not display any significant change in their values. The quantum yield ( $\Phi_{\text{F}}$ ) of compounds **152**, **154** and **155** were measured in different solvents in order to investigate the effect exerted by the solvent on their  $\Phi_{\text{F}}$ . The  $S_0$ - $S_1$  excitation of the fluorophore usually leads to an excited vibrational level of  $S_1$  followed by a loss of some vibrational energy to the solvent. This excess of energy is stabilized by the effect of polar solvent molecules, since typically, the fluorophore has a larger dipole moment in the excited state ( $S_1$ ) than in the ground state ( $S_0$ ).<sup>40</sup> Following this excitation,  $\mu_{\text{E}}$  can produce a reorientation or relaxation of polar solvent molecules around it to lower the energy  $S_1$ . This reduction of energy is seen in the emission in its

increased wavelength; longer wavelengths are less energetic since the energy of emission is inversely proportional to the wavelength as Equation 1 on page 21 illustrates.<sup>40</sup>

Compound	$\Phi_F$ in DCM	$\Phi_F$ in MeOH	$\Phi_F$ in THF
<b>152</b>	0.20	0.15	0.29
<b>154</b>	0.26	0.24	0.34
<b>155</b>	0.03	0.07	0.08

$\Phi_F$  were measured with respect to 4,4-difluoro-8-phenyl-1,3,5,7-tetramethyl-2,6-diethyl-4-bora-3a,4a-diaza-s-indacene ( $\Phi_F = 0.76$ , in tetrahydrofuran)<sup>413</sup>. Dyes were excited at 480 nm.

**Table 4.2  $\Phi_F$  of compounds 152, 154 and 155 in solvents with different polarities.**

The results show a constant trend where the ligand **154** has the highest  $\Phi_F$  value, followed by the phosphonium cation **152** and finally the Cu(II) complex, **155**. The  $\Phi_F$  of the tertiary phosphine **151** has been reported by this group previously;<sup>395</sup> the value is 0.44 using the same fluorescent standard. That value was corroborated by the measurements obtained during the development of this project. This result is interesting since the opposite would be expected considering that the lone pair of electrons in the tertiary phosphine **151** could potentially interact with the fluorophore producing Photoinduced Electron Transfer that could provoke fluorescence quenching. Calculated molecular orbital surfaces already reported by this group show that the tertiary phosphine **151** has no phosphorus character in the HOMO, HOMO-1 or HOMO-2 of this molecule.<sup>395</sup> This suggests that there would be little interaction between the lone pair of electrons on the phosphorus atom and the fluorescent core. The lower  $\Phi_F$  of the phosphonium ion **152** relative to the tertiary phosphine **151** may be explained by its interaction with the solvent. Tetrahydrofuran seems to be the solvent where the highest  $\Phi_F$  values were recorded. This is interesting since this solvent has an intermediate polarity value in between methanol and dichloromethane. Even more interesting is the fact that the  $\Phi_F$  values recorded in dichloromethane were intermediate and those recorded in methanol were the lowest. This could mean that the high polarity of methanol decreases emission for these compounds because of solvent- $\mu_E$  interactions. The values recorded in dichloromethane are lower than those recorded in tetrahydrofuran, even though, the latter solvent has a higher polarity. This might be due to dynamic fluorescence quenching given by the fluorophore colliding with a halogen containing substance, such as dichloromethane. During the

lifetime of the excited state, this collision provokes the return of the fluorophore to the ground state without emission of a photon.<sup>414</sup>

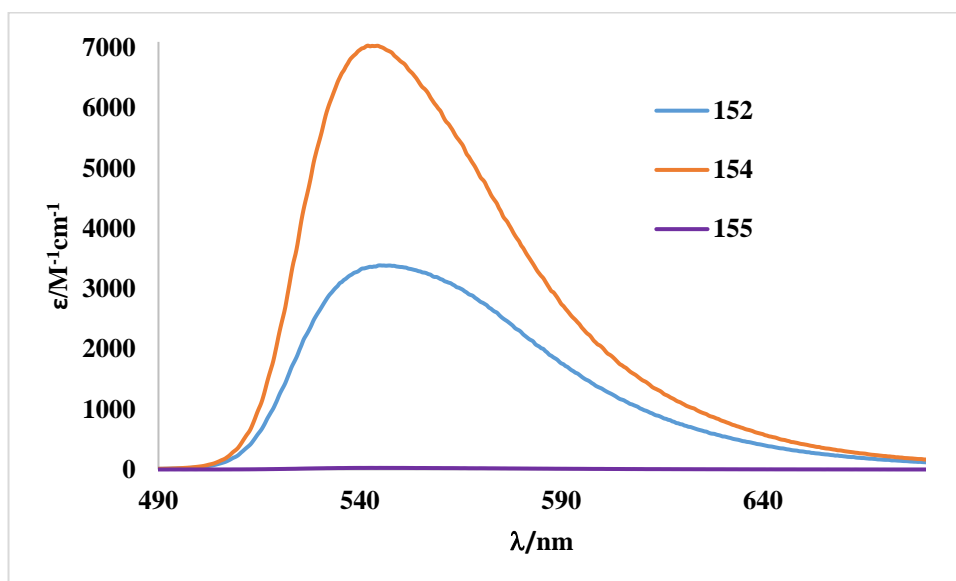


Figure 4.21 Emission spectra of the phosphonium cation **152**, ligand **154** and the complex  $[\text{CuBr}(\text{154})][\text{Br}]_2$  **155**, in tetrahydrofuran (excitation at 480 nm).

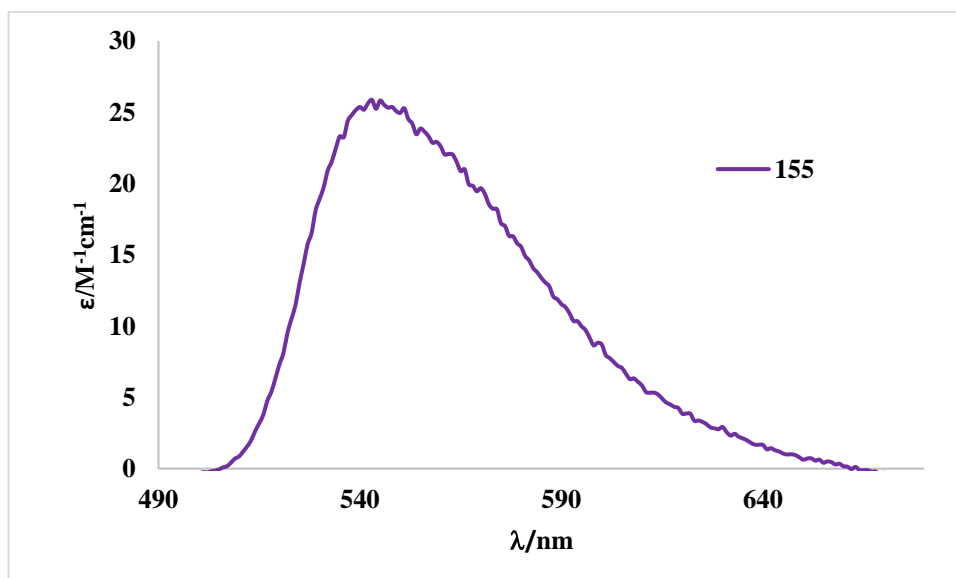


Figure 4.22 Emission spectra of the complex  $[\text{CuBr}(\text{154})\text{Br}][\text{Br}]_2$  **155** in tetrahydrofuran (excitation at 480 nm). The intensity of the emission of complex **155** is much lower than that one of compounds **152** and **154**.

The addition of the chelating moiety to the phosphonium cation **152** decreases the polarity of the product since the resulting ligand **154** contains three *tert*-butyl groups. This might reduce the interactions of the  $\mu_E$  of ligand **154** with the solvent, which could increase the

emission. This can explain the higher  $\Phi_F$  ligand **154** in comparison with its precursor, phosphonium salt **152**. It was not entirely unexpected to observe a reduction of the  $\Phi_F$  of the Cu(II) complex **155**. The presence of the Cu atom may generate the heavy atom effect mentioned in the Section 1.4.1, causing spin-orbit coupling and giving rise to intersystem crossing to a triplet state, which is usually spin forbidden. From the excited triplet state, relaxation predominately happens via non-radiative decay over radiative phosphorescence.<sup>415</sup> The BODIPY-Cu(II) complex **155** has a lower  $\Phi_F$  than compounds **152** and **154** as can be seen in Figure 4.21 and Figure 4.22. However, its  $\Phi_F$  value proves that it is fluorescent, and it can, therefore, be a candidate for fluorescent microscopy.

## 4.6 Summary

Previous reports in the literature show that radiolabelled phosphonium cations can be traced into cancerous tissue since the mitochondria of the cells that form this tissue have a higher  $\Delta\psi_m$ <sup>103, 373, 374</sup>. Positively charged cations can diffuse into living cells and accumulate in the mitochondria.<sup>375-377</sup> This characteristic makes the mitochondria a natural target for drug candidate molecules. Radiolabelled phosphonium cations are traceable in cancerous tissue using PET techniques if they contain a suitable radiolabel.<sup>388, 383, 386</sup> Research on Cu(II) complexes based on phosphonium cations<sup>389, 394</sup> showed that this is an area to be exploited for the development of radiotracers. In this chapter, the synthesis of a fluorescent Cu(II) complex based on a BODIPY phosphonium cation linked to a chelating moiety is reported allowing *in vivo* and *in vitro* imaging. The required phosphonium cation was obtained by reacting 1,4-bis(bromomethyl)benzene with the tertiary phosphine **151**. The resulting phosphonium cation **152** contains a bromide in a benzylic position, which makes it a good leaving group, thereby facilitating the attack of the free amine of the macrocyclic chelating agent **154**. The resulting ligand **154** was then reacted with [Cu(OAc)<sub>2</sub>] producing different complexes identified by HRMS. It was possible to obtain crystals of the main product of this reaction, which were of a high enough quality to be analysed by X-ray crystallography, revealing the structure of the complex obtained. The metallic core of this complex is a penta-coordinated copper centre. The  $\Phi_F$  values of the novel compounds show that the reported  $\Phi_F$  of tertiary phosphine **151**<sup>395</sup> is higher than the phosphonium cation **152**, which could be related to the positive charge on the phosphorus atom (polarity of the salt). Cu(II) complex **155** has the lowest  $\Phi_F$  value, which is likely related to the heavy atom effect prompted by the Cu atom. Nonetheless, the synthesis of a fluorescent Cu(II) complex containing a phosphonium

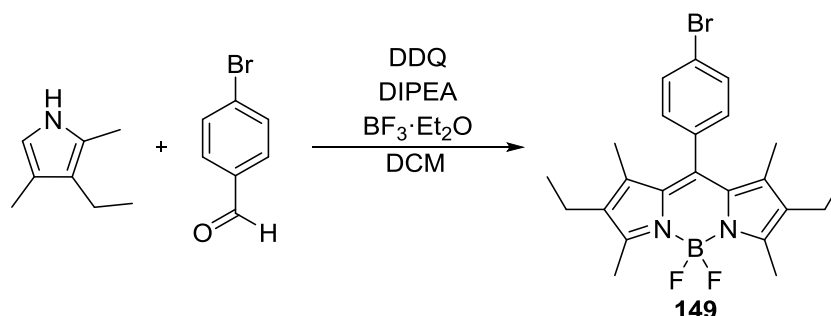
cation was successfully achieved as suggested by the emission spectrum of complex **155**, shown in Figure 4.22.

## 4.7 Experimental

### 4.7.1 General procedure

All air- and/or water-sensitive reactions were performed under a dinitrogen atmosphere using standard Schlenk line techniques. Tetrahydrofuran and toluene were dried over sodium/benzophenone and sodium respectively, dichloromethane was dried over calcium hydride; all solvents used for reactions were distilled prior to use. All starting materials were purchased from Aldrich, Acros Organics, Alfa Aesar or Strem and used as received. Compounds **149**,<sup>397</sup> **150**,<sup>397</sup> and **151**<sup>397</sup> were prepared according to literature procedures. Flash chromatography was performed on silica gel from Fluorochem (silica gel, 40-63u, 60A). Thin-layer chromatography was carried out on Fisher aluminium-based plates with silica gel and fluorescent indicator (254 nm). Melting points were determined in open glass capillary tubes on a Stuart SMP3 melting point apparatus. <sup>1</sup>H, <sup>13</sup>C{<sup>1</sup>H}, <sup>31</sup>P{<sup>1</sup>H}, <sup>19</sup>F{<sup>1</sup>H} and <sup>11</sup>B{<sup>1</sup>H} NMR spectra were recorded on a JEOL Lambda 500 (<sup>1</sup>H 500.16 MHz) or JEOL ECS-400 (<sup>1</sup>H 399.78 MHz) spectrometer at room temperature (21 °C); <sup>1</sup>H and <sup>13</sup>C shifts were relative to tetramethylsilane, <sup>31</sup>P relative to 80% H<sub>3</sub>PO<sub>4</sub>, <sup>11</sup>B relative to BF<sub>3</sub>·Et<sub>2</sub>O and <sup>19</sup>F relative to CFCl<sub>3</sub>. Infrared spectra were recorded on a Varian 800 FT-IR spectrometer. UV-Vis absorption and emission spectra were recorded on a UV-1800 Shimadzu spectrophotometer and RF-6000 Shimadzu spectrofluorometer respectively. Mass spectrometry was carried out by the EPSRC National Mass Spectrometry Service Centre, Swansea.

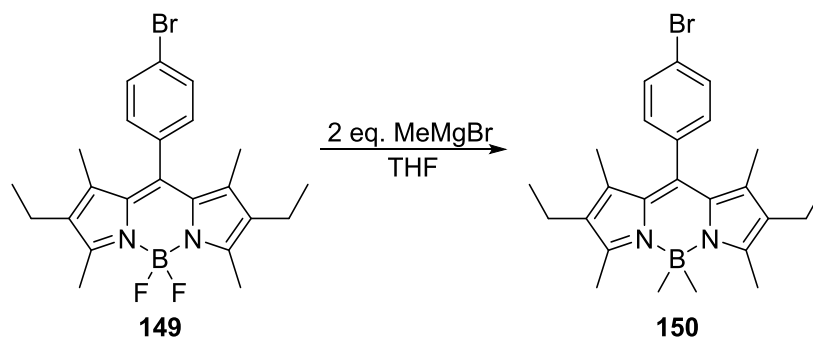
### 4.7.2 8-(4-Bromophenyl)-4,4-difluoro-1,3,5,7-tetramethyl-2,6-diethyl-4-bora-3a,4a-diaza-s-indacene **149**



TFA (3 drops) was added dropwise to a solution of 4-bromobenzaldehyde (15.0 g, 81.0 mmol) and 3-ethyl-2,4-dimethyl-1H-pyrrole (21.9 mL, 162 mmol) in anhydrous

dichloromethane (1500 mL). The reaction was stirred at room temperature under dinitrogen in a darkened flask overnight. DDQ (20.2 g, 81.0 mmol) was added in a single portion, and the reaction was stirred at room temperature for 2 hours. Anhydrous *N,N*-diisopropylethylamine (84.7 mL, 486 mmol) and  $\text{BF}_3 \cdot \text{Et}_2\text{O}$  (80.0 mL, 648 mmol) were added, and the reaction was stirred at room temperature for 4 hours. The reaction mixture was washed with water (3 x 100 mL) and brine (3 x 100 mL). The separated organic fractions were dried over magnesium sulphate, filtered and the solvent removed *in vacuo* yielding a dark-violet solid with a green tint. Purification was achieved using column chromatography on silica gel (toluene,  $R_f=0.5$ ) and afforded a purple solid (20.5 g, 55%). **MP:** 240–244 °C.  **$^1\text{H}$  NMR** (400 MHz,  $\text{CDCl}_3$ )  $\delta$  7.61 (d,  $^3J_{\text{HH}} = 8.2$  Hz, 2H), 7.16 (d,  $^3J_{\text{HH}} = 8.2$  Hz, 2H), 2.51 (s, 6H), 2.29 (q,  $^3J_{\text{HH}} = 7.8$  Hz, 4H), 1.29 (s, 6H), 0.96 (t,  $^3J_{\text{HH}} = 7.8$  Hz, 6H) ppm.  **$^{13}\text{C}\{^1\text{H}\}$  NMR** (100 MHz,  $\text{CDCl}_3$ )  $\delta$  154.7, 138.9, 138.4, 138.2, 135.4, 133.5, 132.3, 130.1, 123.4, 17.0, 14.6, 12.6, 11.9 ppm.  **$^{19}\text{F}\{^1\text{H}\}$  NMR** (376 MHz,  $\text{CDCl}_3$ )  $\delta$  -145.6 (q (equal intensity),  $^1J_{\text{FB}} = 31.8$  Hz, 2F) ppm.  **$^{11}\text{B}\{^1\text{H}\}$  NMR** (128 MHz,  $\text{CDCl}_3$ )  $\delta$  -0.2 (t,  $^1J_{\text{FB}} = 31.8$  Hz, 1B) ppm. **IR** (neat):  $\tilde{\nu} = 2971$  (w), 2901 (w), 1532 (s), 1473 (m), 1405 (s), 1316 (w), 1259 (m), 1182 (s), 1065 (m), 973 (s), 754 (s), 623 (m)  $\text{cm}^{-1}$ .

#### 4.7.3 8-(4-Bromophenyl)-4,4-dimethyl-1,3,5,7-tetramethyl-2,6-diethyl-4-bora-3a,4a-diaza-s-indacene **150**

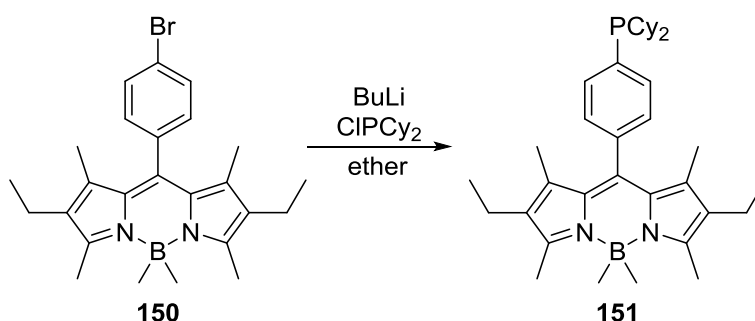


8-(4-Bromophenyl)-4,4-difluoro-1,3,5,7-tetramethyl-2,6-diethyl-4-bora-3a,4a-diaza-s-indacene (**149**) (2.50 g, 5.46 mmol) was dissolved in anhydrous tetrahydrofuran (100 mL). Methylmagnesium bromide (3.8 mL, 11.50 mmol, 3.0M solution in dibutyl ether) was added to this solution dropwise, which caused the solution to turn darker with an orange tint; the solution was stirred at room temperature until complete consumption of the starting material was observed by TLC. The reaction was quenched with water (20 mL) and the solution was extracted with dichloromethane (2 x 100 mL); the combined organic fractions were washed with water (40 mL) and brine (40 mL), and dried over magnesium



sulphate. Purification was performed by column chromatography on silica gel (petroleum ether/toluene 4:1,  $R_f = 0.6$ ) yielding an orange solid (1.00 g, 40%). **MP**: 201-204 °C.  **$^1\text{H}$  NMR** (400 MHz,  $\text{CDCl}_3$ )  $\delta$  7.60 (d,  $^3J_{\text{HH}} = 8.2$  Hz, 2H), 7.36 (d,  $^3J_{\text{HH}} = 8.2$  Hz, 2H), 2.19 (q,  $^3J_{\text{HH}} = 7.3$  Hz, 4H), 1.74 (s, 6H), 1.32 (s, 6H), 0.88 (t,  $^3J_{\text{HH}} = 7.3$  Hz, 6H), 0.22 (s, 6H) ppm.  **$^{13}\text{C}\{^1\text{H}\}$  NMR** (100 MHz,  $\text{CDCl}_3$ )  $\delta$  150.9, 138.8, 136.3, 133.6, 132.6, 132.0, 130.6, 128.8, 122.4, 17.4, 14.7, 14.3, 12.0, 10.4 (br) ppm.  **$^{11}\text{B}\{^1\text{H}\}$  NMR** (128 MHz,  $\text{CDCl}_3$ )  $\delta$  -1.2 ppm. **IR** (neat):  $\tilde{\nu} = 2960$  (w), 1548 (s), 1472 (m), 1385 (s), 1303 (w), 1169 (s), 1140 (m), 1111 (m), 968 (s), 772 (s)  $\text{cm}^{-1}$ .

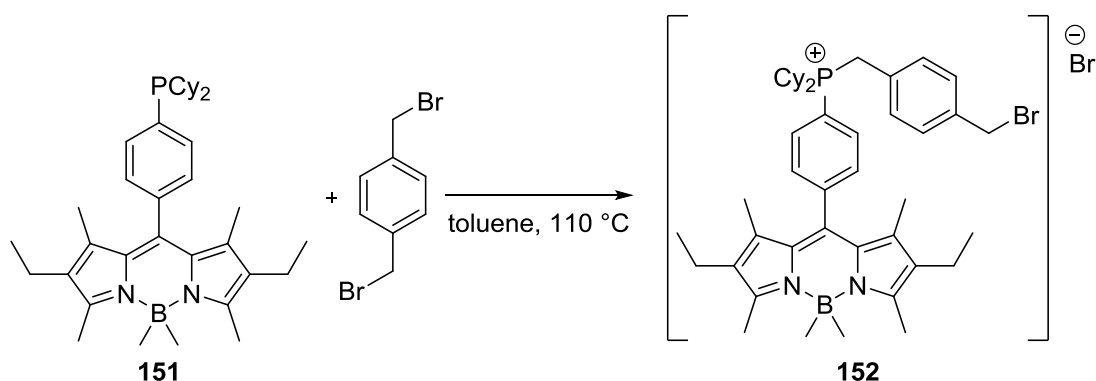
#### 4.7.4 8-((4-Dicyclohexylphosphino)phenyl)-4,4-dimethyl-1,3,5,7-tetramethyl-2,6-diethyl-4-bora-3a,4a-diaza-s-indacene **151**



8-(4-Bromophenyl)-4,4-dimethyl-1,3,5,7-tetramethyl-2,6-diethyl-4-bora-3a,4a-diaza-s-indacene (**150**) (0.50 g, 1.11 mmol) was dissolved in anhydrous diethyl ether (40 mL) and cooled to  $-78$  °C. *n*-BuLi (0.49 mL, 1.22 mmol, 2.5M in hexane) was added dropwise over five minutes and the reaction was allowed to warm to room temperature over 45 minutes. The solution was cooled back to  $-78$  °C and chlorodiphenylphosphine (0.27 mL, 1.22 mmol) was added dropwise. The reaction was allowed to warm to room temperature and was stirred overnight. The reaction mixture was washed with water and extracted with diethyl ether (3 x 30 mL). The combined organic fractions were washed with brine (30 mL) and dried over magnesium sulphate. The solvent was removed *in vacuo* yielding a red/orange solid. The compound was purified using column chromatography on silica gel (chloroform/hexane 1:4,  $R_f = 0.4$ ) and produced an orange solid (0.35 g, 60%).  **$^1\text{H}$  NMR** (400 MHz,  $\text{CDCl}_3$ )  $\delta$  7.47 (m, 2H), 7.21 (d,  $^3J_{\text{HH}} = 8.2$  Hz, 2H), 2.37 (s, 6H), 2.23 (q,  $^3J_{\text{HH}} = 7.3$  Hz, 4H), 1.90-1.56 (m, 12H), 1.36-1.22 (m, 3H), 1.19 (s, 6H), 1.12-0.95 (m, 10H), 0.90 (t,  $^3J_{\text{HH}} = 7.3$  Hz, 6H), 0.21 (s, 6H) ppm.  **$^{13}\text{C}\{^1\text{H}\}$  NMR** (100 MHz,  $\text{CDCl}_3$ )  $\delta$  150.6, 140.2, 137.9, 135.0 (d,  $J_{\text{CP}} = 19.2$  Hz), 134.7 (d,  $J_{\text{CP}} = 19.2$  Hz), 133.8, 132.5, 129.1, 128.3 (d,  $J_{\text{CP}} = 7.7$  Hz), 32.1 (d,  $J_{\text{CP}} = 12.5$  Hz), 28.7 (d,  $J_{\text{CP}} = 6.7$  Hz), 27.1 (d,  $J_{\text{CP}} = 6.7$  Hz), 26.7, 17.6, 14.8, 14.4, 11.9, 10.5 (br) ppm.  **$^{31}\text{P}\{^1\text{H}\}$  NMR** (162 MHz,  $\text{CDCl}_3$ )  $\delta$  2.8

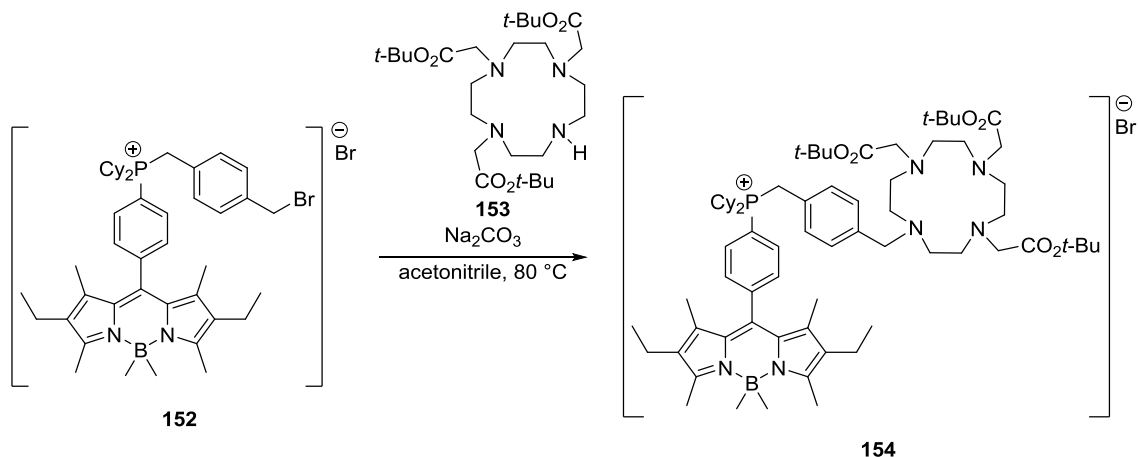
ppm.  $^{11}\text{B}\{^1\text{H}\}$  NMR (128 MHz,  $\text{CDCl}_3$ )  $\delta$  -2.1 ppm. IR (neat):  $\tilde{\nu}$  = 2927 (w), 2856 (w), 1551 (s), 1448 (m), 1321 (m), 1171 (s), 1145 (s), 946 (s)  $\text{cm}^{-1}$ . HRMS ( $\text{AP}^+$ ) calcd. for  $\text{C}_{37}\text{H}_{55}\text{B}_1\text{N}_2\text{P}_1$   $[\text{M}+\text{H}]^+$  requires  $m/z$  569.4198, found  $m/z$  568.4202 (0.1 ppm).

**4.7.5 9-(4-(Bromomethyl)benzyl)-8-((4-dicyclohexyl)phenyl)-4,4-dimethyl-1,3,5,7-tetramethyl-2,6-diethyl-4-bora-3a,4a-diaza-s-indacene phosphonium bromide 152**



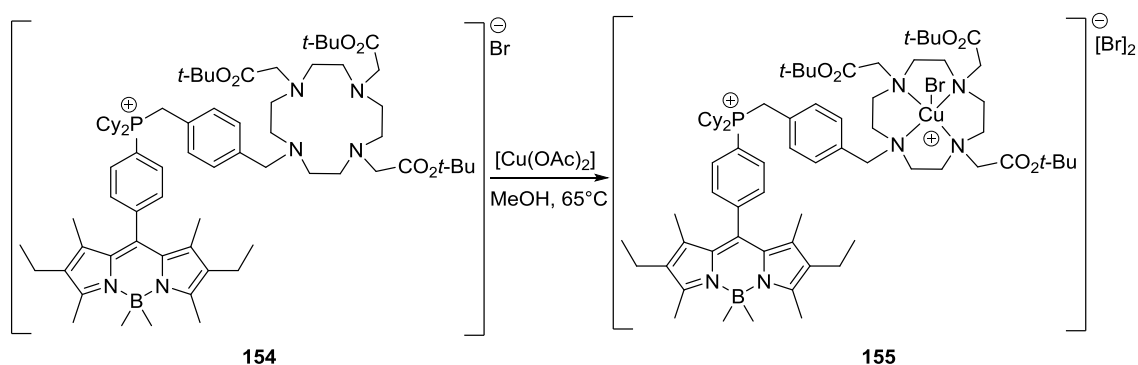
8-((4-Dicyclohexylphosphino)phenyl)-4,4-dimethyl-1,3,5,7-tetramethyl-2,6-diethyl-4-bora-3a,4a-diaza-s-indacene (**151**) (0.60 g, 1.31 mmol) was dissolved in anhydrous toluene (30 mL) and added to a stirred solution of 1,4-bis(bromomethyl)benzene (0.35 g, 1.31 mmol) in anhydrous toluene (30 mL); the resulting red solution was heated to 110 °C overnight. The reaction was monitored by  $^{31}\text{P}\{^1\text{H}\}$  NMR showing the presence of a phosphonium ion. The reaction was allowed to cool to room temperature and the solvent was removed *in vacuo*. The compound was purified using column chromatography on silica gel (chloroform/methanol 9.5:0.5,  $R_f$  = 0.6) and produced a red solid (0.61 g, 55%).  $^1\text{H}$  NMR (400 MHz,  $\text{CDCl}_3$ )  $\delta$  8.07 (m, 2H), 7.59 (d,  $^3J_{\text{HH}}$  = 8.1 Hz, 2H), 7.23 (d,  $^3J_{\text{HH}}$  = 8.1 Hz, 2H), 7.13 (d,  $^3J_{\text{HH}}$  = 8.1 Hz, 2H), 4.92 (d,  $^2J_{\text{HP}}$  = 8.1 Hz, 2H), 4.34 (s, 2H), 2.39 (s, 6H), 2.24 (q,  $^3J_{\text{HH}}$  = 7.3 Hz, 4H), 2.07-1.91 (m, 5H), 1.83-1.62 (m, 7H), 1.47-1.21 (m, 10H), 1.14 (s, 6H), 0.92 (t,  $^3J_{\text{HH}}$  = 7.3 Hz, 6H), 0.22 (s, 6H) ppm.  $^{13}\text{C}\{^1\text{H}\}$  NMR (100 MHz,  $\text{CDCl}_3$ )  $\delta$  151.6, 151.0, 143.9 (d,  $J_{\text{CP}}$  = 3.4 Hz), 138.5 (d,  $J_{\text{CP}}$  = 3.4 Hz), 137.3, 134.2 (d,  $J_{\text{CP}}$  = 8.7 Hz), 133.3, 133.1, 130.9-130.8 (overlapping signals), 129.8, 129.4, 115.6, 114.9, 32.7, 30.9, 30.5, 26.3-26.7 (overlapping signals), 25.5, 17.3, 14.5, 12.0, 10.0 (br) ppm.  $^{31}\text{P}\{^1\text{H}\}$  NMR (162 MHz,  $\text{CDCl}_3$ )  $\delta$  30.2 ppm.  $^{11}\text{B}\{^1\text{H}\}$  NMR (128 MHz,  $\text{CDCl}_3$ )  $\delta$  -1.9 ppm. IR (neat):  $\tilde{\nu}$  = 2929 (m), 2856 (m), 2360 (w), 1549 (s), 1447 (m), 1319 (s), 1171 (s), 1027 (w), 947 (s), 796 (m), 745 (s), 671 (w)  $\text{cm}^{-1}$ . HRMS ( $\text{AP}^+$ ) calcd. for  $\text{C}_{45}\text{H}_{62}\text{B}_1\text{Br}_1\text{N}_2\text{P}_1$   $[\text{M}+\text{H}]^+$  requires  $m/z$  751.3926, found  $m/z$  751.3917 (0.1 ppm).

**4.7.6 9-(4-((4,7,10-Tris(2-(*tert*-butoxy)-2-oxoethyl)-1,4,7,10-tetraazacyclododecan-1-yl)methyl)benzyl)-8-((4-dicyclohexyl)phenyl)-4,4-dimethyl-1,3,5,7-tetramethyl-2,6-diethyl-4-bora-3a,4a-diaza-s-indacene phosphonium bromide 154**



9-(4-(Bromomethyl)benzyl)-8-((4-dicyclohexyl)phenyl)-4,4-dimethyl-1,3,5,7-tetramethyl-2,6-diethyl-4-bora-3a,4a-diaza-s-indacene phosphonium bromide (**152**) (0.10 g, 0.12 mmol), tri-*tert*-butyl 1,4,7,10-tetraazacyclododecane-1,4,7-triacetate (**153**) (0.06g, 0.12 mmol) and Na<sub>2</sub>CO<sub>3</sub> (0.04 g, 0.36 mmol) were dissolved in anhydrous acetonitrile (6 mL) and the resulting red suspension was heated to 80 °C overnight. The reaction was allowed to cool to room temperature and the solvent was removed *in vacuo*. The compound was purified using column chromatography on silica gel (chloroform/methanol 9:1, *R<sub>f</sub>* = 0.3) and produced a red solid (0.09 g, 60%). <sup>1</sup>H NMR (400 MHz, CDCl<sub>3</sub>) δ 8.14 (m, 2H), 7.65 (d, <sup>3</sup>*J*<sub>HH</sub> = 8.6 Hz, 2H), 7.27 (d, <sup>3</sup>*J*<sub>HH</sub> = 7.1 Hz, 2H), 7.18 (d, <sup>3</sup>*J*<sub>HH</sub> = 7.1 Hz, 2H), 4.75 (d, <sup>2</sup>*J*<sub>HP</sub> = 13.6 Hz, 2H), 3.32-3.21 (m, 2H), 3.01-2.95 (m, 2H), 2.88 (s, 2H), 2.84 (s, 2H), 2.39 (s, 6H), 2.24 (q, <sup>3</sup>*J*<sub>HH</sub> = 7.5 Hz, 4H), 2.11-2.01 (m, 5H), 1.98-1.88 (m, 5H), 1.85-1.63 (m, 10H), 1.61-1.47 (m, 6H), 1.43 (s, 18H), 1.39 (s, 9H), 1.29-1.21 (m, 4H), 1.16 (s, 6H), 1.09-0.98 (m, 3H), 0.92 (t, <sup>3</sup>*J*<sub>HH</sub> = 7.5 Hz, 6H), 0.82-0.75 (m, 5H), 0.21 (s, 6H) ppm. <sup>13</sup>C{<sup>1</sup>H} NMR (100 MHz, CDCl<sub>3</sub>) δ 173.7, 172.6, 151.6, 144.0, 137.2, 136.5, 134.3 (d, *J*<sub>CP</sub> = 8.5 Hz), 133.2, 132.8, 131.1-130.9 (overlapping signals), 128.7 (d, *J*<sub>CP</sub> = 7.7 Hz), 128.4, 115.7, 114.9, 83.2, 82.7, 58.5, 56.8, 55.9, 50.6-49.6 (overlapping signals), 30.7, 30.2, 28.1, 28.0, 26.2, 25.7, 20.6, 19.5, 17.6, 14.9, 14.5, 12.2, 11.5, 10.5 (br) ppm. <sup>31</sup>P{<sup>1</sup>H} NMR (162 MHz, CDCl<sub>3</sub>) δ 30.3 ppm; <sup>11</sup>B{<sup>1</sup>H} NMR (128 MHz, CDCl<sub>3</sub>) δ -1.0 ppm. IR (neat):  $\tilde{\nu}$  = 2933 (m), 2860 (m), 2360 (m), 1723 (s), 1550 (m), 1163 (s), 801 (m), 751 (m), 610 (m) cm<sup>-1</sup>. HRMS (AP<sup>+</sup>) calcd. for C<sub>71</sub>H<sub>112</sub>B<sub>1</sub>N<sub>6</sub>O<sub>6</sub>P<sub>1</sub> [M+H]<sup>+</sup> requires *m/z* 593.4237, found *m/z* 593.4231 (0.4 ppm).

#### 4.7.7 [CuBr(154)][Br]<sub>2</sub> 155



9-(4-((4,7,10-Tris(2-(tert-butoxy)-2-oxoethyl)-1,4,7,10-tetraazacyclododecan-1-yl)methyl)benzyl)-8-((4-dicyclohexyl)phenyl)-4,4-dimethyl-1,3,5,7-tetramethyl-2,6-diethyl-4-bora-3a,4a-diaza-s-indacene phosphonium bromide (**154**) (0.12 g, 0.09 mmol) was dissolved in anhydrous methanol (3 mL) and added to a stirred solution of Cu(OAc)<sub>2</sub> (0.02 g, 0.09 mmol) in anhydrous methanol (3 mL). The mixture was stirred at 65 °C for 2 hours and the solvent was removed giving a dark red solid. Purification using column chromatography on silica gel (chloroform/methanol 9:1,  $R_f = 0.3$ ) yielded a red solid (0.06 g, 44%). A sample suitable for X-ray crystallographic analysis was obtained from chloroform. **IR** (neat):  $\tilde{\nu} = 2931$  (m), 2867 (m), 1732 (s), 1558 (s), 1461 (s), 1369 (m), 1322 (m), 1173 (s), 1147 (s), 982 (s), 946 (m) cm<sup>-1</sup>.

## 5 Future Work

The present work shows important developments have been made:

- In chapter 2, the synthesis of the phosphindoles **73-79** proved that it is possible to create analogues with substituents in the C3 position. It was not possible to create a fluorescent derivative using anthracene, naphthalene or benzene as substituents; therefore, it would be interesting to use either a different fluorophore or to add a linker in between the two cyclic functionalities (the phosphindole and the fluorophore). This work also proved that it is possible to add substituents to the phenyl ring of the phosphindole core. To avoid the mixture of regioisomers that was encountered, it would be prudent to use an arene like phenyl that doesn't give rise to this problem. Clearly the mechanism of this reaction – as shown by the *tolyl* derivative – is vulnerable to the generation of undesirable regioisomers.
- In chapter, the synthesis of a pyrene-functionalised tridentate ligand from an air-stable alkyl primary phosphine was described, which opens up the possibility of synthesising primary phosphines featuring different PAHs. The coordination chemistry of **109** was studied since the square planar Pt(II) complex **116** presented here has shown promising anticancer activity against bone osteosarcoma (U2OS) and transformed mammary cancer (HMLER) cells, the next step would be to compare it against similar compounds in order to explain its mechanism of action. Currently, the palladium analogue [PdCl(**109**)]Cl **120** is being tested in the same cells assays as **116** to determine if the latter's mode of action is platinum dependant. Similarly, [(Triphos)PtCl] is also being investigated to establish what role the pyrene plays in the cytotoxicity of **116**.
- Chapter 4 shows that the BODIPY-Cu(II) phosphonium complex **155**, as confirmed by X-ray crystallography was achieved. Further work on this compound wil focus on stablishing that **155** is a useful probe for cell studies by fluorescence microscopy. Studies will take place to determine if **155** localises in mitochondria. Finally, the free ligand **154** will be used to obtain the BODIPY-<sup>64</sup>Cu(II) radiotracer to facilitate imaging studies. Developments are also possible with this novel macrocyclic phosphonium ligand – it should also allow for the synthesis of complexes containing different radioactive metals such as <sup>68</sup>Ga <sup>111</sup>In, <sup>82</sup>Rb, <sup>86</sup>Y and <sup>89</sup>Zr. These metals have different radioactive devay profiles.

In general, this work has led us to synthesise and characterise molecules containing a fluorescent moiety and a second function of biological interest. The BODIPY derivatives in particular appear to be a judicious option for producing fluorescent probes due to their relatively high quantum yield. Although the pyrene derivatives were, they can interact with DNA. As such, two classes of fluorescent transition metal probes have been developed: a BODIPY-Cu(II) phosphonium complex for fluorescence and PET applications and a pyrene-derived Pt complex for DNA intercalation.

## References

1. Patel, D. V. and McGhee, C. N. J., *Clin. Experiment. Ophthalmol.*, **2007**, 35, 71-88.
2. Hoffman, A., Goetz, M., Vieth, M., Galle, P. R., Neurath, M. F. and Kiesslich, R., *Endoscopy*, **2006**, 38, 1275-1283.
3. Bewersdorf, J., Pick, R. and Hell, S. W., *Opt. Lett.*, **1998**, 23, 655-657.
4. Chalfie, M., Tu, Y., Euskirchen, G., Ward, W. W. and Prasher, D. C., *Science*, **1994**, 263, 802-805.
5. Cavanagh, H. D., Petroll, W. M. and Jester, J. V., *Neurosci. Biobehav. Rev.*, **1993**, 17, 477-482.
6. Denk, W., Strickler, J. H. and Webb, W. W., *Science*, **1990**, 248, 73-76.
7. Brynda, M., *Annu. Rep. Med. Chem.*, **2005**, 249, 2013-2034.
8. Katti, K. V., Gali, H., Smith, C. J. and Berning, D. E., *Acc. Chem. Res.*, **1999**, 32, 9-17.
9. Yoshifuji, M., Shibayama, K., Inamoto, N., Matsushita, T. and Nishimoto, K., *Acc. Chem. Res.*, **1983**, 105, 2495-2497.
10. Yoshifuji, M., Shibayama, K., Toyota, K. and Inamoto, N., *Tetrahedron Lett.*, **1983**, 24, 4227-4228.
11. Ramakrishnan, G., Jouaiti, A., Geoffroy, M. and Bernardinelli, G., *J. Phys. Chem.*, **1996**, 100, 10861-10868.
12. Henderson, W. and Alley, S. R., *J. Organomet. Chem.*, **2002**, 656, 120-128.
13. Goodwin, N., Henderson, W., Nicholson, B., Fawcett, J. and Russell, D., *J. Chem. Soc., Dalton Trans.*, **1999**, 0, 1785-1794.
14. Pillarsetty, N., Raghuraman, K., Barnes, C. L. and Katti, K. V., *Acc. Chem. Res.*, **2005**, 127, 331-336.
15. Gali, H., Karra, S. R., Reddy, V. S. and Katti, K. V., *Angew. Chem. Int. Ed.*, **1999**, 38, 2020-2023.
16. Pet, M. A., Cain, M. F., Hughes, R. P., Glueck, D. S., Golen, J. A. and Rheingold, A. L., *J. Organomet. Chem.*, **2009**, 694, 2279-2289.
17. Noble-Eddy, R., Masters, S. L., Rankin, D. W. H., Wann, D. A., Robertson, H. E., Khater, B. and Guillemin, J. C., *Inorg. Chem.*, **2009**, 48, 8603-8612.
18. Scheer, M., Kuntz, C., Stubenhofer, M., Zabel, M. and Timoshkin, A. Y., *Angew. Chem. Int. Ed.*, **2010**, 49, 188-192.
19. Bartlett, R. A., Olmstead, M. M., Power, P. P. and Sigel, G. A., *Inorg. Chem.*, **1987**, 26, 1941-1946.
20. Xie, J., Huang, J. S., Zhu, N., Zhou, Z. Y. and Che, C. M., *Chem. Eur. J.*, **2005**, 11, 2405-2416.
21. Dell'Anna, M. M., Mastrorilli, P., Nobile, C. F., Calmuschi-Cula, B., Englert, U. and Peruzzini, M., *Dalton Trans.*, **2008**, 0, 6005-6013.
22. Bender, M., Niecke, E., Nieger, M. and Pietschnig, R., *Eur. J. Inorg. Chem.*, **2006**, 2006, 380-384.
23. Naseri, V., Less, R. J., Mulvey, R. E., McPartlin, M. and Wright, D. S., *Chem. Commun.*, **2010**, 46, 5000-5002.
24. Brauer, D., Fischer, J., Kucken, S., Langhans, K., Seltzer, O. and Weferling, N., *Z. Naturforsch. B*, **1994**, 49, 1511-1512.
25. Arbuzova, S. N., Brandsma, L., Gusarova, N. K., Van Der Kerk, A. H. T. M., Van Hooijdonk, C. J. M. and Trofimov, B. A., *Synthesis*, **2000**, 2000, 65-66.
26. Reiter, S. A., Nogai, S. D. and Schmidbaur, H., *Dalton Trans.*, **2005**, 0, 247-255.
27. Smith, C. J., Redy, V. S. and Katti, K. V., *Chem. Commun.*, **1996**, 0, 2557-2558.

28. Katti, K. V., Pillarsetty, N. and Raghuraman, K., in *New Aspects in Phosphorus Chemistry III: Topics in Current Chemistry*, ed. Majoral, J. P., Springer Germany, Berlin, Germany, Editon edn., 2003, vol. 229, pp. 121-141.
29. Kothari, K. K., Gali, H., Prabhu, K. R., Pillarsetty, N., Owen, N. K., Katti, K. V., Hoffman, T. J. and Volkert, W. A., *Nucl. Med. Biol.*, **2002**, 29, 83-89.
30. Dorn, H., Singh, R. A., Massey, J. A., Lough, A. J. and Manners, I., *Angew. Chem. Int. Ed.*, **1999**, 38, 3321-3323.
31. Hanaya, T., *Bull. Chem. Soc. Jpn.*, **1989**, 62, 2320-2327.
32. Kyba, E. P., Liu, S. T. and Harris, R. L., *Organometallics*, **1983**, 2, 1877-1879.
33. Ficks, A., Hiney, R. M., Harrington, R. W., Gilheany, D. G. and Higham, L. J., *Dalton Trans.*, **2012**, 41, 3515-3522.
34. Hiney, R. M., Higham, L. J., Muller-Bunz, H. and Gilheany, D. G., *Angew. Chem. Int. Ed.*, **2006**, 45, 7248-7251.
35. Yasui, S., Tojo, S. and Majima, T., *Org. Biomol. Chem.*, **2006**, 4, 2969-2973.
36. Alfassi, Z. B., Neta, P. and Beaver, B., *J. Phys. Chem. A*, **1997**, 101, 2153-2158.
37. Stewart, B., Harriman, A. and Higham, L. J., *Organometallics*, **2011**, 30, 5338-5343.
38. Davies, L. H., Stewart, B. and Higham, L. J., in *Organometallic Chemistry: Volume 39*, eds. Fairlamb, I. J. S. and Lynam, J. M., The Royal Society of Chemistry, Croydon, UK, Editon edn., 2014, vol. 39, pp. 51-71.
39. Davies, L. H., Kasten, B. B., Benny, P. D., Arrowsmith, R. L., Ge, H., Pascu, S. I., Botchway, S. W., Clegg, W., Harrington, R. W. and Higham, L. J., *Chem. Commun.*, **2014**, 50, 15503-15505.
40. Lakowicz, J. R., *Principles of Fluorescence Spectroscopy*, 3rd edn., Springer, New York, 2006.
41. Valeur, B., *Molecular Fluorescence: Principles and Applications*, 2nd edn., Wiley-VCH, Weinheim, 2002.
42. Blacker, T. S., Mann, Z. F., Gale, J. E., Ziegler, M., Bain, A. J., Szabadkai, G. and Duchen, M. R., *Nat. Commun.*, **2014**, 5, 3936.
43. Ghisaidoobe, A. B. T. and Chung, S. J., *Int. J. Mol. Sci.*, **2014**, 15, 22518-22538.
44. Zhu, X.-G., Govindjee, Baker, N. R., Sturler, E., Ort, D. R. and Long, S. P., *Planta*, **2005**, 223, 114-133.
45. Roger, Y. T., *Annu. Rev. Biochem.*, **1998**, 67, 509-544.
46. Lakowicz, J. R. and Weber, G., *Biochemistry*, **1973**, 12, 4161-4170.
47. Birks, J. B., *Rep. Prog. Phys.*, **1975**, 38, 903.
48. Birks, J. B., *Nature*, **1967**, 214, 1187-1190.
49. De Silva, A. P., Gunaratne, H. Q. N., Gunnlaugsson, T., Huxley, A. J. M., McCoy, C. P., Rademacher, J. T. and Rice, T. E., *Chem. Rev.*, **1997**, 97, 1515-1566.
50. Tanaka, K., Miura, T., Umezawa, N., Urano, Y., Kikuchi, K., Higuchi, T. and Nagano, T., *Acc. Chem. Res.*, **2001**, 123, 2530-2536.
51. Ueno, T., Urano, Y., Setsukinai, K., Takakusa, H., Kojima, H., Kikuchi, K., Ohkubo, K., Fukuzumi, S. and Nagano, T., *Acc. Chem. Res.*, **2004**, 126, 14079-14085.
52. Sunahara, H., Urano, Y., Kojima, H. and Nagano, T., *Acc. Chem. Res.*, **2007**, 129, 5597-5604.
53. Murphy, C. B., Zhang, Y., Troxler, T., Ferry, V., Martin, J. J. and Jones, W. E., *J. Phys. Chem. B*, **2004**, 108, 1537-1543.
54. Adronov, A. and Frechet, J. M. J., *Chem. Commun.*, **2000**, 0, 1701-1710.



55. Wan, C. W., Burghart, A., Chen, J., Bergström, F., Johansson, L. B. Å., Wolford, M. F., Kim, T. G., Topp, M. R., Hochstrasser, R. M. and Burgess, K., *Chem. Eur. J.*, **2003**, 9, 4430-4441.
56. Jiao, G. S., Thoresen, L. H. and Burgess, K., *Acc. Chem. Res.*, **2003**, 125, 14668-14669.
57. Hückel, E., *Z. Phys.*, **1931**, 70, 204-286.
58. Roberts, J. D., Streitwieser, A. and Regan, C. M., *Acc. Chem. Res.*, **1952**, 74, 4579-4582.
59. Portella, G., Poater, J. and Solà, M., *J. Phys. Org. Chem.*, **2005**, 18, 785-791.
60. Kim, K. H., Jahan, S. A., Kabir, E. and Brown, R. J. C., *Environ. Int.*, **2013**, 60, 71-80.
61. Ravindra, K., Sokhi, R. and Van Grieken, R., *Atmos. Environ.*, **2008**, 42, 2895-2921.
62. Loeb, L. A. and Harris, C. C., *Cancer Res.*, **2008**, 68, 6863-6872.
63. Baird, W. M., Hooven, L. A. and Mahadevan, B., *Environ. Mol. Mutagen.*, **2005**, 45, 106-114.
64. Slaga, T. J., *Acta Pharmacol. Toxicol.*, **1984**, 55, 107-124.
65. Xue, W. and Warshawsky, D., *Toxicol. Appl. Pharmacol.*, **2005**, 206, 73-93.
66. Kelsell, D. P., Dunlop, J. and Hodgins, M. B., *Trends. Cell. Biol.*, **2001**, 11, 2-6.
67. Aramandla, R., Stormy, A. W., Darryl, B. H., Maria, D. G., Klaus, S. and Eric, H. W., *Int. J. Toxicol.*, **2004**, 23, 301-333.
68. Agarwal, S. K., Sayer, J. M., Yeh, H. J. C., Pannell, L. K., Hilton, B. D., Pigott, M. A., Dipple, A., Yagi, H. and Jerina, D. M., *Acc. Chem. Res.*, **1987**, 109, 2497-2504.
69. Cosman, M., Fiala, R., Hingerty, B. E., Laryea, A., Lee, H., Harvey, R. G., Amin, S., Geacintov, N. E., Broyde, S. and Patel, D., *Biochemistry*, **1993**, 32, 12488-12497.
70. Furst, M. and Kallmann, H., *Phys. Rev.*, **1955**, 97, 583-587.
71. Hell, S. W., Lindek, S., Cremer, C. and Stelzer, E. H. K., *Opt. Lett.*, **1994**, 19, 222-224.
72. Dammers De Klerk, A., *Mol. Phys.*, **1958**, 1, 141-150.
73. Ma, Q., Xu, J., Zhang, X., Zhou, L., Liu, H. and Zhang, J., *Sens. Actuators B Chem.*, **2016**, 229, 434-440.
74. Zhou, X. H., Jiang, Y. R., Zhao, X. J. and Guo, D., *Talanta*, **2016**, 160, 470-474.
75. Mao, G. J., Wei, T. T., Wang, X. X., Huan, S. Y., Lu, D. Q., Zhang, J., Zhang, X. B., Tan, W., Shen, G. L. and Yu, R. Q., *Anal. Chem.*, **2013**, 85, 7875-7881.
76. Stryer, L., *J. Mol. Biol.*, **1965**, 13, 482-495.
77. Sarkar, A. R., Kang, D. E., Kim, H. M. and Cho, B. R., *Inorg. Chem.*, **2014**, 53, 1794-1803.
78. Masanta, G., Lim, C. S., Kim, H. J., Han, J. H., Kim, H. M. and Cho, B. R., *Acc. Chem. Res.*, **2011**, 133, 5698-5700.
79. Paul, B. D. and Snyder, S. H., *Nat. Rev. Mol. Cell Biol.*, **2012**, 13, 499-507.
80. Lefer, D. J., *Proc. Natl. Acad. Sci. U.S.A.*, **2007**, 104, 17907-17908.
81. Ishikawa, J., Sakamoto, H., Nakao, S. and Wada, H., *J. Org. Chem.*, **1999**, 64, 1913-1921.
82. Wang, W., Gao, S. and Wang, B., *Org. Lett.*, **1999**, 1, 1209-1212.
83. Berlman, I., *Handbook of Florescence Spectra of Aromatic Molecules*, 2nd edn., Elsevier, New York, U. S. A., 1971.
84. Sissi, C., Bolgan, L., Moro, S., Zagotto, G., Bailly, C., Menta, E., Capranico, G. and Palumbo, M., *Mol. Pharmacol.*, **1998**, 54, 1036-1045.

85. Quigley, G. J., Wang, A. H., Ughetto, G., Van Der Marel, G., Van Boom, J. H. and Rich, A., *Proc. Natl. Acad. Sci. U.S.A.*, **1980**, 77, 7204-7208.
86. Tacar, O., Sriamornsak, P. and Dass, C. R., *J. Pharm. Pharmacol.*, **2013**, 65, 157-170.
87. Saito, Y., Motegi, K., Bag, S. S. and Saito, I., *Bioorganic. Med. Chem.*, **2008**, 16, 107-113.
88. Ostaszewski, R., Wilczyńska, E. and Wolszczak, M., *Bioorganic. Med. Chem. Lett.*, **1998**, 8, 2995-2996.
89. Wu, X. and Shi, G., *J. Mater. Chem.*, **2005**, 15, 1833-1837.
90. Winnik, F. M., *Chem. Rev.*, **1993**, 93, 587-614.
91. Okamoto, A., Kanatani, K. and Saito, I., *Acc. Chem. Res.*, **2004**, 126, 4820-4827.
92. Telsler, J., Cruickshank, K. A., Morrison, L. E. and Netzel, T. L., *Acc. Chem. Res.*, **1989**, 111, 6966-6976.
93. Mann, J. S., Shibata, Y. and Meehan, T., *Bioconjug. Chem.*, **1992**, 3, 554-558.
94. Kierzek, R., Li, Y., Turner, D. H. and Bevilacqua, P. C., *Acc. Chem. Res.*, **1993**, 115, 4985-4992.
95. Casas-Solvas, J. M., Howgego, J. D. and Davis, A. P., *Org. Biomol. Chem.*, **2014**, 12, 212-232.
96. Pommier, Y., *ACS Chem. Biol.*, **2013**, 8, 82-95.
97. James, J. C., *Annu. Rev. Biochem.*, **2001**, 70, 369-413.
98. Binaschi, M., Zunino, F. and Capranico, G., *Stem Cells*, **1995**, 13, 369-379.
99. Mitscher, L. A., *Chem. Rev.*, **2005**, 105, 559-592.
100. Nitiss, J. L., *Nat. Rev. Cancer*, **2009**, 9, 338-350.
101. Wittig, G. and Schöllkopf, U., *Chem. Ber.*, **1954**, 87, 1318-1330.
102. Murphy, M. P., *Biochim. Biophys. Acta*, **2008**, 1777, 1028-1031.
103. Modica-Napolitano, J. S. and Aprille, J. R., *Cancer Res.*, **1987**, 47, 4361-4365.
104. Yeo, H. M., Ryu, B. J. and Nam, K. C., *Org. Lett.*, **2008**, 10, 2931-2934.
105. Yamaguchi, S., Akiyama, S. and Tamao, K., *J. Organomet. Chem.*, **2002**, 646, 277-281.
106. Real Oliveira, M. E. C. D., Baptista, A. L. F., Coutinho, P. J. G., Castanheira, E. M. S. and Hungerford, G., *Photochem. Photobiol. Sci.*, **2004**, 3, 217-225.
107. Nigam, S., Burke, B. P., Davies, L. H., Domarkas, J., Wallis, J. F., Waddell, P. G., Waby, J. S., Benoit, D. M., Seymour, A. M., Cawthorne, C., Higham, L. J. and Archibald, S. J., *Chem. Commun.*, **2016**, 52, 7114-7117.
108. Loudet, A. and Burgess, K., *Chem. Rev.*, **2007**, 107, 4891-4932.
109. Ulrich, G., Ziessel, R. and Harriman, A., *Angew. Chem. Int. Ed.*, **2008**, 47, 1184-1201.
110. Ziessel, R., Ulrich, G. and Harriman, A., *New J. Chem.*, **2007**, 31, 496-501.
111. Nakanishi, J., Nakajima, T., Sato, M., Ozawa, T., Tohda, K. and Umezawa, Y., *Anal. Chem.*, **2001**, 73, 2920-2928.
112. De Wael, E. V., Pardoën, J. A., Van Koeveringe, J. A. and Lugtenburg, J., *Rec. Trav. Chim. Pays Bas*, **1977**, 96, 306-309.
113. Gómez-Infante, A., Bañuelos, J., Valois-Escamilla, I., Cruz-Cruz, D., Prieto-Montero, R., López-Arbeloa, I., Arbeloa, T. and Peña-Cabrera, E., *Eur. J. Org. Chem.*, **2016**, 2016, 5009-5023.
114. Zhang, X. and Zhang, H. S., *Spectrochim. Acta A*, **2005**, 61, 1045-1049.
115. Zhang, X., Wang, H., Li, J. S. and Zhang, H. S., *Anal. Chim. Acta*, **2003**, 481, 101-108.
116. Oleynik, P., Ishihara, Y. and Cosa, G., *Acc. Chem. Res.*, **2007**, 129, 1842-1843.
117. Baki, C. N. and Akkaya, E. U., *J. Org. Chem.*, **2001**, 66, 1512-1513.

118. Qi, X., Jun, E. J., Xu, L., Kim, S. J., Joong Hong, J. S., Yoon, Y. J. and Yoon, J., *J. Org. Chem.*, **2006**, 71, 2881-2884.
119. Di Cesare, N. and Lakowicz, J. R., *Tetrahedron Lett.*, **2001**, 42, 9105-9108.
120. Lim, S. G. and Blum, S. A., *Organometallics*, **2009**, 28, 4643-4645.
121. Inoue, N., Suzuki, Y., Yokoyama, K. and Karube, I., *Biosci. Biotechnol. Biochem.*, **2009**, 73, 1215-1217.
122. Tasan, S., Zava, O., Bertrand, B., Bernhard, C., Goze, C., Picquet, M., Le Gendre, P., Harvey, P., Denat, F., Casini, A. and Bodio, E., *Dalton Trans.*, **2013**, 42, 6102-6109.
123. Lifschitz, A. M., Shade, C. M., Spokoyny, A. M., Mendez-Arroyo, J., Stern, C. L., Sarjeant, A. A. and Mirkin, C. A., *Inorg. Chem.*, **2013**, 52, 5484-5492.
124. Soh, N., Sakawaki, O., Makihara, K., Odo, Y., Fukaminato, T., Kawai, T., Irie, M. and Imato, T., *Bioorganic Med. Chem.*, **2005**, 13, 1131-1139.
125. Onoda, M., Uchiyama, S., Endo, A., Tokuyama, H., Santa, T. and Imai, K., *Org. Lett.*, **2003**, 5, 1459-1461.
126. Löber, G., *J. Lumin.*, **1981**, 22, 221-265.
127. Georghiou, S., *Photochem. Photobiol.*, **1977**, 26, 59-68.
128. Suh, D. and Chaires, J. B., *Bioorganic Med. Chem.*, **1995**, 3, 723-728.
129. Richards, A. D. and Rodger, A., *Chem. Soc. Rev.*, **2007**, 36, 471-483.
130. Tse, W. C. and Boger, D. L., *Acc. Chem. Res.*, **2004**, 37, 61-69.
131. Leprat, P., Ratinaud, M. H., Maftah, A., Petit, J. M. and Julien, R., *Exp. Cell Res.*, **1990**, 186, 130-137.
132. Nafisi, S., Saboury, A. A., Keramat, N., Neault, J. F. and Tajmir-Riahi, H. A., *J. Mol. Struct.*, **2007**, 827, 35-43.
133. Rescifina, A., Zagni, C., Varrica, M. G., Pistarà, V. and Corsaro, A., *Eur. J. Med. Chem.*, **2014**, 74, 95-115.
134. Pasternack, R. F. and Gibbs, E. J., in *ACS Symposium Series*, ed. Tullius, T. D., ACS Publications, Washington, U. S. A., Editon edn., 1989, vol. 402, pp. 59-73.
135. Chaires, J. B., *Curr. Opin. Struct. Biol.*, **1998**, 8, 314-320.
136. Rosenberg, B., Vancamp, L., Trosko, J. E. and Mansour, V. H., *Nature*, **1969**, 222, 385-386.
137. Pimlott, S. L. and Sutherland, A., *Chem. Soc. Rev.*, **2011**, 40, 149-162.
138. Ido, T., Wan, C. N., Casella, V., Fowler, J. S., Wolf, A. P., Reivich, M. and Kuhl, D. E., *J. Label. Compd. Radiopharm.*, **1978**, 14, 175-183.
139. Vasdev, N., Chio, J., van Oosten, E. M., Nitz, M., McLaurin, J., Vines, D. C., Houle, S., Reilly, R. M. and Wilson, A. A., *Chem. Commun.*, **2009**, 0, 5527-5529.
140. Wadas, T. J., Wong, E. H., Weisman, G. R. and Anderson, C. J., *Chem. Rev.*, **2010**, 110, 2858-2902.
141. Guiyang, H., Ajay, N. S., Orhan, K. O. and Xiankai, S., *Curr. Radiopharm.*, **2011**, 4, 109-121.
142. Smith, S. V., *J. Inorg. Biochem.*, **2004**, 98, 1874-1901.
143. Haynes, N. G., Lacy, J. L., Nayak, N., Martin, C. S., Dai, D., Mathias, C. J. and Green, M. A., *J. Nucl. Med.*, **2000**, 41, 309-314.
144. Zweit, J., Goodall, R., Cox, M., Babich, J. W., Potter, G. A., Sharma, H. L. and Ott, R. J., *Eur. J. Nucl. Med.*, **1992**, 19, 418-425.
145. Obata, A., Kasamatsu, S., McCarthy, D. W., Welch, M. J., Saji, H., Yonekura, Y. and Fujibayashi, Y., *Nucl. Med. Biol.*, **2003**, 30, 535-539.
146. Kobayashi, M., Mori, T., Tsujikawa, T., Ogai, K., Sugama, J., Kiyono, Y., Kawai, K. and Okazawa, H., *Hell. J. Nucl. Med.*, **2015**, 18, 103-107.

147. Ruangma, A., Bai, B., Lewis, J. S., Sun, X., Welch, M. J., Leahy, R. and Laforest, R., *Nucl. Med. Biol.*, **2006**, 33, 217-226.
148. Schmidt, A., Habeck, T., Kindermann, M. K. and Nieger, M., *J. Org. Chem.*, **2003**, 68, 5977-5982.
149. Andreas, S., *Curr. Org. Chem.*, **2004**, 8, 653-670.
150. Cerecetto, H., Gerpe, A., Gonzalez, M., Aran, V. J. and Ocariz, C., *Mini. Rev. Med. Chem.*, **2005**, 5, 869-878.
151. Jennings, A. and Tennant, M., *J. Chem. Inf. Model.*, **2007**, 47, 1829-1838.
152. Hartmann, M., Sommer, M. E., Keppler, B. K., Kratz, F. and Einhäuser, T. J., *J. Inorg. Biochem.*, **1995**, 59, 214.
153. Raffa, D., Daidone, G., Plescia, F., Schillaci, D., Maggio, B. and Torta, L., *Farmaco*, **2002**, 57, 183-187.
154. Grundt, P., Jane Husband, S. L., Luedtke, R. R., Taylor, M. and Newman, A. H., *Bioorganic Med. Chem. Lett.*, **2007**, 17, 745-749.
155. Southan, G. J. and Szabó, C., *Biochem. Pharmacol.*, **1996**, 51, 383-394.
156. Schulz, J. B., Matthews, R. T., Klockgether, T., Dichgans, J. and Beal, M. F., *Mol. Cell. Biochem.*, **1997**, 174, 193-197.
157. Billio, A., Morello, E. and Clarke, M. J., *Cochrane Database Syst. Rev.*, **2010**, 1, 1-2.
158. Sakaguchi, J., Iwasaki, N., Iwanaga, Y., Saito, T., Takahara, E., Kato, H. and Hanaoka, M., *Chem. Pharm. Bull.*, **2001**, 49, 424-436.
159. Harrison, R. G. and O'Donnell, P. J., *Toxicol. Appl. Pharmacol.*, **1970**, 17, 355-360.
160. Pan, S. L., Guh, J. H., Peng, C. Y., Wang, S. W., Chang, Y. L., Cheng, F. C., Chang, J. H., Kuo, S. C., Lee, F. Y. and Teng, C. M., *J. Pharmacol. Exp. Ther.*, **2005**, 314, 35-42.
161. Gavriluta, A., Büchel, G. E., Freitag, L., Novitchi, G., Tommasino, J. B., Jeanneau, E., Kuhn, P. S., González, L., Arion, V. B. and Luneau, D., *Inorg. Chem.*, **2013**, 52, 6260-6272.
162. Zhang, J., Yang, Q., Romero, J. A. C., Cross, J., Wang, B., Poutsiaka, K. M., Epie, F., Bevan, D., Wu, Y., Moy, T., Daniel, A., Chamberlain, B., Carter, N., Shotwell, J., Arya, A., Kumar, V., Silverman, J., Nguyen, K., Metcalf, C. A., Ryan, D., Lippa, B. and Dolle, R. E., *ACS Med. Chem. Lett.*, **2015**, 6, 1080-1085.
163. Souers, A. J., Gao, J., Brune, M., Bush, E., Wodka, D., Vasudevan, A., Judd, A. S., Mulhern, M., Brodjian, S., Dayton, B., Shapiro, R., Hernandez, L. E., Marsh, K. C., Sham, H. L., Collins, C. A. and Kym, P. R., *J. Med. Chem.*, **2005**, 48, 1318-1321.
164. Crestey, F., Collot, V., Stiebing, S. and Rault, S., *Tetrahedron*, **2006**, 62, 7772-7775.
165. Duan, J. X., Cai, X., Meng, F., Lan, L., Hart, C. and Matteucci, M., *J. Med. Chem.*, **2007**, 50, 1001-1006.
166. Fedenok, L. G. and Zolnikova, N. A., *Tetrahedron Lett.*, **2003**, 44, 5453-5455.
167. Fedenok, L. G., Barabanov, I. I., Bashurova, V. S. and Bogdanchikov, G. A., *Tetrahedron*, **2004**, 60, 2137-2145.
168. Shvartsberg, M. S., Ivanchikova, I. D. and Fedenok, L. G., *Tetrahedron Lett.*, **1994**, 35, 6749-6752.
169. Yakaiah, T., Lingaiah, B. P. V., Narsaiah, B., Shireesha, B., Ashok Kumar, B., Gururaj, S., Parthasarathy, T. and Sridhar, B., *Bioorganic Med. Chem. Lett.*, **2007**, 17, 3445-3453.

170. Jones, P., Altamura, S., Boueres, J., Ferrigno, F., Fonsi, M., Giomini, C., Lamartina, S., Monteagudo, E., Ontoria, J. M., Orsale, M. V., Palumbi, M. C., Pesci, S., Roscilli, G., Scarpelli, R., Schultz-Fademrecht, C., Toniatti, C. and Rowley, M., *J. Med. Chem.*, **2009**, 52, 7170-7185.
171. Makhluif, J. H., Wayne, E. C. and Mark, J. K., *Mini. Rev. Med. Chem.*, **2012**, 12, 1293-1300.
172. Avila, B., El-Dakdouki, M. H., Nazer, M. Z., Harrison, J. G., Tantillo, D. J., Haddadin, M. J. and Kurth, M. J., *Tetrahedron Lett.*, **2012**, 53, 6475-6478.
173. Okiyoneda, T., Veit, G., Dekkers, J. F., Bagdany, M., Soya, N., Xu, H., Roldan, A., Verkman, A. S., Kurth, M., Simon, A., Hegedus, T., Beekman, J. M. and Lukacs, G. L., *Nat. Chem. Biol.*, **2013**, 9, 1-27.
174. Farber, K. M., Haddadin, M. J. and Kurth, M. J., *J. Org. Chem.*, **2014**, 79, 6939-6945.
175. Hughes, A. N. and Srivanavit, C., *J. Heterocyclic Chem.*, **1970**, 7, 1-24.
176. Romero-Nieto, C., Merino, S., Rodríguez-López, J. and Baumgartner, T., *Chem. Eur. J.*, **2009**, 15, 4135-4145.
177. Giannousis, P. P. and Bartlett, P. A., *J. Med. Chem.*, **1987**, 30, 1603-1609.
178. Cadierno, V., Donnadiou, B., Igau, A. and Majoral, J. P., *Eur. J. Inorg. Chem.*, **2000**, 2000, 417-421.
179. Samuel, E. and Rausch, M. D., *Acc. Chem. Res.*, **1973**, 95, 6263-6267.
180. Pellissier, H. and Santelli, M., *Tetrahedron*, **2003**, 59, 701-730.
181. Medina, J. M., Mackey, J. L., Garg, N. K. and Houk, K. N., *Acc. Chem. Res.*, **2014**, 136, 15798-15805.
182. Kornev, A. N., Sushev, V. V., Panova, Y. S., Zolotareva, N. V., Baranov, E. V., Fukin, G. K. and Abakumov, G. A., *Eur. J. Inorg. Chem.*, **2015**, 2015, 2057-2066.
183. Kornev, A. N., Galperin, V. E., Sushev, V. V., Zolotareva, N. V., Baranov, E. V., Fukin, G. K. and Abakumov, G. A., *Eur. J. Inorg. Chem.*, **2016**, 2016, 3629-3633.
184. Kabra, V., Kaushik, P. and Ojha, S., *Phosphorus Sulfur Silicon Relat. Elem.*, **2007**, 182, 1093-1102.
185. Pople, J. A. and Santry, D. P., *Mol. Phys.*, **1964**, 8, 1-18.
186. Tolman, C. A., *Chem. Rev.*, **1977**, 77, 313-348.
187. Allen, D. W. and Taylor, B. F., *J. Chem. Soc., Dalton Trans.*, **1982**, 0, 51-54.
188. Ficks, A., Clegg, W., Harrington, R. W. and Higham, L. J., *Organometallics*, **2014**, 33, 6319-6329.
189. Senn, H. M., Deubel, D. V., Blöchl, P. E., Togni, A. and Frenking, G., *J. Mol. Struct.*, **2000**, 506, 233-242.
190. Fey, N., Tsipis, A. C., Harris, S. E., Harvey, J. N., Orpen, A. G. and Mansson, R. A., *Chem. Eur. J.*, **2006**, 12, 291-302.
191. Schmied, A., Straube, A., Grell, T., Jahnigen, S. and Hey-Hawkins, E., *Dalton Trans.*, **2015**, 44, 18760-18768.
192. Aladzheva, I. M., Bykhovskaya, O. V., Nelyubina, Y. V., Klemenkova, Z. S., Artyushin, O. I., Petrovskii, P. V., Vasil'ev, A. A. and Odinet, I. L., *Inorg. Chim. Acta*, **2013**, 395, 203-211.
193. Gampe, C. M. and Carreira, E. M., *Angew. Chem. Int. Ed.*, **2012**, 51, 3766-3778.
194. Yoshida, H., Morishita, T. and Ohshita, J., *Chem. Lett.*, **2010**, 39, 508-509.
195. Bronner, S. M., Bahnck, K. B. and Garg, N. K., *Org. Lett.*, **2009**, 11, 1007-1010.
196. Cheong, P. H. Y., Paton, R. S., Bronner, S. M., Im, G. Y. J., Garg, N. K. and Houk, K. N., *Acc. Chem. Res.*, **2010**, 132, 1267-1269.
197. Hüp, S., Szarvas, L., Nieger, M. and Gudat, D., *Eur. J. Inorg. Chem.*, **2001**, 2001, 2763-2772.

198. Brisdon, A. K., Ali Ghaba, H., Beutel, B., Egjandi, A., Addaraidi, A. and Pritchard, R. G., *Dalton Trans.*, **2015**, 44, 19717-19731.
199. Elder, P. J. W., Chivers, T. and Thirumoorthi, R., *Eur. J. Inorg. Chem.*, **2013**, 2013, 2867-2876.
200. Iijima, S., Nakashima, T. and Kawai, T., *New J. Chem*, **2016**, 40, 10048-10055.
201. Kumaravel, M., Mague, J. T. and Balakrishna, M. S., *Tetrahedron Lett.*, **2014**, 55, 2957-2961.
202. Higashino, T., Yamada, T., Sakurai, T., Seki, S. and Imahori, H., *Angew. Chem. Int. Ed.*, **2016**, 55, 12311-12315.
203. Coogan, M. P. and Harger, M. J. P., *J. Chem. Soc. Chem. Commun.*, **1990**, 0, 1745-1746.
204. Harger, M. J. P., *J. Chem. Soc. Perkin Trans. 2*, **1991**, 0, 1057-1061.
205. Harger, M. J. P., *Chem. Commun.*, **1998**, 0, 2339-2340.
206. Gholivand, K., Mojahed, F., Salehi, M., Naderi-Manesh, H. and Khajeh, K., *J. Enzyme Inhib. Med. Chem.*, **2006**, 21, 521-525.
207. Magde, D., Rojas, G. E. and Seybold, P. G., *J. Photochem. Photobiol.*, **1999**, 70, 737-744.
208. Mataga, N., Kaifu, Y. and Koizumi, M., *Bull. Chem. Soc. Jpn.*, **1956**, 29, 465-470.
209. Appenroth, K., Reichenbacher, M. and Paetzold, R., *J. Photochem. Photobiol.*, **1980**, 14, 39-50.
210. James, T. D., Samankumara-Sandanayake, K. R. A. and Shinkai, S., *Nature*, **1995**, 374, 345-347.
211. Ghosh, K., Masanta, G. and Chattopadhyay, A. P., *J. Photochem. Photobiol. A Chem.*, **2009**, 203, 40-49.
212. Gunnlaugsson, T., Davis, A. P., Hussey, G. M., Tierney, J. and Glynn, M., *Org. Biomol. Chem.*, **2004**, 2, 1856-1863.
213. Wei, P., Li, D., Shi, B., Wang, Q. and Huang, F., *Chem. Commun.*, **2015**, 51, 15169-15172.
214. Zhou, Y., Dong, X., Zhang, Y., Tong, P. and Qu, J., *Dalton Trans.*, **2016**, 45, 6839-6846.
215. Basheer, S. M., Willis, A. C., Pace, R. J. and Sreekanth, A., *Polyhedron*, **2016**, 109, 7-18.
216. Jiang, X. K., Ikejiri, Y., Jin, C. C., Wu, C., Zhao, J. L., Ni, X. L., Zeng, X., Redshaw, C. and Yamato, T., *Tetrahedron*, **2016**, 72, 4854-4858.
217. Anand, T., Sivaraman, G., Iniya, M., Siva, A. and Chellappa, D., *Anal. Chim. Acta*, **2015**, 876, 1-8.
218. Erdemir, S. and Kocyigit, O., *Talanta*, **2016**, 158, 63-69.
219. Maimone, T. J. and Buchwald, S. L., *Acc. Chem. Res.*, **2010**, 132, 9990-9991.
220. Witebsky, F. G., Maclowry, J. D. and French, S. S., *J. Clin. Microbiol.*, **1979**, 9, 589-595.
221. Lancefield, R. C., *J. Exp. Med.*, **1928**, 47, 91-103.
222. Camara, M., Dieng, A. and Boye, C. S. B., *Microbiol. Insights*, **2013**, 6, 71-75.
223. Emadi, A., Jones, R. J. and Brodsky, R. A., *Nat. Rev. Clin. Oncol.*, **2009**, 6, 638-647.
224. Thoen, K. K. and Kenttämää, H. I., *Acc. Chem. Res.*, **1999**, 121, 800-805.
225. Davies, L. H., Stewart, B., Harrington, R. W., Clegg, W. and Higham, L. J., *Angew. Chem. Int. Ed.*, **2012**, 51, 4921-4924.
226. Nyulászi, L., Szieberth, D., Csonka, G. I., Reffy, J., Heinicke, J. and Veszpremi, T., *Struct. Chem.*, **1995**, 6, 1-7.
227. Jiao, X. Y. and Bentrude, W. G., *J. Org. Chem.*, **2003**, 68, 3303-3306.

228. Davies, L. H., Wallis, J. F., Probert, M. R. and Higham, L. J., *Synthesis*, **2014**, 46, 2622-2628.
229. Vilela, S. M. F., Fernandes, J. A., Ananias, D., Carlos, L. D., Rocha, J., Tome, J. P. C. and Almeida Paz, F. A., *CrystEngComm*, **2014**, 16, 344-358.
230. Michaelis, A. and Kaehne, R., *Ber. Dtsch. Chem. Ges.*, **1898**, 31, 1048-1055.
231. Roberts, J. D., Weigert, F. J., Kroschwitz, J. I. and Reich, H. J., *Acc. Chem. Res.*, **1970**, 92, 1338-1347.
232. Bottin-Strzalko, T., Corset, J., Froment, F., Pouet, M. J., Seyden-Penne, J. and Simonnin, M. P., *J. Org. Chem.*, **1980**, 45, 1270-1276.
233. Ficks, A., Sibbald, C., Ojo, S., Harrington, R. W., Clegg, W. and Higham, L. J., *Synthesis (Stuttg.)*, **2013**, 45, 265-271.
234. Nandy, R., Subramoni, M., Varghese, B. and Sankararaman, S., *J. Org. Chem.*, **2007**, 72, 938-944.
235. Iyer, V. M., Stoeckli-Evans, H., D'Aleo, A., Cola, L. D. and Belser, P., *Acta Crystallogr. C*, **2005**, 61, o259-o261.
236. Tribak, Z., Kandri Rodi, Y., Haoudi, A., Essassi, E. M., Capet, F. and Zouihri, H., *IUCrData*, **2016**, 1, x160971.
237. Lee, R., Mason, S. A., Mossou, E., Lamming, G., Probert, M. R. and Steed, J. W., *Cryst. Growth Des.*, **2016**, 16, 7175-7185.
238. Seebach, D., Schaeffer, L., Gessier, F., Bindschädler, P., Jäger, C., Josien, D., Kopp, S., Lelais, G., Mahajan, Y. R., Micuch, P., Sebesta, R. and Schweizer, B. W., *Helv. Chim. Acta*, **2003**, 86, 1852-1861.
239. Larsson, K., *Acta Crystallogr.*, **1966**, 21, 267-272.
240. Kharbach, Y., Kandri Rodi, Y., Haoudi, A., Essassi, E. M., Capet, F. and Zouihri, H., *IUCrData*, **2016**, 1, x160883.
241. Rosen, L. S. and Hybl, A., *Acta Crystallogr. B*, **1972**, 28, 610-617.
242. Zhang, X. Y., Liu, B. N., Wang, P. B. and Liu, D. K., *Acta Crystallogr. E*, **2014**, 70, o1118-o1119.
243. Byrd, H., Clearfield, A., Poojary, D., Reis, K. P. and Thompson, M. E., *Chem. Mater.*, **1996**, 8, 2239-2246.
244. Khrustalev, V. N., Nayani, S. L., Leonova, E. S., Puntus, L. N., Summeth, D. M., Makarov, M. V., Odinets, I. L. and Timofeeva, T. V., *J. Mol. Struct.*, **2013**, 1043, 68-74.
245. Kurz, T., Geffken, D. and Widyan, K., *Tetrahedron*, **2004**, 60, 2409-2416.
246. Glasneck, F., Kobalz, K. and Kersting, B., *Eur. J. Inorg. Chem.*, **2016**, 2016, 3111-3122.
247. Ng, S. W. and Kumar Das, V. G., *Acta Crystallogr. C*, **1996**, 52, 1373-1375.
248. Salin, A. V., Il'in, A. V., Shamsutdinova, F. G., Fatkhutdinov, A. R., Galkin, V. I., Islamov, D. R. and Kataeva, O. N., *Tetrahedron Lett.*, **2015**, 56, 6282-6286.
249. Bichlmaier, I., Kurkela, M., Joshi, T., Siiskonen, A., Ruffer, T., Lang, H., Suchanová, B., Vahermo, M., Finel, M. and Yli-Kauhaluoma, J., *J. Med. Chem.*, **2007**, 50, 2655-2664.
250. Johnson, R. L. and Rao, K. S. S. P., *Bioorganic Med. Chem. Lett.*, **2005**, 15, 57-60.
251. Ainscough, E. W., Brodie, A. M., Burrell, A. K. and Kennedy, S. M. F., *J. Organomet. Chem.*, **2000**, 609, 2-9.
252. Brynda, M., Berclaz, T., Geoffroy, M., Ramakrishnan, G. and Bernardinelli, G., *J. Phys. Chem. A*, **1998**, 102, 8245-8250.
253. Rabiee Kenaree, A., Berven, B. M., Ragogna, P. J. and Gilroy, J. B., *Chem. Commun.*, **2014**, 50, 10714-10717.

254. McMillen, D. F., Trevor, P. L. and Golden, D. M., *Acc. Chem. Res.*, **1980**, 102, 7400-7402.
255. Wicht, D. K., Kourkine, I. V., Lew, B. M., Nthenge, J. M. and Glueck, D. S., *Acc. Chem. Res.*, **1997**, 119, 5039-5040.
256. Aloisi, A., Berthet, J. C., Genre, C., Thuery, P. and Cantat, T., *Dalton Trans.*, **2016**, 45, 14774-14788.
257. King, R. B. and Kapoor, P. N., *Acc. Chem. Res.*, **1971**, 93, 4158-4166.
258. King, R. B., *Acc. Chem. Res.*, **1972**, 5, 177-185.
259. Albrecht, Ł., Albrecht, A., Krawczyk, H. and Jørgensen, K. A., *Chem. Eur. J.*, **2010**, 16, 28-48.
260. Coudray, L. and Montchamp, J. L., *Eur. J. Org. Chem.*, **2008**, 2008, 3601-3613.
261. Kamitani, M., Itazaki, M., Tamiya, C. and Nakazawa, H., *Acc. Chem. Res.*, **2012**, 134, 11932-11935.
262. Costa, E., G. Pringle, P. and Worboys, K., *Chem. Commun.*, **1998**, 0, 49-50.
263. Pringle, P. G. and Smith, M. B., *J. Chem. Soc. Chem. Commun.*, **1990**, 0, 1701-1702.
264. Reedijk, J., *Curr. Opin. Chem. Biol.*, **1999**, 3, 236-240.
265. Garnuszek, P., Licińska, I., Skierski, J. S., Koronkiewicz, M., Mirowski, M., Wiercioch, R. and Mazurek, A. P., *Nucl. Med. Biol.*, 29, 169-175.
266. Budzisz, E., Krajewska, U., Rozalski, M., Szulawska, A., Czyz, M. and Nawrot, B., *Eur. J. Pharmacol.*, **2004**, 502, 59-65.
267. Brabec, V. and Nováková, O., *Drug Resist. Updat.*, 9, 111-122.
268. Sperling, R. A., Rivera Gil, P., Zhang, F., Zanella, M. and Parak, W. J., *Chem. Soc. Rev.*, **2008**, 37, 1896-1908.
269. Buschini, A., Pinelli, S., Pellacani, C., Giordani, F., Ferrari, M. B., Bisceglie, F., Giannetto, M., Pelosi, G. and Tarasconi, P., *J. Inorg. Biochem.*, **2009**, 103, 666-677.
270. Kelkar, A. A., *Tetrahedron Lett.*, **1996**, 37, 8917-8920.
271. Obora, Y., Baleta, A. S., Tokunaga, M. and Tsuji, Y., *J. Organomet. Chem.*, **2002**, 660, 173-177.
272. Bartok, M., Felfoldi, K., Bartok, M., Torok, B. and Bartok, T., *Chem. Commun.*, **1998**, 0, 2605-2606.
273. Rosenberg, B., Van Camp, L. and Krigas, T., *Nature*, **1965**, 205, 698-699.
274. Wang, D. and Lippard, S. J., *Nat. Rev. Drug Discov.*, **2005**, 4, 307-320.
275. Johnstone, T. C., Suntharalingam, K. and Lippard, S. J., *Chem. Rev.*, **2016**, 116, 3436-3486.
276. Pruefer, F. G., Lizarraga, F., Maldonado, V. and Melendez-Zajgla, J., *J. Antimicrob. Chemother.*, **2008**, 20, 348-354.
277. Apps, M. G., Choi, E. H. Y. and Wheate, N. J., *Endocr. Relat. Cancer*, **2015**, 22, R219-R233.
278. Graham, J., Muhsin, M. and Kirkpatrick, P., *Nat. Rev. Drug Discov.*, **2004**, 3, 11-12.
279. Wheate, N. J., Walker, S., Craig, G. E. and Oun, R., *Dalton Trans.*, **2010**, 39, 8113-8127.
280. Holmes, D., *Nature*, **2015**, 527, S218-S219.
281. Stordal, B. and Davey, M., *IUBMB Life*, **2007**, 59, 696-699.
282. Cleare, M. J. and Hoeschele, J. D., *Bioinorg. Chem.*, **1973**, 2, 187-210.
283. Park, G. Y., Wilson, J. J., Song, Y. and Lippard, S. J., *Proc. Natl. Acad. Sci. U.S.A.*, **2012**, 109, 11987-11992.
284. Bimal, K. B. and Frederick, F. B., *Curr. Med. Chem.*, **2001**, 8, 1513-1533.



285. Lerman, L. S., *J. Mol. Biol.*, **1961**, 3, 18-30.
286. Lerman, L. S., *Proc. Natl. Acad. Sci. U.S.A.*, **1963**, 49, 94-102.
287. Champoux, J. J., *Annu. Rev. Biochem.*, **2001**, 70, 369-413.
288. Malonne, H. and Atassi, G., *Anti-Cancer Drugs*, **1997**, 8, 811-822.
289. Parker, C., Waters, R., Leighton, C., Hancock, J., Sutton, R., Moorman, A. V., Ancliff, P., Morgan, M., Masurekar, A., Goulden, N., Green, N., Révész, T., Darbyshire, P., Love, S. and Saha, V., *Lancet*, **2010**, 376, 2009-2017.
290. Weiss, R. B., *Semin. Oncol.*, **1992**, 19, 670-686.
291. Smith, J. C., Reddy, S. V. and Katti, V. K., *J. Chem. Soc., Dalton Trans.*, **1998**, 0, 1365-1370.
292. Handler, A., Peringer, P. and Muller, E. P., *J. Chem. Soc., Dalton Trans.*, **1990**, 0, 3725-3727.
293. Anderson, G. K., Clark, H. C. and Davies, J. A., *Inorg. Chem.*, **1983**, 22, 434-438.
294. Tau, K. D., Uriarte, R., Mazanec, T. J. and Meek, D. W., *Acc. Chem. Res.*, **1979**, 101, 6614-6619.
295. García-Seijo, M. I., Castiñeiras, A., Mahieu, B., Jánosi, L., Berente, Z., Kollár, L. and García-Fernández, M. E., *Polyhedron*, **2001**, 20, 855-868.
296. Garrou, P. E., *Chem. Rev.*, **1981**, 81, 229-266.
297. Sevillano, P., Habtemariam, A., Parsons, S., Castineiras, A., Garcia, M. E. and Sadler, P. J., *J. Chem. Soc., Dalton Trans.*, **1999**, 0, 2861-2870.
298. Housecroft, C. E., Shaykh, B. A. M., Rheingold, A. L. and Haggerty, B. S., *Acta Crystallogr. C*, **1990**, 46, 1549-1551.
299. Vyvyan, J. R., Peterson, E. A. and Stephan, M. L., *Tetrahedron Lett.*, **1999**, 40, 4947-4949.
300. Gildner, P. G. and Colacot, T. J., *Organometallics*, **2015**, 34, 5497-5508.
301. Mitchell, M. B. and Wallbank, P. J., *Tetrahedron Lett.*, **1991**, 32, 2273-2276.
302. Hadizadeh, S., Najafzadeh, N., Mazani, M., Amani, M., Mansouri-Torshizi, H. and Niapour, A., *Biochem. Res. Int.*, **2014**, 2014, 813457.
303. González, M. L., Tercero, J. M., Matilla, A., Niclós-Gutiérrez, J., Fernández, M. T., López, M. C., Alonso, C. and González, S., *Inorg. Chem.*, **1997**, 36, 1806-1812.
304. Iakovidou, Z., Papageorgiou, A., Demertzis, M. A., Mioglou, E., Mourelatos, D., Kotsis, A., Nath Yadav, P. and Kovala-Demertzi, D., *Anti-Cancer Drugs*, **2001**, 12, 65-70.
305. Friebolin, W., Schilling, G., Zöller, M. and Amtmann, E., *J. Med. Chem.*, **2005**, 48, 7925-7931.
306. Garoufis, A., Hadjikakou, S. K. and Hadjiliadis, N., in *Metallotherapeutic Drugs and Metal-Based Diagnostic Agents*, eds. Gielen, M. and Tiekink, E., John Wiley & Sons, Ltd, West Sussex, England, Editon edn., 2005, vol. 1, pp. 399-419.
307. King, R. B., Kapoor, P. N. and Kapoor, R. N., *Inorg. Chem.*, **1971**, 10, 1841-1850.
308. Miller, D. L., Boro, B. J., Grubel, K., Helm, M. L. and Appel, A. M., *Eur. J. Inorg. Chem.*, **2015**, 2015, 5781-5785.
309. Vorce, P. R., Miller, S. M. and Helm, M. L., *Acta Crystallogr. E*, **2009**, 65, m792-m792.
310. Enzmann, A., Eckert, M., Ponikwar, W., Polborn, K., Schneiderbauer, S., Beller, M. and Beck, W., *Eur. J. Inorg. Chem.*, **2004**, 2004, 1330-1340.
311. Bohr, N., *Philos. Mag. Series 6*, **1913**, 26, 1-25.
312. Saum, S. E., Askham, F. R., Laneman, S. A. and Stanley, G. G., *Polyhedron*, **1990**, 9, 1317-1321.

313. Schreiter, W. J., Monteil, A. R., Peterson, M. A., McCandless, G. T., Fronczek, F. R. and Stanley, G. G., *Polyhedron*, **2013**, 58, 171-178.
314. Zhang, Z. Z., Wang, H. K., Wang, H. G., Wang, R. J., Zhao, W. J. and Yang, L. M., *J. Organomet. Chem.*, **1988**, 347, 269-275.
315. Fontaine, X. L. R., Higgins, S. J., Langrick, C. R. and Shaw, B. L., *J. Chem. Soc., Dalton Trans.*, **1987**, 0, 777-779.
316. Tanikaga, R., Hosoya, K., Hamamura, K. and Kaji, A., *Tetrahedron Lett.*, **1987**, 28, 3705-3706.
317. Smith, A. J. and Trimm, D. L., *Annu. Rev. Mater. Res.*, **2005**, 35, 127-142.
318. Thauer, R. K., Diekert, G. and Schönheit, P., *Trends Biochem. Sci.*, **1980**, 5, 304-306.
319. Kasprzak, K. S., Sunderman, F. W. and Salnikow, K., *Mutat. Res.-Fund. Mol. M.*, **2003**, 533, 67-97.
320. Dunnick, J. K., Elwell, M. R., Radovsky, A. E., Benson, J. M., Hahn, F. F., Nikula, K. J., Barr, E. B. and Hobbs, C. H., *Cancer Res.*, **1995**, 55, 5251-5256.
321. Jouad, E. M., Larcher, G., Allain, M., Riou, A., Bouet, G. M., Khan, M. A. and Thanh, X. D., *J. Inorg. Biochem.*, **2001**, 86, 565-571.
322. Ferrari, M. B., Capacchi, S., Reffo, G., Pelosi, G., Tarasconi, P., Albertini, R., Pinelli, S. and Lunghi, P., *J. Inorg. Biochem.*, **2000**, 81, 89-97.
323. Afrasiabi, Z., Sinn, E., Lin, W., Ma, Y., Campana, C. and Padhye, S., *J. Inorg. Biochem.*, **2005**, 99, 1526-1531.
324. Rodríguez-Argüelles, M. C., Ferrari, M. B., Bisceglie, F., Pelizzi, C., Pelosi, G., Pinelli, S. and Sassi, M., *J. Inorg. Biochem.*, **2004**, 98, 313-321.
325. Scanlon, L. G., Tsao, Y. Y., Toman, K., Cummings, S. C. and Meek, D. W., *Inorg. Chem.*, **1982**, 21, 2707-2712.
326. Powell, H. M. and Chui, K. M., *J. Chem. Soc., Dalton Trans.*, **1976**, 0, 1301-1305.
327. Cao, R., Wang, Q. and Sun, H., *Acta Crystallogr. E*, **2008**, 64, m335.
328. Manojlovic-Muir, L., Mirza, H. A., Sadiq, N. and Puddephatt, R. J., *Inorg. Chem.*, **1993**, 32, 117-119.
329. Shelef, M. and Graham, G. W., *Catal. Rev.*, **1994**, 36, 433-457.
330. Westcott, S. A., Stringer, G., Anderson, S., Taylor, N. J. and Marder, T. B., *Inorg. Chem.*, **1994**, 33, 4589-4594.
331. Giordano, G., Crabtree, R. H., Heintz, R. M., Forster, D. and Morris, D. E., in *Inorganic Syntheses*, ed. Shriver, D. F., John Wiley & Sons, Inc., New York, U. S. A., Editon edn., 2007, vol. 19, pp. 218-220.
332. Murphy, L., Congreve, A., Palsson, L. O. and Williams, J. A. G., *Chem. Commun.*, **2010**, 46, 8743-8745.
333. Zhang, K. Y., Li, S. P. Y., Zhu, N., Or, I. W. S., Cheung, M. S. H., Lam, Y. W. and Lo, K. K. W., *Inorg. Chem.*, **2010**, 49, 2530-2540.
334. Leung, S. K., Kwok, K. Y., Zhang, K. Y. and Lo, K. K. W., *Inorg. Chem.*, **2010**, 49, 4984-4995.
335. Kastl, A., Wilbuer, A., Merkel, A. L., Feng, L., Di Fazio, P., Ocker, M. and Meggers, E., *Chem. Commun.*, **2012**, 48, 1863-1865.
336. Gull, A. M., Fanwick, P. E. and Kubiak, C. P., *Organometallics*, **1993**, 12, 2121-2125.
337. Ha-Thi, M. H., Penhoat, M., Drouin, D., Blanchard-Desce, M., Michelet, V. and Leray, I., *Chem. Eur. J*, **2008**, 14, 5941-5950.
338. Kaloudi-Chantzea, A., Karakostas, N., Raptopoulou, C. P., Psycharis, V., Saridakis, E., Griebel, J., Hermann, R. and Pistolis, G., *Acc. Chem. Res.*, **2010**, 132, 16327-16329.

339. Wu, W., Zhao, J., Sun, J., Huang, L. and Yi, X., *J. Mater. Chem. C*, **2013**, 1, 705-716.
340. Okamoto, M. and Teranishi, H., *J. Phys. Chem.*, **1984**, 88, 5644-5646.
341. Gacal, B. N., Koz, B., Gacal, B., Kiskan, B., Erdogan, M. and Yagci, Y., *J. Polym. Sci. A*, **2009**, 47, 1317-1326.
342. Birks, J. B. and Christophorou, L. G., *Spectrochim. Acta*, **1963**, 19, 401-410.
343. Maeda, H., Maeda, T., Mizuno, K., Fujimoto, K., Shimizu, H. and Inouye, M., *Chem. Eur. J*, **2006**, 12, 824-831.
344. Donald, S. M., *J. Chem. Phys.*, **1949**, 17, 905-913.
345. N. Berberan Santos, M., *PhysChemComm*, **2000**, 3, 18-23.
346. Michael, K., *J. Chem. Phys*, **1952**, 20, 71-74.
347. Harriman, A., *J. Chem. Soc. Faraday Trans. 1*, **1981**, 77, 369-377.
348. Harriman, A., *J. Chem. Soc. Faraday Trans. 1 Phys. Chem.*, **1980**, 76, 1978-1985.
349. Fonin, A. V., Sulatskaya, A. I., Kuznetsova, I. M. and Turoverov, K. K., *PLOS ONE*, **2014**, 9, 1-8.
350. Tedeschi, C., Möhwald, H. and Kirstein, S., *Acc. Chem. Res.*, **2001**, 123, 954-960.
351. Parker, C. A. and Hatchard, C. G., *Trans. Faraday Soc.*, **1963**, 59, 284-295.
352. Smyre, C. L., Saluta, G., Kute, T. E., Kucera, G. L. and Bierbach, U., *ACS Med. Chem. Lett.*, **2011**, 2, 870-874.
353. Kheradi, A. R., Saluta, G., Kucera, G. L., Day, C. S. and Bierbach, U., *Bioorganic Med. Chem. Lett.*, **2009**, 19, 3423-3425.
354. Martins, E. T., Baruah, H., Kramarczyk, J., Saluta, G., Day, C. S., Kucera, G. L. and Bierbach, U., *J. Med. Chem.*, **2001**, 44, 4492-4496.
355. Baruah, H., Day, C. S., Wright, M. W. and Bierbach, U., *Acc. Chem. Res.*, **2004**, 126, 4492-4493.
356. Choudhury, J. R. and Bierbach, U., *Nucleic Acids Res.*, **2005**, 33, 5622-5632.
357. Guddneppanavar, R., Saluta, G., Kucera, G. L. and Bierbach, U., *J. Med. Chem.*, **2006**, 49, 3204-3214.
358. Ding, S., Qiao, X., Kucera, G. L. and Bierbach, U., *Chem. Commun.*, **2013**, 49, 2415-2417.
359. Cusumano, M., Di Pietro, M. L. and Giannetto, A., *Chem. Commun.*, **1996**, 0, 2527-2528.
360. Loehrer, P. J. and Einhorn, L. H., *Ann. Intern. Med.*, **1984**, 100, 704-713.
361. Matsunaga, Y., Takechi, K., Akasaka, T., Ramesh, A. R., James, P. V., Thomas, K. G. and Kamat, P. V., *J. Phys. Chem. B*, **2008**, 112, 14539-14547.
362. Yassin, A., Jimenez, P., Lestriez, B., Moreau, P., Leriche, P., Roncali, J., Blanchard, P., Terrisse, H., Guyomard, D. and Gaubicher, J., *Chem. Mater.*, **2015**, 27, 4057-4065.
363. Masseroni, D., Biavardi, E., Genovese, D., Rampazzo, E., Prodi, L. and Dalcanale, E., *Chem. Commun.*, **2015**, 51, 12799-12802.
364. Friedman, J. R. and Nunnari, J., *Nature*, **2014**, 505, 335-343.
365. McBride, H. M., Neuspiel, M. and Wasiak, S., *Curr. Biol.*, **2006**, 16, R551-R560.
366. Frantz, M. C. and Wipf, P., *Environ. Mol. Mutagen.*, **2010**, 51, 462-475.
367. Benz, R., *Biochim. Biophys. Acta Rev. Biomembranes*, **1994**, 1197, 167-196.
368. Schirmer, T., *J. Struct. Biol.*, **1998**, 121, 101-109.
369. Klebba, P. E., *J. Bacteriol.*, **2005**, 187, 8232-8236.
370. Perry, S. W., Norman, J. P., Barbieri, J., Brown, E. B. and Gelbard, H. A., *Biotechniques*, **2011**, 50, 98-115.
371. Guido, K., Bruno, D. and Michèle, R. R., *Annu. Rev. Physiol.*, **1998**, 60, 619-642.
372. Cooperstein, S. J., Dixit, P. K. and Lazarow, A., *Anat. Rec.*, **1960**, 138, 49-66.

373. Johnson, L. V., Walsh, M. L. and Chen, L. B., *Proc. Natl. Acad. Sci. U.S.A.*, **1980**, 77, 990-994.
374. Summerhayes, I. C., Lampidis, T. J., Bernal, S. D., Nadakavukaren, J. J., Nadakavukaren, K. K., Shepherd, E. L. and Chen, L. B., *Proc. Natl. Acad. Sci. U.S.A.*, **1982**, 79, 5292-5296.
375. Lan Bo, C., *Annu. Rev. Cell Biol.*, **1988**, 4, 155-181.
376. Liberman, E. A., Topaly, V. P., Tsofina, L. M., Jasaitis, A. A. and Skulachev, V. P., *Nature*, **1969**, 222, 1076-1078.
377. Emaus, R. K., Grunwald, R. and Lemasters, J. J., *Biochim. Biophys. Acta Bioenergetics*, **1986**, 850, 436-448.
378. Brennan, N. K., Hall, J. P., Davies, S. R., Gollnick, S. O., Oseroff, A. R., Gibson, S. L., Hilf, R. and Detty, M. R., *J. Med. Chem.*, **2002**, 45, 5123-5135.
379. Sun, X., Wong, J. R., Song, K., Hu, J., Garlid, K. D. and Chen, L. B., *Cancer Res.*, **1994**, 54, 1465-1471.
380. Mendling, W., Weissenbacher, E. R., Gerber, S., Prasauskas, V. and Grob, P., *Arch. Gynecol. Obstet.*, **2016**, 293, 469-484.
381. Modica-Napolitano, J. S. and Aprille, J. R., *Adv. Drug Deliv. Rev.*, **2001**, 49, 63-70.
382. Modica-Napolitano, J. S., Koya, K., Weisberg, E., Brunelli, B. T., Li, Y. and Chen, L. B., *Cancer Res.*, **1996**, 56, 544-550.
383. Madar, I., Anderson, J. H., Szabo, Z., Scheffel, U., Kao, P. F., Ravert, H. T. and Dannals, R. F., *J. Nucl. Med.*, **1999**, 40, 1180-1185.
384. Madar, I., Weiss, L. and Izbicki, G., *J. Nucl. Med.*, **2002**, 43, 234-238.
385. Ravert, H. T., Madar, I. and Dannals, R. F., *J. Label. Compd. Radiophar.*, **2004**, 47, 469-476.
386. Madar, I., Ravert, H. T., Du, Y., Hilton, J., Volokh, L., Dannals, R. F., Frost, J. J. and Hare, J. M., *J. Nucl. Med.*, **2006**, 47, 1359-1366.
387. Cheng, Z., Subbarayan, M., Chen, X. and Gambhir, S. S., *J. Label. Compd. Radiophar.*, **2005**, 48, 131-137.
388. Min, J. J., Biswal, S., Deroose, C. and Gambhir, S. S., *J. Nucl. Med.*, **2004**, 45, 636-643.
389. Zhou, Y. and Liu, S., *Bioconjug. Chem.*, **2011**, 22, 1459-1472.
390. Wang, J., Yang, C. T., Kim, Y. S., Sreerama, S. G., Cao, Q., Li, Z. B., He, Z., Chen, X. and Liu, S., *J. Med. Chem.*, **2007**, 50, 5057-5069.
391. Yang, C. T., Li, Y. and Liu, S., *Inorg. Chem.*, **2007**, 46, 8988-8997.
392. Kim, Y. S., Yang, C. T., Wang, J., Wang, L., Li, Z. B., Chen, X. and Liu, S., *J. Med. Chem.*, **2008**, 51, 2971-2984.
393. Yang, C. T., Kim, Y. S., Wang, J., Wang, L., Shi, J., Li, Z. B., Chen, X., Fan, M., Li, J. J. and Liu, S., *Bioconjug. Chem.*, **2008**, 19, 2008-2022.
394. Zhou, Y., Kim, Y. S., Shi, J., Jacobson, O., Chen, X. and Liu, S., *Bioconjug. Chem.*, **2011**, 22, 700-708.
395. Davies, L. H., Harrington, R. W., Clegg, W. and Higham, L. J., *Dalton Trans.*, **2014**, 43, 13485-13499.
396. Liu, S., Kim, Y. S., Zhai, S., Shi, J. and Hou, G., *Bioconjug. Chem.*, **2009**, 20, 790-798.
397. Davies, L. H., Stewart, B., Harrington, R. W., Clegg, W. and Higham, L. J., *Angew. Chem. Int. Ed.*, **2012**, 51, 4921-4924.
398. Kee, H. L., Kirmaier, C., Yu, L., Thamyongkit, P., Youngblood, W. J., Calder, M. E., Ramos, L., Noll, B. C., Bocian, D. F., Scheidt, W. R., Birge, R. R., Lindsey, J. S. and Holten, D., *J. Phys. Chem. B*, **2005**, 109, 20433-20443.

399. Goze, C., Ulrich, G., Mallon, L. J., Allen, B. D., Harriman, A. and Ziessel, R., *Acc. Chem. Res.*, **2006**, 128, 10231-10239.
400. Baltusis, L., Frye, J. S. and Maciel, G. E., *Acc. Chem. Res.*, **1986**, 108, 7119-7120.
401. McQuaker, S. J., Quinlan, C. L., Caldwell, S. T., Brand, M. D. and Hartley, R. C., *ChemBioChem*, **2013**, 14, 993-1000.
402. Morrison, D. E., Aitken, J. B., De Jonge, M. D., Issa, F., Harris, H. H. and Rendina, L. M., *Chem. Eur. J.*, **2014**, 20, 16602-16612.
403. Laughlin, B. J., Burdette, M. K., Powell, C. R., Levy, B. E., Tennyson, A. G. and Smith, R. C., *Eur. J. Org. Chem.*, **2014**, 2014, 5998-6009.
404. Podgoršek, A., Stavber, S., Zupan, M. and Iskra, J., *Tetrahedron*, **2009**, 65, 4429-4439.
405. Burke, B. P., Greenman, P., Smith, A. M. and Archibald, S. J., *Acta Crystallogr. E*, **2012**, 68, o3202-o3202.
406. Cao, Y., Liu, M., Zhang, K., Zu, G., Kuang, Y., Tong, X., Xiong, D. and Pei, R., *Biomacromolecules*, **2017**, 18, 150-158.
407. Springborg, J. and Sotofte, I., *Acta Chem. Scand.*, **1997**, 51, 357-366.
408. Riesen, A., Zehnder, M. and Kaden, T. A., *Helv. Chim. Acta*, **1986**, 69, 2067-2073.
409. Sastri, C. V., Eswaramoorthy, D., Giribabu, L. and Maiya, B. G., *J. Inorg. Biochem.*, **2003**, 94, 138-145.
410. Dimiza, F., Papadopoulos, A. N., Tangoulis, V., Psycharis, V., Raptopoulou, C. P., Kessissoglou, D. P. and Psomas, G., *Dalton Trans.*, **2010**, 39, 4517-4528.
411. Akasaka, K., Suzuki, T., Ohru, H. and Meguro, H., *Anal. Lett.*, **1987**, 20, 731-745.
412. Pan, J., Downing, J. A., McHale, J. L. and Xian, M., *Mol. Biosyst.*, **2009**, 5, 918-920.
413. Coskun, A. and Akkaya, E. U., *Acc. Chem. Res.*, **2005**, 127, 10464-10465.
414. Apicella, B., Ciajolo, A. and Tregrossi, A., *Anal. Chem.*, **2004**, 76, 2138-2143.
415. Weissman, S. I. and Lipkin, D., *Acc. Chem. Res.*, **1942**, 64, 1916-1918.

## Appendix

### Crystallography

Crystal structure of **69**

Table 1 Crystal data and structure refinement for **69**.

Empirical formula	C <sub>31</sub> H <sub>24</sub> NZrBr <sub>0.5</sub> Cl <sub>0.5</sub>
Formula weight	559.41
Temperature/K	150.15
Crystal system	monoclinic
Space group	P2 <sub>1</sub> /c
a/Å	7.71380(10)
b/Å	18.1990(3)
c/Å	17.3229(3)
α/°	90
β/°	96.714(2)
γ/°	90
Volume/Å <sup>3</sup>	2415.17(7)
Z	4
ρ <sub>calc</sub> /cm <sup>3</sup>	1.538
μ/mm <sup>-1</sup>	1.358
F(000)	1132.0
Crystal size/mm <sup>3</sup>	0.45 × 0.2 × 0.15
Radiation	MoKα (λ = 0.71073)
2θ range for data collection/°	5.77 to 57.02
Index ranges	-10 ≤ h ≤ 10, -23 ≤ k ≤ 20, -17 ≤ l ≤ 22
Reflections collected	14345
Independent reflections	5158 [R <sub>int</sub> = 0.0226, R <sub>sigma</sub> = 0.0308]
Data/restraints/parameters	5158/0/314
Goodness-of-fit on F <sup>2</sup>	1.038
Final R indexes [I ≥ 2σ (I)]	R <sub>1</sub> = 0.0259, wR <sub>2</sub> = 0.0639
Final R indexes [all data]	R <sub>1</sub> = 0.0346, wR <sub>2</sub> = 0.0653
Largest diff. peak/hole / e Å <sup>-3</sup>	0.43/-0.54

### Crystal structure of **73**

Table 2 Crystal data and structure refinement for **73**.

Empirical formula	C <sub>25</sub> H <sub>22</sub> NPS
Formula weight	399.46
Temperature/K	150.0(2)
Crystal system	orthorhombic
Space group	Pbca
a/Å	14.47762(13)
b/Å	13.63301(11)
c/Å	21.14832(15)
α/°	90
β/°	90
γ/°	90
Volume/Å <sup>3</sup>	4174.12(6)
Z	8
ρ <sub>calc</sub> /cm <sup>3</sup>	1.271
μ/mm <sup>-1</sup>	2.163
F(000)	1680.0
Crystal size/mm <sup>3</sup>	0.23 × 0.15 × 0.09
Radiation	CuKα (λ = 1.54184)
2θ range for data collection/°	8.362 to 133.824
Index ranges	-17 ≤ h ≤ 17, -15 ≤ k ≤ 16, -25 ≤ l ≤ 18
Reflections collected	28327
Independent reflections	3713 [R <sub>int</sub> = 0.0348, R <sub>sigma</sub> = 0.0190]
Data/restraints/parameters	3713/0/256
Goodness-of-fit on F <sup>2</sup>	1.027
Final R indexes [I ≥ 2σ (I)]	R <sub>1</sub> = 0.0304, wR <sub>2</sub> = 0.0807
Final R indexes [all data]	R <sub>1</sub> = 0.0345, wR <sub>2</sub> = 0.0840
Largest diff. peak/hole / e Å <sup>-3</sup>	0.25/-0.27

## Crystal structure of **74**

Table 3 Crystal data and structure refinement for **74**.

Empirical formula	C <sub>21</sub> H <sub>20</sub> NPS
Formula weight	349.41
Temperature/K	150.0(2)
Crystal system	monoclinic
Space group	P2 <sub>1</sub> /c
a/Å	11.1317(2)
b/Å	14.2985(2)
c/Å	12.3847(2)
α/°	90
β/°	111.841(2)
γ/°	90
Volume/Å <sup>3</sup>	1829.74(6)
Z	4
ρ <sub>calc</sub> /cm <sup>3</sup>	1.268
μ/mm <sup>-1</sup>	2.388
F(000)	736.0
Crystal size/mm <sup>3</sup>	0.2 × 0.16 × 0.1
Radiation	CuKα (λ = 1.54184)
2θ range for data collection/°	8.558 to 133.874
Index ranges	-13 ≤ h ≤ 12, -17 ≤ k ≤ 16, -14 ≤ l ≤ 14
Reflections collected	13100
Independent reflections	3248 [R <sub>int</sub> = 0.0383, R <sub>sigma</sub> = 0.0312]
Data/restraints/parameters	3248/0/220
Goodness-of-fit on F <sup>2</sup>	1.021
Final R indexes [I ≥ 2σ (I)]	R <sub>1</sub> = 0.0324, wR <sub>2</sub> = 0.0812
Final R indexes [all data]	R <sub>1</sub> = 0.0412, wR <sub>2</sub> = 0.0873
Largest diff. peak/hole / e Å <sup>-3</sup>	0.29/-0.22



Crystal structure of **75**

Table 4 Crystal data and structure refinement for **75**.

Empirical formula	C <sub>17</sub> H <sub>18</sub> NPS
Formula weight	299.35
Temperature/K	150.0(2)
Crystal system	monoclinic
Space group	P2 <sub>1</sub> /c
a/Å	11.02573(16)
b/Å	20.3758(3)
c/Å	7.04987(11)
α/°	90
β/°	99.1072(14)
γ/°	90
Volume/Å <sup>3</sup>	1563.84(4)
Z	4
ρ <sub>calc</sub> /cm <sup>3</sup>	1.271
μ/mm <sup>-1</sup>	2.702
F(000)	632.0
Crystal size/mm <sup>3</sup>	0.36 × 0.18 × 0.11
Radiation	CuKα (λ = 1.54184)
2θ range for data collection/°	8.122 to 134.06
Index ranges	-13 ≤ h ≤ 13, -24 ≤ k ≤ 24, -8 ≤ l ≤ 7
Reflections collected	42773
Independent reflections	2795 [R <sub>int</sub> = 0.0503, R <sub>sigma</sub> = 0.0157]
Data/restraints/parameters	2795/0/184
Goodness-of-fit on F <sup>2</sup>	1.063
Final R indexes [I ≥ 2σ (I)]	R <sub>1</sub> = 0.0288, wR <sub>2</sub> = 0.0740
Final R indexes [all data]	R <sub>1</sub> = 0.0325, wR <sub>2</sub> = 0.0763
Largest diff. peak/hole / e Å <sup>-3</sup>	0.31/-0.25

Crystal structure of **76**

Table 5 Crystal data and structure refinement for **76**.

Empirical formula	C <sub>33</sub> H <sub>32</sub> NOPS
Formula weight	521.63
Temperature/K	150(2) K
Crystal system	triclinic
Space group	P1
a/Å	10.4544(5)
b/Å	12.6185(7)
c/Å	12.7281(7)
α/°	67.862(5)
β/°	69.229(4)
γ/°	67.350(4)
Volume/Å <sup>3</sup>	1391.56(13)
Z	2
ρ <sub>calc</sub> /cm <sup>3</sup>	1.245
μ/mm <sup>-1</sup>	0.200
F(000)	552
Crystal size/mm <sup>3</sup>	0.42 × 0.40 × 0.35
Radiation	CuKα (λ = 1.54184)
2θ range for data collection/°	3.1 to 28.4
Index ranges	-13 to 12, k -16 to 15, l -14 to 16
Reflections collected	11486
Independent reflections	5748 (R <sub>int</sub> = 0.0149)
Data/restraints/parameters	5748 / 0 / 355
Goodness-of-fit on F <sup>2</sup>	1.065
Final R indexes [I ≥ 2σ (I)]	R1 = 0.0409, wR2 = 0.1090
Final R indexes [all data]	R1 = 0.0603, wR2 = 0.1164
Largest diff. peak/hole / e Å <sup>-3</sup>	0.30 and -0.50

## Crystal structure **77**

Table 6 Crystal data and structure refinement for **77**.

Empirical formula	C <sub>25</sub> H <sub>22</sub> NPSe
Formula weight	446.36
Temperature/K	150.0(2)
Crystal system	orthorhombic
Space group	Pbca
a/Å	14.46942(11)
b/Å	13.83807(10)
c/Å	21.17154(15)
α/°	90
β/°	90
γ/°	90
Volume/Å <sup>3</sup>	4239.15(5)
Z	8
ρ <sub>calc</sub> /cm <sup>3</sup>	1.399
μ/mm <sup>-1</sup>	3.173
F(000)	1824.0
Crystal size/mm <sup>3</sup>	0.24 × 0.17 × 0.06
Radiation	CuKα (λ = 1.54184)
2θ range for data collection/°	8.352 to 133.772
Index ranges	-17 ≤ h ≤ 17, -12 ≤ k ≤ 16, -25 ≤ l ≤ 25
Reflections collected	57128
Independent reflections	3774 [R <sub>int</sub> = 0.0460, R <sub>sigma</sub> = 0.0160]
Data/restraints/parameters	3774/0/256
Goodness-of-fit on F <sup>2</sup>	1.047
Final R indexes [I ≥ 2σ (I)]	R <sub>1</sub> = 0.0300, wR <sub>2</sub> = 0.0809
Final R indexes [all data]	R <sub>1</sub> = 0.0353, wR <sub>2</sub> = 0.0850
Largest diff. peak/hole / e Å <sup>-3</sup>	0.58/-0.57

## Crystal structure **78**

Table 7 Crystal data and structure refinement for **78**.

Empirical formula	C <sub>21</sub> H <sub>20</sub> NPSe
Formula weight	396.31
Temperature/K	150.0(2)
Crystal system	monoclinic
Space group	P2 <sub>1</sub> /c
a/Å	11.25631(18)
b/Å	14.45813(18)
c/Å	12.3901(2)
α/°	90
β/°	112.1141(19)
γ/°	90
Volume/Å <sup>3</sup>	1868.10(5)
Z	4
ρ <sub>calc</sub> /cm <sup>3</sup>	1.409
μ/mm <sup>-1</sup>	3.523
F(000)	808.0
Crystal size/mm <sup>3</sup>	0.24 × 0.17 × 0.15
Radiation	CuKα (λ = 1.54184)
2θ range for data collection/°	8.48 to 133.91
Index ranges	-13 ≤ h ≤ 12, -16 ≤ k ≤ 17, -14 ≤ l ≤ 14
Reflections collected	13781
Independent reflections	3317 [R <sub>int</sub> = 0.0320, R <sub>sigma</sub> = 0.0233]
Data/restraints/parameters	3317/0/220
Goodness-of-fit on F <sup>2</sup>	1.033
Final R indexes [I ≥ 2σ (I)]	R <sub>1</sub> = 0.0251, wR <sub>2</sub> = 0.0610
Final R indexes [all data]	R <sub>1</sub> = 0.0322, wR <sub>2</sub> = 0.0656
Largest diff. peak/hole / e Å <sup>-3</sup>	0.29/-0.26

## Crystal structure **79**

Table 8 Crystal data and structure refinement for **79**.

Empirical formula	C <sub>17</sub> H <sub>18</sub> NPSe
Formula weight	346.25
Temperature/K	150.0(2)
Crystal system	monoclinic
Space group	P2 <sub>1</sub>
a/Å	8.5322(3)
b/Å	8.2843(3)
c/Å	11.2269(4)
α/°	90
β/°	94.181(3)
γ/°	90
Volume/Å <sup>3</sup>	791.44(5)
Z	2
ρ <sub>calc</sub> /cm <sup>3</sup>	1.453
μ/mm <sup>-1</sup>	2.463
F(000)	352.0
Crystal size/mm <sup>3</sup>	0.2079 × 0.1842 × 0.0913
Radiation	MoKα (λ = 0.71073)
2θ range for data collection/°	5.798 to 54.952
Index ranges	-10 ≤ h ≤ 11, -10 ≤ k ≤ 10, -14 ≤ l ≤ 14
Reflections collected	12450
Independent reflections	3427 [R <sub>int</sub> = 0.0470, R <sub>sigma</sub> = 0.0501]
Data/restraints/parameters	3427/1/184
Goodness-of-fit on F <sup>2</sup>	1.038
Final R indexes [I ≥ 2σ (I)]	R <sub>1</sub> = 0.0326, wR <sub>2</sub> = 0.0553
Final R indexes [all data]	R <sub>1</sub> = 0.0418, wR <sub>2</sub> = 0.0582
Largest diff. peak/hole / e Å <sup>-3</sup>	0.52/-0.29
Flack parameter	-0.009(6)

Crystal structure **80**

Table 9 Crystal data and structure refinement for **80**.

Empirical formula	C <sub>25</sub> H <sub>23</sub> NPSCl
Formula weight	435.92
Temperature/K	150.01(10)
Crystal system	monoclinic
Space group	P2 <sub>1</sub> /n
a/Å	14.8440(2)
b/Å	17.6553(3)
c/Å	17.6310(3)
α/°	90
β/°	107.5083(17)
γ/°	90
Volume/Å <sup>3</sup>	4406.59(13)
Z	8
ρ <sub>calc</sub> /cm <sup>3</sup>	1.314
μ/mm <sup>-1</sup>	3.182
F(000)	1824.0
Crystal size/mm <sup>3</sup>	0.2442 × 0.1045 × 0.0842
Radiation	CuKα (λ = 1.54184)
2θ range for data collection/°	6.846 to 132.742
Index ranges	-8 ≤ h ≤ 17, -20 ≤ k ≤ 20, -20 ≤ l ≤ 20
Reflections collected	33799
Independent reflections	7703 [R <sub>int</sub> = 0.0458, R <sub>sigma</sub> = 0.0351]
Data/restraints/parameters	7703/480/529
Goodness-of-fit on F <sup>2</sup>	1.022
Final R indexes [I ≥ 2σ (I)]	R <sub>1</sub> = 0.0337, wR <sub>2</sub> = 0.0844
Final R indexes [all data]	R <sub>1</sub> = 0.0432, wR <sub>2</sub> = 0.0894
Largest diff. peak/hole / e Å <sup>-3</sup>	0.46/-0.36

Crystal structure **81**

Table 10 Crystal data and structure refinement for **81**.

Empirical formula	C <sub>26</sub> H <sub>25</sub> NPSCl
Formula weight	449.95
Temperature/K	150.00(10)
Crystal system	monoclinic
Space group	P2 <sub>1</sub> /n
a/Å	10.0581(5)
b/Å	22.5806(10)
c/Å	10.3541(5)
α/°	90
β/°	93.929(4)
γ/°	90
Volume/Å <sup>3</sup>	2346.07(18)
Z	4
ρ <sub>calc</sub> /cm <sup>3</sup>	1.274
μ/mm <sup>-1</sup>	0.333
F(000)	944.0
Crystal size/mm <sup>3</sup>	0.3256 × 0.1642 × 0.1448
Radiation	MoKα (λ = 0.71073)
2θ range for data collection/°	5.754 to 59.018
Index ranges	-13 ≤ h ≤ 13, -29 ≤ k ≤ 30, -13 ≤ l ≤ 14
Reflections collected	76161
Independent reflections	6037 [R <sub>int</sub> = 0.0552, R <sub>sigma</sub> = 0.0290]
Data/restraints/parameters	6037/309/286
Goodness-of-fit on F <sup>2</sup>	1.212
Final R indexes [I ≥ 2σ (I)]	R <sub>1</sub> = 0.0639, wR <sub>2</sub> = 0.1237
Final R indexes [all data]	R <sub>1</sub> = 0.0835, wR <sub>2</sub> = 0.1306
Largest diff. peak/hole / e Å <sup>-3</sup>	0.41/-0.39

Crystal structure **94**

Table 11 Crystal data and structure refinement for **94**.

Empirical formula	C <sub>17</sub> H <sub>13</sub> P
Formula weight	248.24
Temperature/K	150.0(2)
Crystal system	monoclinic
Space group	P2 <sub>1</sub> /n
a/Å	11.2924(2)
b/Å	8.81898(12)
c/Å	13.4847(3)
α/°	90
β/°	113.882(2)
γ/°	90
Volume/Å <sup>3</sup>	1227.92(4)
Z	4
ρ <sub>calc</sub> /cm <sup>3</sup>	1.343
μ/mm <sup>-1</sup>	1.765
F(000)	520.0
Crystal size/mm <sup>3</sup>	0.25 × 0.17 × 0.1
Radiation	CuKα (λ = 1.54184)
2θ range for data collection/°	8.662 to 134.01
Index ranges	-13 ≤ h ≤ 13, -10 ≤ k ≤ 10, -16 ≤ l ≤ 16
Reflections collected	32162
Independent reflections	2185 [R <sub>int</sub> = 0.0380, R <sub>sigma</sub> = 0.0119]
Data/restraints/parameters	2185/0/169
Goodness-of-fit on F <sup>2</sup>	1.047
Final R indexes [I ≥ 2σ (I)]	R <sub>1</sub> = 0.0608, wR <sub>2</sub> = 0.1799
Final R indexes [all data]	R <sub>1</sub> = 0.0693, wR <sub>2</sub> = 0.1901
Largest diff. peak/hole / e Å <sup>-3</sup>	0.39/-0.70



## Crystal structure **95**

Table 12 Crystal data and structure refinement for **95**.

Empirical formula	C <sub>20</sub> H <sub>19</sub> P
Formula weight	290.32
Temperature/K	150.00(10)
Crystal system	monoclinic
Space group	P2 <sub>1</sub> /n
a/Å	7.5163(4)
b/Å	29.1986(9)
c/Å	7.5464(3)
α/°	90
β/°	114.466(6)
γ/°	90
Volume/Å <sup>3</sup>	1507.46(13)
Z	4
ρ <sub>calc</sub> /mg/mm <sup>3</sup>	1.279
m/mm <sup>-1</sup>	1.510
F(000)	616.0
Crystal size/mm <sup>3</sup>	0.263 × 0.115 × 0.051
Radiation	CuKα (λ = 1.54184)
2θ range for data collection	6.054 to 133.462°
Index ranges	-8 ≤ h ≤ 8, -33 ≤ k ≤ 34, -8 ≤ l ≤ 8
Reflections collected	7524
Independent reflections	2451 [R <sub>int</sub> = 0.0328, R <sub>sigma</sub> = 0.0314]
Data/restraints/parameters	2451/6/199
Goodness-of-fit on F <sup>2</sup>	1.045
Final R indexes [I ≥ 2σ (I)]	R <sub>1</sub> = 0.0394, wR <sub>2</sub> = 0.1040
Final R indexes [all data]	R <sub>1</sub> = 0.0469, wR <sub>2</sub> = 0.1106
Largest diff. peak/hole / e Å <sup>-3</sup>	0.33/-0.23

## Crystal structure of **100**

Table 13 Crystal data and structure refinement for **100**.

Empirical formula	C <sub>21</sub> H <sub>21</sub> O <sub>3</sub> P
Formula weight	352.35
Temperature/K	150.01(10)
Crystal system	triclinic
Space group	P-1
a/Å	8.6981(3)
b/Å	9.7858(4)
c/Å	11.3382(4)
α/°	90.893(3)
β/°	102.740(3)
γ/°	112.373(4)
Volume/Å <sup>3</sup>	865.15(6)
Z	2
ρ <sub>calc</sub> /cm <sup>3</sup>	1.353
μ/mm <sup>-1</sup>	1.547
F(000)	372.0
Crystal size/mm <sup>3</sup>	0.22 × 0.19 × 0.12
Radiation	CuKα (λ = 1.54184)
2θ range for data collection/°	8.044 to 132.52
Index ranges	-10 ≤ h ≤ 10, -11 ≤ k ≤ 11, -13 ≤ l ≤ 13
Reflections collected	23420
Independent reflections	3030 [R <sub>int</sub> = 0.0339, R <sub>sigma</sub> = 0.0151]
Data/restraints/parameters	3030/258/249
Goodness-of-fit on F <sup>2</sup>	1.044
Final R indexes [I ≥ 2σ (I)]	R <sub>1</sub> = 0.0404, wR <sub>2</sub> = 0.1044
Final R indexes [all data]	R <sub>1</sub> = 0.0448, wR <sub>2</sub> = 0.1081
Largest diff. peak/hole / e Å <sup>-3</sup>	0.39/-0.33

## Crystal structure **102**

Table 14 Crystal data and structure refinement for **102**.

Empirical formula	C <sub>20</sub> H <sub>17</sub> Br
Formula weight	337.24
Temperature/K	150.01(10)
Crystal system	triclinic
Space group	P-1
a/Å	6.99019(14)
b/Å	7.7048(2)
c/Å	15.4327(3)
α/°	81.785(2)
β/°	84.5942(17)
γ/°	65.973(2)
Volume/Å <sup>3</sup>	750.77(3)
Z	2
ρ <sub>calc</sub> /mg/mm <sup>3</sup>	1.492
m/mm <sup>-1</sup>	2.728
F(000)	344.0
Crystal size/mm <sup>3</sup>	0.313 × 0.196 × 0.132
Radiation	MoKα (λ = 0.71073)
2θ range for data collection	5.828 to 52.742°
Index ranges	-8 ≤ h ≤ 8, -9 ≤ k ≤ 9, -19 ≤ l ≤ 19
Reflections collected	36958
Independent reflections	3071 [R <sub>int</sub> = 0.0393, R <sub>sigma</sub> = 0.0145]
Data/restraints/parameters	3071/0/190
Goodness-of-fit on F <sup>2</sup>	1.107
Final R indexes [I ≥ 2σ (I)]	R <sub>1</sub> = 0.0185, wR <sub>2</sub> = 0.0492
Final R indexes [all data]	R <sub>1</sub> = 0.0200, wR <sub>2</sub> = 0.0500
Largest diff. peak/hole / e Å <sup>-3</sup>	0.29/-0.31

Crystal structure **103**.

Table 15 Crystal data and structure refinement for **103**.

Empirical formula	C <sub>24</sub> H <sub>27</sub> O <sub>3</sub> P
Formula weight	394.42
Temperature/K	150.01(10)
Crystal system	monoclinic
Space group	P2 <sub>1</sub> /c
a/Å	8.1515(4)
b/Å	26.7594(10)
c/Å	9.5127(5)
α/°	90
β/°	106.984(5)
γ/°	90
Volume/Å <sup>3</sup>	1984.50(17)
Z	4
ρ <sub>calc</sub> /mg/mm <sup>3</sup>	1.320
m/mm <sup>-1</sup>	0.161
F(000)	840.0
Crystal size/mm <sup>3</sup>	0.232 × 0.182 × 0.152
Radiation	MoKα (λ = 0.71073)
2θ range for data collection	6 to 52.73°
Index ranges	-10 ≤ h ≤ 10, -33 ≤ k ≤ 33, -11 ≤ l ≤ 11
Reflections collected	16477
Independent reflections	4045 [R <sub>int</sub> = 0.0342, R <sub>sigma</sub> = 0.0299]
Data/restraints/parameters	4045/0/255
Goodness-of-fit on F <sup>2</sup>	1.020
Final R indexes [I ≥ 2σ (I)]	R <sub>1</sub> = 0.0391, wR <sub>2</sub> = 0.0949
Final R indexes [all data]	R <sub>1</sub> = 0.0502, wR <sub>2</sub> = 0.1011
Largest diff. peak/hole / e Å <sup>-3</sup>	0.27/-0.47

## Crystal structure **116**

Table 16 Crystal data and structure refinement for **116**.

Empirical formula	C <sub>48</sub> H <sub>45</sub> Cl <sub>2</sub> P <sub>3</sub> Pt
Formula weight	980.74
Temperature/K	150.0(2)
Crystal system	triclinic
Space group	P-1
a/Å	9.3188(3)
b/Å	16.0163(7)
c/Å	16.0188(8)
α/°	114.587(4)
β/°	95.249(3)
γ/°	106.127(3)
Volume/Å <sup>3</sup>	2028.99(16)
Z	2
ρ <sub>calc</sub> /cm <sup>3</sup>	1.605
μ/mm <sup>-1</sup>	9.055
F(000)	980.0
Crystal size/mm <sup>3</sup>	0.09 × 0.08 × 0.02
Radiation	CuKα (λ = 1.54184)
2θ range for data collection/°	6.246 to 134.194
Index ranges	-10 ≤ h ≤ 9, -19 ≤ k ≤ 19, -19 ≤ l ≤ 18
Reflections collected	29025
Independent reflections	7166 [R <sub>int</sub> = 0.0775, R <sub>sigma</sub> = 0.0688]
Data/restraints/parameters	7166/158/499
Goodness-of-fit on F <sup>2</sup>	0.987
Final R indexes [I ≥ 2σ (I)]	R <sub>1</sub> = 0.0348, wR <sub>2</sub> = 0.0619
Final R indexes [all data]	R <sub>1</sub> = 0.0547, wR <sub>2</sub> = 0.0685
Largest diff. peak/hole / e Å <sup>-3</sup>	1.25/-0.66

## Crystal structure **120**

Table 17 Crystal data and structure refinement for **120**.

Empirical formula	C <sub>48</sub> H <sub>45</sub> Cl <sub>2</sub> P <sub>3</sub> Pd
Formula weight	892.05
Temperature/K	150.0(2)
Crystal system	triclinic
Space group	P-1
a/Å	9.3424(3)
b/Å	15.9663(7)
c/Å	15.9893(5)
α/°	114.613(4)
β/°	95.230(3)
γ/°	106.190(3)
Volume/Å <sup>3</sup>	2022.80(16)
Z	2
ρ <sub>calc</sub> /cm <sup>3</sup>	1.465
μ/mm <sup>-1</sup>	0.744
F(000)	916.0
Crystal size/mm <sup>3</sup>	0.25 × 0.16 × 0.12
Radiation	MoKα (λ = 0.71073)
2θ range for data collection/°	5.878 to 57.46
Index ranges	-12 ≤ h ≤ 12, -19 ≤ k ≤ 19, -19 ≤ l ≤ 21
Reflections collected	32276
Independent reflections	8975 [R <sub>int</sub> = 0.0416, R <sub>sigma</sub> = 0.0458]
Data/restraints/parameters	8975/599/523
Goodness-of-fit on F <sup>2</sup>	1.036
Final R indexes [I ≥ 2σ (I)]	R <sub>1</sub> = 0.0373, wR <sub>2</sub> = 0.0749
Final R indexes [all data]	R <sub>1</sub> = 0.0528, wR <sub>2</sub> = 0.0820
Largest diff. peak/hole / e Å <sup>-3</sup>	0.53/-0.44

## Crystal structure **121**

Table 18 Crystal data and structure refinement for **121**.

Empirical formula	$C_{48}H_{45}Cl_2NiP_3$
Formula weight	844.36
Temperature/K	150.0(2)
Crystal system	monoclinic
Space group	$P2_1/n$
$a/\text{\AA}$	19.5203(3)
$b/\text{\AA}$	7.39919(9)
$c/\text{\AA}$	28.7444(4)
$\alpha/^\circ$	90
$\beta/^\circ$	107.6135(14)
$\gamma/^\circ$	90
Volume/ $\text{\AA}^3$	3957.04(9)
Z	4
$\rho_{\text{calc}}/\text{g/cm}^3$	1.417
$\mu/\text{mm}^{-1}$	3.359
F(000)	1760.0
Crystal size/ $\text{mm}^3$	$0.27 \times 0.18 \times 0.08$
Radiation	$\text{CuK}\alpha$ ( $\lambda = 1.54184$ )
$2\theta$ range for data collection/ $^\circ$	4.868 to 133.962
Index ranges	$-22 \leq h \leq 23, -8 \leq k \leq 8, -34 \leq l \leq 32$
Reflections collected	29006
Independent reflections	7017 [ $R_{\text{int}} = 0.0494, R_{\text{sigma}} = 0.0377$ ]
Data/restraints/parameters	7017/0/487
Goodness-of-fit on $F^2$	1.045
Final R indexes [ $I \geq 2\sigma(I)$ ]	$R_1 = 0.0344, wR_2 = 0.0835$
Final R indexes [all data]	$R_1 = 0.0472, wR_2 = 0.0920$
Largest diff. peak/hole / $e \text{\AA}^{-3}$	0.43/-0.23

## Crystal structure **155**

Table 19 Crystal data and structure refinement for **155**.

Empirical formula	$C_{71}H_{111}BBr_3CuN_6O_6P$
Formula weight	1489.70
Temperature/K	150.0(2)
Crystal system	triclinic
Space group	P-1
a/Å	12.7536(3)
b/Å	16.2685(3)
c/Å	22.2666(4)
$\alpha/^\circ$	103.401(2)
$\beta/^\circ$	93.393(2)
$\gamma/^\circ$	102.018(2)
Volume/Å <sup>3</sup>	4367.51(16)
Z	2
$\rho_{\text{calc}}/\text{cm}^3$	1.133
$\mu/\text{mm}^{-1}$	2.478
F(000)	1562.0
Crystal size/mm <sup>3</sup>	0.27 × 0.08 × 0.03
Radiation	CuK $\alpha$ ( $\lambda = 1.54184$ )
2 $\theta$ range for data collection/ $^\circ$	7.132 to 133.77
Index ranges	-15 ≤ h ≤ 15, -19 ≤ k ≤ 19, -26 ≤ l ≤ 26
Reflections collected	61659
Independent reflections	15402 [ $R_{\text{int}} = 0.0495$ , $R_{\text{sigma}} = 0.0406$ ]
Data/restraints/parameters	15402/1111/1010
Goodness-of-fit on F <sup>2</sup>	1.032
Final R indexes [ $I \geq 2\sigma(I)$ ]	$R_1 = 0.0611$ , $wR_2 = 0.1668$
Final R indexes [all data]	$R_1 = 0.0746$ , $wR_2 = 0.1790$
Largest diff. peak/hole / e Å <sup>-3</sup>	1.97/-1.22